**Célia Marisa Costa Figueiredo Silveira**
Licenciada em Bioquímica

# Development of electrochemical nitrite biosensors using cytochrome *c* nitrite reductase from *Desulfovibrio desulfuricans* ATCC 27774

Dissertação para obtenção do Grau de Doutor em
Química Sustentável

Orientador: Doutora Maria Gabriela Machado de Almeida,
Investigadora Auxiliar da Faculdade de Ciências e Tecnologia
da Universidade Nova de Lisboa

Co-orientador: Doutor José João Galhardas de Moura,
Professor Catedrático Aposentado da Faculdade de Ciências
e Tecnologia da Universidade Nova de Lisboa

Júri:

Presidente: Doutora Maria Rosa Santos de Paiva
Arguentes: Doutor Lo Gorton
Doutor Christopher Michael Ashton Brett
Vogais: Doutora Margarida Maria Portela Correia dos Santos Romão
Doutor Pedro Miguel Leal Rodrigues
Doutora Patrícia Mira Paes de Sousa Videira

FACULDADE DE CIÊNCIAS E TECNOLOGIA
UNIVERSIDADE NOVA DE LISBOA

**Novembro 2011**

2011

# Development of electrochemical nitrite biosensors using cytochrome *c* nitrite reductase from *Desulfovibrio desulfuricans* ATCC 27774

**Célia Marisa Costa Figueiredo Silveira**

CÉLIA MARISA COSTA FIGUEIREDO SILVEIRA
Licenciada em Bioquímica

# DEVELOPMENT OF ELECTROCHEMICAL NITRITE BIOSENSORS USING CYTOCHROME *C* NITRITE REDUCTASE FROM *DESULFOVIBRIO DESULFURICANS* ATCC 27774

Dissertação apresentada para a obtenção do Grau de Doutor em Química Sustentável pela Universidade Nova de Lisboa, Faculdade de Ciências e Tecnologia

Orientador: Doutora Maria Gabriela Machado de Almeida, Investigadora Auxiliar da Faculdade de Ciências e Tecnologia da Universidade Nova de Lisboa
Co-orientador: Doutor José João Galhardas de Moura, Professor Catedrático Aposentado da Faculdade de Ciências e Tecnologia da Universidade Nova de Lisboa

Júri
Presidente: Doutora Maria Rosa Santos de Paiva
Arguentes: Doutor Lo Gorton
Doutor Christopher Michael Ashton Brett
Vogais: Doutora Margarida Maria Portela Correia dos Santos Romão
Doutor Pedro Miguel Leal Rodrigues
Doutora Patrícia Mira Paes de Sousa Videira

Lisboa
2011

# Development of electrochemical nitrite biosensors using cytochrome *c* nitrite reductase from *Desulfovibrio desulfuricans* ATCC 27774

Copyright by Célia Marisa Costa Figueiredo Silveira, Faculdade de Ciências e Tecnologia da Universidade Nova de Lisboa e Universidade Nova de Lisboa

Novembro 2011

A Faculdade de Ciências e Tecnologia e a Universidade Nova de Lisboa tem o direito, perpétuo e sem limites geográficos, de arquivar e publicar esta dissertação através de exemplares impressos reproduzidos em papel ou de forma digital, ou por qualquer outro meio conhecido ou que venha a ser inventado, e de a divulgar através de repositórios científicos e de admitir a sua cópia e distribuição com objectivos educacionais ou de investigação, não comerciais, desde que seja dado crédito ao autor e editor.

Nº Arquivo

## Acknowledgments

Many people have given me valuable help during my Ph.D. project. I owe them much and I hope that I will meet them again in the future.

First of all I would like to express my gratitude to my supervisors: Prof. José J.G. Moura, who gave me the opportunity to work in his lab and enabled my studies and research and also for the light shedding discussions. To Prof. M. Gabriela Almeida, I have to thank the opportunity she gave me to come (and go ✈) work in these projects, for all her support, teachings, ideas, encouragement and a lot more that, as she knows, I don't have much talent to express.

I thank Prof. Isabel Moura for allowing me to work in her lab and for all the helpful discussions and support over these years.

I would like to acknowledge all the collaborators, which have contributed for this work and made it possible.

To Stephane Besson for all his help in the kinetic studies and also to Sergey Bursakov.

Thanks to the sol-gel team from Faculdade de Farmácia, Universidade do Porto: Conceição Montenegro, Alberto Araújo and Sofia Gomes who kindly received me in their lab in Porto.

I would like to thank Serge Cosnier and his group in CNRS Grenoble for the help in the carbon nanotubes work and for the scientific discussions. To Michael Holzinger, Karine Gorgy, Arielle LePellec and of course to Jessica Baur, who kept my electrodes working after I came back to Portugal, thanks.

To Ana Viana from Faculdade de Ciências, Universidade de Lisboa, for the AFM analysis; to Smijla Todorovic, for the Raman spectroscopy studies in ITQB and to Rui Silva from CENIMAT FCT-UNL, for the SEM analysis, I thank all the inputs to the work, helping in the morphological characterization of the biosensors, and for the helpful discussions.

From CCMar Universidade do Algarve, thanks to Pedro Rodrigues for having me in his lab and allowing me to perform the DIGE experiments and to Odete Cordeiro and Mahaut De Vareilles for all their help.

Thanks to Prof. Manuel F.R. Pereira from Laboratório Associado LSRE/LCM, Departamento de Engenharia Química, Faculdade de Engenharia, Universidade do Porto for providing the MWCNTs samples.

I thank Professor Bart Devreese from the University of Ghent, Mass Spectrometry Proteomics group (L-ProBE), for the mass spectrometry analysis.

A special thank you to Ana Teresa Lopes, the lab technician for Grupo de Bioinorgânica and Grupo de Biofísica e Bioquímica de Proteínas at REQUIMTE, for putting up with all my questions, requests and everything else I kept asking of her all these years. Also thanks for the teachings in anaerobic bacteria cultures.

To Beth Sommerville, who worked in the proteomics project, I thank all her patience and hard effort.

I thank Marta Pimpão for all her work in the carbon nanotubes biosensors and for all the good times in the lab.

I express my appreciation to all my present and past colleagues from Grupo de Bioinorgância and Grupo de Biofísica e Bioquímica de Proteínas. I will remember always their friendship, help, advices and shared knowledge, in and out of the lab. I have learned with all and I thank them. For the ones who accompanied me in these last times, Gabi, Pablo, Sofia, Marta Carepo, Raquel, Patricia, Catarina, Natália, Luís, Jacopo, Simone, Susana, Rui Almeida, Leonardo, Luisa, Américo, Cristiano, Ana Teresa, Alexandra, thanks for everything.

A special thank you to Luisa Maia, for listening to me, always knowing how to cheer me up, and helping me put everything in the right perspective.

To Alexandra Serra I thank for sharing knowledge and lab space with me and for being my Ph.D. partner and friend.

Agradeço ao Rui Duarte, colega de laboratório e de gabinete pela ajuda e pelos momentos divertidos que passamos. Ficarão sempre na minha memória, tal como ele.

Agradeço aos meus pais e irmã por me aturarem e ao resto da família e amigos por perguntarem e demonstrarem sempre o seu apoio durante este percurso.

Finally, I thank for the financial support provided by REQUIMTE and Fundação para a Ciência e Tecnologia (POCI/QUI/58026/2004 and SFRH/BD/28921/2006).

## Abstract

This thesis describes the construction of novel nitrite biosensors based on the cytochrome *c* nitrite reductase (cc*NiR*) from the sulfate reducing bacteria *Desulfovibrio desulfuricans* ATCC 27774.

The kinetic behavior of the enzyme was firstly evaluated using spectrophotometric methods and a direct electrochemical approach. Due to cc*NiR*'s fast kinetics, electron delivering from reduced mediators was rate-limiting in solution assays, so only apparent kinetic constants can be estimated. Overall, the methods produced comparable results and showed that the binding affinity for nitrite decreases whereas turnover increases with the reduction potential.

The biosensing strategies presented have used amperometric/voltammetric transduction and explored the fact that cc*NiR* displays a non-mediated electrochemical response to nitrite when adsorbed onto pyrolytic graphite electrodes. Different strategies were proposed for protein immobilization.

In the sol-gel biosensor the protein was successfully incorporated in a porous silica glass while promptly displaying catalytic currents. The minimum detectable nitrite concentration was 120 nM. The biosensor's response was stable up to two weeks and the analysis of nitrite in freshwaters, using the standard addition method, was highly accurate.

Nanostructured configurations based on single- and multi-walled carbon nanotubes deposits greatly enhanced the direct electron transfer of cc*NiR*. At optimal conditions, the sensitivity to nitrite was 2.4 $A.M^{-1}.cm^{-2}$, the highest reported in nitrite biosensing. The addition of protective coatings (*e.g.* laponite clay) increased the bioelectrode stability (60% response after 248 days).

Surfactant films provided suitable microenvironments for cc*NiR* direct electrochemical response. The biomembrane-like modifiers enabled a considerable augmentation of catalytic currents when compared to bare electrodes (10 fold and 30% increased sensitivity with n-dodecyl-β-D-maltoside).

A preliminary proteome analysis of *D. desulfuricans* cells grown with nitrate or sulfate as electron acceptor was performed by 2D electrophoresis. It was shown that the oxidizing substrate influences the protein expression, with *ca.* 15% of proteins having significant changes.

**Keywords:** nitrite biosensors, cytochrome *c* nitrite reductase, direct electron transfer, sol-gel, carbon nanotubes, surfactants, proteomics.

## Resumo

Esta tese teve por objectivo a construção de biossensores para a quantificação de nitrito baseados na redutase do nitrito multihémica (cc*c*NiR) extraída de *Desulfovibrio desulfuricans* ATCC27774.

Em primeiro lugar, as características cinéticas da enzima foram estudadas recorrendo a métodos espectrofotométricos e electroquímicos. Devido à elevada eficiência catalítica, a cinética enzimática é limitada ao nível do redutor (mediador electrónico), pelo que as constantes cinéticas são sempre aparentes. Os dois métodos usados produziram resultados comparáveis e indicaram que a afinidade para o substrato diminui, enquanto que a constante catalítica aumenta, com o potencial de redução.

A transdução da resposta dos biossensores assentou em técnicas voltamétricas/amperométricas, explorando o facto da cc*c*NiR apresentar uma resposta electroquímica não mediada para nitrito quando adsorvida em eléctrodos de grafite pirolítica. Para a imobilização da proteína foram testados diferentes materiais.

No biossensor preparado com sol-gel, a enzima apresentou respostas catalíticas rápidas enquanto incorporada numa matrix não condutora. O limite de detecção de nitrito foi de 120nM. A resposta do sensor foi estável durante duas semanas e a quantificação de nitrito em amostras reais foi bastante exacta.

Depósitos nano-estruturados à base de nanotubos de carbono permitiram aumentar significativamente a resposta electroquímica da cc*c*NiR. Em condições optimizadas, a sensibilidade para nitrito foi 2.4 $A.M^{-1}.cm^{-2}$, o valor mais elevado até agora reportado. A adição de camadas protectoras de laponite garantiu o prolongamento da estabilidade do eléctrodo até 248 dias (60% da resposta inicial).

A utilização de filmes de surfactantes providenciaram um ambiente adequado ao aumento da resposta catalítica da cc*c*NiR. Com o n-dodecyl-β-D-maltoside, foi observado um incremento de 30% na sensibilidade da resposta e de 10x nas correntes máximas.

A análise preliminar do proteoma de células de *D. desulfuricans,* crescidas com diferentes substratos oxidantes (nitrato ou sulfato) foi realizada por electroforese 2D. O substrato respiratório provou ter influência na expressão proteica, com cerca de 15% de proteínas a apresentarem alterações.



**Palavras-chave:** biossensores de nitrito, redutase do nitrito multihémica, transferência electrónica directa, sol-gel, nanotubos de carbono, surfactantes, proteómica.

## Table of contents

## Figure Index

## Table Index

## List of abbreviations and symbols

| | |
|---|---|
| 2DE | two-dimensional gel electrophoresis |
| $\%m_O$ | mass percentage of oxygen on surface |
| 3-APTMS | 3-(aminopropyl)trimethoxy-silane |
| A | electrode area |
| Abs | absorbance |
| AFM | atomic force microscopy |
| AQS | anthraquinone-2-sulphonate |
| ASB-14 | amidosulfobetaine-14 |
| ATCC | American Type Cell Culture |
| ATP | adenosine triphosphate |
| BET | Brunauer-Emmet-Teller |
| BSA | bovine serum albumin |
| BV | benzyl viologen |
| CAPS | 3-(cyclohexylamino)-1-propanesulfonic acid |
| *cc*NiR | cytochrome c nitrite reductase |
| *cd*$_1$NiRs | cytochrome *cd*$_1$ nitrite reductases |
| CHAPS | 3-[(3-cholamidopropyl)dimethylammonio]-1-propanesulfonate |
| CMC | critical micellar concentration |
| CNT | carbon nanotubes |
| CPG | controlled pore glass |
| CTAB | cetyltrimethylammonium bromide |
| CuNiRs | copper-containing nitrite reductases |
| CV | cyclic voltammogram |
| cyt | cytochrome |
| DDAB | didodecyldimethyl ammonium bromide |
| DDM | n-dodecyl-β-D-maltoside |
| $\Delta E_p$ | peak potential separation |
| DET | direct electron transfer |
| DHP | dihexadecyl-phosphate |
| $\Delta I_{cat}$ | catalytic current after baseline subtraction |
| DIGE | differential in gel electrophoresis |
| DMF | dimethylformamide |
| DMPC | dimyristoylphosphatidyl-choline |
| DNA | desoxyribonucleic acid |

| | |
|---|---|
| DNase | desoxiribonuclease |
| DQ | diquat |
| DTT | dithiotreitol |
| E | potential |
| $\varepsilon$ | molar extinction coefficient |
| $E^{0'}$ | formal reduction potential |
| $E_{1/2}$ | half-wave potential |
| EC | mechanism of electrochemical reaction followed by chemical reaction |
| EDS | energy dispersive X-ray spectrometer |
| EDTA | ethylenediamine-tetra-acetic acid |
| EETMS | 2-(3,4-epoxycyclohexyl)-ethyltrime-thoxysilane |
| $E_p$ | peak potential |
| $E_{pa}$ | anodic peak potential |
| $E_{pc}$ | cathodic peak potential |
| ET | electron transfer |
| EU | European Union |
| F | Faraday constant |
| FEG | field emission guns |
| FIB | focused ion beam |
| $\Gamma$ | surface coverage |
| GC | glassy carbon |
| HEPES | 4-(2-hydroxyethyl)piperazine-1-ethanesulfonic acid sodium salt |
| HPU | hydrophilic polyurethane |
| HS | high spin |
| Hsp | heat shock protein |
| I | current |
| $I_0$ or $I_c$ | current in the absence of nitrite |
| IC | indigo carmine |
| $I_{cat}$ | catalytic current |
| IEF | isoelectric focusing |
| $I_{max}$ | maximum current |
| $I_p$ | peak current |
| $I_{pa}$ | anodic peak current |
| $I_{pc}$ | cathodic peak current |
| IPG | immobiline dry strip |
| $J_{0\ or\ initial}$ | current density in the absence of nitrite |

| | |
|---|---|
| $J_{max}$ | maximum current density |
| $k_{cat}$ | turnover number |
| $k_{cat}^{app}$ | apparent turnover number |
| $K_M$ | Michaelis-Menten constant |
| $K_M^{app}$ | apparent Michaelis-Menten constant |
| LDH | layered double hydroxide |
| LOD | lower limit of detection |
| LS | low spin |
| μ | specific growth rate |
| MALDI | matrix-assisted laser desorption ionization |
| MES | 2-(N-morpholino)ethanesulfonic acid hemisodium salt |
| MET | mediated electron transfer |
| MS | mass spectrometry |
| MV | methyl viologen |
| MW | relative molecular weight |
| MWCNT | multi-walled carbon nanotubes |
| ν | scan rate |
| n | number of electrons transferred |
| NA | not applicable |
| NADH | nicotinamide adenine dinucleotide |
| ND | not determined |
| NEDA | n-(1-naphtil)ethylenediamine |
| NHE | normal hydrogen electrode |
| NiR | nitrite reductase |
| NL | non-linear pH gradient |
| NOCs | carcinogenic *N*-nitroso compounds |
| NOx | nitric oxides |
| Nr | number |
| *nrf* | nitrate reduction by formate |
| Ø | diameter |
| OD | optical density |
| ox | oxidized |
| PAGE | polyacrylamide gel electrophoresis |
| PAH | poly(allylamine hydrochloride) |
| PAPS-$SO_3$H-V | viologen-modified sulfonated polyaminopropylsiloxane |
| Paz | pseudoazurine |

| | |
|---|---|
| PBV | poly(benzyl viologen) |
| PEG | poly(ethylene glycol) |
| PFV | protein film voltammetry |
| PG | pyrolytic graphite |
| PGE | pyrolytic graphite electrode |
| $pH_{PZC}$ | point of zero charge |
| pI | isoelectric point |
| pmf | peptide mass fingerprinting |
| PPB | N-(3-pyrrol-1-yl-propyl)-4,4´-bipyridinium |
| PPV | poly(pyrrole-viologen) |
| PS | phenosafranine |
| PSA | ammonium persulfate |
| Q | charge |
| red | reduced |
| Ref | reference |
| RNA | ribonucleic acid |
| RNase | ribonuclease |
| rpm | rotations *per* minute |
| RR | resonance Raman |
| SAM | self-assembled monolayer |
| $S_{BET}$ | Brunauer-Emmet-Teller surface area |
| SCE | saturated calomel electrode |
| SDS | sodium dodecyl sulfate |
| SE | secondary electrons detector |
| SEM | scanning electron microscopy |
| Sens | sensitivity |
| SRB | sulfate reducing bacteria |
| STM | scanning tunneling microscopy |
| SWCNT | single-walled carbon nanotubes |
| Td | doubling time |
| TEMED | tetramethylethylenediamine |
| TEOS | tetraethoxysilane |
| TES | N-[tris(hydroxymethyl)methyl]-3-aminopropanesulfonic acid |
| THF | tetrahydrofurane |
| TMOS | tetramethylsilane |
| TOF | time-of-flight |

| | |
|---|---|
| Tris | tris(hydroxymethyl)aminomethane |
| U | unit of enzyme activity |
| Usp | universal stress protein |
| UV-vis | ultra violet – visible |
| $v_0$ | initial rate reaction |
| $V_{max}$ | maximum rate of reaction |
| Zwitt | Zwittergent 3-10 |

## Microorganisms

| | |
|---|---|
| *A. faecalis* | *Alcaligenes faecalis* S-6 |
| *A. radiobacter* | *Agrobacterium radiobacter* |
| *D. desulfuricans* | *Desulfovibrio desulfuricans* ATCC 27774 |
| *D. vulgaris* | *Desulfovibrio vulgaris* Hildenborough |
| *E. coli* | *Escherichia coli* |
| *M. hydrocarbonoclasticus* | *Marinobacter hydrocarbonoclasticus* |
| *N. vulgaris* | *Nitrobacter vulgaris* |
| *P. denitrificans* | *Parococcus denitrificans* |
| *P. pantotrophus* | *Paracoccus pantotrophus* |
| *R. sphaeroides* | *Rhodopseudomonas sphaeroides* |
| *S. deleyianum* | *Sulfospirillum deleyianum* |
| *W. succinogenes* | *Wolinella succinogenes* |

# Chapter 1

# General Introduction

# Chapter 1 - General Introduction

Biosensing has captured attention from the scientific community for a long time. Even though the number of products introduced in the market is far behind the growth in publications, the potentialities of this technology are well acknowledged and keep driving the research forward. Nitrite has been indicated as an interesting analyte for biosensing, as clear markets exist in food industry, pollution control and clinical diagnostics.

In this chapter a brief introduction to biosensors is first presented, highlighting interest, applications and some of the advantages over other analytical methodologies. This topic is followed by the issue of nitrite determination: reasons, risks to human health and environmental and physiological occurrence. A description of nitrite determination methods is then presented with the main focus on enzyme based biosensors, to which this thesis is dedicated. Finally, the biological component of the biosensor studies here presented - cytochrome *c* nitrite reductase from *Desulfovibrio desulfuricans* ATCC 27774 - is described and characterized.

## 1.1) Biosensors

Research in biosensors was first introduced by Clark and Lyons in 1962 with the development of an enzyme biosensor for glucose [1]. Since then, the interest in biosensor technology has grown as a multidisciplinary research and development area involving the fields of physics, chemistry, biochemistry, molecular biology, material science and electronics, among others.

A biosensor is a self-contained integrated device composed of a biological recognition system (bioreceptor) in direct contact with a physicochemical transducer. It converts the bioreceptor's response to a specific analyte into an analytically useful signal (Figure 1.1). This signal can be proportional to the concentration of the analyte or simply an indication of its existence in the sample [2].

A wide variety of biological elements can be exploited in biosensors including enzymes, nucleic acids, cell receptors, organelles, antibodies, tissues and whole cells [2-6]. Moreover,

ever growing developments in molecular biology and engineering expand the list of possible biological and biological mimicking biorecognition elements.

The transducers may be electrochemical (the most common and widespread), optical, piezoelectric, magnetic, thermal, etc. [2-4,6]. Advances in transduction methodologies are supported by the constant evolution in electronics, informatics, data mining and computer technologies.

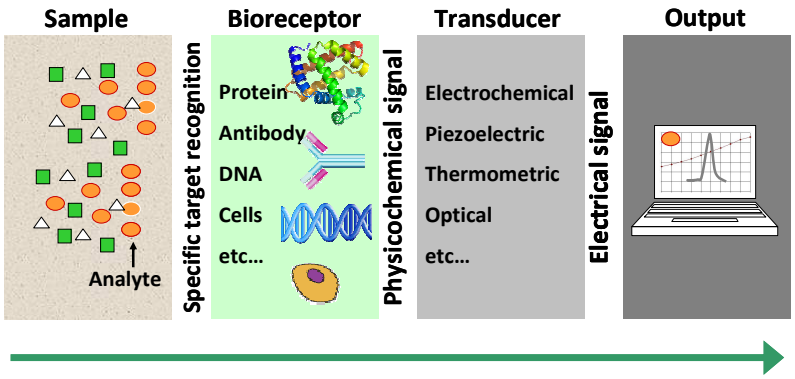


**Figure 1.1 -** Schematic representation of the working principle of biosensors.

The coupling between the bioreceptor and the transducer is a critical step in biosensor development. It is important to preserve the biorecognition activity and guarantee robustness and reproducibility to the sensor. The most commonly used methods for immobilization are membrane and matrix entrapment, physical adsorption and covalent binding [2-3]. The materials to be used should maximize the capabilities of the biological component of the biosensors and at the same time provide a stable and protective environment.

Biosensing strategies benefit from the high specificity of the biological element and the sensitivity of the transducer mechanisms, making it possible to recognize and quantify specific molecules in complex samples. The use of biosensor technology for analysis has thus been considered advantageous in comparison to other analytical techniques [4]. In addition, biosensors are simple to use, they can provide short response times and therefore allow real-time measurements. They should also be easy and cheap to fabricate in miniature dimensions, turning a long and elaborated laboratory protocol into a simple task, quickly executed on-site [5]. As reagentless devices, biosensors may be viewed as environmentally friendly analytical tools.

Biosensors have been designed for applications in a wide range of areas such as medical/clinical analysis, agriculture, food quality, environmental analysis and defense/ bioterrorism prevention [7-8]. The most successful one is undoubtedly the glucose biosensor. It is used worldwide by millions of diabetics to monitor glucose levels in blood; hence, there is a huge demand in the clinical market, pushing forward the investment and research in this particular area. This biosensor typically uses an electrochemical detection method for monitoring the electron transfer associated to glucose degradation, catalysed by glucose oxidase. Very recently, implantable glucose sensors, that allow continuous monitoring, were launched in the market.

Stricter legislation within the United States of America and the European Union demands improved and fast analysis of a growing number of analytes, especially in the environmental sector. Accordingly, biosensing is surely able to grow in importance within the analytical methodologies [5,7]. Nonetheless, a more widespread implementation of biosensor technology for analysis still faces some challenges. These lie not only on market sizes for the analytes or even in the competition with other analytical methods such as chromatography, immunoassays and mass spectrometry, that are also being fast developed and offer high precision results and low detection limits; the challenges are yet related with the conception of biosensors, for example with the stability of the biocomponents, sensitivity, selectivity and lifetime of the devices, either in use or in storage [6].

## 1.2) Nitrite assessment

Nitrite ($NO_2^-$) and nitrate ($NO_3^-$) salts are naturally present in environmental and physiological systems. On top of their natural occurrence, anthropogenic inputs derive from their use as fertilizers and food preservatives, for example. Nitrite and nitrate chemistries are practically indissociable and they are generally coexistent in all types of sources. If in excessive levels, these ions can have an adverse impact on public health and on ecological systems. Nitrite is the foremost toxic agent, but the fairly inert nitrate is easily reduced to nitrite by bacterial action in the soil, in food products or within the digestive system [9-10]. Not surprisingly, the concerns of potential toxicity have generated an increasing interest on the measurement of nitrite and nitrate for some time now.

In order to manage environmental and health risks, deriving from exposure to these ions, governmental agencies have implemented rules and directives to restrict the levels of $NO_3^-$ and $NO_2^-$ in drinking waters and food products. European directive 98/83/EC has established the maximum admissible levels of nitrate and nitrite in drinking water at 50 and 0.1 ppm, respectively. Likewise, the World Health Organization has set these limits at 50 ppm ($NO_3^-$) and 3 ppm ($NO_2^-$) (WHO/SDE/WSH/07.01/16). More recently, following the European Food Safety Authority recommendations, 2006/52/EC directive has reduced the authorized levels for these ions in meat and other food products, which should be controlled on the basis of added rather than residual amounts (*e.g.* 150 mg/kg of nitrites in meat products). Furthermore, the determination of nitrite in human physiological fluids is also commonly used for clinical diagnosis [11].

### 1.2.1) Human health risks

Human exposure to nitrate and nitrite ions results largely from dietary ingestion of food products. Only a minor percentage comes from drinking water, where the levels of these compounds usually comply with regulation [9,12]. Nitrate occurs naturally in plants, which are the main source of intake; lettuce, spinach, beetroot, radishes and celery, for example, are nitrate-rich vegetables. Yet, large accumulation of $NO_3^-$ is typically observed if vegetables are grown in soils overloaded with nitrogen fertilizers [12-13]. Nitrite ions are essentially supplied by processed foods; along with nitrate (E251, E252), nitrite salts (E249, E250) have been largely used in the manufacturing of processed and cured meats, fishes and some cheeses as anti-microbial and conserving agents and as enhancers of organoleptic properties like color and flavor [14-15].

***Methemoglobinemia*** is the principal adverse health effect caused by over-exposition to $NO_3^-$/$NO_2^-$. Nitrite can irreversibly oxidize hemoglobin to methemoglobin, which is unable to bind oxygen, endangering its transport through the body. This can cause clinical cyanosis among other symptoms. Infants are particularly susceptible to nitrite induced methemoglobinemia, often referred to as the blue-baby syndrome; a small number of fatal cases has been reported, generally associated to the consumption of water resources that failed drinking water standards (*e.g.* private wells) [9,12].

A second concern with nitrite effects on human health is the potential role of nitrite in forming ***carcinogenic N-nitroso compounds*** (NOCs) via reaction with secondary amines [16-17]. Although many NOCs have been shown to be genotoxic in animal models, the relationship between $NO_3^-$/$NO_2^-$ intake and the risk of cancer in humans has not been unequivocally proved so far [12]. No matter the controversy, the information generated from the analytical surveillance of nitrite in food products is fundamental for the management of health risks.

### 1.2.2) Environmental issues

Accumulation of nitrate in the environment derives mainly from the use of nitrogen fertilizers in agriculture; its conversion to nitrite is favored by anaerobic conditions [9]. Nitrite, on the other hand, is extensively used in textile, metal, petroleum and pharmaceutical industries [18-19]. The anthropogenic input of $NO_3^-$ and $NO_2^-$ to the environment can also occur through the photochemical conversion of atmospheric nitrogen oxides (NOx) generated by all sorts of combustion processes (industrial, domestic and automobile) [10,20-21].

An excessive input of nitrite and nitrate into the environment disturbs the biogeochemical nitrogen cycle by interfering with the denitrification/nitrification processes [20,22]. These highly soluble ions have high mobility through the soil which can lead to the contamination of ground-waters supplies. Another concern regarding the accumulation of $NO_3^-$ and $NO_2^-$ in the environment is the eutrophication of aquatic ecosystems, whose normal balance is disrupted by enrichment with nitrogen nutrients that stimulate the overgrowth of some algae species. The buildup of nitrite levels in intensive fish culture is another issue. The inefficient dispersion of wastes and the lack of local replenishment with oxygenated waters create the ideal conditions for microbial activity, resulting in an increase in ammonia and nitrite concentrations. If left unattended this can affect the fish stock [9,22-23].

### 1.2.3) Physiological significance/Biological activity

Besides the input from dietary sources, $NO_3^-$ and $NO_2^-$ are also produced endogenously in tissues. The chemical reactions of these ions in the physiological environment are strongly

related to the nitric oxide (NO) metabolism. Nitric oxide is an important mediator in cell signal transduction. It has a major role in regulating cardiovascular functions and in modulating inflammatory, infectious and degenerative disorders [12,24]. As a consequence, abnormal production of NO has been implicated in a number of pathological conditions such as acute lung disease, atherosclerosis and septic shock [25-26]. Nitric oxide is an unstable species with a very short lifetime; it is metabolized to nitrite and nitrate by reaction with oxygen. NO formation can, thus, be indirectly determined through $NO_3^-$ and $NO_2^-$ ions [25,27].

Recent studies have brought attention to nitrite itself as an important molecule in physiology, associating it with intracellular signaling functions [26,28]. The concept of a potential therapeutic use of nitrate and nitrite in human health has emerged afterwards [12,24]. These current trends contribute for the enduring scientific and public interest on the quantification of nitrite [25,28].

### 1.2.4) Detection methods

Given that nitrite and nitrate are simultaneously present in various types of samples, their detection is intimately associated and some methodologies can, in fact, be used for both ions. This implies the reduction of nitrate to nitrite, using copper or cadmium columns or nitrate reductases [10].

Probably due to the diversity and complexity of the target samples, whether they are physiological, from the environment, food or industry, a consensus on how to measure these ions is far from being reached. There are numerous analytical methods available for the determination of nitrite and nitrate ions: UV-Vis spectrophotometry (Griess reaction), fluorescence spectrophotometry, capillary electrophoresis, ionic and gas chromatography (associated with various detection systems, such as UV-vis, fluorimetry, electrochemistry and mass spectrometry), electrochemistry, among others [9-11,29-32]. However, most of these methods have shown important limitations such as sample pre-treatment stages, susceptibility to matrix interferences, insufficient detection limits, low selectivity, long analysis time and lack of portability. As a result, the analytical field is searching for innovative and improved tools such as biosensors.

As mentioned in section 1.1 biosensors can offer a series of advantages over other analytical methods, namely the inherent specificity and selectivity of the biorecognition reactions. At this stage the discussion will be set on nitrite detection only. Nitrite reductase enzymes are the sensing elements most commonly used in nitrite biosensors. Additionally, heme proteins, like myoglobin and hemoglobin [33-34], and microbial based biosensors [35-36] have been employed in the quantitative determination of nitrite.

Nitrite biosensors will be described in more detail in the following sections. These devices are generally characterized by high sensitivity and low limits of quantification, thereby indicating biosensors as reliable options for nitrite detection. The main issues in nitrite biosensing are the availability and cost of the proteins and the low stability of the devices, a consequence of the fragile and complex nature of both the immobilizing layers and of the proteins themselves [9-10].

## 1.3) Nitrite biosensors

Over the last fifteen years, biosensor technology has been exploited as a route to provide reliable nitrite quantification in complex samples. Accordingly, diverse protein electrodes and optical devices were presented in the literature. The strategies proposed for protein immobilization have relied on a variety of materials, ranging from non-conducting polymers, electropolymerized films, redox active clays, sol-gel silica glasses, carbon nanotubes and DNA tethers, either alone or in composite formulations.

The main obstacles of electrochemical biosensors are the firm immobilization of the protein without denaturation or leakage and the achievement of an efficient electronic communication between proteins and electrodes. In the context of nitrite biosensors, the majority of proposals have employed redox mediators (*e.g.* viologen derivatives) that display a fast and reversible electrochemical response and are able to shuttle electrons rapidly to the protein redox centers, following the transducing scheme depicted in Figure 1.2A. In accordance to an EC' mechanism (electrochemical reaction followed by a chemical one), the increase in cathodic peak current resulting from the regeneration of the oxidized mediator by the catalytic reaction step is directly related to the amount of substrate being processed. Mediatorless approaches based on the direct electron transfer (DET) between the redox

active enzyme and the electrode material were also reported (Figure 1.2B); in this situation, the increase in catalytic currents results from the direct regeneration of enzyme cofactors. This type of communication with the electrode is typically harder to achieve due to the insulating nature of protein polypeptide chains and the location of redox centers which are commonly deeply buried within the protein structure. In addition, the protein molecules can have an unfavorable orientation on the transducer surface, thus hindering the electron exchange and sometimes contributing to an increased distance between the electroactive centers and the electron transfer partner (the electrode).

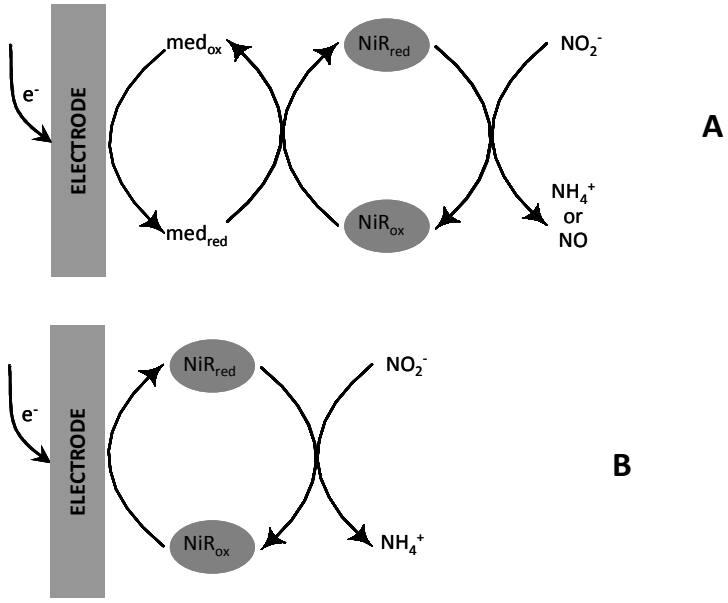


**Figure 1.2 -** Schematic representations of the working principles of enzymatic nitrite biosensors: **A)** Mediated transduction, **B)** Direct transduction. ($med_{ox}$ – mediator in the oxidized form; $med_{red}$ – mediator in the reduced form; $NiR_{ox}$ – NiR oxidized state; $NiR_{red}$ – NiR reduced state).

Besides dictating the efficiency of electrochemical transduction, the biosensor design also plays a fundamental role in defining the response features. For example, sensitivity and response time, which strongly depend on mass transfer limitations, are particularly influenced by the characteristics of the immobilization matrix.

In the next section the nitrite biosensors reported in the literature will be described. These devices were categorized into two main groups: microbial based biosensors and nitrite reductase biosensors. Furthermore, the latter section was grouped according to the type of

transduction in amperometric/voltammetric (to which a special emphasis was given), potentiometric, condutimetric and optical devices.

### 1.3.1) Microbial based biosensors

Microorganism based sensors for the detection of nitrite make use of bacterial cells that contain enzymes with activity for the reduction or oxidation of nitrite.

Reshetilov et al. proposed a microorganism biosensor for nitrite detection based on the nitrite oxidizing activity of *Nitrobacter vulgaris* [36]. These cells were adsorbed on chromatographic paper and attached to an amperometric oxygen electrode through a nylon net. The sensor activity was tested in the presence of various potential interfering compounds showing good selectivity towards nitrite. The detection limit was 10 μM. The stability of the device was probably affected by the weak immobilization system; still, it kept *ca.* 40% of initial activity after seven days of continuous measurements [36].

In another work, denitrifying bacteria (*Agrobacterium radiobacter*) were used as the biological component in a device used for the on-line determination of nitrate/nitrite in activated sludge from a waste-water treatment plant [35]. The bacteria cells reduced $NO_3^-$ /$NO_2^-$ ions to nitrous oxide that was subsequently detected at a palladium microsensor, set at 0.1 V *vs* SCE (saturated calomel electrode). The electron equivalents for the reduction reactions diffused to the bacteria chamber from a reservoir. The cells were immobilized with an ion permeable membrane (cut-off 100 Dalton) that covered the tip of the biosensor. The sensor's operational stability was 5 days, since membrane detachment hindered its use for a longer period. The detection limit was 3.6 μM and the calibration curve was linear from 0-86 μM of N, the range of $NO_3^-$/ $NO_2^-$ concentrations observed in the activated sludge [35].

This type of sensors provides a simpler bioreceptor preparation procedure, and consequential lower costs, since it makes use of integral cells instead of highly purified proteins. Moreover, the enzymatic activities essential for analyte recognition will be confined in the bacterial cells, protected from any harsh conditions the biosensors may be used in. The activities can be constantly replenished due to cell growth [35]. But, this may also be viewed as a potential problem since the expression and activity of the enzymes will be conditioned by the bacteria growth conditions and by being able to keep the cells viable.

### 1.3.2) Biosensors based on nitrite reductases

Nitrite reducing enzymes (NiRs) are innate candidates for playing the role of biorecognition elements in nitrite biosensing devices. Four classes of NiRs have been recognized so far, all of which were already featured in biosensor applications. They can be grouped according to the type of co-factors and reaction product [37-39].

There are two types of ammonia forming nitrite reductases: ***cytochrome c nitrite reductases*** (cc NiRs), which are multi-heme enzymes isolated from sulfate or sulfur reducing bacteria, and ***sirohemic nitrite reductases***, which contain a siroheme and an iron-sulfur cluster and are commonly purified from photosynthetic organisms such as plants, algae and cyanobacteria. This group of enzymes is able to catalyze the six electron reduction of nitrite to ammonia, according to the following equation:

$$NO_2^- + 8H^+ + 6e^- \rightarrow NH_4^+ + 2H_2O \quad (1.1)$$

The nitric oxide forming nitrite reductases are dissimilatory NiRs involved in bacterial denitrification; they catalyze the one electron reduction of nitrite to nitric oxide (equation 1.2). There are two different types: the ***copper-containing nitrite reductases*** (CuNiRs), with type-I and type-II copper centers, and the ***cytochrome $cd_1$ nitrite reductases*** ($cd_1$NiRs) that comprise a *c*-type and a $d_1$-type heme [37-39].

$$NO_2^- + 2H^+ + e^- \rightarrow NO + H_2O \quad (1.2)$$

#### 1.3.2.1) Amperometric and voltammetric biosensors

The group of enzyme based nitrite biosensors with amperometric/voltammetric transduction was sub-divided into mediated and non-mediated approaches. The analytical parameters of these and other enzyme based nitrite biosensors were compiled in Table 1.1. Attention should be given to the fact that the direct comparison of the analytical features of each proposal is not straightforward since the assessment of relevant parameters, such as stability and selectivity, lacked standardization. Furthermore, if a full comparison is required, experimental conditions that may vary from system to system (*e.g.* temperature, pH or ionic strength) should also be taken into account.

**Table 1.1 -** Description and analytical parameters of nitrite reductase based biosensors (NA – not applicable; ND – not determined; MET – mediated electron transfer; DET – direct electron transfer; * – original values were converted to the same final unit).

| Enzyme | Source | Sensor preparation | Transducing mode | Electron transfer | Linear Range | Detection Limit | Sensitivity | Ref |
|---|---|---|---|---|---|---|---|---|
| Sirohemic NiR | Spinach leafs | enzyme + BSA + glutaraldehyde | Potentiometric | NA | 0.1-50 mM | ND | ND | [40] |
| ccNiR | *D. desulfuricans* | GC/ casting of enzyme + polyacrylamide (mediator in solution) | Voltammetric | MET (methyl viologen) | up to 200 µM | ND | ND | [41] |
| ccNiR | *D. desulfuricans* | GC/ casting of enzyme + polyacrilamide | | DET | up to 200 µM | ND | ND | |
| ccNiR | *D. desulfuricans* | GC/ dispersion of poly(pyrrole-viologen) + enzyme mixture followed by electropolymerization | Voltammetric | MET (poly(pyrrole-viologen)) | 5.4-43.4 µM | 5.4 µM | 1721 mA $M^{-1}cm^{-2}$ | [42] |
| ccNiR | *D. desulfuricans* | GC/ casting of Nafion + enzyme/ incorporation of mediator | Voltammetric | MET (methyl viologen) | 75-800 µM | 60 µM | 445 mA $M^{-1}cm^{-2}$ | [43] |
| ccNiR | *D. desulfuricans* | GC/ casting of [ZnCr-AQS] LHD + enzyme/ glutaraldehyde vapor cross-linking | Amperometric | MET (AQS) | 0.015-2.350 µM | 4 nM | 1824 mA $M^{-1}cm^{-2}$ | [44] |
| ccNiR | *D. desulfuricans* | gold/ casting of Nafion + enzyme + mediator + glycerol + BSA/ glutaraldehyde vapor cross-linking | Conductimetric | MET (methyl viologen) | 0.2-120 µM | 0.05 µM | 0.194 µS/µM | [45] |
| ccNiR | *S. deleyianum* | graphite and mediator composite/ casting of enzyme + poly(carbamoyl sulfonate) hydrogel membrane | Amperometric | MET (phenosafranin) | up to 250 µM | 1 µM | 446.5 mA $M^{-1}cm^{-2}$ | [46] |
| $cd_1$NiR | *P. denitrificans* | graphite/ enzyme entrapment through dialysis membrane (mediator in solution) | Amperometric | MET (1-methoxy PMS) | 4.35-65.2 µM* | ND | ND | [47] |
| $cd_1$NiR | *P. denitrificans* | graphite / enzyme entrapment with dialysis membrane (mediator in solution) | Amperometric | MET (1-methoxy PMS) | up to 750 µM | 10 µM | 33 mA $M^{-1}cm^{-2}$ | [46] |
| $cd_1$NiR | *P. pantotrophus* | enzyme incorporated in bulk sol-gel monoliths of TEOS | Optical | NA | 0.075-1.250 µM | 0.075 µM | ND | [48] |
| $cd_1$NiR | *P. pantotrophus* | enzyme in controlled pore glass beads of isothiocyanate | Optical | NA | 0-4 mM | 0.93 µM | 19.5 $nM^{-1}$ | [49] |
| $cd_1$NiR | *M. hydrocarbono-clausticus* | graphite/ casting of polyvinyl alcohol + enzyme + mediator followed by photopolymerization | Amperometric | MET (cyt-$c_{552}$) | 10-200 µM | 7 µM | 2.49 A $cm^2$ $\mu M^{-1}$ | [50] |
| CuNiR | *R. sphaeroides* | GC/ electropolimerization of PPB/ casting of enzyme + PBV | Voltammetric | MET (PPB) | up to 50 µM | 1 µM | 789 mA $M^{-1}cm^{-2}$* | [51] |
| CuNiR | *R. sphaeroides* | GC/ casting of poly(vinyl alcohol) + mediator + enzyme/ casting of poly(allylamine hydrochloride)/ casting of hydrophilic polyurethane | Amperometric | MET (methyl viologen) | 1.5-260 µM | 1.5 µM | 170 mA $M^{-1}cm^{-2}$* | [52] |
| CuNiR | *R. sphaeroides* | GC/ casting of PAPS-$SO_3$H-V + enzyme/ casting HPU | Amperometric | MET (PAPS-$SO_3$H-V) | 0-18 µM | 60 nM | 170 mA $M^{-1}cm^{-2}$* | [53] |
| CuNiR | *A. faecalis* | gold/ enzyme entrapped with dialysis membrane (mediator in solution) | Amperometric | MET (1-methoxy PMS) | 0-22 µM* | 0.22 µM* | ND | [54] |
| CuNiR | *A. faecalis* | gold/ dip-coating in (cysteine) thiolated hexapeptide (enzyme and mediator in solution) | Voltammetric | MET (pseudoazurine) | 200-1500 µM | ND | ND | [55] |
| | | gold/ dip-coating in (cysteine) thiolated hexapeptide (enzyme and mediator in solution) | | MET (ruthenium hexamine) | 1-100 µM | ND | ND | |

As stated before, a biosensor is generally described as a contained unit which integrates a biorecognition element in direct physical contact with a signal transducer element [2,6]. In a mediated biosensor the electron carrier should also make part of the biorecognition system. For this reason, it must be immobilized in conjunction with the biological component. Hence, nitrite biosensing proposals in which the electron donor is added to the electrolyte solution should not be viewed as biosensors. Such non-integrated systems are, nonetheless, worth mentioning efforts that somewhat inspired further studies on the development of electrochemical enzyme devices for nitrite quantification.

#### 1.3.2.1.1) Biosensors based on mediated electrochemistry

Several studies have been described in the literature concerning the mediated electrochemistry of different NiRs. In this context, a wide range of ***synthetic electron carriers***, either in solution or immobilized, were tested prospecting the development of mediated nitrite biosensing devices [46-47,52]. Although NiRs are able to accept electrons from a variety of redox mediators, electron donors with quite negative redox potentials, such as viologen dyes, are usually chosen since the biosensor analytical performances are superior [42-43,51-53]. Yet, the high polarization potentials required complicate biosensor operation, given that side reactions (inevitably from oxygen, for example) will interfere in the analytical process. For this reason, nitrite biosensors based on reducing enzymes are almost exclusively anaerobic devices, *i.e.*, they are employed in previously deoxygenated solutions. Whenever possible it is advisable to select mediators with higher potentials. Phenazines [46-47,54], safranines [46] and anthraquinones [44] are such examples featured in NiR based biosensors.

More recently, mediated biosensor constructions based on the interaction of NiRs and their ***natural electron-transfer partner proteins*** have been proposed [50,55-56]. This type of mediation may prove advantageous relatively to biosensors based on artificial mediators, given that it mimics more faithfully the electron transfer processes occurring *in vivo*. Very importantly, avoiding the synthetic electronic mediators (which are frequently hazardous and general catalysts) turns the method more environmentally friendly and improves detection selectivity. The bioreceptor/mediator couples CuNiR/pseudoazurine (Paz) from *Alcaligenes faecalis* S-6 (*A. faecalis*) and $cd_1$NiR/ cytochrome-$c_{552}$ (cyt-$c_{552}$) purified from

*Marinobacter hydrocarbonoclasticus* (*M. hydrocarbonoclasticus*) were used in such approach. The nitrite detection capabilities of these systems gain from the use of the enzyme's physiological partners as proved in Astier et al. work where a wider linear range was attained with pseudoazurine in comparison with an inorganic mediator, ruthenium hexamine, also tested as mediating species to CuNiR (Table 1.1) [55]. In the $cd_1$NiR/cyt-$c_{552}$ based sensor described by Serra et al. the cyt-$c_{552}$ also delivered high-quality mediating properties. Besides favoring ET (electron transfer) to $cd_1$NiR, much reducing unspecific electronic reactions, it also enabled to work at -0.1 V (*vs* Ag/AgCl), therefore avoiding problematic high polarization potentials [50].

***a) Immobilization***

The co-immobilization of enzymes and mediators is a key factor to take into account when designing a biosensor. From the proteins standpoint, it is important to protect them from harsh environments which can cause losses of activity or denaturation. Regarding mediators, these usually small molecules can easily diffuse through membranes, and thus it is necessary to find strategies to retain them conveniently on the sensor, avoiding instability setbacks.

***a.1) Enzyme immobilization:***

The enzyme immobilization strategies utilized in nitrite biosensors include entrapment with dialysis membranes or with polymeric matrices (by casting or by electropolymerization of the polymer/enzyme mixtures on electrode surfaces) and interaction with DNA tethers or with peptides.

Entrapment with ***dialysis membranes*** was used in non-integrated devices for nitrite detection. Strelihtz and co-workers used it for the immobilization of $cd_1$NiR from *Parococcus denitrificans* (*P. denitrificans*) on graphite electrodes [46-47]. Sasaki et al. followed a similar approach using a recombinant CuNiR from *A. faecalis* overexpressed in *Escherichia coli* (*E. coli*), which had the double of the enzyme activity displayed by the wild type protein. The enzyme was entrapped on a gold surface with filter paper and a dialysis membrane [54]. In both cases amperometric measurements were done using mediating species in solution (Table 1.1). Although this method was quite convenient for testing a broad list of synthetic

electron donors in Strelihtz et al. work [46], the stability of such configurations is rather poor, probably due to the weak immobilization methods [54].

Several nitrite bioelectrodes based on casting of polymer/enzyme mixtures on electrode surfaces have been reported. A diversity of ***non-conducting polymers*** were used such as Nafion [43] and polyacrilamide gel [41] in *Desulfovibrio desulfuricans* ATCC 27774 cc*c*NiR based biosensors, poly(carbamoyl sulfonate) hydrogel in *cd*$_1$NiR (*P. denitrificans*) and cc*c*NiR (*S. deleyianum*) biosensors [46] or a photopolymerisable polyvinyl alcohol derivative with azide pendant groups (PVA-AWP) in a nitrite biosensor based on the co-immobilization of the protein couple *cd*$_1$NiR/cyt-*c*$_{552}$ [50]. A more complex system was presented by De Quan et al., where after the casting of a poly(vinyl alcohol), mediator and enzyme [a CuNiR from *Rhodopseudomonas sphaeroides (R. sphaeroides*)] mixture on a glassy carbon transducer surface, extra protective coats of poly(allylamine hydrochloride) and finally hydrophilic polyurethane were added [52].

Enzyme incorporation into ***redox active matrices*** is another methodology used in the construction of electrochemical nitrite biosensors. The enzymes are entrapped and at the same time electrically wired, so a better electrical connection is achieved. As a consequence, the resulting biosensors are usually very sensitive. Following this trend a redox active [ZnCr-AQS] layered double hydroxide (LDH) - an anionic exchange material doped with anthraquinone-2-monosulfonate - and an electropolymerizable poly(pyrrole-viologen) were successfully employed in the encapsulation of *D. desulfuricans*'s cc*c*NiR [42,44]. Wu et al. used a similar strategy with the CuNiR from *R. sphaeroides* which was immobilized on a glassy carbon electrode modified with a pyrrol electropolymerized film of N-(3-pyrrol-1-yl-propyl)-4,4´-bipyridinium and poly(benzyl viologen) [51]. That same enzyme was co-immobilized on a glassy carbon electrode with a viologen-modified sulfonated polyaminopropylsiloxane (PAPS-$SO_3$H-V) and hydrophilic polyurethane (HPU) [53]. The CuNiR/PAPS-$SO_3$H-V/HPU biosensor was prepared by drop-coating and the HPU membrane was the responsible for the immobilization of both the CuNiR and the PAPS-$SO_3$H-V mediator. Still, the immobilizing layer can be considered as an electroactive matrix since the viologen is covalently attached to the siloxane backbone.

Alternative strategies, making use of ***biomaterials as immobilizing agents*** were presented for CuNiR/pseudoazurine based nitrite sensing electrodes. Tepper has immobilized this set

of proteins on a SAM-modified (self-assembled monolayers) gold electrode using specific DNA tethers [56]. Both PAz and CuNiR were modified with complementary DNA tags which were allowed to hybridize with the gold anchored SH-DNA strands. This method enabled a tight association of the two proteins with the electrode surface and, at the same time, granted appropriate mobility and proximity for electron shuttling and catalytic turnover. Nevertheless, the analytical performance of this proposal was not fully explored [56]. Astier et al. used the same set of proteins on gold electrodes surfaces which were made more biocompatible through modification with cysteine-containing hexapeptides. In the presence of the CuNiR, pseudoazurine and nitrite, all in solution, both heterogeneous and intermolecular electron transfer occurred, enabling the detection of enzyme turnover [55].

### *a.2) Mediator immobilization*

When addressing mediator immobilization, it is important to choose polymers that allow an efficient retention on the bioelectrode. In De Quan et al. work, previously referred, the second polymeric coat of poly(allylamine hydrochloride) helped preventing mediator leakage, since this positively charged film was able to maintain the cationic mediator (methyl viologen) in place, by electrostatic repulsion [52]. An electrostatic interaction was also taken as the basis for methyl viologen immobilization in the Nafion/*cc*NiR film deposited on a glassy carbon surface in the work by Almeida et al. [43]. The polymer/enzyme modified electrode was immersed on a mediator containing solution, thus allowing it to incorporate the film. The cationic exchange nature of Nafion was in this way exploited to retain methyl viologen on the biosensor. The stability of this configuration was somewhat poor seeing that there was a progressive decay of mediator levels, due to its leakage from de Nafion/*cc*NiR film. A reproducible response could nonetheless be obtained for two days if matrix mediator levels were kept constant, by re-immersing the electrode in methyl viologen solution [43].

Another possibility concerning mediator containment in polymer based biosensors is the use of materials with redox mediating groups incorporated in their structure. Electropolymerizable poly(pyrroles) [42,51], a [ZnCr-AQS] LDH [44] and a viologen-modified sulfonated polyaminopropylsiloxane (PAPS-$SO_3$H-V) [53] are examples of such matrices. These materials have the double role of binding layers and redox mediators, thus allowing efficient enzyme wiring.

An alternative proposal for mediator immobilization was presented in Strehlitz et al. study. The mediator phenosafranine was directly integrated on carbon paste working electrodes (mixed on graphite-epoxy composites) [46].

***b) Analytical parameters***

Among the NiR and mediated electron transfer based sensors, the ones prepared by casting of enzyme/polymer on electrode surfaces usually provide the widest linear ranges. The polymeric coats act as diffusion barriers to nitrite, contributing for the extension of the linear catalytic current response. Accordingly, the linear range's upper limits are around 200 to 260 μM of nitrite, with the exception of the Nafion/*cc*NiR sensor [43] and the poly(carbamoyl sulphonate)/$cd_1$NiR [46] which have two of the highest limits reported to date, 800 and 750 μM, respectively. However, the analytical performance of these examples is the worst in terms of the detection limits which are quite high, limiting their application in real samples (see Table 1.1). The sensitivities are also on the low range level.

In what respects the biosensors employing redox active matrices, they share a common feature of having low detection limits [42,44,51,53]; the biosensor presented by Chen et al. based on the redox active [ZnCr-AQS] LDH offered the lowest limit - 4 nM. These configurations are also generally characterized by a high current sensitivity to nitrite, a fact that is most likely related to the superior electrical electrode/enzyme connection [42,44,51].

***c) Stability***

Sensor stability seldom exceeds a few days [42-43,51] or uses [46]. Protein deactivation is generally pointed out as the most important parameter accounting for the biosensor's response decay [42,43]. Still, some configurations presented reasonable storage stability, determined as the maintenance of 80% of the sensors initial activity, set at 24 and 51 days [52-53]. Also the [ZnCr-AQS] LDH based sensor was considered fairly stable, since it kept up to 60% of the initial response to nitrite after 32 days. This was an indication of the good biocompatibility of this immobilizing material [44].

***d) Real sample analysis***

In what concerns application in real samples the biosensors thus far tested have shown interesting qualities; in most cases the determinations are very accurate when compared with control methods [41]. Still general difficulties were found regarding the use in non-deoxygenated solutions [54].

***e) Response times***

The response times of the amperometric nitrite biosensors described in the literature are generally affected by the immobilizing layer. Thick polymeric coats like the poly(carbamoyl sulfonate) hydrogel used for *cc*NiR immobilization in Strehlitz el at. work [46] and the hydrophilic polyurethane layer used in the CuNiR/PAPS-$SO_3$H-V/HPU biosensor by Quan et al. [53] provided moderate long response times, $t_{95}$% 3 min and $t_{90\%}$ 60 s, respectively. More reasonable response times were obtained with the redox active matrix [ZnCr-AQS] LDH based sensor ($t_{90\%}$ < 5 s) [44].

**1.3.2.1.2) Biosensors based on direct electrochemistry**

A nitrite biosensor based on the DET between enzymes and electrodes has also been presented [41]. The prerequisites for achieving an efficient heterogeneous electron transfer reaction include the correct orientation of the protein molecules on the electrode surface and a sufficiently short distance between the redox active site and the electrodic interface. If no tethering system is used to control molecular spatial organization, in addition to enzyme turnover and substrate diffusion, the catalytic current may also reflect the average of individual interfacial ET rates. Very importantly, the operating potential in DET based devices is directly related to the redox potential of the enzyme, usually upgrading selectivity and avoiding interfering reactions. The biosensor's manufacturing is also simplified since fewer reagents are required.

Thus far, *cc*NiR of *D. desulfuricans* is the only NiR that has been used in DET biosensors, the first results being presented by Scharf and co-workers. In parallel to a methyl viologen mediated approach a direct electrochemical response of the enzyme entrapped on a polyacrilamide gel layer deposited on GC (glassy carbon) electrodes was observed [41].

#### 1.3.2.2) Potentiometric biosensors

Kiang and collaborators pioneered on the field of nitrite biosensors based on nitrite reducing enzymes. In their work, a sirohemic NiR extracted from spinach leaves was incorporated in a co-polymer made up of bovine serum albumine (BSA) and glutaraldehyde prepared by a freeze-thaw process. Dithionite ($S_2O_4^{2-}$) reduced methyl viologen was employed as the enzyme electron donor. The ammonia generated from the nitrite reduction reaction could be detected with a potentiometric electrode [40].

#### 1.3.2.3) Condutimetric biosensors

A conductimetric nitrite biosensor was developed by Zhang et al. by immobilizing the c*c*NiR from *D. desulfuricans* in the presence of BSA, Nafion, methyl viologen, glycerol and glutaraldehyde vapor (as cross-linking agent). The sensor was prepared by casting the enzyme preparation and a control mixture without c*c*NiR on a pair of gold interdigitated electrodes - the working and the reference electrodes, respectively. The reaction was initiated by the addition of sodium dithionite, in order to reduce the immobilized redox mediator, which in turn further activated c*c*NiR. The reaction generates conductance variation inside the miniaturized cell, which could be measured and correlated with nitrite concentration present in solution. This biosensor displayed a prompt response (10 s) with a linear range and detection limit of 0.2 - 120 µM and 0.05 µM, respectively. The response was stable for at least one week, gradually dropping after this period. Interference studies showed little or no response (lower than 5%) to common ions present in water. The biosensor was used to determine the nitrite in river water samples with recovery rates between 105-109 % [45].

#### 1.3.2.4) Optical biosensors

Similar works published by Ferreti et al. [48] and Rosa et al. [49] have suggested the employment of *cd*$_1$NiR from *Paracoccus pantotrophus* (*P. pantotrophus*) in optical nitrite biosensors. In both cases, signal transduction was based on the intensity variation of the absorption band assigned to the catalytic $d_1$-type heme ($\lambda$ = 460 nm) following nitrite addition. Prior to measurements, the sensors were exposed to sodium dithionite for enzyme activation. In a first report, sol-gel/enzyme matrices were used in two different

configurations [48]. Firstly, *cd*$_1$NiR was encapsulated in bulk sol-gel monoliths of tetramethylsilane (TMOS), which were deposited on the optical face of a spectrophotometric cuvette. The sensor had a detection limit of 0.075 μM and a linear range up to 1.250 μM nitrite. Sensitivity was determined to be 7.9 $nM^{-1}$ (Table 1.1). As an alternative approach, a sol-gel sandwich sensor configuration was investigated where the protein was deposited between two tetraethoxysilane (TEOS) sol-gel thin films, enabling to speed up the response time from 15 to 5 minutes [48]. A second optical *cd*$_1$NiR biosensor was proposed using controlled pore glass (CPG) beads of isothiocyanate for enzyme immobilization [49]. Since the matrix caused high levels of radiation scattering, the authors have chose to obtain signal transduction by visible light diffuse reflectance using a purposely designed apparatus, instead of common spectrophotometric equipments. However, this system showed a poorer analytical performance, with a detection limit of 0.93 μM, a linear range of 0-4 μM and a sensitivity of 18.5 $nM^{-1}$ [49].

## 1.4) Cytochrome *c* nitrite reductase

In the following chapters the cytochrome *c* nitrite reductase from *D. desulfuricans* will be used as the biorecognition element of non-mediated amperometric biosensors for nitrite detection. This enzyme is involved in the pathway of dissimilatory nitrate reduction to ammonia, thereby playing an important role in the biogeochemical nitrogen cycle.

c*c*NiR catalyzes the six-electron reduction of nitrite to ammonia ($NH_4^+$) (equation 1.1). Its existence has been demonstrated in bacterial strains from almost every taxonomic branch, however, the best studied c*c*NiRs were isolated from proteobacteria belonging to the subdivisions γ (ex: *Escherichia coli*) [57], δ (ex: *D. desulfuricans*) [58] or ε (ex: *Wolinella succinogenes* or *Sulfospirillum deleyianum*) [59-60]. The enzyme's production is favored by growing the bacteria in nitrate rather than sulfate containing media [61]. The reaction mechanism of c*c*NiR has been particularly well studied in *W. succinogenes*. The proposed model was based on the crystallographic observation of reaction intermediates and density functional calculations and suggests that nitrite is reduced to ammonia without the release of nitric oxide, hydroxylamine or any other intermediate [62]. In addition to nitrite, some c*c*NiRs were shown to reduce other substrates but always at lower rates than nitrite, these

include the intermediates nitric oxide and hydroxylamine, o-methylhydroxylamine [63] and sulfite [64-65].

*cc*NiR is usually found as a soluble periplasmic protein or as a membrane associated complex with the NrfH subunit. The physiological form of the enzyme is believed to be a double trimer of 2 NrfA and 1 NrfH subunits [66] (Figure 1.3A); *in vitro*, the protein complexes associate each other forming large aggregates (min. 890 kDa) [67].

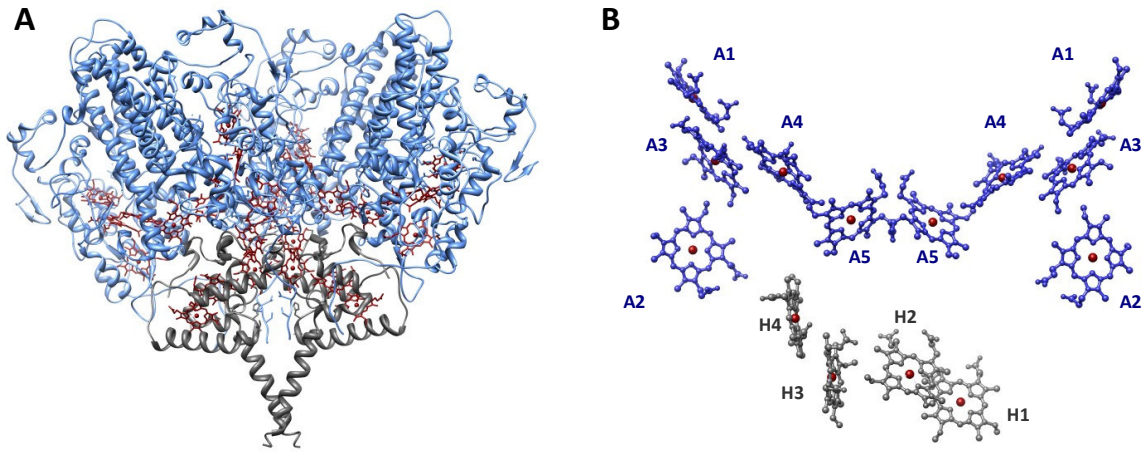


**Figure 1.3 -** *Desulfovibrio vulgaris* Hildenborough *cc*NiR **A)** view of the $NrfA_4NrfH_2$ complex: the catalytic subunit (NrfA) is depicted in blue and the electron donor subunit (NrfH) in gray, heme groups are shown in dark red; **B)** relative spatial arrangement of heme groups in a $NrfA_2NrfH$ complex, NrfA and NrfH hemes are tagged $A_n$ and $H_n$, respectively. Figure was prepared with Chimera software with pdb entry 2J7A from Brookhaven protein Data Bank [68].

In ε and δ bacteria *cc*NiR is found in association to the NrfH membrane subunit; the interaction is thought to be stronger in δ species seeing that they are only separated in the presence of strong detergents, like sodium dodecyl sulfate, while in ε (ex: *W. succinogenes*) it has also been purified as an isolated protein in the periplasm. In γ proteobacteria like *E. coli* only a soluble form of NiR has been encountered; in this case no membrane NrfH subunit is present, instead NrfA receives electrons from another periplasmic pentaheme cytochrome, NrfB [59,67,69-70].

The catalytic subunit NrfA (61 kDa), which is associated to the periplasmic membrane, is a pentaheme cytochrome *c*-type where the short distances between hemes allow a fast and efficient electron transfer [60,71]. In addition, the iron-to-iron distance between the heme 5 groups positioned at the interface of the two NrfA subunits of the $NrfA_2NrfH$ complex should also allow rapid electron transfer between monomers (Figure 1.3B). Hemes 1, 3 and 4 form an almost coplanar group with midpoint reduction potentials of -80, -480 and -400 mV *vs* NHE (normal hydrogen electrode), respectively (at pH 7.6) [71]. They are arranged in a very close parallel stack and π-electron interaction between porphyrin rings is likely to occur [60]. Hemes 2 (-50 mV) and 5 (+150 mV) are further apart and both have been postulated as the entry point of electrons from the NrfH subunit, as they are the closest to the hemes in that subunit [60,66-67].

The catalytic reaction occurs at heme 1, a high spin penta-coordinated heme group with an unusual binding motif. A lysine residue serves as proximal ligand to the heme iron, thus replacing the conventional histidine residue. The distal position in the hemic iron is free to accommodate the substrate molecule. Hemes 2 to 5 have the typical cytochrome *c*-type binding motif (bis-His) and are thought to constitute storage and transfer sites for the electrons flowing to the catalytic heme [60,71].

The catalytic site of NrfA can be assessed by two channels that reach the protein surface. They are supposed to be the substrate and product channels because they have an overall electrostatic charge opposed to the anion $NO_2^-$ substrate and cation $NH_4^+$ product that should flow through them. This is thought to contribute to the high catalytic activity of this enzyme [57,71-72]. The product channel in *D. desulfuricans* cc*NiR is partially blocked by a polypeptide segment; accordingly, the product may have to find a different route to exit the active site or a conformational change may allow this to occur through the designated product channel [71]. Interestingly, the rate of nitrite reduction was found to be lower in *D. desulfuricans* in comparison with *E. coli* and *S. deleyianum* cc*NiRs [73].

NrfH (19 kDa) is a small membrane-bound cytochrome comprising four *c*-type heme groups and it serves a double purpose. On one hand, it anchors the catalytic subunits to the membrane and on the other hand, it serves as a quinol oxidase, transferring electrons from the quinone pool to the catalytic subunits [66-67]. It is composed of a transmembrane helix and a globular hydrophilic domain that houses the four hemes. The NrfH subunit interacts

with the NrfA dimmer in an asymmetrical way, with only one of the catalytic monomers receiving electrons directly from NrfH. Heme 1 is in close contact with the membrane, in a position that should be optimal for interaction with the quinone pool. It is a high-spin heme with an unusual coordination, *i.e.*, a methionine as a proximal ligand and aspartate as distal ligand. Heme 4 has a his-lys coordination with the lysine residue coming from the NrfA subunit. This heme has quite small distances to both heme 2 and 5 in NrfA, suggesting that both can accept electrons from this subunit [66].

c*c*NiR displays typical cytochrome *c*-type spectroscopy. The UV-vis spectrum of the oxidized protein has absorption maxima at 279, 409 and 534 nm and an additional band at *ca.* 630 nm, which has been attributed to the high-spin ferric hemes [74]. In a dithionite reduced state the enzyme presents $\alpha$ and $\beta$ maximums at 523.5 and 553.5 nm and a Soret band at 420.5 nm [75].

c*c*NiR activity has been studied by Protein Film Voltammetry (PFV) mainly on pyrolytic graphite edge orientated electrodes [76-81] . These electrochemical studies have revealed interesting features of the mechanism of substrate reduction. The redox transformations on c*c*NiR occur across a wide range of potentials (150 to -480 mV *vs* NHE in *D. desulfuricans*) and the heme centers oxidation state appears to regulate the interaction of c*c*NiR with substrate through some electronic or structural changes [77,78,80].

Non-turnover signals indicating the direct reduction of the heme centers have only been reported when the film was prepared with highly concentrated enzyme solutions [76]. The large reversible peaks observed are thought to be the contribution of the 14 hemes of the $NrfA_2NrfH$ complex overlapping in a broad unresolved peak. The catalytic heme reduction potential was -200 ± 20 mV *vs* NHE, which was in fair agreement with previous spectroscopic studies. However, the highly concentrated films are not favorable for catalytic experiments, due to the high turnover of the enzyme, substrate diffusion and mass transport constrains within the surely multiple layered films. The absence of non-turnover signals when using films of only a few picomoles of enzyme is probably due to a well below monolayer (sub-monolayer) coverage of the adsorbed films [77], as confirmed by *in situ* STM (scanning tunneling microscopy) in gold electrodes [82]. Nevertheless, clear catalytic currents are always observed in the presence of nitrite.

In the cyclic voltammetry studies in the presence of nitrite (current=activity *vs* potential profiles) the enzyme activity is detected as a negative current beginning bellow -0,1 V *vs* NHE. The steep slope of the catalytic signal is in agreement with a two-electron transfer process controlling the catalytic rate, probably the reduction of hemes 1 (catalytic center) and 3 [77]. Interestingly, under substrate-limited turnover (typically below the $K_M$), increasing the driving force attenuates the nitrite reduction rate. Redox triggered conformational changes have been pointed as responsible for this decreased activity, through the reduction of other heme groups in the enzyme (4 and 5 in *E. coli* NrfA are reduced at this lower potential regions, -323 mV, while in *D. desulfuricans* only heme 4 has a lower potential, -400 mV) [77,78,80]. The rate attenuation is absent at high substrate concentration, where catalysis is enzyme limited; the electron flux is in this case higher and thus there is not sufficient time for the conformational changes to occur [78].

The high activity of the enzyme prevents voltammetry from being recorded in conditions under which substrate limitation is entirely absent. The kinetic parameters are therefore usually determined at high revolving rotating disk electrodes (3000 rpm) [77]. The electrochemical turnover rates are seldom calculated, since it is very difficult to attain the non-catalytic signals corresponding to the oxidation and reduction of the centers of the enzyme that could provide the measurement of surface coverage. The Michaelis-Menten constants are quite similar to the ones from solution studies indicating that no major perturbations are expected in the adsorbed enzyme [77,83].

The possibility to attain a high catalytic efficiency of this enzyme with electrochemical methods makes it a suitable candidate for the development of nitrite biosensors.

## 1.5) Objectives

This thesis is dedicated to the construction of nitrite biosensors with amperometric/ voltammetric transduction platforms. The work should allow the implementation of new methodologies for the determination of nitrite in complex matrices (environmental, physiological, foodstuff).

The work is focused on third generation biosensor devices, where the response is based on the direct interaction of the enzyme (cytochrome *c* nitrite reductase) with electrode

surfaces (pyrolytic graphite and glassy carbon). The enzyme will be imprisoned in diverse matrices namely, sol-gel glasses, electroactive polymers, inorganic clays and surfactants.

In a parallel work, the kinetic behavior of the enzyme, still poorly understood, will be studied in order to recognize the best conditions to explore the potentialities of this enzyme.

A proteomic study of the respiratory flexibility of *D. desulfuricans* will be carried out, aiming to study the regulation mechanisms that allow its adaptability to different environmental conditions and learn how the c*c*NiR enzyme expression in favored.

# Chapter 2

# Kinetic characterization of cytochrome *c* nitrite reductase

# Chapter 2 - Kinetic characterization of cytochrome *c* nitrite reductase

## 2.1) Introduction

Kinetic studies of *cc*NiR have been largely based on classical spectrophotometric methods using viologen dyes as electron sources (*e.g.* methyl viologen (MV) and benzyl viologen (BV)) [57-58,63-65,69,84]. They are based on the measurement of the rate of MV or BV re-oxidation in the presence of enzyme and substrate or on the quantitative determination of nitrite or ammonia after a fixed time assay also using the same type of redox mediators. In Table 2.1 a list of kinetic parameters for cytochrome *c* nitrite reductases from different bacterial sources is presented. Although the protocols provide a satisfactory turnover, they appear to give variable results when used to estimate other kinetic parameters. This has been attributed to an insufficient control of the concentration of reduced mediators in the assays (particularly in fixed time assays) and also to interferences from other reagents, like the frequently used reducing agents, dithionite and zinc. For example, the $K_M$ constants, for most NrfA enzymes studied so far, are set in the region of 30-40 μM of nitrite when determined by MV re-oxidation rates, but they can be overestimated when colorimetric assays based on nitrite or ammonia quantification are used.

**Table 2.1 -** Activities and kinetic parameters for NrfA from different bacterial sources.
* – original values were converted to the same final unit.

| Bacteria | Specific activity (μmol/min/mg) | $K_M$ | $k_{cat}$ ($s^{-1}$) | Method | Ref |
|---|---|---|---|---|---|
| *D. desulfuricans* | 344.6 | 1.14 mM | - | Ammonia quantification | [58] |
| *D. desulfuricans* | - | 22 μM | 769 | MV oxidation rate | [69] |
| *D. desulfuricans* | 453 | - | - | Ammonia quantification | [65] |
| *E. coli* | 870 | 28 μM | 770 | MV oxidation rate | [57] |
| *E. coli* | - | 33 μM | 629 | MV oxidation rate | [85] |
| *E. coli* | - | 38 μM | 625 | MV oxidation rate | [69] |
| *D. vulgaris* | 685 | - | - | Ammonia quantification | [74] |
| *W. succinogenes* | 1483* | 0.1 mM | 417* | MV oxidation rate | [84] |
| *W. succinogenes* | 414 | - | - | Ammonia quantification | [64] |
| *S. deleyianum* | 1050 | - | - | Ammonia quantification | [63] |

Therefore, the investigation of *cc*NiR kinetics requires a more systematic study. The use of a variety of artificial electron donors, with different redox potentials or ionic charges, might shed light on electron entry points, donor-protein interactions and provide rigorous criteria to establish new reliable protocols. However, practical details on the experimental conditions (mediator concentration should not be limiting, subtraction of non catalytical reactions, etc.) are rarely taken into account. Moreover, the list of available redox mediators is not long: besides being suitable electron carriers to the enzyme, they must also have chromophore groups that enable the reaction monitoring by UV-Vis spectrophotometry.

Protein Film Voltammetry is a promising alternative to the conventional methods used in kinetic studies. In this technique, an extremely small amount of a redox protein is adsorbed onto a solid electrode as an electroactive film. By applying a driving force (potential difference) the protein molecules exchange electrons directly with the electrode surface and the resultant current flow is recorded as a function of the electrode potential. In the case of an enzyme, and with a continuous delivery of its substrate to the electrode surface (what is usually achieved by using a rotating disk electrode at high revolving rates, typically 2000 to 3000 rpm), the catalytic process results in a steady-state electron flow whose detection allows instantaneous measurement of turnover rates [86,87]. The electrode itself works as the redox partner of the enzyme; as so, no electron shuttle species or co-substrates are mediating the process and no inhibition or interference reactions are expected [69].

Pyrolytic graphite (PG) electrodes have shown to be very suitable for the direct electrochemical study of redox proteins. Nonetheless, following immobilization on the electrode surface, enzymes may retain or not their catalytic properties [86,87]. Previous studies have shown that PFV can be used with *cc*NiRs, giving important insights into the activity of these enzymes. Most of the work has been done in pyrolytic graphite edge orientated electrodes and has revealed interesting features on the catalytic mechanism, on the redox center potentials and also on potential modulation of activity and enzyme interaction with substrates and inhibitors [76-81,83].

In this chapter different experimental approaches to assess *cc*NiR activity are compared and discussed, thereby contributing to the development of an efficient method, applicable in a broad range of experimental conditions. The kinetic behavior of the enzyme was studied

by two spectrophotometric techniques and also by an electrochemical assay, according to the experimental schemes depicted in Figure 2.1.

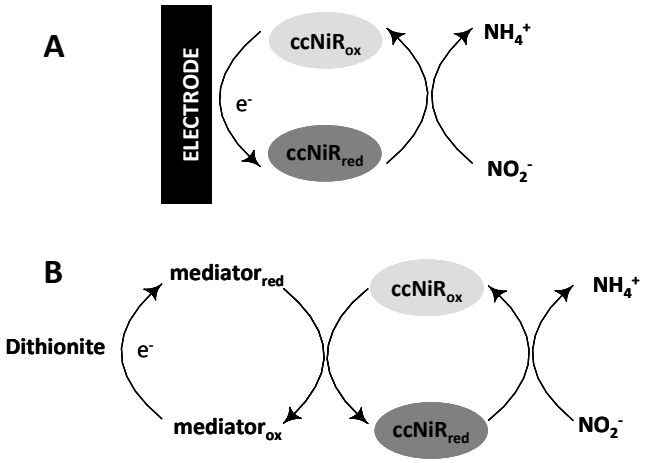


**Figure 2.1 -** Reaction schemes for electrochemical **A)** and solution **B)** assays of *cc*NiR activity.

For the spectrophotometric techniques several redox mediators were used, namely MV, Diquat (DQ), Phenosafranine (PS), Anthraquinone-2-sulphonate (AQS) and Indigo Carmine (IC) (see Table 2.2).

This preliminary work could be quite relevant for the mechanistic study of nitrite reduction by *cc*NiR as well as for paving the way towards the construction of new nitrite biosensors. In fact, several of the proposals of *D. desulfuricans* *cc*NiR based nitrite biosensors have used different electronic mediators (MV and AQS) for enzyme activation [41-45]. In order to find the optimal conditions for biosensor operation and to make a consistent comparison between the analytical properties of the proposed systems, one should fully control the correspondent homogeneous enzyme kinetics.

## 2.2) Experimental

### 2.2.1) Reagents

The cytochrome *c* nitrite reductase (1.0 $mg.mL^{-1}$) was purified from *D. desulfuricans* ATCC 27774 cells as previously described in [58,75] and stored in 0.1 M phosphate buffer pH7.6, at -20°C. The enzyme purification procedure is described in Annex 1. The protein concentration was determined with the Bicinchoninic Acid Protein Assay Kit (Sigma) using horse heart cytochrome *c* (Sigma) as standard.

1,1'-dimethyl-4,4'-bipyridinium dichloride (methyl viologen, MV), hydroxylamine, n-(1-naphtil)ethylenediamine and phenol were purchased from Sigma. Sodium nitroprusside, 3,7-diamino-5-phenylphenazinium chloride (phenosafranine, PS), 5,5'-indigo sulfonic acid disodium (indigo carmine, IC), deiquat monohydrate (diquat, DQ), anthraquinone-2-sulphonate (AQS), sodium dithionite, potassium chloride, sodium nitrite, ammonium chloride, disodium hydrogen phosphate, sodium dihydrogen phosphate and sulphanilamide were all from Merck. Hydrochloric acid was from Riedel-de-Haen. All chemicals were of analytical grade.

### 2.2.2) Enzyme assays

The enzymatic activity of *cc*NiR was determined by three different assays: two spectrophotometric (discontinuous and continuous) and one electrochemical.

#### 2.2.2.1) Discontinuous assay

The discontinuous assay involved two steps: first the enzymatic conversion of nitrite to ammonia, followed by the quantitative determination of both nitrite and ammonia present in the reaction mixture.

For the ***enzymatic step***, a 1 mL solution assay was prepared containing 0.2 M phosphate buffer pH 7.6, 0.5 mM sodium nitrite, 0.5 mM of electron donor (Table 2.2) (in the case of PS, AQS and IC the concentration was 0.25 mM) and appropriately diluted enzyme (0.7 nM for MV, DQ and PS assays, 7 nM for AQS and 14 nM for IC). In order to obtain comparable results, the mediator concentrations were leveled to provide the same reducing equivalents,

since PS, AQS and IC supply 2 electrons *per* molecule and the other mediators are one electron donors (when dithionite reduced). The reaction was initiated by the addition of 0.5 mM of sodium dithionite (prepared in a buffered solution) and after a specific incubation period (from 2 to 10 minutes) at 37°C, the reaction was stopped by oxidation of dithionite through vigorous stirring.

The ***quantification of nitrite and ammonia*** was performed by the Griess [88] and indophenol blue [89] methods, respectively. Absorbance measurements were performed with a UV-Vis spectrophotometer (Shimadzu UV – 160A). For each set of data the errors were determined as the standard deviation of the average from a minimum of three experimental assays. No ammonia formation (or nitrite consumption) was detected in any of the three control experiments performed: 1) without enzyme, 2) using acid inactivated enzyme and 3) without substrate.

One unit of enzyme activity (1 U) is defined as the amount of enzyme that catalyzes the reduction of 1 µmol of nitrite *per* minute. It can equally be defined as the amount of enzyme that catalyzes the production of 1 µmol of ammonia *per* minute.

**a) Determination of ammonia - Indophenol blue method**

For the determination of ammonia, 0.1 mL of the enzymatic reaction mixture was added to 0.5 mL of phenol reagent [1% (m/V) phenol and 0.005% (m/V) sodium nitroprusside], 0.5 mL of phosphate buffer 0.5 M pH 12.1 and 4.2 µL of commercial bleach. This reaction mixture was immediately mixed by vortex and placed in a water bath at 37°C, for 20 minutes. The absorbance was then measured at 630 nm. Ammonium chloride standards (0 - 50 nmol) were tested in the same way.

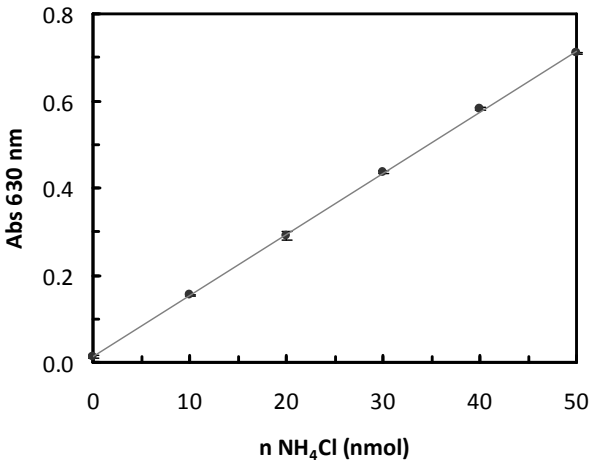


**Figure 2.2 -** Ammonia calibration curve determined by the indophenol blue method. Cell volume 1.104 mL. Linear regression y = 0.0140 x + 0.0143, $R^2$ = 0.9997.

**b) Determination of nitrite - Griess method**

For the quantification of nitrite, 0.1 mL of the enzymatic reaction mixture were added to 0.9 mL of phosphate buffer 0.2 M, pH 7.6, followed by the sequential addition of 0.5 mL of each of the Griess reagents: sulphanilamide [1% (m/V) in 9% (m/V) HCl] and NEDA [0.02% (m/V)]. This mixture was vortex mixed and incubated at room temperature for 20 minutes. The absorbance at 540 nm was recorded. Standard samples of sodium nitrite (0 - 50 nmol) were prepared in water and evaluated using the same protocol.

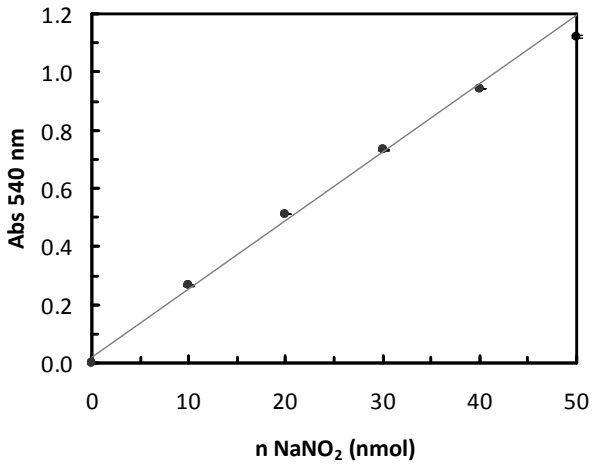


**Figure 2.3 -** Nitrite calibration curve determined by the Griess method. Cell volume 2 mL. Linear regression y = 0.0234 x + 0.0220, $R^2$ = 0.9974.

**Table 2.2 -** Mediators structure, formal reduction potential and molecular extinction coefficient.

| Mediator | | $E^{0'}$ (mV) vs NHE | $\lambda_{max}$ (nm) | $\varepsilon_{max}$ ($mM.cm^{-1}$) |
|---|---|---|---|---|
| **Indigo carmine** | 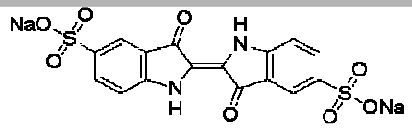 | -125 | 602 | 10.2 |
| **Anthraquinone-2-sulphonate** | 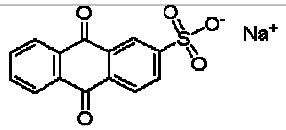 | -225 | 380 | 9.7 |
| **Phenosafranine** | 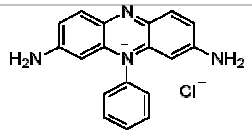 | -255 | 540 | 18.4 |
| **Diquat** | 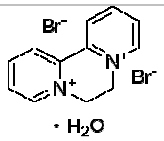 | -350 | 460 | 2.7 |
| **Methyl viologen** | 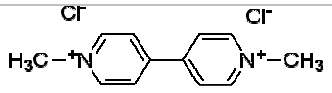 | -440 | 604 | 13.6 |

### 2.2.2.2) Continuous enzymatic assay

In this method, kinetic data was obtained by monitoring the re-oxidation of the mediators used as electron sources for enzyme turnover. The assay mixtures were prepared in a septum-stopered quartz cell containing 0.16 mM of each mediator (except for PS - 0.08 mM) and suitably diluted *cc*NiR. The enzyme concentration in the assays with the different electron donors was varied to allow the determination of the initial rate of reaction within a time interval of 10 to 15 seconds. Total cell volume was 2.5 mL completed with phosphate buffer 0.2 M, pH 7.6. The cell was purged with argon for 10 minutes before starting the reaction, while it was being incubated at 37°C. An appropriate volume of sodium dithionite was then added to the cell with a syringe to reduce the mediators (typically around 20 µL to achieve a final concentration in the cell of 0.16 mM, or 10 µL when using PS). The total volume varied slightly from assay to assay due to some dithionite degradation following the solution deoxygenation step. The complete reduction of the mediators was assured by controlling the absorbance of their reduced forms.

The absorbance was measured for 30 seconds to establish a baseline (the rate of the non-enzymatic re-oxidation of the mediator, to be subtracted from the nitrite reduction rates) and the reaction was subsequently started by the addition of sodium nitrite stock solutions (1 or 10 mM). The kinetic measurements were made by following the rate of the change of the light absorption of the mediators in the presence of nitrite [604 nm for MV ($\varepsilon_{604nm}$=13.6 $mM.cm^{-1}$) 460 nm for DQ ($\varepsilon_{460nm}$=2.7 $mM.cm^{-1}$) and 540 nm for PS ($\varepsilon_{540nm}$=18.4 $mM.cm^{-1}$)]. Control assays performed in the absence of nitrite or enzyme showed little or no bleaching of the reduced mediators. The absorbance variation over time was measured on a Diode array spectrophotometer (Agilent Technologies 8453A UV-Vis), equipped with a thermo-settable single-cell holder in an open compartment. Each experimental point is the average of a minimum of three independent; errors bars represent the standard deviation. Kinetic parameters $K_M$ and $k_{cat}$ were determined by an iterative nonlinear least squares method using the software GraphPad Prism 4.

### 2.2.2.3) Electrochemical assay

#### a) Electrochemistry

Chronoamperometry experiments (electrode potential was stepped while the current was measured) were performed with an Autolab electrochemical analyzer (PGSTAT12, Eco Chemie) under the control of GPES software (Eco Chemie). The working potentials are referred in the results section. Electrode rotation was driven with an electrode rotator (Eco Chemie) also controlled by GPES. The experiments were performed with a speed rotation of 600 rpm. A three-electrode cell configuration was used, composed of a silver/silver chloride reference electrode (Ag/AgCl) (Radiometer), a platinum (Pt) wire counter electrode (Radiometer) and a PG working electrode (self-made). All potentials were quoted against NHE (+197 mV Ag/AgCl). The experiments were carried out at 37°C in a single compartment cell (Metrohm) containing 20 mL of supporting electrolyte (0.1 M phosphate buffer, pH 7.6). The solution in the electrochemical cell was purged with argon before measurements and the argon atmosphere was maintained during the experiments by continuously flushing the cell.

#### b) Electrode preparation

Protein films were prepared by depositing a 10 µL drop of enzyme solution (1.0 mg/mL) on the electrode surface. After 10 minutes, the electrode was washed with buffer and placed in the electrochemical cell. Protein surface coverage (*ca.* 4.3 pmol.cm$^{-2}$) was determined, according to the method described in [76], from the area of the non-catalytic peaks of *cc*NiR cyclic voltammograms performed in the absence of nitrite. The electrode response to nitrite was evaluated by successively adding small volumes of sodium nitrite stock solutions (1, 10 and 100 mM), while continuously recording the current activity. Control experiments showed no detectable faradaic current in the absence of *cc*NiR.

### 2.2.3) Molecular Docking Simulations

The atomic coordinates of *D. desulfuricans* *cc*NiR were obtained from the Brookhaven protein Data Bank (entry 1OAH.pdb) [71]. The structures of the mediators were obtained

from the PubChem database [entries 15939 (MV), 6795 (DQ), 65733 (PS), 8551 (AQS), and 5284351 (IC)]. The atomic coordinates of the mediators and *cc*NiR were used as input files for the docking algorithm PatchDock [90-91], which creates potential complexes sorted according to shape complementarity criteria. The obtained complexes are sorted by a scoring function that considers both geometric fit and atomic desolvation energy. A root mean square deviation clustering of 4 Å is then applied to the complexes to discard redundant solutions. With this algorithm, the native result is always found in the top 100 solutions and often among the top 10. Noticeably, the top 20 solutions obtained in this study were very similar to each other. Thus, to avoid the construction of confusing pictures only the first five are shown in the figures. Structure manipulation was done with the UCSF Chimera package [92].

## 2.3) Results and Discussion

### 2.3.1) Mediated spectrophotometry

#### 2.3.1.1) Determination of *cc*NiR enzymatic reaction product

The influence of the enzyme's electron donor in the product formation was investigated. In particular, it was checked if nitrite is directly converted to ammonia and no intermediates are accumulated during the course of the enzymatic reaction. A simple fixed-time method (discontinuous) was used, in which direct measurements of the reaction substrate and product were made [58]. Nitrite consumption and ammonia formation curves, traced in the presence of methyl viologen, diquat, phenosafranine, anthraquinone-2-sulphonate and indigo carmine, are represented in Figure 2.4.

The enzyme concentration was different in some assays in order to guarantee that all the nitrite/ammonia progression curves would vary linearly with time within the interval chosen to stop the enzymatic reactions. Comparing the ammonia and nitrite contents (at 4 minutes, within the linear part of product formation) it was confirmed that there is 100% conversion of nitrite into ammonia with all the mediators, except for indigo carmine (75%) as shown in Figure 2.5. Since the latter has the highest reduction potential (-145 mV *vs* NHE), one may speculate that the reaction is not complete and less reduced intermediates or products other than ammonium may be formed. No further studies were performed to corroborate this result, since efficient quantitation methods for reaction intermediates have yet to be established [64].

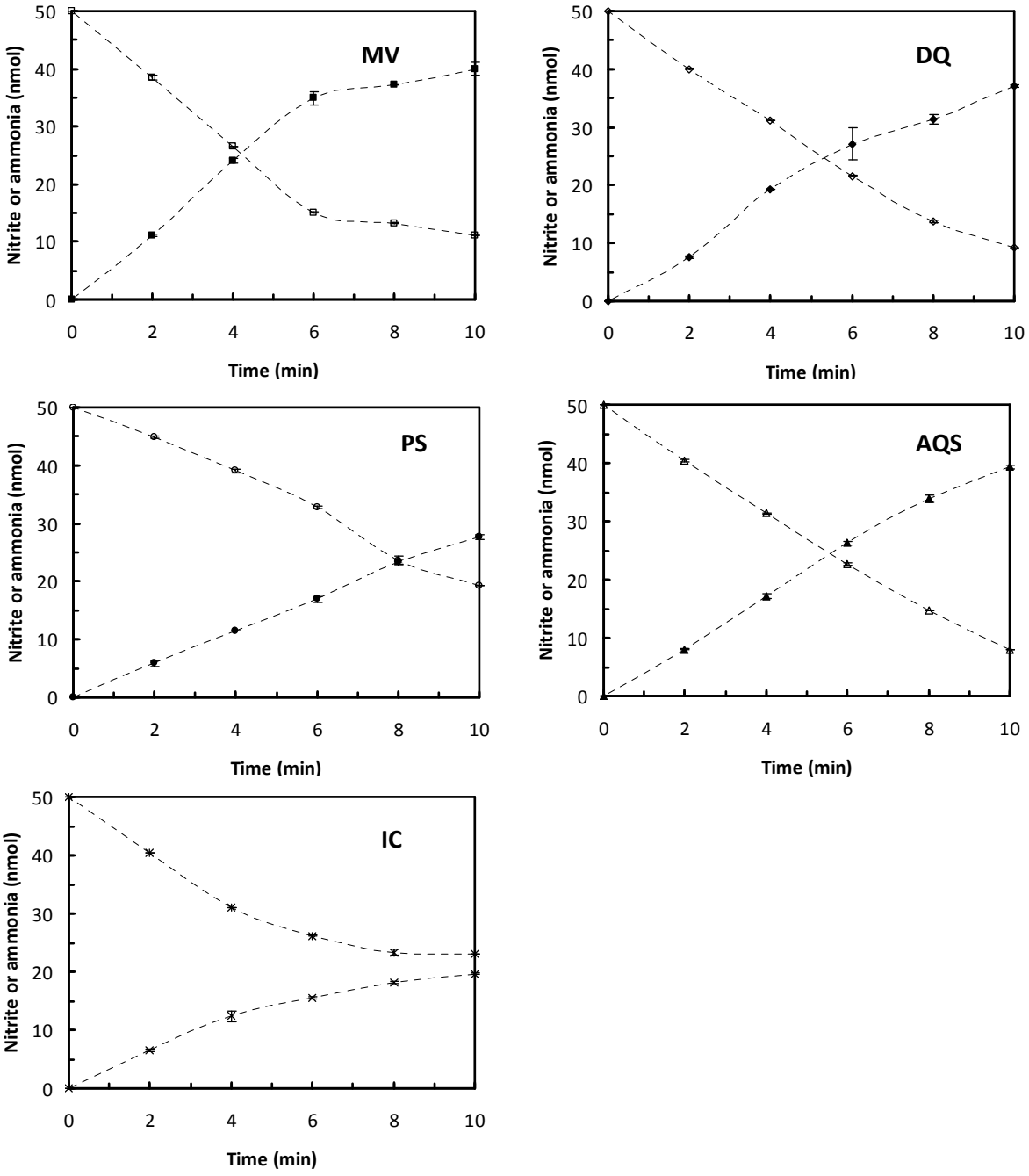


**Figure 2.4 -** Progression curves for ammonia (filled symbols) and nitrite (open symbols) for *cc*NiR reaction, in the presence of equivalent electron concentrations of dithionite reduced mediators MV (■□); DQ (◆◇); PS (●○); AQS (▲△) and IC (ж). Enzyme concentration was 0.7 nM for MV, DQ, and PS assays, 7 nM for AQS, and 14 nM for IC. All assays were performed at 37°C. In the case of DQ assays the values for ammonia detection were corrected by adding a 25% to the final value, since a consistent 25% error was found in control experiments where ammonia was quantified in DQ containing solutions.

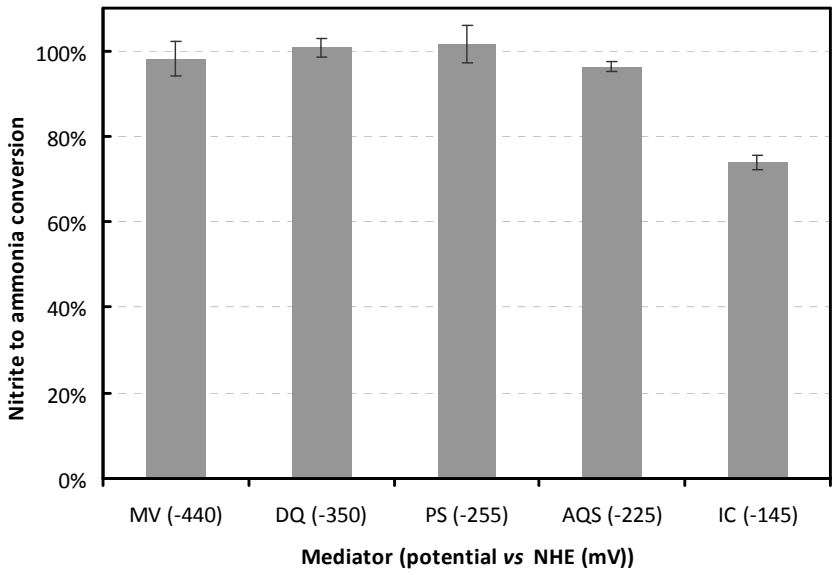


**Figure 2.5 -** Percentage of conversion of nitrite to ammonia in the presence of each mediator. Values were determined as the average of three enzymatic assays performed as described in the experimental section (reaction time 4 minutes). Dithionite was used as reducing agent. All assays were performed at 37°C. Enzyme concentration was 0.7 nM for MV, DQ and PS assays, 7 nM for AQS, and 14 nM for IC.

The specific activity of *cc*NiR for both nitrite and hydroxylamine was determined with all the mediators, using this discontinuous method. The activity for hydroxylamine reduction was obtained by determining the amount of ammonia produced in the assay (hydroxylamine conversion percentages were not calculated, given that this substrate was not quantified). As shown in Figure 2.6, the activities for $NH_2OH$ were at least 10 times lower than the activities for nitrite, thus confirming nitrite as the specific substrate for *cc*NiR. A similar result was observed for *Wolinella succinogenes* *cc*NiR in which the activity for hidroxylamine was 10% of the activity to the nitrite (with methyl viologen as electron donor) [84].

The specific activity values were found to decrease with the potential of the electron carrier, indicating methyl viologen (the mediator with the lowest potential) as the most suitable electron donor for the enzyme. Activities are in the range found for *cc*NiRs from other organisms (Table 2.1).

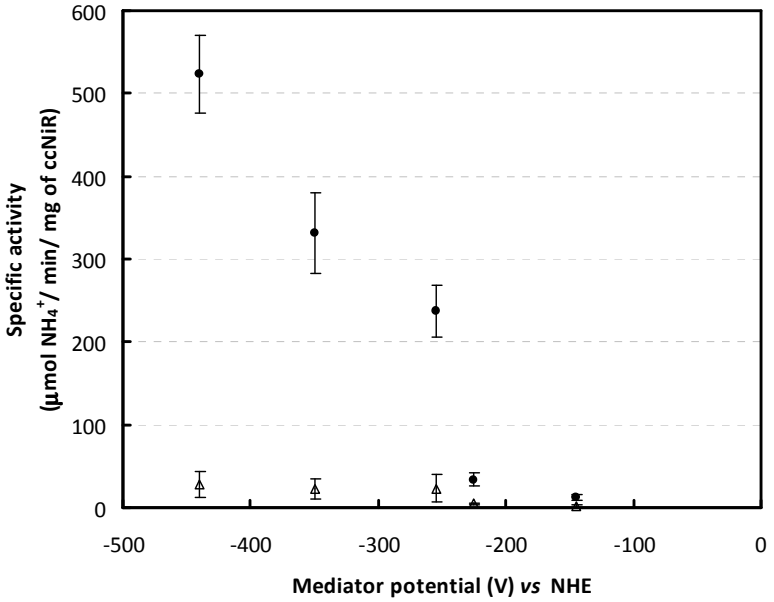


**Figure 2.6 -** *cc*NiR specific activities determined with an equivalent electron concentration of the mediators and with a saturating nitrite (●) and hydroxylamine (△) concentration. Incubation time was 4 minutes, that is, within the range of ammonia production at a linear rate. Dithionite was used as reducing agent. All assays were performed at 37°C. Enzyme concentration was 0.7 nM for MV, DQ and PS assays, 7 nM for AQS, and 14 nM for IC.

### 2.3.1.2) Molecular interaction between *cc*NiR and redox mediators

The molecular docking studies were performed to investigate the interaction between *cc*NiR and the redox mediators (Figure 2.7). From the best five solutions obtained with the molecular docking algorithm PatchDock [90-91], MV was validated as a convenient mediator for *cc*NiR reduction, since it interacts with a region closer to the electron transfer heme groups of the protein. Benzyl viologen, a similar redox mediator that has been used in kinetic studies with *Wolinella succinogenes* NrfA has also been indicated to react directly with heme 1 [70,93]. In contrast, the highest potential mediators IC and AQS, which provided the lowest specific activities for nitrite reduction, interact with the enzyme in the interface between the two catalytic subunits, distant from any electron transfer hemes. Most of the top five solutions found for PS and DQ were also located in regions distant from the heme clusters, with the exception of DQ that has one putative docking site close to the catalytic heme.

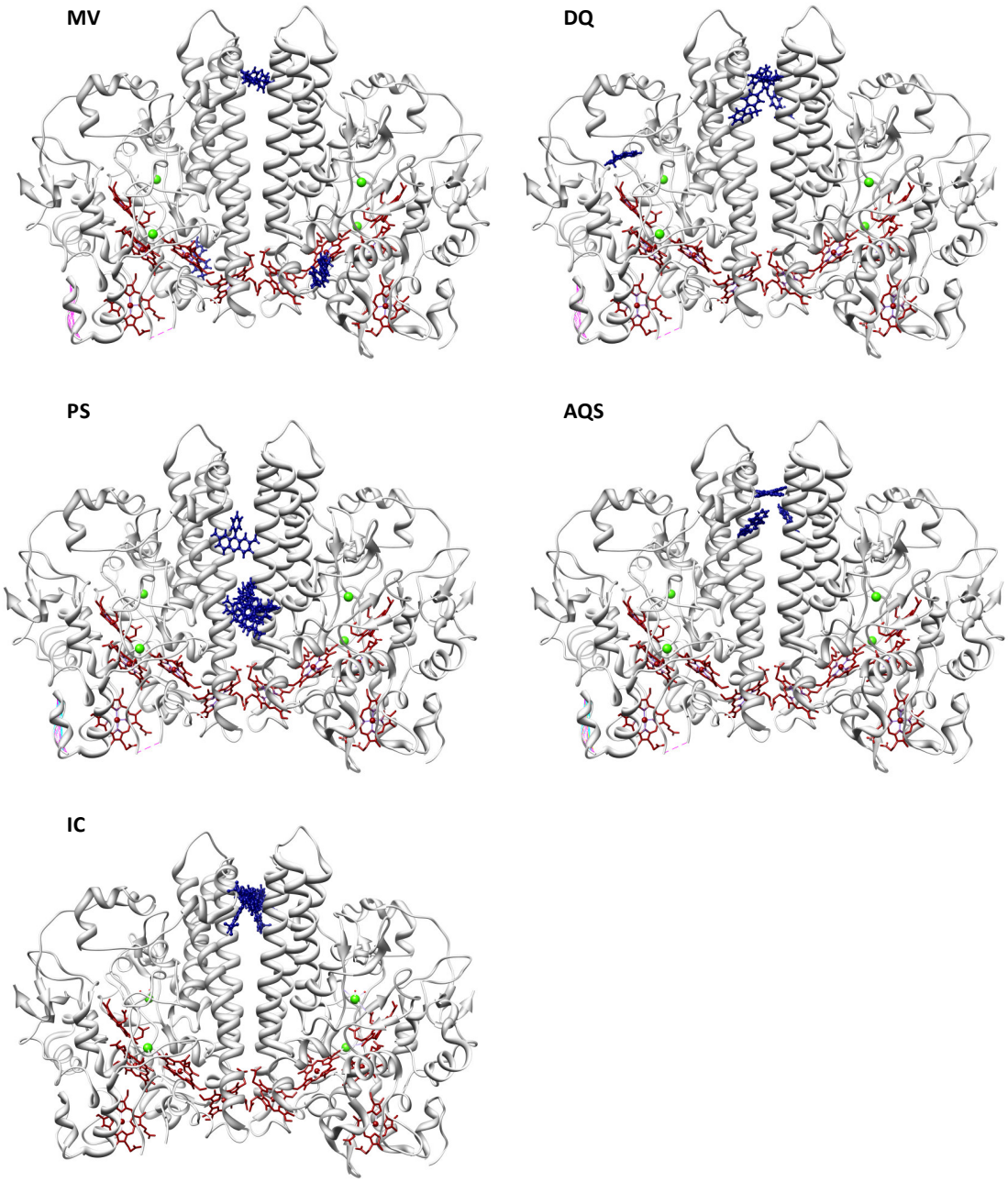


**Figure 2.7 -** Interaction complexes of *cc*NiR with the mediators MV, DQ, PS, AQS and IC. First five solutions obtained with the molecular docking algorithm PatchDock. Heme groups are depicted in dark red and mediators are represented in blue.

#### 2.3.1.3) Determination of *cc*NiR's kinetic parameters

The kinetic parameters for nitrite reductases are usually determined using a continuous spectrophotometric assay, in which the rate of re-oxidation of a mediator co-substrate gives an indirect measurement of enzyme activity [57,64,74]. Although time-consuming, this method offers advantages relatively to the discontinuous assay applied previously, since it allows direct tracking of the progress curve of the reaction, therefore making it relatively easy to estimate initial rates, spot any deviations from the initial linear phase of the reaction and detect anomalous behavior [94].

The initial rates of *cc*NiR reaction were calculated from the changes in absorbance over time. In other words, the initial rate of mediator re-oxidation, upon nitrite injection, was calculated by taking the first derivative of the first part of the progression curve, thus considering a pseudo-1$^{st}$-order reaction. In some cases the initial linear portion of the assay was sufficiently prolonged to allow the calculation of the initial rate reaction just by plotting a tangent to the first part of the assay curve, therefore considering a zero-order reaction rate. A detailed description of the methods used to calculate the initial rates of reactions can be found in Annex 2, as well as the equations for the reaction with the mediators.

To determine the kinetic parameters for nitrite reduction it is important to ensure that the co-substrate of the reaction - the mediator - is at saturating levels in the reaction, thus not affecting the rate of nitrite reduction by *cc*NiR. For this reason the initial reaction rates were measured over a range of concentrations of each mediator within the normal parameters used in spectrophotometric assays (absorbance values between 0.5 and 1.2). Only the three lowest potential mediators (MV, DQ, and PS) were selected for this study, seeing that the specific activity with the other two mediators was quite low.

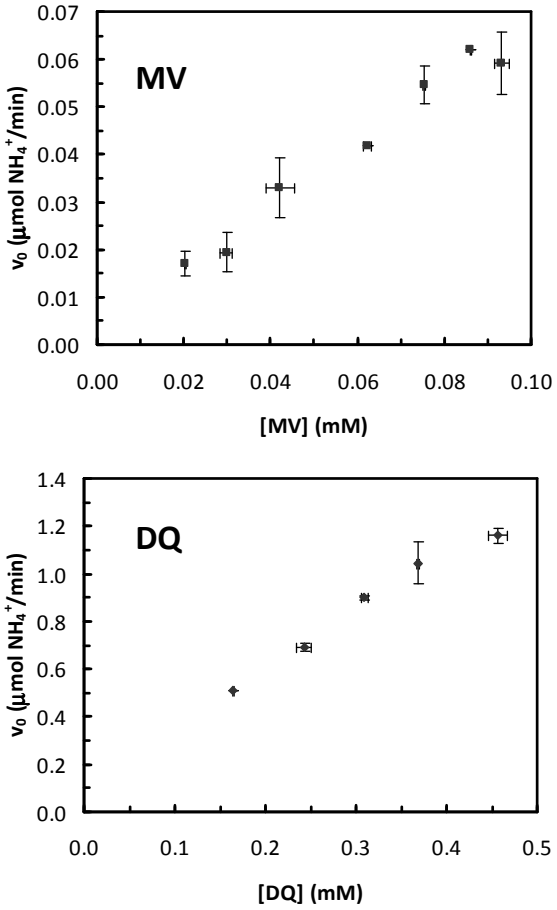


**Figure 2.8 -** Enzyme activities determined using 0.16 mM of nitrite at 37°C, with increasing concentrations of MV (■) and DQ (●), corresponding to absorbance values in the range 0.5 to 1.2. Enzyme concentration was 0.6 nM for MV and 7.4 nM for DQ assays.

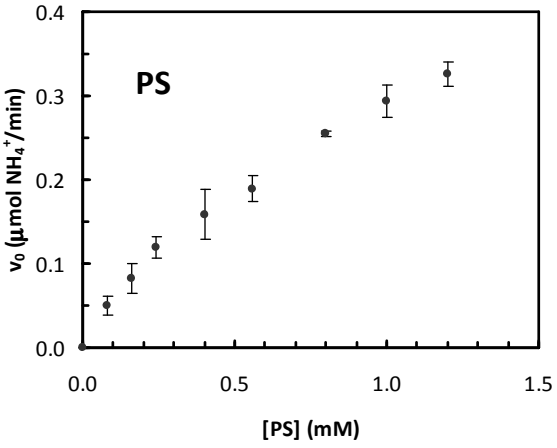


**Figure 2.9 -** Enzyme activities determined using 0.16 mM of nitrite with increasing concentrations of PS. Enzyme concentration was 7.4 nM. Assays were conducted in 50 mM tris-HCl pH 7.6 at 37°C.

In Figures 2.8 and 2.9 the reaction rates determined in the presence of a saturating nitrite concentration (0.16 mM) were plotted as a function of mediator concentration. The concentrations were varied between 0.02 to 0.09 mM and 0.17 to 0.45 mM for methyl viologen and diquat, respectively, which corresponded to absorbance values from 0.5 to 1.2. In order to improve the solubility of the other electron donor, phenosafranine, the ionic strength of the buffer system was lowered (50 mM of tris-HCl instead of 0.2 M of phosphate). The reduced form of phenosafranine was colorless and thus allowed the study to be performed with higher concentrations, within the range 0.1 to 1.2 mM.

The first conclusion that must be drawn from the obtained results is that the reactions are not taking place at saturating mediator levels as required. In fact, the initial reaction rates measured over a range of concentrations of MV, DQ, and PS are influenced by the mediator concentration (Figures 2.8 and 2.9). Electron delivering from reduced electron donors is rate limiting in this type of assay. This is not surprising since the need of six electrons *per* substrate molecule, associated to the high catalytic rates of *cc*NiR demands a great supply of reducing equivalents. Therefore, the amount of electron donor in the reaction vessel should be increased, but this involves experimental challenges. The concentration of colored mediators, such as MV and DQ (reduced forms), is always limited by the validity range of the Lambert-Beer's law; the absorbance eventually reaches such high levels that the apparatus no longer responds linearly to the increasing concentrations. Problem solving could have been provided by the non-absorbing reduced form of phenosafranine, but its low solubility has constituted another obstacle. At the maximum concentration achieved, 1.2 mM, this mediator was also not saturating.

Without a perfect option, and with the aim of obtaining a set of comparable kinetic data, it was decided to level the concentration of the reducing equivalents that each mediator supplies (*cf.* experimental section). The results obtained are shown in Figure 2.10. In the presence of varying substrate concentrations the nitrite reducing activity follows a Michaelis-Menten profile for all mediators.

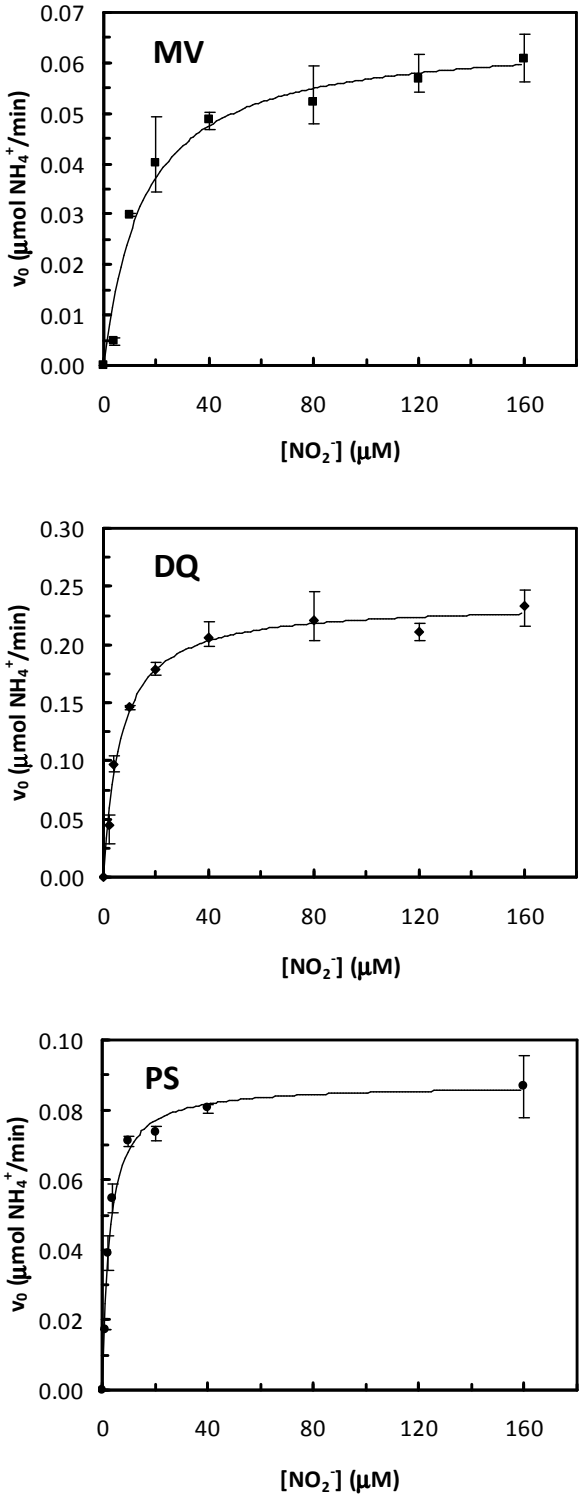


**Figure 2.10 -** Enzyme activities determined using equivalent electron concentrations (0.16 mM) of MV (■), DQ (◆), PS (●), at 37°C, with increasing nitrite concentrations. The solid lines represent the simulations to the Michaelis-Menten equation. Enzyme concentration was 0.6 nM for MV, 1.5 nM for DQ, and 7.4 nM for PS assays.

The apparent $K_M$ and turnover numbers were calculated from the least square data fitting to the Michaelis-Menten equation (equation 2.1).

$$v_0 = \frac{V_{max} * [NO_2^-]}{K_M + [NO_2^-]} \quad (2.1)$$

where $v_0$ is the initial rate of reaction, $V_{max}$ is the limiting rate, $[NO_2^-]$ is the substrate concentration and $K_M$ is the Michaelis-Menten constant. The turnover number ($k_{cat}$) was determined according to the following equation (equation 2.2).

$$k_{cat} = V_{max} * [ccNiR] \quad (2.2)$$

The kinetic parameters are listed in Table 2.3 along with the catalytic efficiency, determined by the ratio $k_{cat}/K_M$.

Although they are in the same order of magnitude, there is no coherent variation of the catalytic constant with the potential. In particular, the electronic carrier that gave the highest $k_{cat}$ value was diquat, which has an intermediate reduction potential. This indicates a clear influence of the mediator nature on the measured activities, determined by other aspects than the reduction potential. Perhaps the electron transfer rate from DQ to the protein is much faster, enabling higher turnovers. In fact, according to the docking studies (*cf.* section 2.3.1.2) DQ may interact differently with c*c*NiR, having some chances to deliver electrons directly to the catalytic site (Figure 2.7). The high $k_{cat}$ value for DQ was also unexpected since in the discontinuous assay, the highest specific activity was observed for MV. A possible explanation can come from the fact that anaerobic conditions were maintained in the continuous method, but not in the discontinuous. As a result, in the latter assay the concentration of the reduced species is not properly controlled, as it is in the continuous mode (*e.g.*, incomplete diquat reduction). This brings attention to the artifacts that can be generated by indirect enzymatic assays based on measurements of electronic carriers.

The binding affinity for nitrite decreased consistently with the reduction potential ($K_M$ rise). Possibly, in a fully reduced state the protein may adopt a structural conformation that somewhat diminishes the affinity for nitrite (see below, the electrochemistry results).

**Table 2.3 -** Kinetic parameters for the nitrite reduction reaction catalyzed by *D. desulfuricans* *cc*NiR obtained by the continuous spectrophotometric assay.

| Mediator/ Potential (*vs* NHE) | $K_M^{app}$ (μM) | $k_{cat}^{app}$ ($s^{-1}$) | $k_{cat}/K_M$ ($s^{-1}$. $\mu M^{-1}$) |
|---|---|---|---|
| **Phenosafranine / -255 mV** | $2.7 \pm 0.4$ | $79 \pm 3$ | 29 |
| **Diquat / -350 mV** | $6.4 \pm 0.6$ | $1064 \pm 23$ | 166 |
| **Methyl viologen / -440 mV** | $15.0 \pm 3.6$ | $738 \pm 45$ | 49 |

### 2.3.2) Direct electrochemistry

The alternative method for determining nitrite reductase activity relied on a heterogeneous electron transfer reaction using an electrochemical technique (PFV). Herein, c*c*NiR was adsorbed on the surface of a PG electrode that delivered electrons directly to the enzyme, thus converting it into its active state (Figure 2.1A).

Due to the high activity of multihemic nitrite reductases it is difficult to eliminate mass-transport limitations in these experiments [77]. At low concentrations of substrate, the catalytic response is limited by its transport to the enzyme film, an effect that becomes less important at saturating concentrations of nitrite. The effect of electrode rotation rate was thus tested by measuring the catalytic current in the presence of a relatively low amount of nitrite (10 μM), at different rotation speeds.

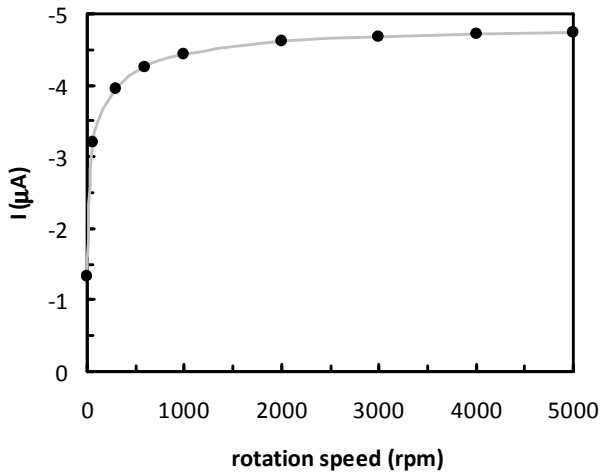


**Figure 2.11 -** Effect of electrode rotation speed on the current response of a *cc*NiR film on a PG electrode. The assays were carried out at 37°C in the presence of 10 μM of nitrite.

An electrode rotation speed of 600 rpm was chosen to be used in this work, which corresponds to 95% of the limiting current (not affected by mass transport), as observed in Figure 2.11. This was considered as a sufficient reflection of the steady-state activity of *cc*NiR. In this way, we were also able to avoid turbulence and flow irreproducibility observed at high electrode rotation speeds, which are generally ascribed to eddy currents and vortices forming around the edges of the revolving electrode [95].

The *cc*NiR activity for nitrite was determined by amperometric titration (Figure 2.12A) performed at potentials equivalent to the ones provided by the redox mediators used in the spectrophotometric assays (-440 mV for MV, -350 mV for DQ, and -255 mV for PS). Thus, in spite of varying the protein reduction level, the experimental conditions are fully comparable.

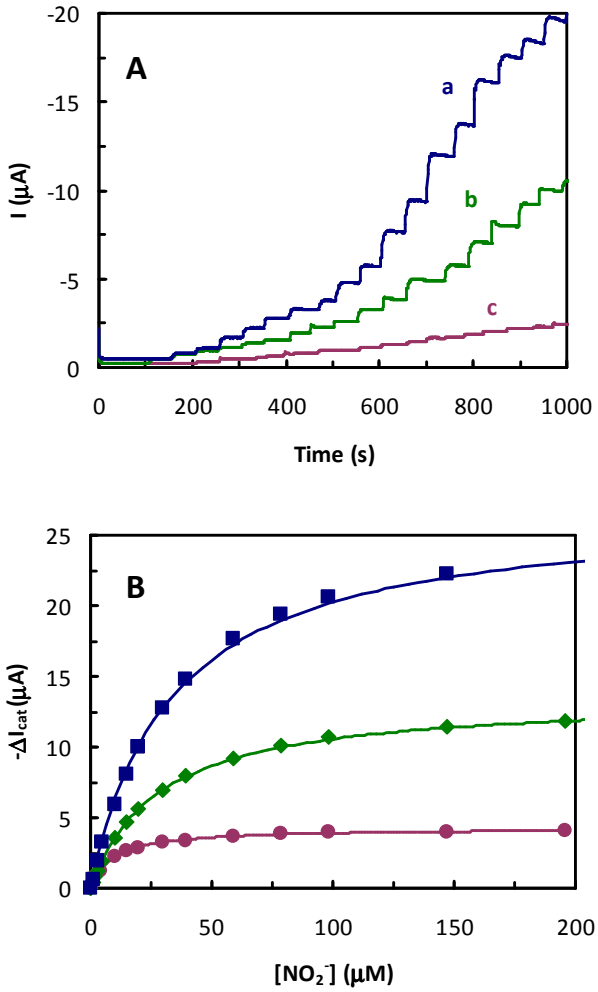


**Figure 2.12 - A)** Amperomograms of PG electrodes with immobilized *cc*NiR, in the presence of increasing amounts of nitrite, recorded at (a) −440 mV, (b) −350 mV, and (c) − 255mV. **B)** Calibration curves performed at − 440mV (■), − 350mV (◆) and − 255mV (●). The assays were carried out at 37°C in 0.1 M phosphate buffer, pH 7.6, with an electrode rotation speed of 600 rpm. The enzyme amount on the electrodes was *ca.* 4.3 ± 0.6 pmol.cm$^{-2}$. The solid lines represent the Michaelis-Menten simulations of enzyme kinetics.

In Figure 2.12B the catalytic currents ($I_{cat}$) of *cc*NiR films were plotted as a function of nitrite concentration. The current values attained in the presence of nitrite were corrected with the baseline value, at zero nitrite concentration ($\Delta I_{cat}=I_{cat}-I_0$). The data were least square fitted to a hyperbolic expression equivalent to the Michaelis-Menten equation where the kinetic currents are analogous to the solution rates of reaction (equation 2.3).

$$I_{cat} = \frac{I_{max} * [NO_2^-]}{K_M + [NO_2^-]} \quad (2.3)$$

In this equation $I_{max}$ is the maximum current which is given by,

$$I_{max} = nFA\Gamma k_{cat} \quad (2.4)$$

with *n* as the number of electrons (*n*=6 for nitrite reduction by *cc*NiR), F is the Faraday constant, A is the electrode area, and $\Gamma$ is the surface concentration of enzyme. This equation was used for the calculation of turnover numbers, according to the method described in [76]. The protein surface coverage on the electrode was determined from the area of the non-catalytic peaks of cyclic voltamograms performed in the absence of nitrite and taking into account that *cc*NiR's $NrfA_2NrfH$ complex complete reduction involves 14 electrons [76] (equation 2.5):

$$Q = nFA\Gamma \quad (2.5)$$

The typical value determined for enzyme surface coverage was 4.3 ± 0.6 pmol.cm$^{-2}$. This value is consistent with the formation of a *cc*NiR monolayer on the electrode [77].

The *cc*NiR films on the PG electrodes exhibited turnovers equivalent to those measured in the solution assays (Table 2.4). Hence, it is assumed that the catalytic activity of the biofilm was greatly maintained. More importantly, the expected trend of increasing $k_{cat}$ with the electrode reductive driving force was here observed. This should be related to the use of the same electron delivering system (the PG working electrode) at the three operating potentials, thus eliminating any variability coming from the use of different electronic mediators.

The Michaelis-Menten constants were higher than those obtained in the solution assays. This may reflect a small effect of enzyme adsorption, making it more difficult for nitrite to access the active site, or of mass transport, since substrate flow to the electrode could be slightly hampered by the compromise rotation speed used in the experiments. Yet, as in the solution assays, the trend of decreasing binding affinity for nitrite with the reduction potential was also observed. The same behavior was observed for the *cc*NiR from *E. coli*,

with the $K_M$ for nitrite reduction changing from 12 ± 2 μM at -0.3 V to 30 ± 4 μM at -0.4 V [83]. When considering the $k_{cat}/K_M$ factor, the catalytic efficiency increases slightly with the reducing power regardless of the experimental approach.

**Table 2.4 -** Kinetic parameters for nitrite reduction catalyzed by *D. desulfuricans* *cc*NiR obtained by the continuous spectrophotometric and the amperometric assays. * – Turnover number was determined according to [76].

| | **Homogeneous** | | | **Electrochemical** | | |
|---|---|---|---|---|---|---|
| **Mediator / Potential (*vs* NHE)** | **$K_M^{app}$ (μM)** | **$k_{cat}^{app}$ ($s^{-1}$)** | **$k_{cat}/K_M$ ($s^{-1}$. $\mu M^{-1}$)** | **$K_M^{app}$ (μM)** | **$k_{cat}^{app}$* ($s^{-1}$)** | **$k_{cat}/K_M$ ($s^{-1}$. $\mu M^{-1}$)** |
| **Phenosafranine / -255 mV** | $2.7 \pm 0.4$ | $79 \pm 3$ | 29 | $9.2 \pm 0.1$ | $120 \pm 1$ | 13 |
| **Diquat / -350 mV** | $6.4 \pm 0.6$ | $1064 \pm 23$ | 166 | $28.1 \pm 0.4$ | $382 \pm 2$ | 14 |
| **Methyl viologen / -440 mV** | $15.0 \pm 3.6$ | $738 \pm 45$ | 49 | $33.3 \pm 0.7$ | $762 \pm 4$ | 23 |

## 2.4) Temperature effect on *cc*NiR kinetic parameters

Although the studies here presented were all performed at 37°C, *i.e.*, the physiological temperature at which the strain of bacteria, from which the enzyme is obtained from, is grown, it was decided to evaluate the influence of temperature on *cc*NiR's activity.

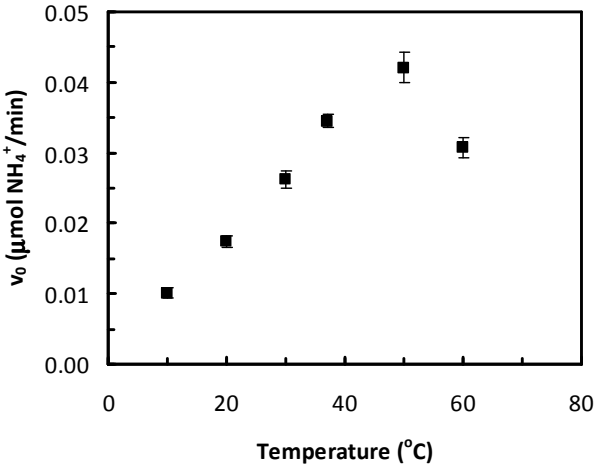


**Figure 2.13 -** Temperature effect on the specific activity of c*c*NiR. Assays were performed with 0.6 nM of c*c*NiR, 160 µM of nitrite and *ca.* 0.08 mM of dithionite reduced MV (Abs 604 nm *ca.* 1) in 0.2 M phosphate buffer, pH7.6.

As observed in Figure 2.13 the catalytic activity follows an expected bell-shaped trend with temperature, with a maximum of activity set at around 50°C. The maximum activity for this enzyme had previously been observed at 57°C in [75]. This result confirms the high stability of the enzyme, a very promising and attractive property when considering its application in a commercial biosensor device.

## 2.5) Conclusions

The kinetic properties of *cc*NiR were studied by different methods. One of the objectives was to determine the influence of the electron donor of the reaction on the homogeneous kinetic parameters. As shown, below a sufficient reducing power (E < −250 mV), nitrite was always converted stoichiometrically to ammonia, whatever the mediator used. However, the chemical structure of the electronic carrier may have a certain impact on *cc*NiR activity, most likely at the level of the mediator-protein interaction and the subsequent intermolecular electron transfer. Apparently, the enzyme has a greater affinity for diquat than for the others mediators, seeing that the highest turnover (with the continuous spectrophotometric method) was attained in its presence.

Methyl viologen was confirmed as the most suitable electron donor for *in vitro* measurements, since it provided the highest specific activity for nitrite, although at an improbable physiologic driving force. Moreover, it was the mediator that interacted more closely with the electron transfer hemes of *cc*NiR, as observed in the molecular docking studies.

It was also observed that it is very difficult to perform assays with saturating mediator conditions when using spectrophotometric techniques. As so, rate-limiting by electron donors is a pending issue and only apparent kinetic constants can be assessed. The data presented in the literature should thus be evaluated carefully, and take the experimental conditions into consideration.

Although the present study does not provide a way for determining real parameters describing the homogeneous kinetics, it indicates electrochemistry as a good alternative to techniques depending on chromophore mediators. The enzyme activities reported by the electrochemical method are thought to be limited mainly by the kinetic properties of *cc*NiR and not by the experimental conditions (*e.g.* reducing equivalents availability).

The analysis of *cc*NiR kinetic parameters shows that the driving force at which the reaction takes place influences the activity. With a higher degree of enzyme reduction (achieved at lower potentials) the turnover and catalytic efficiency are superior. Nonetheless, this enzyme is efficient even at relatively high potentials and within a wide range of temperatures. This does make it a very interesting candidate for application in a biosensor for nitrite screening.

# Chapter 3

# Sol-gel based biosensor

# Chapter 3 - Sol-gel based biosensor

## 3.1) Introduction

### 3.1.1) Direct electron transfer based biosensors

The last decades have witnessed a budding demand for improved analytical tools to enable the reliable inspection of the chemical or biological composition of every material that interacts with Consumers or Nature. In this context, biosensor technology constitutes a very important field of Research and Development. Electrochemical enzyme based biosensors are of particular interest due to their operational simplicity, low cost fabrication, portability and real time monitoring ability. Nevertheless, it is often hard to achieve an efficient electronic communication between the enzyme and the signal transducer since the limited exposure of the redox active sites prevents facile electron transfer towards the electrode. Several approaches have been proposed to solve this issue. In the first generation of biosensors, the strategy relies on the measurement of an electroactive substrate or product of the enzymatic reaction, while in second generation devices the reaction is monitored by a natural or artificial redox mediator. Major improvements, such as the elimination of mediator leakage, were obtained with the introduction of biosensors where the redox communication is ensured by enzyme wiring or electron relays [96-97]. Yet, the ideal approach allows direct electron transfer between the oxidoreductase and the electrode thereby increasing selectivity, simplifying the manufacturing process and requiring fewer reagents [98-99]. However, several issues still challenge the direct protein wiring: i) adsorption of impurities or denaturated forms of the biomolecules on the electrode surface may hinder the electron exchange; ii) unfavorable protein orientation on the transducer surface can result in low accessibility to the biomolecules redox centers; iii) denaturation and loss of biological activity due the uncontrolled adsorption to the electrode surface. These problems can make DET hard to achieve. Therefore, the development of appropriate electrode interfaces and protein immobilization methods to promote DET, while retaining biological activity, is crucial.

This chapter describes the construction of a truly non-mediated amperometric biosensor for nitrite ($NO_2^-$) determination. The previous attempts to construct a nitrite biosensor using

the cytochrome *c* nitrite reductase from *Desulfovibrio desulfuricans* ATCC 27774 as the biorecognition element are described in Chapter 1. The majority made use of artificial electroactive compounds as electron shuttles [42-45]. Nevertheless, c*c*NiR is also able to display a DET response when simply adsorbed onto a pyrolytic graphite electrode [76]. This feature was used for the development of the DET based amperometric biosensor for nitrite determination. To construct a suitable analytical device based on this system, enzyme incorporation in a protective matrix is strongly recommended. This may provide the protein with greater stability and act as a barrier against fouling and interfering species. However, the high molecular weight of the c*c*NiR aggregates and their partial hydrophobic character [67] may hamper the encapsulation process. This chapter describes a successful way of entrapping c*c*NiR in a porous membrane losing neither the catalytic activity nor the direct electronic contact with the electrode surface. A sol-gel matrix was used for this purpose.

### 3.1.2) Sol-gel based biosensors

Sol-gel is frequently used for the encapsulation of biomolecules in biosensors. This material is usually produced under mild conditions which biomolecules can withstand, without losing bioactivity, native conformations or being denaturated (in the case of proteins) [100-101]. The porous structures allow efficient encapsulation and simultaneously the diffusion of small substrate molecules to the immobilized biomolecules [102-105].

Sol-gel matrices are produced from a starting colloidal suspension of sol-gel precursors – the sol – which undergoes hydrolysis and condensation reactions to form the gel (Figure 3.1). The precursors are metals or metalloid elements surrounded by reactive ligands; metal alkoxydes, and alkoxysilanes in particular, are the most common ones, since they react easily with water. Nonetheless, several other types of precursors are available such as aluminates, titanates, borates, etc. [106-107]. The reactions take place in the presence of water, a catalyst (acid or base) and a solvent (generally an alcohol). The hydrolysis of the alkoxysilanes results in the formation of silanol groups (Si-OH) which will react to generate siloxane (Si-O-Si) bonds through condensation reactions, thus leading to the formation of polymer networks in the sol and eventually interconnecting into rigid porous structures - gel

state. The solvents are then excluded from the network, while the material dries to form the dry state porous matrix – the xerogel [107-111].

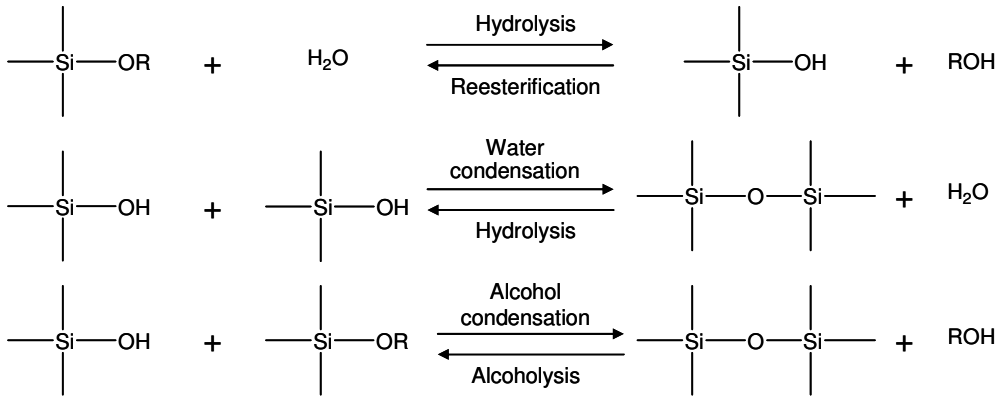


**Figure 3.1 -** Sol-gel formation reactions from silica based alkoxide precursors.

The successful use of sol-gel in biosensors is quite remarkable seeing that the fragile nature and high sensitivity of biomolecules imposes the need to maintain mild conditions (close to native environments) upon their immobilization. Biomolecules are faced with the reactants in which the sol-gel reactions occur: the alcohols (as solvents), the acids or bases (catalysts), and the monomer precursors themselves, whose reactivity can alter protein surfaces. They also have to surpass the effects of solvent evaporation and structure change during the drying and aging stages of the sol-gel process, which is frequently accompanied by shrinkage of the gels, therefore further constricting the immobilized biomaterial and potentially giving rise to cracking of the sol-gel, degradation and leaching [108]. Proper orientation and accessibility to protein active sites inside the sol-gel is another concern, and this is not easily attained inside the pores of the matrix [103,107]. In spite of these potential drawbacks, sol-gels materials are undoubtedly capable of providing good immobilization platforms for the construction of biosensors. This is attested by the numerous proposals described in the literature using several proteins such as glucose oxidase [112-114], urease [115], peroxidases [116], lactate oxidases and dehydrogenases [117-118], nitrate and nitrite reductases [48,119], myoglobin, hemoglobin, catalase [120], among others.

The reactions in the sol-gel process are regulated by several parameters like the nature of the precursor, water:silane ratio, pH, temperature, catalyst, solvent, etc. All of these greatly

influence the sol-gel matrices and allow morphological and structural control over their structure [102,108-109,121]. Accordingly, the sol-gel process gives a number of possibilities in terms of the types of materials and configurations that can be obtained [103,109,122]. The ability to create materials with the desired properties, such as thickness, porous structure, diffusion within the matrix, highlights the sol-gel process as a valuable resource in the constructions of electrochemical biosensors.

Besides the mentioned versatility and the mild/low temperature fabrication conditions of sol-gel, it gathers numerous other attractive features such as the chemical inertness, negligible swelling, mechanical and thermal stability and simple processing. Of great interest is also the possibility to combine sol-gel with other types of compounds, in this way producing sol-gel composites or hybrid materials with a higher range of applicability [103,110]. Sol-gel matrices have been used in combination with gold nanoparticles [116], zeolites, detergents, polymers, gold [123-124] and carbon powders [125-126], among others. By introducing modifiers into sol-gel precursors it is possible to create materials with specific functionalities, such as anchoring sites or mediating species [127], thiolated sol-gels for self-assembly on gold electrodes [128-129], materials with hydrophobic or hydrophilic character, more biocompatible precursors, etc. [103,110].

Considering the hydrophobic nature of c*c*NiR, it was decided to test the quite hydrophobic sol-gel precursors tetraethoxysilane (TEOS) and 2-(3,4-epoxycyclohexyl)-ethyltrimethoxysilane (EETMS), which is often used in combination with 3-(aminopropyl)trimethoxysilane (3-APTMS) [112-114,117]. The water:silane molar ratio, the reaction medium and the enzyme concentration used to prepare sol-gel/c*c*NiR films were first optimized. Taking into account the large dimensions of the c*c*NiR aggregates, the recipes started from high water:silane molar ratios. A composite graphite-silica material was later prepared in order to improve the conductivity of the silica glass.

## 3.2) Experimental

### 3.2.1) Reagents

cc*c*NiR was purified from *D. desulfuricans* ATCC 27774 cells as described in Annex 1. The specific activity was 300 U/mg and the protein content 1.0 mg/mL, in 0.1 M phosphate buffer pH 7.6. The protein used for scanning electron microscopy studies was exchanged to HEPES buffer 0.1 M pH 7.6.

The sol-gel precursors 3-APTMS, EETMS and TEOS were obtained from Fluka. Hydroxylamine and methyl viologen were purchased from Sigma. Sodium nitrite, sodium sulphite, ammonium chloride, tris(hydroxymethyl)aminomethane, potassium chloride, sodium hydrogenphosphate and sodium dihydrogenphosphate were all from Merck. Poly(ethylene glycol) 6000 (PEG 6K) was from Aldrich. Ethanol was from Panreac and hydrochloric acid from Riedel-de-Haen. Graphite powder was from Sigma (particles size <20 µM). Solutions were prepared with deionized water (18 MΩcm) from a Millipore MilliQ water purification system. All chemicals were analytical grade and were used without further purification.

### 3.2.2) Enzyme assays

The enzymatic activity was determined as described in Chapter 2 (section 2.2.2). The assay mixture contained 0.16 mM of zinc reduced methyl viologen and 0.6 nM cc*c*NiR in 0.3 M phosphate buffer, pH 7.6. All assays were performed anaerobically at 20°C.

### 3.2.3) Electrochemical measurements

A conventional three electrode electrochemical cell was used, with an Ag/AgCl reference electrode (Radiometer), a Pt counter electrode (Radiometer) and a self-made PG electrode (∅ = 4mm) modified with the sol-gel/cc*c*NiR film, as working electrode. The electrochemical cell (Metrohm), containing 20 mL of 0.1 M KCl in 0.05 M tris-HCl buffer pH 7.6 as supporting electrolyte, was thoroughly purged with argon before and during the experiments.

Measurements were performed with a potentiostat Autolab PSTAT 12 (EcoChemie) monitored by the control and data acquisition software GPES 4.9 (EcoChemie).

Cyclic voltammetry experiments were performed with a 20 mV/s scan rate in a potential window of -0.1 to -0.9 V. To evaluate the biosensors response to nitrite, the electrochemical cell was successively spiked with standard solutions of sodium nitrite (0.01, 0.1 and 1 M). After each addition, the cell was again purged with argon for *ca.* 30 s and the CV (cyclic voltammogram) was recorded. Nitrite catalytic currents were determined at the inversion potential -0.9 V.

For amperometric experiments the electrode was poised at -0.9 V, unless stated otherwise, with a speed rotation of 600 rpm (kinetic studies) or argon bubbling (calibration). The catalytic current was calculated from the height of each current step following a nitrite addition to the cell.

For each experimental condition a minimum of three independent assays was performed. The values presented in the graphs and tables represent the average of three assays; error values and bars represent the standard deviation. All potentials were quoted against the Ag/AgCl reference electrode (-197 mV *vs* NHE).

### 3.2.4) Biosensor preparation

Prior to coating, the PGEs were polished with alumina slurry (0.3 μm) from Buehler. The electrodes were then thoroughly washed with water and ethanol and ultra-sonicated for 5 min. Finally, the electrodes were washed with water and dried with compressed air.

The TEOS sol-gel mixtures were prepared by mixing different molar ratios of water and precursor (50:1; 250:1 and 500:1) with 8% ethanol (or 0.2 mg/mL PEG 6K) and 10 mM HCl. The same was done for the 3-APTMS/EETMS and EETMS containing mixtures. A detailed description of these sol-gel formulations is presented in Table 3.1. The mixtures with ethanol were magnetically stirred for 30 min (for the TEOS based preparations, an ice bath was used to prevent premature gel formation), while the PEG 6K ones were sonicated for 30 min. Next, a 10 μL drop of mixture was placed onto the PGE and left at room temperature, for sol development (*ca.* 45 min). This procedure was later repeated suspending 1 mg/mL graphite particles in the precursors containing solution. Before starting the gelation process, the sol

layer was impregnated with enzyme solution (4-92 pmol) and left for a 24 h aging period, at room temperature. The modified electrodes were finally washed and stored in supporting electrolyte at 4°C.

**Table 3.1 -** Compositions of sol-gel based nitrite biosensors prepared with 3-APTMS, EETMS and TEOS in various water:silane proportions and different solvents.

| Precursors | Water:precursor molar ratio | PEG 6K (mg/mL) | Ethanol % | HCl (mM) |
|---|---|---|---|---|
| **3-APTMS & EETMS** | 30:1 | 1 | - | 1 |
| | 130:1 | | | |
| | 50:1 | 1 | - | 1 |
| | 225:1 | | | |
| | 100:1 | 1 | - | 1 |
| | 450:1 | | | |
| **3-APTMS** | 50:1 | 1 | - | 1 |
| | 100:1 | 1 | - | 1 |
| **EETMS** | 65:1 | 1 | - | 3 |
| | 225:1 | 1 | - | 3 |
| | 450:1 | 1 | - | 3 |
| | 40:1 | - | 11 | 2 |
| | 225:1 | - | 11 | 2 |
| | 450:1 | - | 11 | 2 |
| **TEOS** | 50:1 | - | 8 | 10 |
| | 250:1 | - | 8 | 10 |
| | 500:1 | - | 8 | 10 |
| | 50:1 | 0.2 | - | 10 |
| | 250:1 | 0.2 | - | 10 |
| | 500:1 | 0.2 | - | 10 |

### 3.2.5) Characterization of the sol-gel/*cc*NiR film

#### 3.2.5.1) Scanning electron microscopy (SEM)

The scanning electron microscopy (SEM) analysis were performed in a Zeiss model DSM 962, with a secondary electrons detector (SE) and an energy dispersive X-ray spectrometer (EDS) from Oxford Instruments (model INCAx-sight) with an ultra thin window able to detect low atomic number elements. The electrode surface was previously coated with gold to increase electrical conductivity during examination. For these experiments some of the electrodes were prepared with HEPES 0.1 M pH 7.6 buffer.

#### 3.2.5.2) Atomic force microscopy (AFM)

Tapping mode AFM images were obtained in a Multimode Nanoscope IIIa Microscope (Digital Instruments, Veeco) in air, using etched silicon cantilevers with spring constants of *ca.* 300 kHz (Tap300, BudgetSensors). The images were acquired at a scan rate of 1.5-1.8 Hz.

#### 3.2.5.3) UV-vis spectroscopy

The electronic absorption spectra were obtained at a Shimadzu UV1800 spectrophotometer. The protein doped glass slides were prepared on top of the inner face of a quartz cuvette (UV-Vis). After sol-gel aging, the cuvette was filled up with electrolyte solution.

#### 3.2.5.4) Resonance Raman spectroscopy

Resonance Raman (RR) measurements were performed with a confocal microscope coupled to a Raman spectrometer (Jobin Yvon U1000) equipped with 1200 l/mm grating and liquid nitrogen cooled back-illuminated CCD detector. The *cc*NiR containing glass slides were formed on microscopy lamellas. Following the sol-gel aging period, the samples were excited with the 413 nm line from a krypton ion laser (Coherent Innova 302). RR spectra of hydrated sample were measured with variable (750 μW-1.5 mW) laser power and (10-40 s) accumulation time, at room-temperature, at different spots on the matrix. Experimental RR spectra, that represent an average of 4-10 spectra taken from different spots, were submitted to component analysis by a home made software.

## 3.3) Results and discussion

### 3.3.1) Biosensor optimization

The optimum membrane composition was selected from a group of sol-gel/*cc*NiR formulations prepared with different precursors, water:monomer molar ratios and enzyme quantities. The bioelectrodes were characterized by cyclic voltammetry. A typical catalytic shape current-potential curve was always observed in the presence of nitrite (Figure 3.2A) due to the non-mediated electroenzymatic reduction of the substrate, according with the EC' mechanism depicted in Figure 3.2B. In control experiments using sol-gel modified electrodes without c*c*NiR, no catalytic reaction was detected following substrate addition.

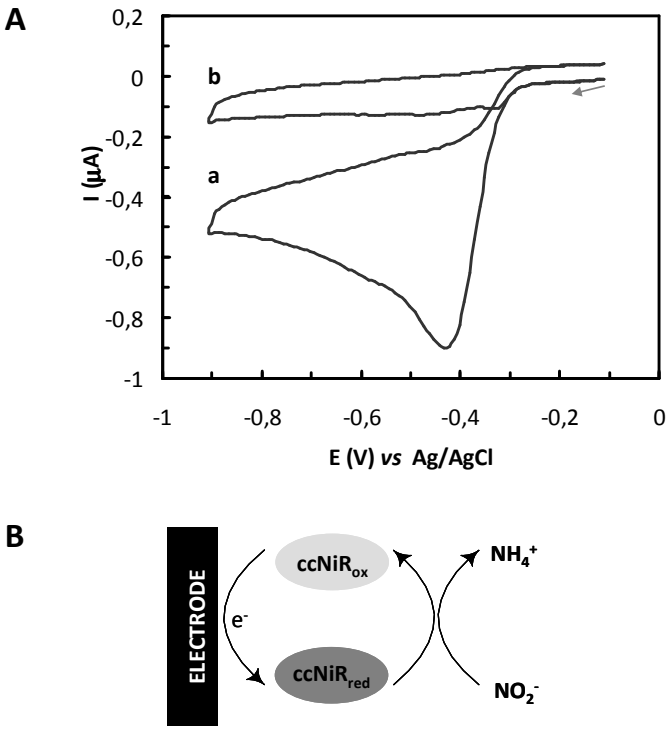


**Figure 3.2 - A)** Cyclic voltammograms of a sol-gel/*cc*NiR film **(a)** with (10 µM) and **(b)** without nitrite. The sol-gel was prepared with the optimal composition 225:1 $H_2O$:EETMS molar ratio and 74 pmol of c*c*NiR. **B)** Schematic representation of the reaction mechanism that describes the voltammograms profile, *i.e.*, the enzyme undergoes a reversible electrochemical reduction followed by an irreversible chemical reaction (EC').

The analytical performance of the bioelectrodes was evaluated according to the sensitivity to nitrite, the detection limit and the amplitude of the linear range. Table 3.2 summarizes the results concerning the effects of the nature and amount of the sol-gel precursor.

**Table 3.2 -** Analytical properties of sol-gel/*cc*NiR based biosensors prepared with various precursors, in different water:silane proportions. ND – not determined.

| Precursors | Water:precursor molar ratio | Solvent & Catalyst | Linear range (µM $NO_2^-$) | Sensitivity ($mA.M^{-1}.cm^{-2}$) | $I_{cat}/I_c$ |
|---|---|---|---|---|---|
| **3-APTMS & EETMS** | 30:1<br>130:1 | PEG 6K & HCl | sol-gel/*cc*NiR films detached from the electrode | | |
| | 50:1<br>225:1 | | | | |
| | 100:1<br>450:1 | | | | |
| **3-APTMS** | 50:1 | | | | |
| | 100:1 | | | | |
| **EETMS** | 65:1 | PEG 6K & HCl | 0.25 - 40 | 53 ± 1 | 0.7 ± 0.1 |
| | 225:1 | | 0.5 - 20 | 243 ± 9 | 3.8 ± 0.2 |
| | 450:1 | | 1 - 15 | 257 ± 4 | 3.4 ± 0.1 |
| | 40:1 | ethanol & HCl | 20/200 - 2000 | 0.054 - 0.24 | ND |
| | **225:1** | | **0.25 - 50** | **430 ± 23** | **6.6 ± 1.1** |
| | 450:1 | | 0.25 - 5 | 274 ± 34 | 1.9 ± 0.2 |
| **TEOS** | 50:1 | PEG 6K & HCl | 0.5 - 15 | 332 ± 9 | 3.3 ± 0.4 |
| | 250:1 | | 0.25 - 25 | 198 ± 8 | 1.0 ± 0.3 |
| | 500:1 | | ND | ND | ND |
| | 50:1 | ethanol & HCl | 0.5 - 20/40 | 311 ± 41 | 3.5 ± 0.4 |
| | 250:1 | | 0.5 - 25/40 | 261 ± 20 | 1.4 ± 0.1 |
| | 500:1 | | 0.5 - 25/35 | 69 ± 25 | 1.6 ± 0.2 |

Regarding the TEOS based formulations the linear range did not change much with the decreasing amount of silane whereas the sensitivity dropped progressively, especially from 250:1 to 500:1 $H_2O$:TEOS with the ethanol based formulations. This was, most likely, due to the silica pores being too big to withhold the protein molecules. All biosensing films had a thin and glassy appearance, but a high tendency to fracture during the drying process, occasionally loosing small pieces of glass. As a consequence the reproducibility was rather low and TEOS was discarded.

Next, sol-gel/enzyme films were prepared with the combination of two precursors: 3-APTMS and EETMS. These have been used for the successful encapsulation of glucose oxidase and lactate oxidase in platinum electrodes, the resulting sol-gel network providing a remarkable microstructure, biocompatibility and stability with homogeneously distributed protein [112-114,117]. However, preliminary results have demonstrated that 3-APTMS/ EETMS films completely detached from the pyrolytic graphite electrodes, and accordingly no activity was detected. The same was observed for sol-gel formulations with 3-APTMS only. In light of this, the more hydrophobic component of the mix, EETMS, was solely used for sol-gel preparation.

The EETMS modified electrodes were smooth and shiny after the sol-gel development period (24 h) although the surface became a bit cracked once the aging process took place, as later confirmed by SEM (see below section 3.3.2.1). This behavior has been shown to be related with the EETMS hydrophobicity that generates small wettable areas and brittle surfaces [108,112-113]. The EETMS results were not only better than those obtained with TEOS, but they were more reproducible. These formulations also displayed the highest catalytic efficiency, expressed as the quotient between the peak reduction currents in the presence ($I_{cat}$ at 10 μM) and absence of nitrite ($I_c$) (Table 3.2). Due to the presence of the bulky epoxycyclohexyl group, EETMS is likely to decrease the rate of hydrolysis and condensation [108], producing a more adequate network for both *cc*NiR encapsulation and DET.

Overall the formulations with ethanol were better than the PEG based ones. The compositions with the lowest water content (40:1 and 65:1 $H_2O$:EETMS for ethanol and PEG

preparations, respectively) gave the poorest analytical parameters, marked by an abnormally low sensitivity to nitrite (Table 3.2). Several factors could account for this situation: i) the low amount of water produced pores too small to accommodate the large size aggregates of c*c*NiR and/or generated an extremely strong barrier to nitrite diffusion, as judged by the extensive linear range; ii) the sol-gel polymerization under a low water:silane ratio stimulated enzyme aggregation, producing lower activities; iii) the reduced wettability of the film decreased both capacitive and Faradaic currents [113]. In opposition, as suggested by the lower sensitivities and narrower linear ranges seen in Table 3.2, the highest $H_2O$:silane ratio (450:1) produced pores too large in size and the enzyme encapsulation was less efficient. A good balance between sensitivity to nitrite and linear range amplitude was obtained with the ethanol formulation based on the 225:1 ratio (highlighted in Table 3.2).

Subsequently, several electrode configurations using the latter $H_2O$:EETMS combination and varying amounts of c*c*NiR (from 4 to 92 pmol) were tested. The linear range is wider when using 74 pmol of enzyme, while the biosensor sensitivity to nitrite reaches a maximum value at 15 pmol, stays fairly constant up to 74 pmol and then decays significantly (Figure 3.3). Similar bell-shaped curves were observed in biosensor optimization studies with this enzyme [44] and with a CuNiR from *R. sphaeroides* [53], thus allowing to find an optimal amount of protein to be used in the biosensors. Although the activity is expected to increase with the amount of protein, at a certain point increasing the surface concentration of enzyme will no longer benefit the sensor response due to an electrode passivation effect.

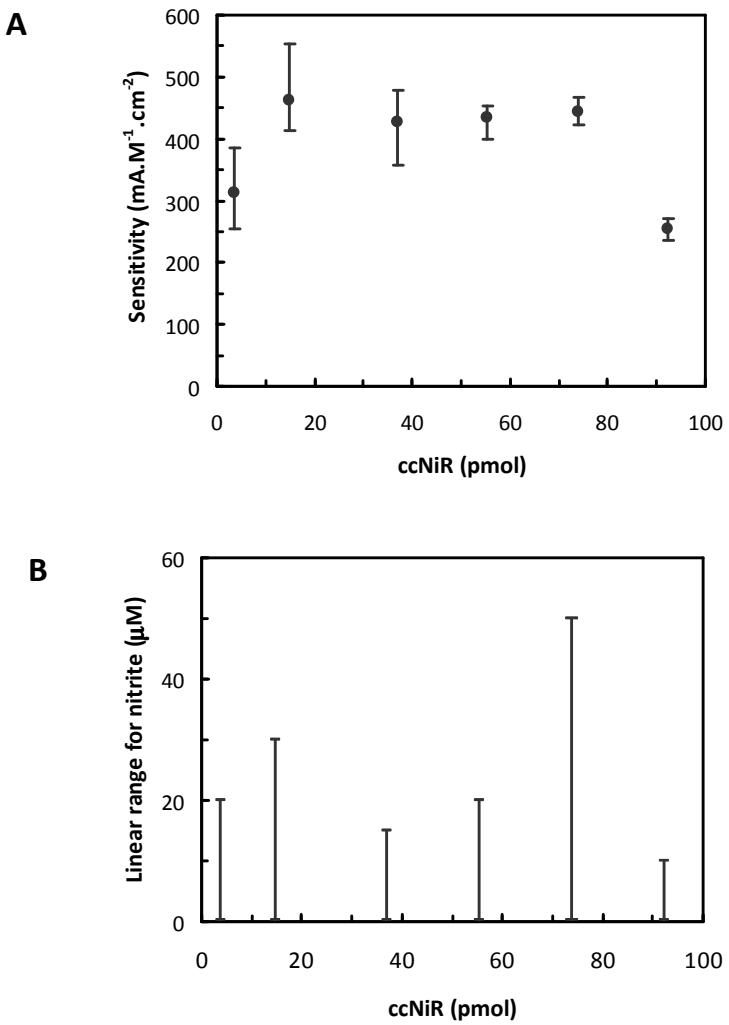


**Figure 3.3 -** Effect of the enzyme amount on the biosensor's response to nitrite, as determined by cyclic voltammetry experiments. Sol-gel prepared with 1:225 EETMS:$H_2O$ molar proportion. **A)** sensitivity; **B)** linear range.

The reduction of activity at high enzyme loadings could be related to a hyper-aggregation of the protein complexes within the sol-gel network and/or to a much slower diffusion of the substrate across the highly doped ceramic material [130]. For further studies, we selected a c*c*NiR amount of 74 pmol since it combined a good sensitivity with a broader linearity range and better reproducibility.

The sol-gel/c*c*NiR films obtained in the optimized conditions were morphologically characterized and the analytical performance of the bioelectrodes was further evaluated by amperometry.

### 3.3.2) Characterization of the sol-gel/*cc*NiR membrane

#### 3.3.2.1) Morphology

The global inspection of the modified sol-gel/*cc*NiR electrode by SEM (Figure 3.4) reveals a very smooth surface, randomly interrupted by cracks. The film is partially covered by layers of deposited materials that also surround the sol-gel fissures.

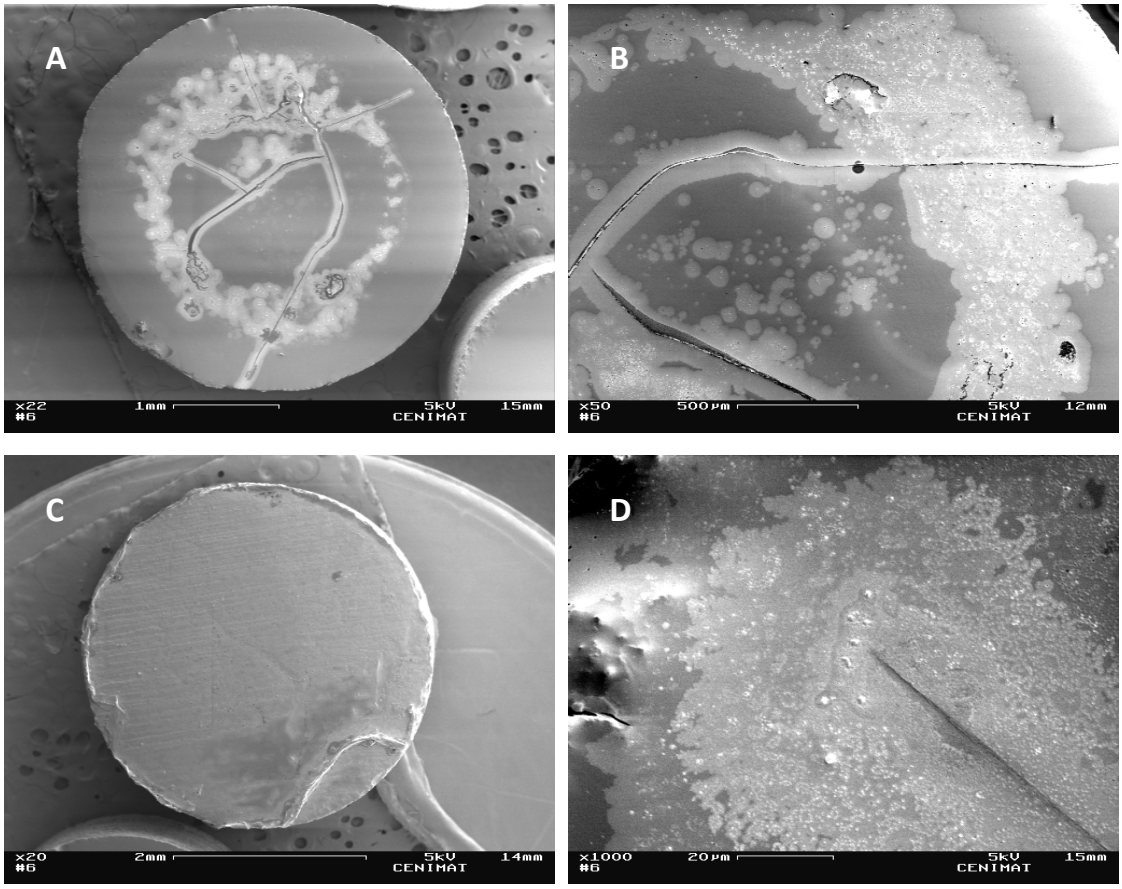


**Figure 3.4 -** SEM micrographs of **A)** sol-gel/*cc*NiR film (signal amplification ×22, 5 kV), **B)** sol-gel/*cc*NiR film (signal amplification ×50, 5 kV), **C)** *cc*NiR in HEPES buffer doped sol-gel film (signal amplification ×50, 5 kV) and **D)** sol-gel film with phosphate buffer (signal amplification ×1000, 5 kV). The sol-gel was prepared with 74 pmol of enzyme and a 225:1 $H_2O$:EETMS molar ratio and was deposited on pyrolytic graphite disks.

According to the SEM-EDS analysis (Figure 3.5), these deposits are particularly rich in P, K and O elements, probably from the phosphate salts ($K_2HPO_4$ and $KH_2PO_4$) that compose the buffer solution. Results suggest that this salt solution is expelled from the silica network essentially through the sol-gel cracks, forming small pools that, upon drying, create salt deposits. The further away from the sol-gel fissure the less salt is present, supporting the hypothesis of its exclusion from the sol-gel matrix (*cf.* Figure 3.5A and D).

This phenomenon was not seen on control films where the enzyme solution was replaced by an equal volume of deionized water or by enzyme in HEPES buffer instead of phosphate buffer (Figure 3.4C). On the other hand, it was observed in control electrodes were phosphate buffer was used instead of the enzyme solution (Figure 3.4D). Therefore, it can be concluded that the presence of phosphate salts stimulates cracking in EETMS based silicas. This is understandable since this ceramic material has a strong hydrophobic character. Nevertheless, one should be aware that this effect may seem particularly accentuated due to the longer sol-gel drying period (*ca.* 72h) imposed by the SEM analysis. For biosensing purposes, the bioceramic film was not allowed to dry for such a long time. So, the formation of cracks and salt deposits should be less important in this case. Even though phosphate salts are a frequent component of enzyme containing buffer solutions used in the construction of sol-gel based biosensors, the rejection of these salts from silicate films has not been reported so far.

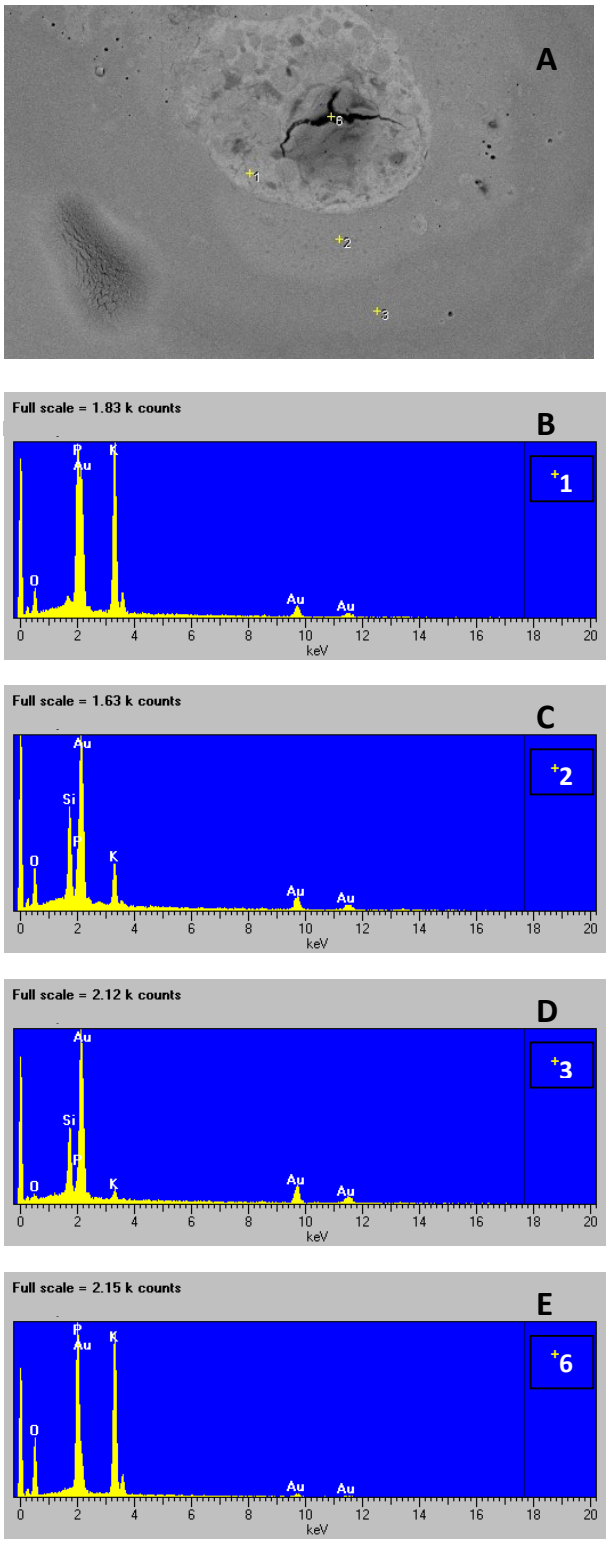


**Figure 3.5 -** SEM-EDS analysis of a ccNiR doped sol-gel film (74 pmol of enzyme and 225:1 $H_2O$:EETMS molar ratio). **A)** SEM micrograph (signal amplification x500, 5kV), EDS graph of points in A: **B)** 1, **C)** 2, **D)** 3 and **E)** 6.

A closer look to the micrographs of the sol-gel/*cc*NiR films demonstrates that although the electrode coverage is not completely uniform, ordered microstructure areas may be found. These zones were further investigated using AFM (Figure 3.6A). In all the inspected regions the surface was rather flat and there was no evidence of large protein aggregates outside the silica layer, suggestive of an effective enzyme entrapment inside the silica network. The *cc*NiR/silicate surface presented both large and small pores, ranging from an upper diameter of about 1 µm down to tens of nanometers. This heterogeneity was not caused by protein incorporation since sol-gel films prepared in its absence were also characterized by a nano to sub-microporosity (Figure 3.6B).

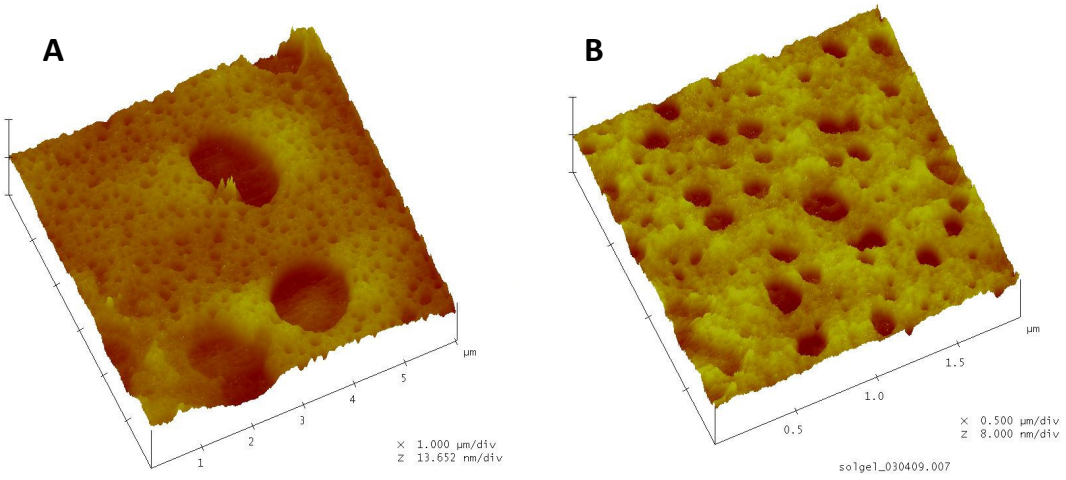


**Figure 3.6 -** AFM images of **A)** sol-gel/*cc*NiR film, **B)** sol-gel/phosphate buffer film (control electrode) deposited on highly oriented pyrolytic graphite.

### 3.3.2.2) Spectroscopy

In order to inspect the effect of the immobilization procedure on the structural integrity of the microenvironment of the heme cofactors of *cc*NiR, enzyme doped sol-gel films were examined by spectroscopic techniques.

The UV-Vis spectra of the entrapped *cc*NiR, in both oxidized and dithionite reduced forms (Figure 3.7A), are quite similar to the ones observed in solution (Figure 3.7B) an in [67]. In fact, the spectroscopic features assigned to *c*-type hemes (Soret, Q, α and β bands) did not

change upon protein encapsulation, keeping constant both wavelength maxima and band width. The only difference resides in a decrease of peak intensity of the Soret band (410 nm). In light of the fact that protein unfolding induces visible alterations in the hemes spectroscopic signature in terms of position, intensity and broadening [131], the obtained data give good indications about the biocompatibility of the microenvironment produced by the EETMS based silica matrix.

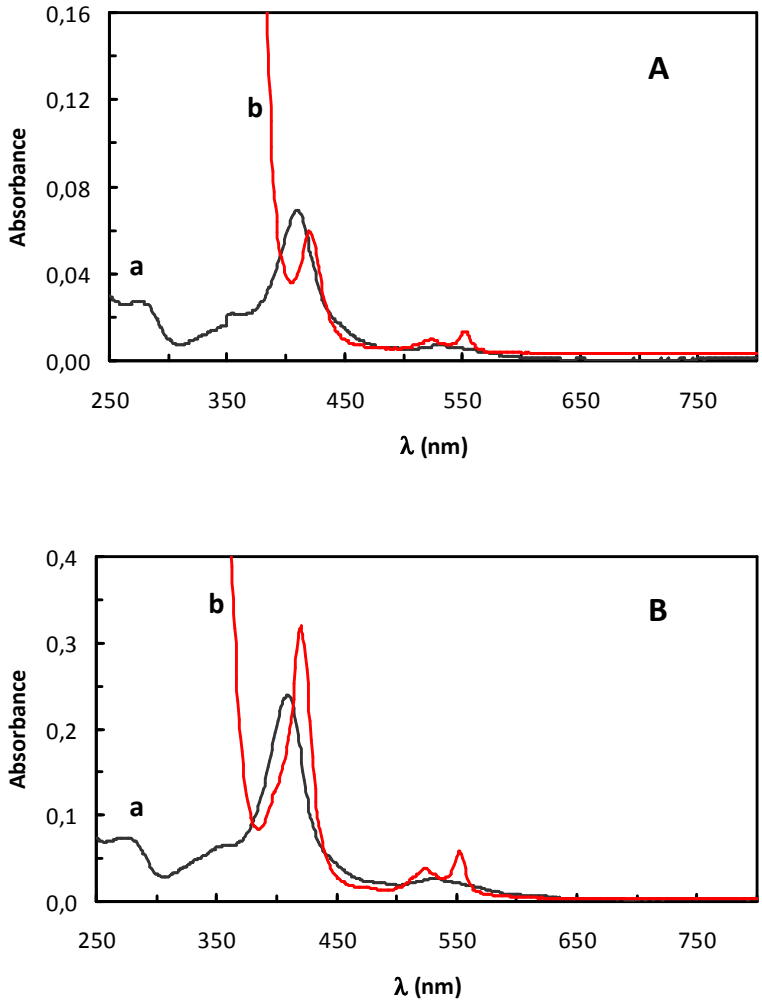


**Figure 3.7 -** UV-Vis spectra of ccNiR: **A)** immobilized in sol-gel matrix in a glass slide hydrated in supporting electrolyte, **B)** in 0.1 M phosphate buffer pH 7.6, in the **(a)** oxidised and **(b)** dithionite reduced forms.

The maintenance of the structural integrity of *cc*NiR in the sol-gel films was also supported by resonance Raman (RR) data (Figure 3.8). Namely, the high frequency region spectra of the encapsulated enzyme obtained under Soret excitation revealed typical features of a multiple *c*-type heme containing protein. The frequencies of the heme oxidation and spin state marker bands, $\nu_3$ (1504 $cm^{-1}$), $\nu_2$ (1587 $cm^{-1}$) and $\nu_{10}$ (1637 $cm^{-1}$) indicate that the predominant species is in the low spin (LS) state, as expected. Component analysis revealed the presence of high spin (HS) species with downshifted frequencies at 1367 $cm^{-1}$ and 1495 $cm^{-1}$ for $\nu_4$ and $\nu_3$ modes, respectively. The observed frequencies for both HS and LS modes are in agreement with those found in solution RR spectra of *cc*NiR (not shown), and the values reported for *bis*-His and 5 coordinated HS **c**-type hemes [132]. Therefore, no indications of denaturation or conformational changes of heme groups upon encapsulation of *cc*NiR into the sol-gel matrix were detected in the RR spectra. A shoulder at 1360 $cm^{-1}$ in the experimental spectrum originates from partial photoreduction of the protein; the intensity of this band is in direct correlation with the exposure of the sample to the laser beam, being present in the spectra even for the shortest accumulation times and laser power.

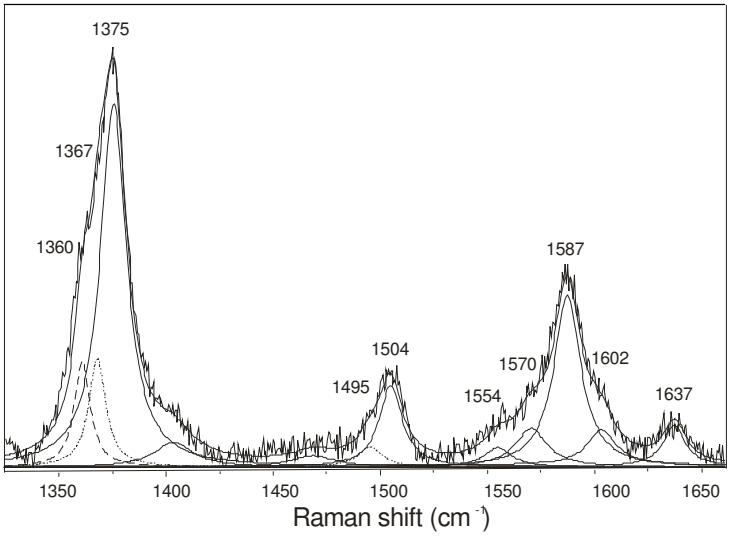


**Figure 3.8 -** Experimental and component resonance Raman spectra of a *cc*NiR doped glass slide. Experimental spectrum is an average of 4, measured from different spots on the surface with 413 nm excitation, 20 s accumulation time and 750 mW laser power. The most prominent oxidation/spin state marker bands are indicated; dotted bands (1367 $cm^{-1}$ and 1495 $cm^{-1}$) are assigned to the high spin species and dashed band to photoreduced protein.

#### 3.3.2.3) Electrochemistry

In the absence of nitrite, a very small non catalytic peak was observed (Figure 3.2A(b)). This attests for the capacity of c*c*NiR to exchange electrons directly with the solid electrode, especially if one considers that the large enzyme aggregates are most likely randomly oriented inside a nonconductive silica matrix. The signal appears in the same potential region of the broad wave previously identified when using c*c*NiR directly adsorbed on a PG electrode [76]. The absence of a peak shift upon entrapment suggests that this process did not significantly disturb the formal potential of the protein cofactors. However, the corresponding anodic peak was difficult to detect and the peak definition at all the tested scan rates was rather poor. These setbacks hindered a detailed analysis of the electrochemical process and eventual assessment of valuable parameters such as protein coverage and heterogeneous electron transfer rate constants.

### 3.3.3) Response to nitrite

To settle the operating potential for the bioelectrode calibration, amperometric measurements were carried out at three different voltages, all of them close to or well below the reduction potential of the catalytic heme (-200 ± 20 mV *vs* NHE, pH 7, *i.e.* -0.4 V *vs* Ag/AgCl) *i.e.*, the site of interaction with the substrate [76]. In this way, the supply of the minimal reduction power needed for enzyme activity is guaranteed. Nevertheless, some of the remaining hemes from both subunits have reduction potentials above that value. This may provide extra electron tunneling pathways between the active site and the enzyme surface, contributing to the amplification of heterogeneous ET. Figure 3.9 shows the amperometric responses and corresponding calibration curves obtained at -0.9, -0.7 and -0.5 V *vs* Ag/AgCl.

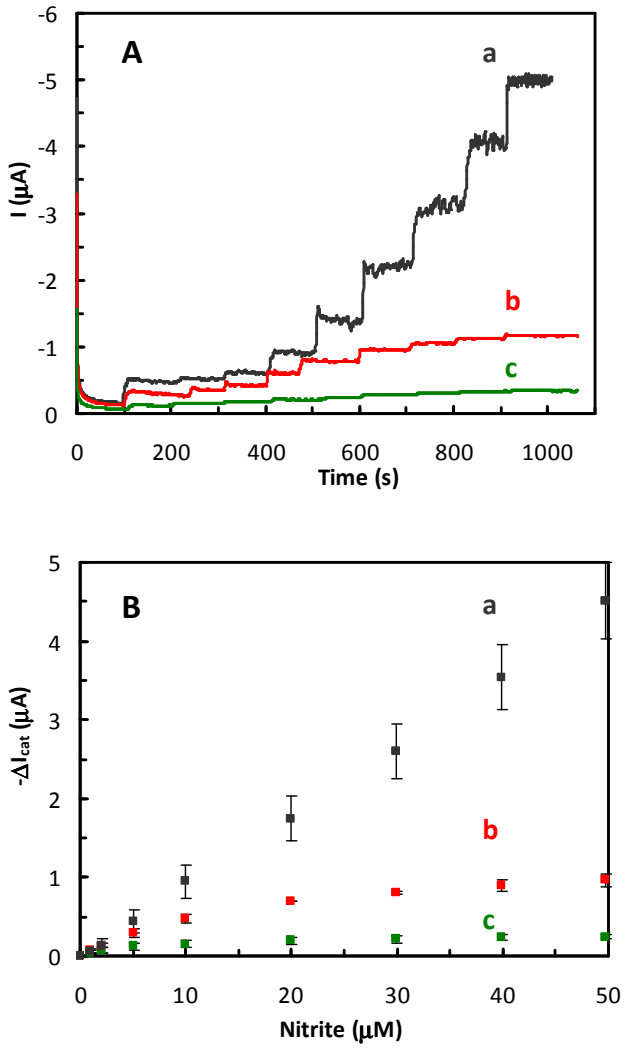


**Figure 3.9 - A)** Current response for sol-gel/*cc*NiR modified electrodes to successive nitrite injections **B)** Calibration curves registered at different working potentials: **(a)** -0.9 V, **(b)** -0.7 V and **(c)** -0.5 V *vs* Ag/AgCl. Sol-gel/*cc*NiR formulation: 74 pmol of enzyme and 225:1 $H_2O$:EETMS molar ratio.

The amperometric response upon nitrite addition was always prompt and reached a maximum within 5 s, indicative of fast heterogeneous ET. Although the enzyme cofactors are only slightly reduced, a small catalytic activity could be detected at the highest voltage tested (-0.5 V). As the reduction potential decreased the linear response of the biosensor towards nitrite became wider (Table 3.3). In fact, the subjection of the electrode to a stronger driving force helped interfacial ET and increased enzyme reduction, promoting catalytic activity. However, the probability of having background interference from complex

samples increases at very negative potentials and sample degassing is mandatory to eliminate the interference from oxygen, for example. In this regard, a less negative working potential is preferred.

**Table 3.3 -** Analytical properties of sol-gel/*cc*NiR based biosensors tested at different working potentials. Sol-gel/*cc*NiR formulation 74 pmol of enzyme and 225:1 $H_2O$:EETMS molar ratio.

| Working potential (V *vs* Ag/AgCl) | Linear range (μM $NO_2^-$) | Sensitivity ($mA.M^{-1}.cm^{-2}$) |
|---|---|---|
| -0.9 | 0.25 - 50 | 430 ± 23 |
| -0.7 | 0.25 - 10 | 345 ± 15 |
| -0.5 | 0.25 - 2 | 391 ± 62 |

Since the sensitivity of the biosensor through a range of different voltages is quite similar (*ca.* 10% variation), the working potential can be adjusted as a balance between the desired quantification limits and the interferences risks. A potential of -0.9 V was chosen for further analytical characterizations, thus allowing the broader analytical performance of the bioelectrode. At this voltage, the response of the biosensor to the enzyme substrate was linear from 0.25 to 50 μM, the detection limit was 120 nM (at a signal-to-noise ratio of 3) and the sensitivity to nitrite, given by the slope of the calibration curve, was 430 ± 23 $mA.M^{-1}.cm^{-2}$ (Table 3.3).

The sensitivity variation between electrode preparations is most likely related to the enzyme immobilization method, given that it consists on the simple cast of sol-gel and *cc*NiR drops on top of the electrode. The reproducibility of the response depends on the exact amount of protein entrapped within the sol-gel layer and, very importantly, on the proper orientation of the protein molecules towards the electrode surface, which can vary from preparation to preparation [98,131].

In order to improve the analytical parameters of the biosensor a conductivity enhancer was added to the silica glass [102,109]. As shown in Figure 3.10 doping of the biosensing membrane with graphite particles amplified the amperometric response up to 200 μM.

Despite, the sensitivity to nitrite was nearly the same (414 ± 20 $mA.M^{-1}.cm^{-2}$) as the bioelectrodes without graphite, the maximum current intensity, on the other hand, increased about 3 times. The electrochemical transduction of the biosensor was facilitated by this sol-gel-graphite composite.

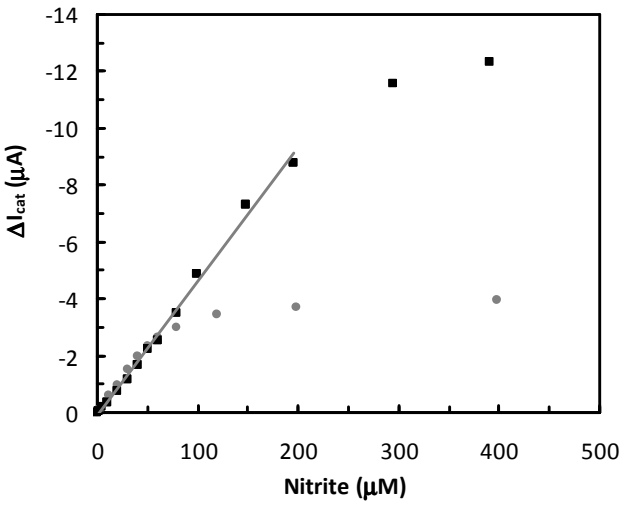


**Figure 3.10 -** Calibration curves of a sol-gel/*cc*NiR (●) and a sol-gel/*cc*NiR–graphite (■) biosensor. Sol-gel/*cc*NiR formulations: 74 pmol of enzyme, 225:1 $H_2O$:EETMS molar ratio and 1 mg/mL of graphite for the doped preparation. The assays were carried out at -0.9V *vs* Ag/AgCl. Linear regression y = -0.0493 x + 0.1844, $R^2$ = 0.9945.

To determine the kinetic parameter $K_M$ of *cc*NiR in the immobilized state, the amperometric analysis was repeated using a rotating electrode, in order to avoid mass transport control. Figure 3.11 shows the current response of a sol-gel/*cc*NiR biosensor to increasing substrate concentrations. Above 100 μM, the plot of catalytic current *vs* nitrite concentration (Figure 3.11B) reaches a pseudo-plateau consistent with Michaelis-Menten enzyme kinetics. According to the data fitting, the $K_M^{app}$ is 27.5 ± 1.3 μM, 7.5 times higher than the value determined in bulk solution (3.6 μM at 20°C) and almost 4 times the one previously obtained from non-encapsulative direct electrochemistry (7 μM, 20°C) [76]. The increasing factor of the Michaelis constant is typical for immobilized enzymes and it is attributed to the creation of a barrier to substrate diffusion by the host matrix, in this case,

the sol-gel layer. Therefore, it is unlikely that the affinity for the substrate has been significantly affected; the difference in $K_M$ is probably a consequence of the immobilization procedure.

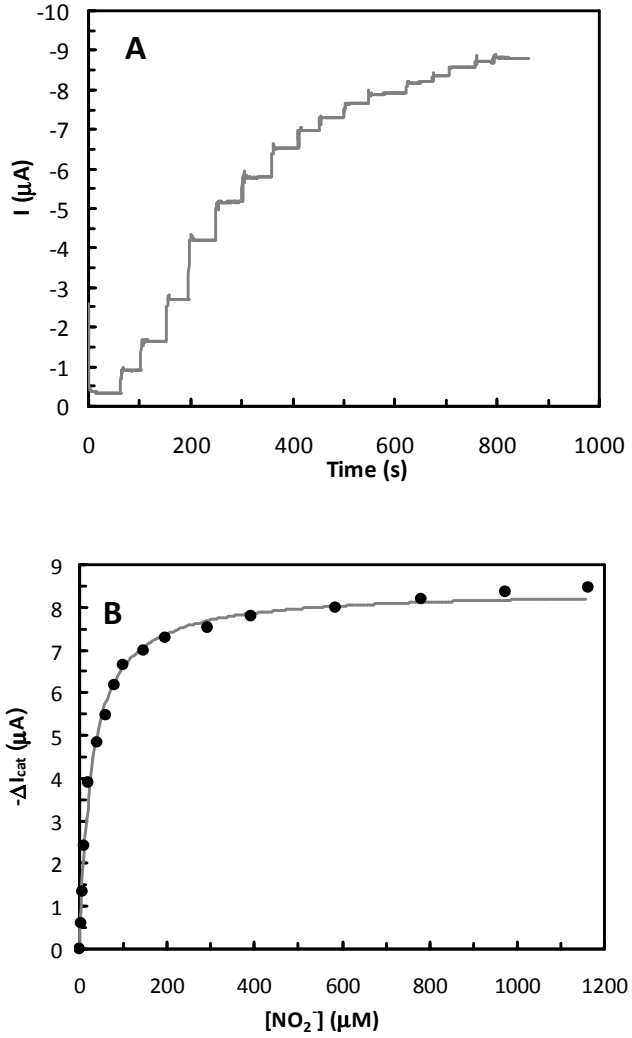


**Figure 3.11 - A)** Current response of a PGE/sol-gel/*cc*NiR biosensor to successive nitrite injections, **B)** Calibration curve (●) and Michaelis-Menten simulations of enzyme kinetics (—). Sol-gel/*cc*NiR formulation: 74 pmol of enzyme, 225:1 $H_2O$:EETMS molar ratio and 1 mg/mL of graphite. The assays were carried out at -0.9V *vs* Ag/AgCl with an electrode rotation speed of 600 rpm.

### 3.3.4) Interferences

The biosensor response to potential interferences was studied by comparing the magnitude of the catalytic response to 20 μM (within the calibration curve) and 500 μM (saturating concentration) of nitrite with the one obtained after adding the same concentration of a second chemical species.

**Table 3.4 -** Response of the sol-gel/*cc*NiR biosensor to potential interfering species: percentage of nitrite current response in the presence of an equal amount of interferent. Sol-gel/*cc*NiR formulation: 74 pmol of enzyme and 225:1 $H_2O$:EETMS molar ratio.

| Interfering species | $[NO_2^-]$ = 20 μM | $[NO_2^-]$ = 500 μM |
|---|---|---|
| **Nitrite ($NO_2^-$)** | 100% | 100% |
| **Nitrate ($NO_3^-$)** | 0.0% | 0.0% |
| **Sulfite ($SO_3^{2-}$)** | -2.5% | -1.6% |
| **Ammonium ($NH_4^+$)** | 0.0% | 0.3% |
| **Hydroxylamine ($NH_2OH$)** | 1.2% | 2.2% |

As shown in Table 3.4 the biosensor did not show any activity for nitrate ions which are often present in nitrite containing samples. Also, no catalytic response was observed for sulfite, on the contrary a small inhibition effect was detected (*ca.* -2%). Ammonium, the final product of nitrite reduction by *cc*NiR, did not affect the biosensor response either. In the presence of hydroxylamine, the bioelectrode increased its response by 1.2 and 2.2% at 20 and 500 μM of nitrite, respectively. This is a very low value when compared with other *cc*NiR based biosensing systems [43]. Hence, the sol-gel/*cc*NiR biosensor has drastically diminished the hydroxylamine interference. The explanation for such a low activity is unclear for now, but it is probably related to the specificities of the silica matrix and its interactions with the substrate molecules.

### 3.3.5) Biosensor stability

The sol-gel/*cc*NiR modified electrodes were stored in tris-HCl buffer pH 7.6, at 4°C, and tested for stability. Calibration curves were periodically traced and the linear range and sensitivity for nitrite were evaluated. In spite of a nearly daily utilization, both the linear range and sensitivity were quite stable (>90%) during the first two weeks (Figure 3.12). Thus, the silica matrix hosts the enzyme in a biocompatible cage, simultaneously preventing denaturation and lixiviation. Thereafter, the biosensor activity started to decrease progressively, keeping just 15% of the initial activity after thirty days. This deteriorating response is most likely due to the enzyme inactivation, related (or not) to the sol-gel aging process. Interestingly, the bioelectrode retained a residual activity over an extremely long period of time (up to six months).

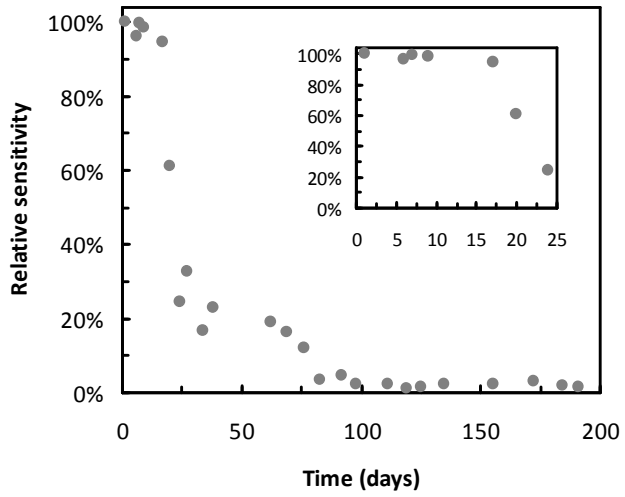


**Figure 3.12 -** Time effects on the biosensor sensitivity for nitrite determination. Sensitivity values were given by the slope of calibration curves performed periodically throughout 180 days. **Inset:** first 25 days of calibration. Sol-gel/*cc*NiR formulation: 74 pmol of enzyme and 225:1 $H_2O$:EETMS molar ratio. Catalytic currents were measured at -0.9V *vs* Ag/AgCl.

### 3.3.6) Biosensor application in real samples

The sol-gel/*cc*NiR biosensor was used to determine the concentration of nitrite in two real samples collected from surface waters of a Portuguese river, without any treatment, using the standard addition method and according to the voltammetric procedure described in Section 3.2.3. Each sample was examined in three independent assays (n = 3), using two different bioelectrode assemblies. The results are listed in Table 3.5.

**Table 3.5 -** Analytical results of the sol-gel/*cc*NiR biosensor for two real water samples from Portuguese rivers. Sol-gel/*cc*NiR formulation: 74 pmol of enzyme and 225:1 $H_2O$:EETMS molar ratio. Catalytic currents were measured at -0.9V *vs* Ag/AgCl.

| Sample | Standard method (μM $NO_2^-$) | Biosensor (μM $NO_2^-$) |
|---|---|---|
| **A** | 2.13 | 2.12 ± 0.14 |
| **B** | 11.44 | 11.47 ± 0.26 |

The biosensor results were identical to the values obtained by the colorimetric method described in the Standard Methods for the Examination of Water and Wastewater (4500-$NO_2^-$,B). This experiment attests the high accuracy of the analysis and indicates that the proposed biosensor can be reliably applied to nitrite determination in freshwaters.

## 3.4) Conclusions

Due to the inherent properties of cc*c*NiR and to the tunable porosity and hydrophobicity of the silica immobilizing layer it was possible to achieve a direct electrochemical response of cc*c*NiR when coupled to pyrolytic graphite interfaces. In this way, a non-mediated biosensing system was constructed, that provided an efficient way for assessing nitrite.

The sol-gel/cc*c*NiR biosensor displays a good analytical performance when compared to the formerly proposed bioelectrodes (*cf.* Table 1.1). The enhanced selectivity towards nitrite and the high stability of operation clearly constitute the most important advances. The sensitivity is satisfactory and the LOD (lower limit of detection) (120 nM) is well below the EU rules for nitrite in drinking waters (<0.1 ppm, *i.e.*, 2.2 μM). When using a silica-carbon conductive matrix, linearity extends over a two order magnitude range. Furthermore, the proposed biosensing system is easy to fabricate and works as a starting platform that can be modulated as a function of the analytical requirements. In particular, the parameters influenced by the analyte mass transport can be tuned by simply adjusting the diffusion barrier (*e.g.*, depositing an additional polymeric layer).

A drawback faced by encapsulation approaches when associated to DET is the lack of control of the spatial arrangement of the protein molecules, lowering both electronic communication and reproducibility. The development of a reliable nitrite amperometric biosensor for mass production should overcome this issue. In this regard, the proposed device shows great potential for improvement due to the versatility of the sol-gel chemistry for imparting geometric order to entrapped molecules. A promising strategy is silica functionalization via introduction of mercapto-groups used for protein anchoring.

The elimination of oxygen interferences is another pending question. Again, further developments of the sol-gel/cc*c*NiR system may optimize the working potential of the proposed biosensor since it offers some chances to operate at reduction potentials slightly above oxygen reduction. Perhaps an improved interfacial ET may decrease the driving force needed for enzyme activation.

# Chapter 4

# Carbon nanotubes based biosensors

# Chapter 4 - Carbon nanotubes based biosensors

## 4.1) Introduction

Carbon nanotubes (CNTs) have been gaining increasing popularity as promoters of direct electron transfer between biomolecules and electrode surfaces [133-134]. These carbon nanostructures are characterized by quite unique physical and chemical properties making them very interesting materials for a number of fields. They have application potential in areas such as electronics, scanning probe microscopy, chemical and electrochemical sensing, reinforced composite materials, energy storage and conversion, etc. In what respects electrochemistry, CNTs have shown improved performance when compared to the normally used carbon materials (glassy carbon and graphite). They share advantages with the other types of carbon electrodes, such as the wide potential windows and the relatively inert electrochemistry, but special structural and electronic features are responsible for the superior performance of CNTs as promoters of heterogeneous electron transfer [135]. In fact, CNTs have demonstrated remarkable behavior in electrochemical studies as electrocatalysts and in facilitating the direct electrochemistry of some proteins; this has contributed for their successful use in several electroanalytical applications, namely as electrochemical sensors and biosensors [136-144].

Carbon nanotubes are composed of graphene sheets rolled up to form tubes of varying diameter, length and termination [135]. The walls of the tubes are similar to basal plane graphite, with their hexagonal honeycomb structure of polyaromatic hydrocarbons, while the tubes ends can be terminated by fullerene like structures incorporating pentagons or by functional groups similar to the ones on edge plane graphite (oxygen-containing functional groups) [145-147].

CNTs are usually classified in two types: single-walled carbon nanotubes (SWCNTs), which consist of a single graphene sheet rolled into a nanometer diameter tube (from 0.4 to 2 nm) and multi-walled carbon nanotubes (MWCNTs), which are composed of multiple concentric tubes sharing a common axis (2-100 nm in diameter). Their lengths can vary between several hundred nanometers to several micrometers [135,148]. Nanotubes can be metallic or semi-

conducting according to the number of carbon hexagons around the circumference of the tube and their chiral angle with the tube axis [135,149-151].

Although the chemical composition of CNTs is quite simple, the special structure confers them remarkable properties. One of the most striking is the high specific surface (length to diameter ratio) granted by the helical arrangement of the carbon atom hexagons around the tube axis and the nanometric diameters [152]. Another remarkable feature, significant for electrochemistry, is the electrical conductivity. Other interesting properties include: intrinsic structural robustness, thermal stability, flexibility and reactivity [135].

Carbon nanotubes can be prepared by various processes, the most common are: electric-arc discharge, laser ablation and chemical vapor deposition [153-155]. Most methods make use of catalysts (nanoparticles of transition metals for the most) and can generate impurities; accordingly, CNTs are often purified after production [156-158]. In fact, pre-treatments and surface functionalization is very important to improve CNTs electrochemistry. The treatments should help to eliminate impurities and also introduce structural defects and functional groups that have been demonstrated to be relevant for CNT reactivity and electroactivity [159-161]. Chemical oxidation (using strong acids such as $HNO_3$ and $H_2SO_4$) and thermal exposure are the most common treatments performed on CNTs [156]. These modifications are usually associated with shortening of the tubes, opening of the end caps and introduction of oxyde functional groups (*e.g.* carboxyl). Increasing the number of oxygenated groups on carbon nanotubes has shown to enhance the rate of electron transfer rates [140]. In effect, some studies have attributed the good performance of CNT modified electrodes to the oxide species present on the carbon nanostructure [147,162]. The nanotubes can be further functionalized with amides and thiols groups, metal nanoparticles, polymers, amino acids, biomolecules etc. [156,163-166]. The treatments change the structural and electronic properties of the nanotubes, helping to improve CNT solubility and biocompatibility and facilitating heterogeneous electron transfer [156,160-161,164].

In practical terms, the use of CNTs in electrochemical applications has been associated with gain in currents and sensitivities, lower overpotentials and enhanced electron transfer rates [138-144,156]. CNTs can be used as modifiers over conventional working electrodes or

as electrode materials themselves. The later case is related with the use of CNT paste electrodes (CNT/binder composite electrodes), prepared by combining CNTs with binders [159,167-170] and screen-printed electrodes made of CNT inks [171]. Still, the vast majority of applications of carbon nanotubes in electrochemical studies rely on electrode surface modification by casting and evaporating suspensions of CNTs in organic solvents, polymers, surfactants and sol-gel matrices. Ultrasonication is usually necessary to disperse the nanotubes, since they are insoluble in most solvents. Typically the CNTs are randomly orientated over the surface of the electrode, and this can lower the reproducibility. More organized coatings, of controlled arrangement, can be obtained with self-assembled aligned carbon nanotubes [172-173], nanotubes grown on electrode surfaces [174] and layer-by-layer assemblies [175]. Accordingly, the amount and distribution of carbon nanotubes on the electrodes can be more easily controlled.

CNTs have been successfully employed in the (bio)electroanalytical field, showing improved behavior in the study of biologically important molecules, such as dopamine, norepinephrine, NADH, hydrogen peroxide and L-tyrosine [145,162,170,174,176-177]. As above mentioned, the special features of carbon nanotubes allows them to undergo fast electron transfer with the electroactive species, to detect them at lower potentials when compared to other types of electrodes and to improve their electrochemical reversibility [170,176-177].

CNTs have also been used for promoting the direct electrochemistry of several redox proteins and in electrochemical biosensors (enzyme, DNA and antibody based). Good electrochemical performance has been achieved with glucose oxidase [178-179], peroxidases [180], catalases [181-182], cytochrome c [183], myoglobin [184], hemoglobin [134,184], among others. The biomolecules can be immobilized by interaction with functional groups present on the nanotubes or by unspecific physical adsorption. The improved performance of CNT electrodes in these applications has been related with the larger surface areas generated by the three dimensional porous structures the CNT deposits bestow the electrodes. Also, these will be able to accommodate higher loadings of active biomolecules. In addition, the nano-scaled geometry of the nanotubes may have an

important contribution, allowing the enhanced wiring of proteins by shortening the distances to their redox centers [138-141,179].

In this context, this chapter describes innovative amperometric nitrite biosensors based on the heterogeneous electron exchange between *D. desulfuricans* cc*c*NiR and carbon nanotubes modified electrodes.

In a first approach, highly purified SWCNTs were used to form multilayered films, on GC and PG electrodes, which greatly enhanced the direct electrochemistry of cc*c*NiR. After bioelectrode optimization, the addition of a functionalized polypyrrole layer or an inorganic clay was explored with the aim of stabilizing the bioelectrode response. In part B of this chapter the same basic strategy was used to study the interaction of cc*c*NiR with modified MWCNTs deposited over PG electrodes. The surface properties of these modified materials were related with the MWCNT/cc*c*NiR bioelectrodes response to nitrite.

## 4.2) Experimental

**Part A – Single-walled carbon nanotubes biosensor**

### 4.2.1) Reagents

c*c*NiR (1.0 mg/mL; 300 U/mg) was purified from *D. desulfuricans* ATCC 27774 cells as described in Annex 1 and stored in 0.1 M phosphate buffer pH 7.6 at -20°C. Sodium nitrite, dipotassium hydrogen phosphate and potassium dihydrogen phosphate were from Merck. Tetrahydrofurane (THF) was from Fisher, dimethylformamide (DMF) and diethyl ether were from Sigma. $LiClO_4$ was provided by Fluka. All chemicals were of analytical grade. The synthetic hectorite laponite was obtained from Laporte industries. The amphiphilic pyrrole, (11-pyrrolyl-1-undecyl) triethylammonium tetrafluoroborate, was synthesized by Serge Cosnier group (Université Joseph Fourier, Grenoble, France) as previously described [185]. The solutions were prepared with deionized water (18 ΩM.cm resistivity) from a Millipore MilliQ system.

Purified SWCNTs were purchased from Unidym (production by HiPco® process). In order to obtain better dispersions, as received nanotubes (20 mg), were sonicated in 300 mL of THF for 2h. The solvent of the inhomogeneous dispersion was then evaporated under vacuum to recover a fine powder of carbon nanotubes. The solid was diluted with 200 mL DMF and sonicated for further 2h at room temperature. After sedimentation of undispersed nanotubes, the supernatant was filtered over a PTFE membrane filter (pore size 0.45 µm) and washed with THF. The residue was not allowed to dry during filtration. Thus, the wet sludge cake was put in a few millilitres of diethyl ether and mechanically stirred and ground until dryness to avoid re-aggregation of the SWCNTs. The SWCNTs were allowed to dry overnight at 70°C. Using such pre-treated nanotubes, stable and homogeneous dispersions in THF (0.1 mg/mL) could be obtained after only 15 min of sonication [186].

### 4.2.2) Electrochemical measurements

Electrochemical measurements were performed with a Potentiostat Autolab PGSTAT30 monitored by the control and data acquisition software GPES 4.9, both from Eco-Chemie. The experiments were done in a three-electrode cell system (Metrohm), with a saturated calomel reference electrode (SCE) from Radiometer, a platinum wire (placed in a separated compartment containing the supporting electrolyte) as a counter electrode and a pyrolytic graphite (self-made) or glassy carbon (Radiometer) disk as working electrode. The experiments were carried out at room temperature (20 ± 2°C) in argon-purged 20 mL of 0.1 M phosphate buffer (pH 7.6) maintained under an argon atmosphere.

The cyclic voltammograms were plotted using a scan rate of 20 mV/s in a potential window of -0.1 to -0.8 V. After each addition, the cell was again purged with argon for *ca.* 30 s and the CV was recorded. Nitrite catalytic currents were determined at the CV inversion potential -0.8 V.

To evaluate the bioelectrode response to nitrite, the cell was consecutively spiked with small volumes of $NaNO_2$ standard solutions (0.01, 0.1 and 1 M).

The values presented in the graphs and tables are the average of three independent experimental determinations; error values and bars represent the standard deviation. All potentials were quoted against SCE (-242 mV *vs* NHE).

### 4.2.3) Bioelectrode preparation

Prior to enzyme coating, the GC and PG working electrodes (diameters 3-5 mm) were polished with diamond paste on felt pads and successively washed with ethanol, acetone and deionized water. The SWCNT modification was made by depositing successive layers of 10 µL of the THF dispersion and drying the solvent of each layer, one by one, under vacuum. Up to 15 layers of SWCNTs were formed on the electrode surface in this manner (layer-by-layer construction). The electrodes were then rinsed with THF and water to remove the unattached SWCNTs and residues of the organic solvent. A drop of enzyme (7 µL) was then applied onto the modified electrodes and left for air drying for 30 min. Next, the bioelectrodes were immersed in fresh electrolyte solutions; when not in use, they were stored at 4°C, in a semi-dry state, *i.e.*, leaving a small droplet of buffer solution on top, to

maintain a moist environment. Control electrodes were prepared by deposition of enzyme directly on the surface of GC or PG electrodes and leaving them for air drying for 30 minutes.

For laponite electrodes (PG/SWCNT/c*c*NiR/laponite) the clay colloidal suspension (2 mg/mL) was prepared by dispersion in deionized water and overnight stirring. A 10 µL drop was placed on the surface of the PG/SWCNT/c*c*NiR electrodes and dried under vacuum.

In the case of the polymer electrodes (PG/SWCNT/c*c*NiR&polypyrrole), a mixture of 10 µL of the monomer dispersion (3.0 mM) and 7 µL (7 µg) of c*c*NiR were deposited on a PG/SWCNT electrode and dried under vacuum. Polymerization of the adsorbed monomer was then performed at 0.8 V in deoxygenated 0.1 M $LiClO_4$ aqueous solution.

### 4.2.4) Scanning electron microscopy (SEM)

Enzyme and nanotube films were prepared for SEM measurements by deposition on a glassy carbon plate. FEG-SEM images were recorded using an ULTRA 55 FESEM based on the GEMINI FESEM column (in-lens SE detector) with beam booster (Nanotechnology Systems Division, Carl Zeiss NTS GmbH, Germany) and tungsten gun (acceleration voltage 5 kV).

## Part B - Modified multi-walled carbon nanotubes biosensor

### 4.2.5) Reagents

c*c*NiR (1.0 mg/mL; 300 U/mg) was purified from *D. desulfuricans* ATCC 27774 cells as described in Annex 1 and stored in 0.1 M phosphate buffer, pH 7.6 at -20°C. Sodium nitrite, tris(hydroxymethyl)aminomethane and potassium chloride were from Merck. Tetrahydrofurane (THF) was from Fisher. Solutions were prepared with deionized water (18 MΩ cm) from a Millipore MilliQ water purification system. All chemicals were analytical grade and were used without further purification.

The MWCNT samples were provided by Prof. Manuel F.R. Pereira from Laboratório Associado LSRE/LCM, Departamento de Engenharia Química, Faculdade de Engenharia, Universidade do Porto. Five samples were tested: MWCNT_orig (as purchased material, with no treatment), MWCNT_$HNO_3$ (oxidation with $HNO_3$), MWCNT_$HNO_3$_$N_2$_400 (oxidation with $HNO_3$ followed by thermal treatment under $N_2$ flow at 400°C for 1h),

MWCNT_$HNO_3$_$N_2$_600 (oxidation with $HNO_3$ followed by thermal treatment under $N_2$ flow at 600°C for 1h) and MWCNT_$O_2$ (oxidation with 5% $O_2$ in $N_2$ flow at 500°C for 3h) [187]. Table 4.1 summarizes the main textural and chemical properties of the MWCNT samples and classifies the stability of the water and THF dispersions.

**Table 4.1 -** Textural and chemical characterization of the MWCNT samples [187] and respective dispersion stability. $S_{BET}$ – Brunauer-Emmet-Teller surface area, $\%m_O$ – mass percentage of oxygen on the surface, $pH_{PZC}$ – point of zero charge.

| Sample | $S_{BET}$ ($m^2g^{-1}$) | % $m_O$ | $pH_{PZC}$ | Water dispersion | THF dispersion |
|---|---|---|---|---|---|
| **MWCNT_orig** | 331 | 0.84 | 7.0 | X | unstable |
| **MWCNT_$HNO_3$** | 476 | 8.7 | 3.0 | Stable | unstable |
| **MWCNT_$HNO_3$_$N_2$_400** | 483 | 5.6 | 3.8 | very stable | x |
| **MWCNT_$HNO_3$_$N_2$_600** | 504 | 2.8 | 5.9 | Stable | x |
| **MWCNT_$O_2$** | 508 | 2.5 | 5.2 | Stable | unstable |

### 4.2.6) MWCNT dispersions

The carbon nanotube dispersions (0.1 mg/mL) were prepared in tetrahydrofuran (THF) or deionized water by sonication during 30 minutes. The samples that were not homogeneous 30 minutes after being prepared or during the time necessary to prepare the electrodes were labeled as unstable.

### 4.2.7) Bioelectrode preparation

The MWCNT modification was made by depositing successive layers of 10 µL of nanotube dispersions in THF or water, and drying the solvent of each layer, one by one, inside an oven set at 65°C (in between, there were no rinsing steps). Up to 20 layers of MWCNTs were formed on the electrode surface in this manner. After all layers had been deposited, the electrodes prepared with THF dispersions were rinsed with THF to remove any unattached MWCNTs. A drop of enzyme (7 µL – 7 µg) was then applied onto the modified electrodes and dried at room temperature for 30 minutes. Next, the bioelectrodes were immersed in electrolyte solutions. When not in use, they were stored at 4°C, in a semi-dry state, i.e., leaving a small droplet of buffer solution on top, to maintain a moist environment.

### 4.2.8) Electrochemical measurements

Electrochemical measurements were carried out with a Potentiostat Autolab PGSTAT12 (Eco-Chemie) monitored by the control and data acquisition software GPES 4.9 (Eco-Chemie). The experiments were done in a three-electrode cell system (Metrohm), with a SCE reference electrode (Radiometer), a platinum wire, as a counter electrode (Radiometer) and a pyrolytic graphite disk as working electrode (self-made). The experiments were performed at room temperature (20 ± 2°C) under an argon atmosphere. The supporting electrolyte was 0.1 M KCl in 0.050 M tris-HCl buffer pH 7.6 (20 mL).

The cyclic voltammetry experiments were performed as described in section 4.2.2.

### 4.2.9) Scanning electron microscopy (SEM)

The enzyme and nanotube films (MWCNT_$O_2$) for SEM were prepared by deposition on a pyrolytic graphite disks. The analysis was done in a FEI Strata 235-Dual Beam FIB (focused ion beam) both in surface and cross section.

## 4.3) Results and Discussion

**Part A – Single-walled carbon nanotubes biosensor**

### 4.3.1) Morphologic characterization

A representative SEM image of a typical deposit of unmodified SWCNTs is shown in Figure 4.1A. The nanotubes are arranged in no particular structure, displaying a network of interconnected tubes and bundles spread randomly on multiple layers. This mesh arrangement is the typical framework that results from the layer-by-layer deposition of CNTs [188]. Such entangled nanotube bundles offer a highly porous matrix with pore sizes of several tens of nanometers. After immobilization of *cc*NiR, a homogeneous protein layer can be seen over the nanotube deposit (Figure 4.1B). This confirms the two level architecture of the bioelectrode composed of a 3D network of CNTs covered by a protein layer.

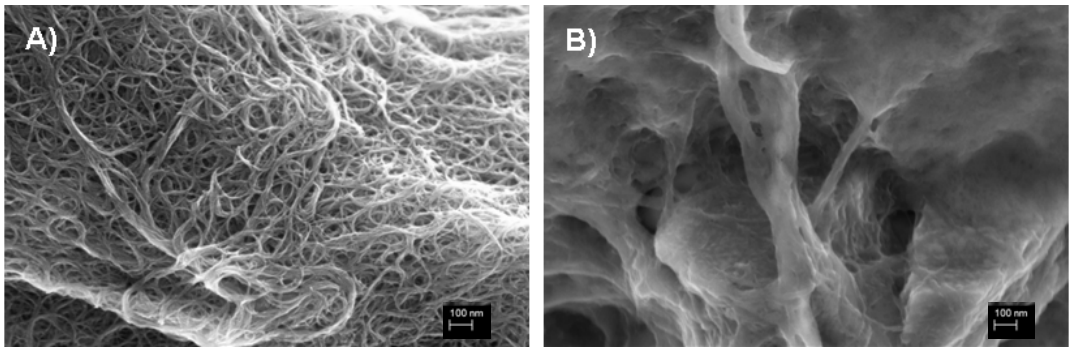


**Figure 4.1 -** SEM images of **A)** glassy carbon plate electrode covered with 12 layers of SWCNTs without enzyme coating; **B)** Same setup as (A) following immobilization of *cc*NiR. SEM conditions: beam length 4.8-5.2 mm, magnification x50 000, acceleration voltage 5 kV.

### 4.3.2) Bioelectrode optimization

Cyclic voltammograms for SWCNT/*cc*NiR films deposited on GC and PG electrodes were recorded in 0.1 M phosphate buffer pH 7.6, both in the presence and absence of nitrite. When compared to *cc*NiR films deposited on bare electrodes, the SWCNT/*cc*NiR coatings

showed higher background and faradaic currents, as exemplified in Figure 4.2 for PG and GC 12-SWCNT/*cc*NiR electrodes. This is most likely related to the higher surface area provided by the carbon nanotubes [138,175,189]. The large separation between the cathodic and anodic scans in CV is typical on CNT modified electrodes; it arises from the high capacive currents afforded by the CNTs [140].

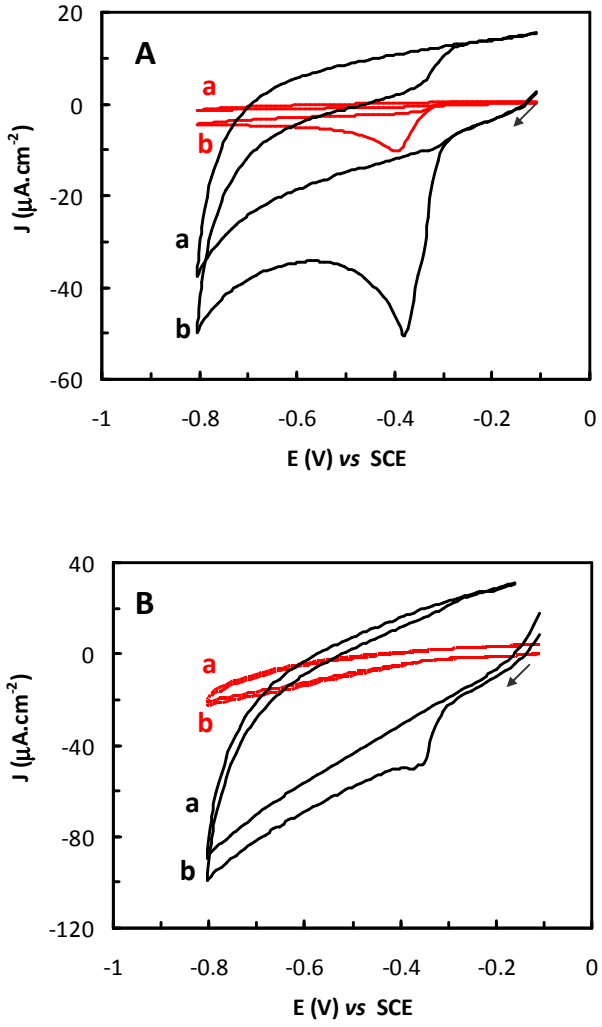


**Figure 4.2 -** Cyclic voltammograms of **A)** PG/*cc*NiR electrode (—) and of a PG/12-SWCNT/*cc*NiR electrode (—): **(a)** without $NO_2^-$ and **(b)** with 10 µM $NO_2^-$. **B)** Same set of experiments performed with GC electrodes.

In the presence of the enzyme's substrate, the PG/*cc*NiR control electrode exhibited a catalytic peak at *ca.* -0.380 V *vs* SCE, which reflects the electroenzymatic reduction of nitrite to ammonium and hence, a direct electrical connection of *cc*NiR to the electrode surface. In a similar experiment carried out with a PG/SWCNT/*cc*NiR electrode, a much higher catalytic current (*ca.* 10 times) was displayed at the same potential.

In fact, carbon nanotubes can supply more electroactive sites than plain PG electrodes and they can also act as a porous matrix that is able to retain greater amounts of enzyme and provide a favourable microenvironment to exchange electrons with the working electrodes [175]. Consequently, the electroenzymatic reduction of nitrite was greatly enhanced. It should be noted that no direct reduction of nitrite was observed, in the same potential range, at PG/SWCNT electrodes to which no enzyme was added (not shown).

Interestingly, the amplifying effect of carbon nanotubes on the DET of *cc*NiR was much more obvious for the glassy carbon electrodes: in the absence of SWCNTs, no electrochemical peak signals could be observed, even in the presence of nitrite (although a small increase of current was detected – Figure 4.2B red (b)). Yet, when the surface was modified with carbon nanotubes, a catalytic peak was clearly detected at *ca.* -0.380 V, as for the PG electrodes. On the other hand, the PG support by itself, also contributes to the direct charge transfer to *cc*NiR, since the nitrite dependent current densities were always higher when using PG rather GC as working electrode. This result reinforces the notion that graphene based materials in general, and highly graphitized nanotubes in particular, have a great capacity for improving the electrochemical transduction of nitrite biocatalysis.

The influence of the amount of deposited SWCNT on the electrochemical response of *cc*NiR was evaluated for both PG and GC electrodes, taking into consideration the maximum current density ($J_{max}$) of the catalytic wave observed at saturating nitrite concentrations. The number of layers of SWCNTs was varied between 3 and 15. As shown in Figure 4.3, $J_{max}$ increases gradually with the number of layers of SWCNT up to 9-12, and stabilizes above this value. This profile has indicated the optimal amount of carbon nanotubes that should be used for immobilizing and wiring *cc*NiR to the electrode, in the current experimental conditions; therefore, for further analysis all electrodes were prepared by depositing 12 layers of SWCNTs on the PG surfaces.

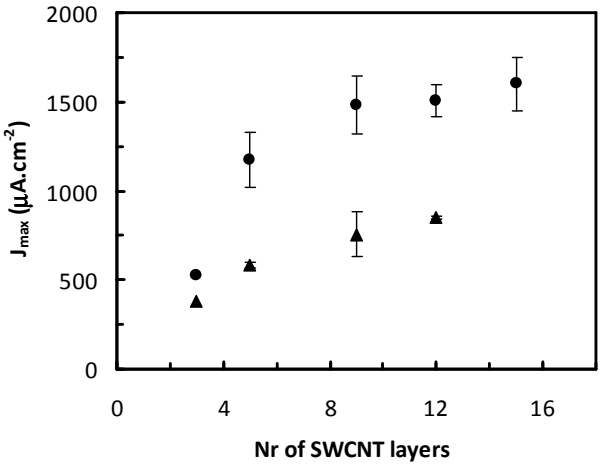


**Figure 4.3 -** Effect of SWCNT layers on the maximum current values determined for the reduction of nitrite by SWCNT/*cc*NiR modified PG (●) and GC (▲) electrodes.

### 4.3.3) Bioelectrode response to nitrite

To assess the dependence of the catalytic current on the concentration of the substrate, cyclic voltammograms of the PG/12-SWCNT/*cc*NiR modified electrodes were registered at various nitrite concentrations (Figure 4.4).

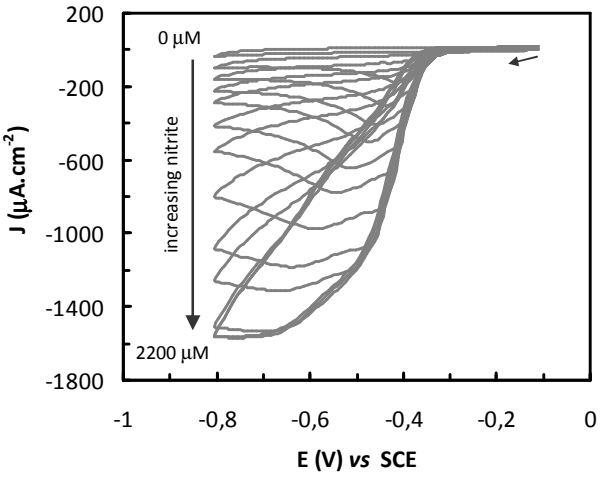


**Figure 4.4 -** Cyclic voltammograms of a PG/12-SWCNT/*cc*NiR bioelectrode in the presence of varying nitrite concentrations.

The results presented in Figure 4.5 show the relation between the catalytic currents and nitrite concentration for PG/12-SWCNT/*cc*NiR electrodes. A steady increase of the catalytic currents is observed, with a linear range extending up to 150 µM of nitrite and reaching a plateau at higher concentrations. This profile was fitted to a Michaelis-Menten kinetics with the following parameters $K_M^{app}$ = 715 ± 51 µM and $J_{max}^{app}$ = 2150 ± 65 µA $cm^{-2}$.

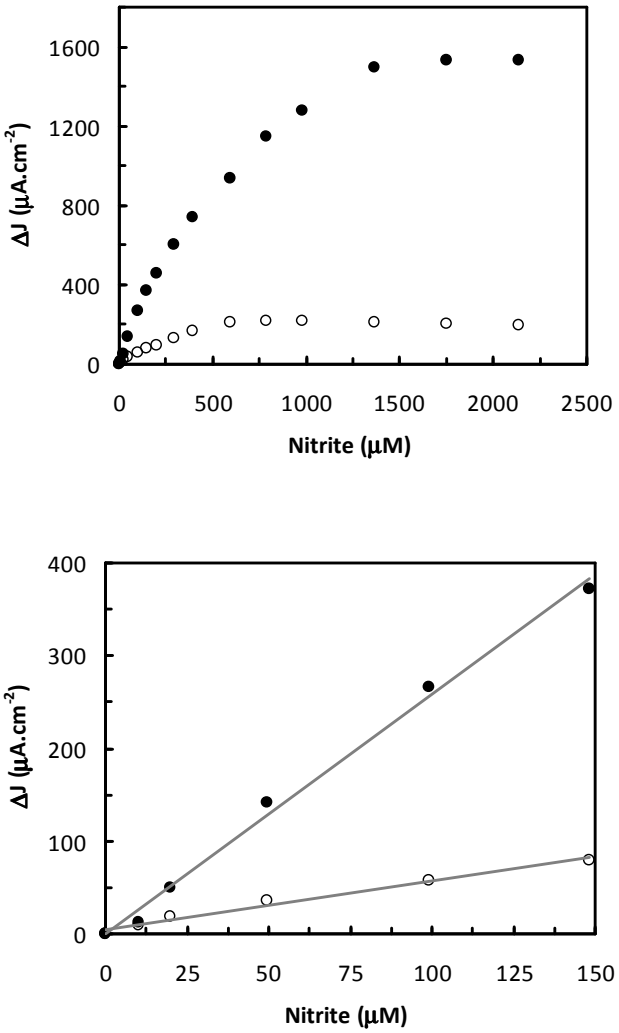


**Figure 4.5 - A)** Calibration plot for nitrite response and **B)** correspondent linear regions, for (●) PG/12-SWCNT/*cc*NiR and (○) PG/*cc*NiR electrodes.

The sensitivity of the bioelectrode, as determined by the slope of the linear part of the calibration curve (Figure 4.5B), was 2.4 ± 0.1 $A.M^{-1}.cm^{-2}$ and $J_{max}$ was 1500 ± 90 $\mu A \cdot cm^{-2}$. This sensitivity is much higher than most of the values reported for the preceding nitrite biosensors constructed with the same enzyme [42-44]. In contrast, the sensitivity and $J_{max}$ values were significantly lower in the absence of the SWCNT coating (Figure 4.5), *i.e.*, 0.52 ± 0.03 $A.M^{-1}.cm^{-2}$ and 216 $\mu A \cdot cm^{-2}$, demonstrating once again the beneficial role played by SWCNTs as a host and connecting material.

The lower detection limit was 2.1 µM, at a signal to noise ratio of 3; this value is higher than the LODs obtained with some other biosensing systems also based on *cc*NiR from *D. desulfuricans* (*cf.* reference [44] and Chapter 3), and it is not enough for nitrite monitoring in drinking waters according to the European Union rules (maximum admissible level <0.1 ppm, *i.e.*, 2.2 µM). Nevertheless, further optimization using different amounts of enzyme and number of SWCNTs layers may improve the LOD of the SWCNT/*cc*NiR based electrode.

Despite the simplicity of the method used to prepare these bioelectrodes, the PG/12-SWCNT/*cc*NiR biosensors were quite reproducible, with a variation in sensitivity of *ca.* 6% between electrodes.

### 4.3.4) Interferences

The effect of potential interfering substances (nitrate, sulfite, sulfate, hydroxylamine, ammonium) on the bioelectrode response was evaluated by comparing the magnitude of the catalytic current obtained in the presence of nitrite only (50 µM), with the one obtained after adding a second chemical species. The results were expressed in percentage variation and are listed in Table 4.2. The ionic species had little (nitrate, sulfite and sulfate) or negligible (ammonium) effect, which can be caused by minor variations of the ionic strength. However, in the presence of hydroxylamine, the catalytic response increased 20%; in fact, this compound was previously recognized as having reactivity with *cc*NiR, probably being an intermediary species of the *cc*NiR catalysed reduction of nitrite to ammonium [43].

**Table 4.2 -** Percentage variation of the bioelectrode response to 50 µM nitrite in the presence of the same concentration of a potential interfering species.

| Interferent | Response Variation |
|---|---|
| **Nitrate ($NO_3^-$)** | 3% |
| **Sulfite ($SO_3^{2-}$)** | 2% |
| **Sulfate ($SO_4^{2-}$)** | 2% |
| **Hydroxylamine ($NH_2OH$)** | 20% |
| **Ammonium ($NH_4^+$)** | 0.5% |

### 4.3.5) Bioelectrode stability

To evaluate the stability of the PG/12-SWCNT/*cc*NiR electrodes, their sensitivity to nitrite was periodically determined (Figure 4.6). A progressive decrease is observed from day one to day forty (36% of initial activity). Then the response remains stable for two months, subsequently decreasing and totally disappearing after six months.

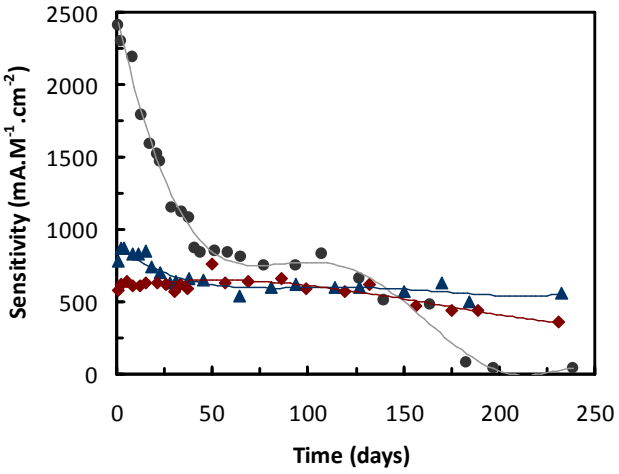


**Figure 4.6 -** SWCNTs based biosensors sensitivity for nitrite as a function of time for PG/12-SWCNT/*cc*NiR (●); PG/12-SWCNT/*cc*NiR&polypyrrole (▲) and PG/12-SWCNT/*cc*NiR/laponite (◆) electrodes. Sensitivity values were given by the slope of calibration curves performed periodically throughout 248 days.

With the aim of improving the stability and lifetime of the bioelectrode, the deposition of two different materials was investigated for preventing enzyme leakage and protecting its microenvironment. Specifically, an inorganic clay (laponite) and an electropolymerized amphiphilic pyrrole were used for enzyme entrapment and preservation of its catalytic activity.

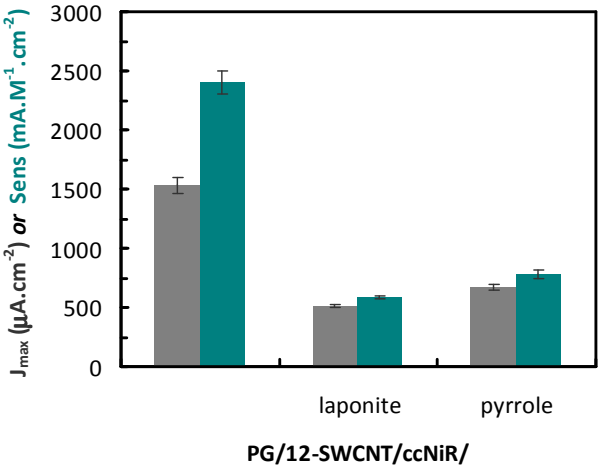


**Figure 4.7 -** Matrix effect on the biosensors response to nitrite: maximum current density (■); sensitivity (■), as determined by the slope of the calibration curves for the first day calibration of the three types of electrode.

Figure 4.7 shows the maximum current densities obtained at a saturating nitrite concentration (above 1 mM) for the SWCNT/*cc*NiR bioelectrodes modified with protective matrices, as well as the sensitivity for the calibration curves attained with each configuration. The initial sensitivity of the biosensors with laponite and polypyrrole was 25% and 32%, respectively, of the one recorded for the PG/12-SWCNT/*cc*NiR electrode. In addition, the maximum current densities decreased to 33% (laponite) and 44% (polypyrrole) when compared with the non-protected electrode. Most likely, these inorganic or polymeric layers create steric hindrances towards nitrite diffusion, which account for the lowered parameters. Another possibility is that less enzyme is in fact electroactive, when these protective layers are present, due to a different arrangement of the biofilm, lower enzyme accessibility or denaturation. This hypothesis was not further looked into since the surface

coverage of the different bioelectrodes was not determined (the non-catalytic signals had very low intensity (*cf.* Figure 4.2A)).

Despite the fact that the activity of the modified bioelectrodes was lowered, the stability increased considerably since 90% of the initial sensitivity was maintained after two weeks for polypyrrole and no significant variation was observed for laponite over a period of three months (Figure 4.6). Clearly, the presence of these additional coatings greatly extends the biosensor lifetime given that *ca.* 60 % of the initial nitrite sensitivity is still observed after 248 days, for both encapsulating matrices. These configurations are the most stable when compared to the previously reported cc*c*NiR based biosensors [41-45] and Chapter 3.

## Part B - Modified multi-walled carbon nanotubes biosensor

The enhancement of the electrocatalytic activity of cc*c*NiR through the employment of carbon nanotubes was further investigated with various samples of thermally and chemically modified multi-walled carbon nanotubes. In particular, these materials had previously been subjected to oxidative and thermal treatments in order to create MWCNTs with different oxygen-containing surface groups, conferring the CNTs specific surface chemical properties [187]. The characteristics of the materials are listed in Table 4.3.

**Table 4.3 -** Textural and chemical characterization of the MWCNT samples [187]. $S_{BET}$ – Brunauer-Emmet-Teller surface area, $\%m_O$ – mass percentage of oxygen on the surface, $pH_{PZC}$ – point of zero charge.

| Sample | $S_{BET}$ ($m^2g^{-1}$) | % $m_O$ | $pH_{PZC}$ |
|---|---|---|---|
| **MWCNT_orig** | 331 | 0.84 | 7.0 |
| **MWCNT_$HNO_3$** | 476 | 8.7 | 3.0 |
| **MWCNT_$HNO_3$_$N_2$_400** | 483 | 5.6 | 3.8 |
| **MWCNT_$HNO_3$_$N_2$_600** | 504 | 2.8 | 5.9 |
| **MWCNT_$O_2$** | 508 | 2.5 | 5.2 |

### 4.3.6) Non-catalytic signals

The non-catalytic signals of cc*c*NiR immobilized in PG electrodes modified with five layers of the different types of MWCNTs were evaluated by cyclic voltammetry (Figure 4.8). The non-turnover currents should reflect the amount of immobilized enzyme molecules and their ability to interact with the modified electrode. However, as in the case of the PG/SWCNT electrodes (*cf.* Figure 4.2A), only a broad peak with low intensity (*ca.* -0.380 V *vs* SCE) can be observed in the cathodic potential scan, in these experimental conditions. The only exception is the sample of MWCNT_$O_2$, for which a more defined peak shape was obtained (Figure 4.8B).

Just as for the SWCNTs modified electrodes the cyclic voltammograms with MWCNT/cc*c*NiR had higher background and faradaic currents in comparison with cc*c*NiR films deposited on bare PG surfaces. This is related to the larger surface area provided by the MWCNTs. Nonetheless, the position and shape of the non-catalytic signals displayed by cc*c*NiR when adsorbed on PG/CNTs or bare PG are similar. Thus, it was assumed that the change from a PG surface to a MWCNT modified one had no significant effect on the cc*c*NiR electrochemical profile.

The MWCNT_$HNO_3$_$N_2$_600 sample rich in lactones and carboxylic anhydrides produced the higher currents, pointing it out as the most adequate material to enhance heterogeneous electron transfer. Nonetheless, no direct relations could be found between the properties of the MWCNT (percentage of oxygen on the nanotubes surface, surface area, $pH_{PZC}$) and the intensity of the non-catalytic signals. Perhaps the type of oxygenated groups and not the amount is the crucial factor in this case.

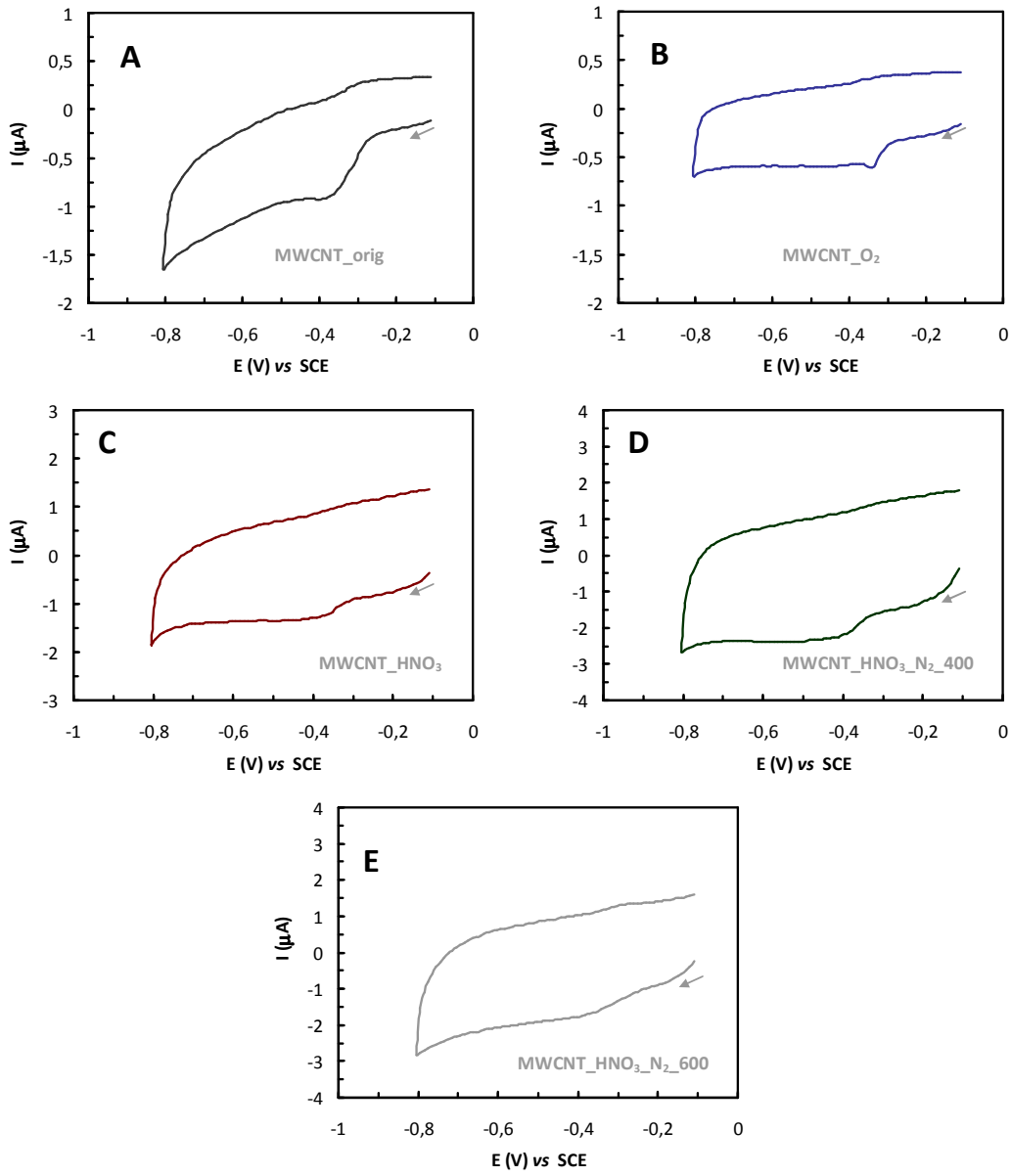


**Figure 4.8 -** Cyclic voltammograms of PG/5-MWCNT/ccNiR electrodes: **A)** MWCNT_orig (THF suspension), **B)** MWCNT_$O_2$, **C)** MWCNT_$HNO_3$, **D)** MWCNT_$HNO_3$_$N_2$_400 and **E)** MWCNT_$HNO_3$_$N_2$_600.

### 4.3.7) Bioelectrodes response to nitrite

All the PG electrodes prepared with the different samples of MWCNTs and c*c*NiR were tested in the presence of nitrite by cyclic voltammetry. The current-potential profiles were identical to those of the PG/SWCNT/c*c*NiR electrodes previously obtained (Figure 4.4). The catalytic response to nitrite was characterized in terms of the linear range, sensitivity within this linear range, maximum current and catalytic efficiency, defined as the ratio "maximum current (at saturating nitrite concentration 1 mM)/initial current" (Table 4.4). These parameters should reflect the material's "friendliness" for c*c*NiR activity.

**Table 4.4 -** Effect of the type of modified MWCNT on the bioelectrode response to nitrite. All electrodes were prepared with five layers of nanotubes on PG surfaces. *The CNT dispersion was prepared in THF.

| CNT sample | Linear range (µM) | Sensitivity ($mA.M^{-1}.cm^{-2}$) | $J_{max}$ ($\mu A.cm^{-2}$) | $I_{max}/I_{initial}$ |
|---|---|---|---|---|
| **MWCNT_orig *** | 1 - 200 | 431 ± 41 | 187 ± 26 | 120 |
| **MWCNT_$O_2$** | 1 - 100 | 1081 ± 120 | 807 ± 43 | 378 |
| **MWCNT_$HNO_3$** | 1 - 200 | 531 ± 49 | 287 ± 29 | 71 |
| **MWCNT_$HNO_3$_$N_2$_400** | 1 - 100 | 889 ± 87 | 308 ± 54 | 131 |
| **MWCNT_$HNO_3$_$N_2$_600** | 1 - 600 | 626 ± 43 | 1143 ± 67 | 199 |

The best results were obtained with the MWCNT_$O_2$ and MWCNT_$HNO_3$_$N_2$_600 bioelectrodes, which presented the highest maximum current densities and catalytic efficiencies. Interestingly, no direct correlation was observed between the initial current densities (non-catalytic) and the maximum current densities obtained in the presence of nitrite (catalytic). For example, although the MWCNT_$O_2$ electrodes produced the lowest currents in the absence of nitrite (Figure 4.8B), they displayed relatively high currents in its presence. Apparently, this material is not so good for heterogeneous ET, but is much more adequate for enzyme catalysis. The MWCNT_$HNO_3$_$N_2$_600 provided both high catalytic and non-catalytic currents, however seeing that the MWCNT_$O_2$ material provided the highest

sensitivity for nitrite and catalytic efficiency, it was chosen for further studies (see following sections).

In order to interpret the different behaviors of the bioelectrodes in respect to the surface properties of the CNTs, the maximum current densities (only for the modified MWCNTs) were plotted against their main surface properties, *i.e.*, the $pH_{PZC}$, the percentage of oxygen on the surface and the specific surface (Figure 4.9).

The surface area variation between nanotubes is quite small (476 to 508 $m^2g^{-1}$), and therefore should not be a major factor accounting for the differences on bioelectrode activity. Nonetheless, there does seem to be an increased enzyme activity when the MWCNTs have a higher surface area (Figure 4.9A). This could be related to the increasing availability of contact sites between the nanotubes and the enzyme molecules.

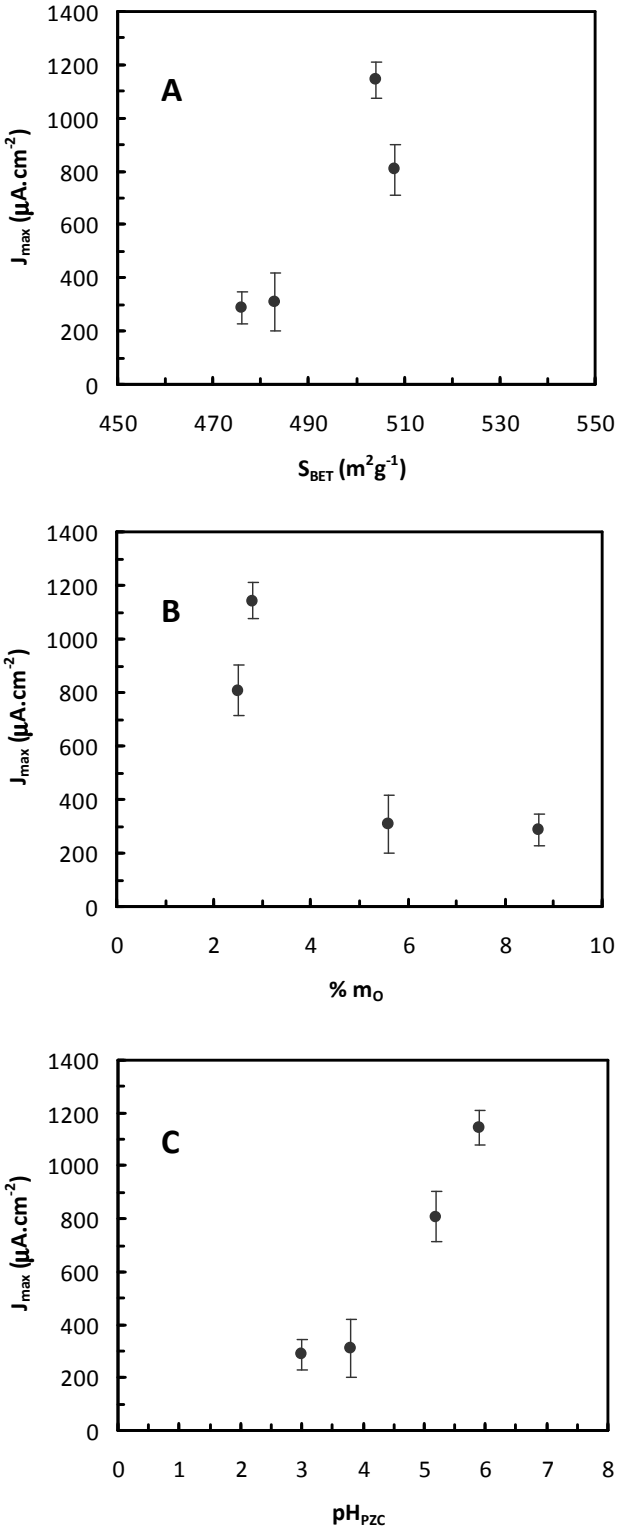


**Figure 4.9 -** Effect of the surface chemical properties of the MWCNT on the maximum currents obtained with PG/5-MWCNT/*cc*NiR electrodes. **A)** BET (Brunauer-Emmet-Teller) surface area, **B)** mass percentage of oxygen on the surface, **C)** point of zero charge.

Regarding the influence of mass percentage of oxygen on the MWCNT surface it can be observed in Figure 4.9B that a higher percentage of oxygen is related with lower $J_{max}$. Although it was expected that the presence of oxygenated groups could provide more compatible sites [140] for enzyme attachment it is probably the nature of these groups on the carbon surface and not their total amount that governs the interactions with the enzyme. Also, there is an inverse relation between the surface area of the nanotubes and mass percentage of oxygen on their surface [187] (see Table 4.3) and, as shown previously, the higher surface areas correlate with higher c*c*NiR catalytic activity.

The other property of the MWCNTs, the $pH_{PZC}$, is related to their acid-base character and is mainly governed by the type of oxygenated groups present. In this case, a less charged surface was more convenient for enzyme turnover (Figure 4.9C). At the pH used in these studies all the nanotubes should be negatively charged, however, the ones containing less acidic groups, *i.e.*, the MWCNT_$O_2$ and MWCNT_$HNO_3$_$N_2$_600, provided the highest currents. These were described as being rich in carbonyls, phenols and quinones groups (the last two mainly for the MWCNT_$O_2$) giving them a more neutral and basic character than the carboxylic acids and anhydrides rich materials MWCNT_$HNO_3$ and MWCNT_$HNO_3$_$N_2$_400. Apparently the surface charge had the strongest influence on the electrochemical response of the bioelectrodes.

### 4.3.8) Bioelectrode optimization

As expected from the previous study with SWCNTs, both the non-catalytic and catalytic currents of PG/MWCNT_$O_2$/c*c*NiR electrodes increased with the number of nanotubes layers (Figure 4.10), meaning that more material is available for immobilizing electroactive enzyme.

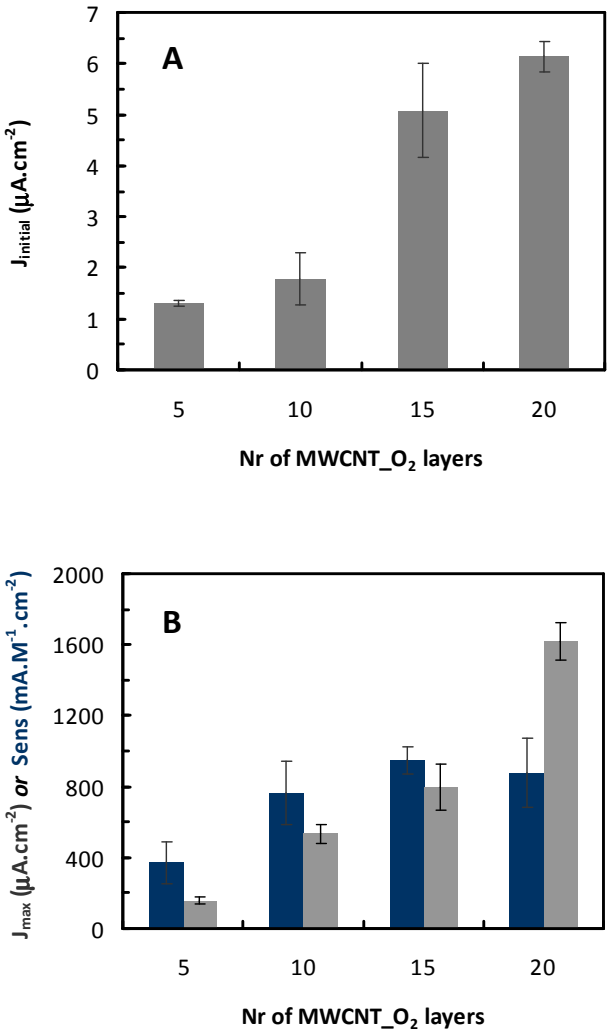


**Figure 4.10 -** Effect of the number of deposited nanotube layers on the non-catalytic and catalytic response of PG/MWCNT_$O_2$/*cc*NiR biosensors. **A)** Current density in the absence of nitrite (determined at -0.380 V *vs* SCE), **B)** (▒) Maximum current density values for nitrite reduction (measured at saturating concentrations of nitrite) and (■) sensitivity, as determined by the slope of the calibration curves.

Even at 20 layers of deposited material, the biosensor's performance still showed some improvement. The linear range was further extended: 1-400 to 1-800 µM for 15 and 20 layers respectively, and the maximum currents were also higher. This could indicate the presence of more enzyme in the 20 layer configurations. On the other hand, the sensitivity to nitrite stabilized between 15 and 20 layers of CNTs, demonstrating that at these experimental conditions (enzyme concentration) no further improvement was expected in

terms of substrate detection at low concentrations. The preparation of electrodes with 20 or more layers is rather tedious and not viable and therefore the 15 layer configuration was considered as a good balance, since it did show a rather important enhancement of cc*c*NiR's catalytic response. In the future, other methods should be considered for preparing the electrodes, such as co-deposition of mixtures of enzyme and highly concentrated dispersions of CNTs in a one-step biosensor preparation.

Given that the modifications in the nanotubes made them water dispersible, it was decided to prepare mixed films of enzyme and nanotubes, therefore simplifying the preparation of the biosensor. In order to achieve similar amounts of deposited material on the electrode highly concentrated dispersions of CNTs had to be prepared. However, this proved to be very difficult with some of the materials, which were unable to reach such high dispersion levels. One of the most important barriers related to the use of CNTs in electrochemistry is in fact the reproducible preparation of modified surfaces. This material has a high tendency to aggregate [140] due to the hydrophobicity of the carbon walls. It is therefore quite important to introduce modifications into these materials in order to improve both solubility and biocompatibility [137].

### 4.3.9) Morphological characterization

The SEM images of 15 layers of MWCNT_$O_2$ deposited over pyrolytic graphite disks and of the reproduction of the 15-MWCNT_$O_2$/cc*c*NiR electrodes (Figure 4.11) were very similar to the images obtained with the SWCNTs (Figure 4.1).

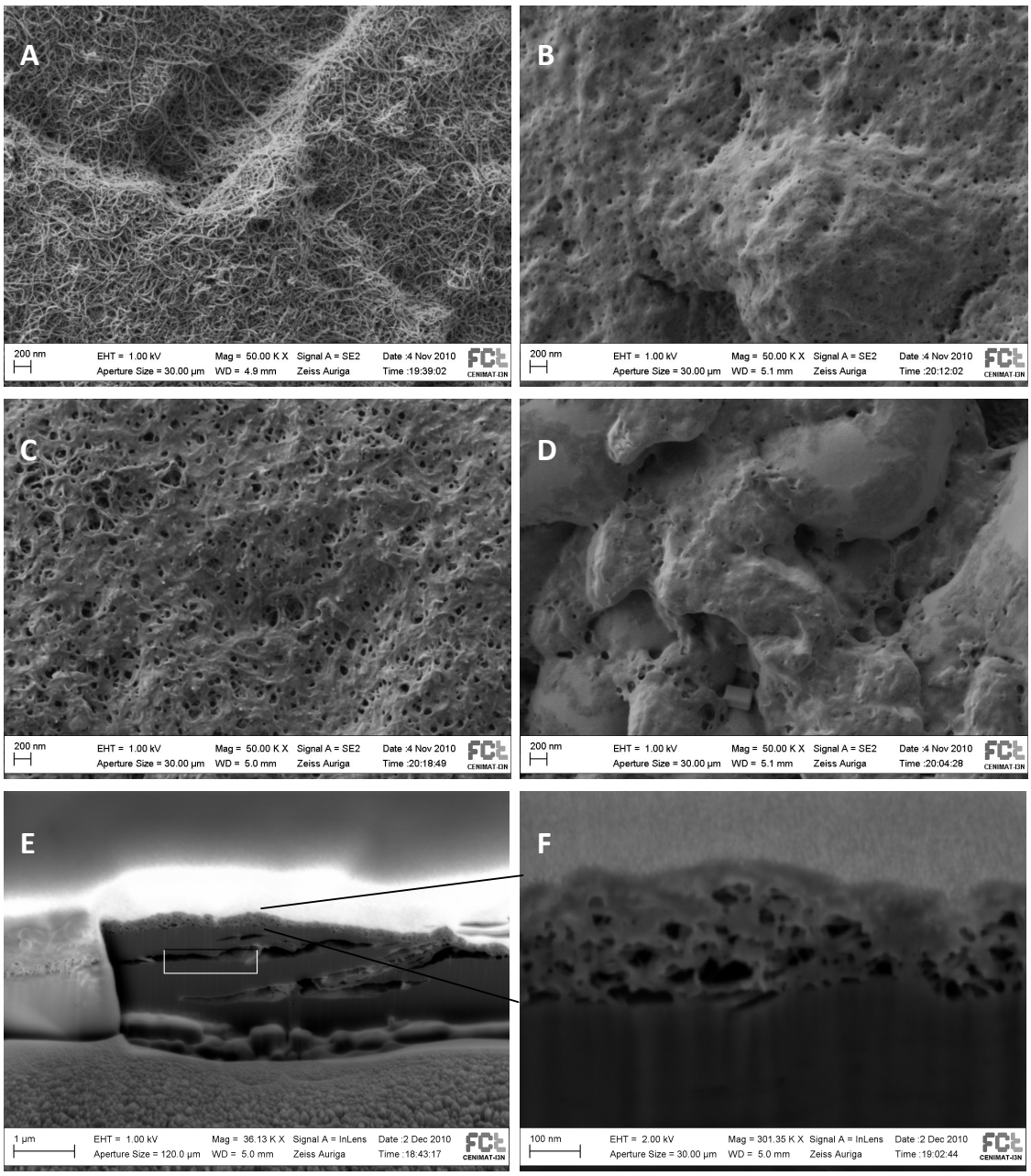


**Figure 4.11 -** Representative SEM images of MWCNT_$O_2$ and c*c*NiR deposited on pyrolytic graphite. **A)** 15 layers of MWCNT_$O_2$, **B)** same setup as (A) after c*c*NiR immobilization, **C)** mixed film of c*c*NiR and MWCNT_$O_2$; **D)** layer of c*c*NiR directly over the PG, **E)** sectional cut of setup (A), **F)** same sample at higher magnification.

The carbon nanotubes are disposed with no defined arrangement, creating a porous structure of intertwined material (Figure 4.11A). When covered with the c*c*NiR layer, the

underlying nanotubes deposits are somewhat recognizable, as suggested by the comparison between the MWCNT_$O_2$/c*c*NiR and c*c*NiR samples, Figures 4.11B and 4.11D, respectively. The sample containing the mixture of c*c*NiR and MWCNTs applied in one-step (Figure 4.11C) is intermediate to the one where the enzyme is added after the CNT deposition (Figure 4.11B) and the nanotubes alone (Figure 4.11A); the protein layer is easily identified, but it seems more intertwined with the nanotubes. This shows that the protein was able to enter/adsorb to the 3D network structure of the carbon nanotubes constituting a more uniform film. The sectional cuts of the control sample 15-MWCNT clearly reveal the porous network that is formed by the carbon nanotubes on the graphite electrode. The film is approximately 200 nm thick. Unfortunately it was not possible to obtain sectional images of the MWCNT_$O_2$/c*c*NiR electrodes – the beam appeared to destroy the enzyme layer.

## 4.4) Conclusions

The electrocatalytic response of cc*NiR can be enhanced to a great extent by using nanostructured electrodes based on carbon nanotubes. The CNT coatings provide a larger surface area and allow the immobilization of higher amounts of electroactive cc*NiR, thus amplifying interfacial electron exchange with this oxidoreductase.

When cc*NiR/CNTs films were deposited on pyrolytic graphite surfaces, the catalytic response was higher than the one obtained on glassy carbon. This highlights the excellent role of graphene based materials for promoting electron delivery to cc*NiR. It is worth to mention that very recently, a renewed interest has been devoted to graphene based electrodes for the construction of electrochemical (bio)sensors, mainly due their improved electrocatalytic efficiency [190].

In terms of direct electron transfer with the enzyme the carbon nanotubes did not facilitate the process, since the reduction potential of the enzyme was maintained while changing from a PG to a CNT modified electrode surface. The shape of the cyclic voltammograms of cc*NiR immobilized in a MWCNT_$O_2$ modified electrode in the absence of nitrite was slightly different from the usual broad band shape obtained for all other nanostructured materials and pyrolytic graphite itself. A defined peak shape was present at similar potentials in the PG/MWCNT_$O_2$/cc*NiR electrodes. This material probably had a different interaction with the enzyme, as later confirmed by a high catalytic efficiency of the enzyme deposited in this sample.

The amount of carbon nanotubes present in the CNT/cc*NiR bioelectrodes influenced their response to nitrite. Typically up to 9-12 and 15-20 layers, of 0.1 mg/mL dispersions of SWCNTs and MWCNT_$O_2$, respectively, the response to nitrite increased, stabilizing afterwards. This showed that the performance of the bioelectrodes is governed by the increased electrode surface area.

The higher amounts of nanotubes provided higher enzyme activities; though, the layer-by-layer deposition methodology is not feasible for more than 20 layers and so other types of preparation should be looked into. The possibility to use water dispersions in the case of the modified MWCNT samples is a great advantage in this respect since it enables the mixing of CNTs with enzyme and its application in a single step.

The bioelectrodes were simple and easy to prepare and provided a very sensitive method for electrochemical determination of nitrite. Regarding the SWCNTs/*cc*NiR electrodes, the presence of additional clay or polymer layers preserved efficiently the electroenzymatic activity of the device for several months. Although several other proposals of SWCNT-heme protein assemblies have been reported, this is the first association of CNTs with a reductase enzyme, according to the literature surveyed.

In what respects the different MWCNT samples, better results were obtained with higher surface area and less charged materials. Overall the presence of oxide surface groups on carbon nanotubes enabled better results, as confirmed by the higher activities obtained with all the MWCNTs treated samples, compared to the non-modified MWCNTs.

Regarding the surface characterization of these bioelectrodes, they are constituted by very porous structures with the enzyme layer being quite dominating, however without losing the underlying nanostructure. This suggests that the enzyme infiltrates the CNT films.

As shown in this chapter, CNTs are capable of facilitating protein electrochemistry. The modified electrodes provided a very sensitive method for the electrochemical determination of nitrite, contributing for the implementation of DET based biosensors. Nevertheless, it is important to keep in mind the difficulties of working with such materials, namely obtaining uniform and stable dispersions. Future endeavours should focus on preparing nanostructured surfaces in a controlled and robust manner aiming for the mass production of this type of devices.

# Chapter 5

# Cytochrome *c* nitrite reductase direct electron transfer in surfactant films

# Chapter 5 - Cytochrome *c* nitrite reductase direct electron transfer in surfactant films

## 5.1) Introduction

The immobilization of proteins in surfactant films has been indicated as a good approach to promote electron transfer with electrodes. Research studies have shown that the films are quite stable in aqueous solution and that the proteins can retain their native structures [191-193]. This strategy has been widely used in the study of the redox properties of proteins and has potential for application in biosensors and bioreactors [194-198].

Surfactants are surface active agents composed of a charged or polar head group and a hydrophobic nonpolar tail. The tail is generally a hydrocarbon chain with 6-22 carbon atoms. The hydrophilic region of the molecule – the head group – may be positive, negative, neutral or zwitterionic, thus categorizing the surfactant as cationic, anionic, nonionic or zwitterionic [199-200]. Surfactants can behave as detergents which are indispensable to the isolation and purification of membrane proteins and are also commonly used for protein crystallization [199-200]. The steroid based surfactants (*e.g.* cholic acid) usually lead to less inactivation of proteins when compared to linear hydrocarbon compounds with similar headgroups. Surfactants with longer hydrocarbon chains are also less prone to denature proteins than short chained compounds. Zwittergents (amphoteric sulfobetaines) are usually more inactivating than non-ionic reagents [199-200].

Surfactant molecules can be adsorbed at the interface between two bulk phases, such as the electrode/solution interface; they lower the interfacial tension between the two and facilitate the contact. Therefore, these surface active agents are capable of modifying and controlling electrode surface properties [197]. Surfactant molecules can aggregate to form supra-molecular structures with specific regions of hydrophilic and hydrophobic character. In aqueous solution, above the critical micellar concentration (CMC), they form spherical micelles with the hydrophilic head groups facing the solution and the hydrocarbon chains oriented towards the interior of the structure (Figure 5.1A) [200]. The CMC is characteristic of each surfactant and in addition to micelle formation it is also correlated with abrupt

changes or sharp discontinuities in the physical properties of the surfactant, such as conductivity and surface tension.

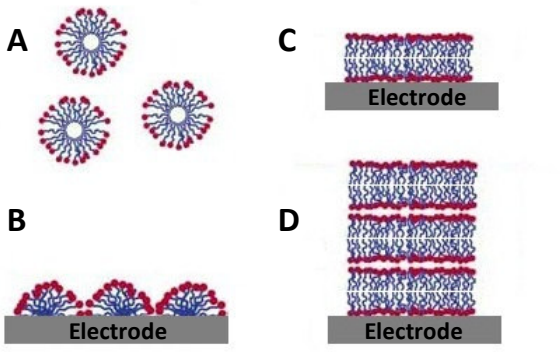


**Figure 5.1 -** Schematic representations of surfactants in various forms, the headgroups are represented by the red circles and the hydrophobic tails are in blue. **A)** Spherical micelles, **B)** hemimicelles, **C)** bilayers and **D)** multilayers on electrode surfaces.

Surfactants are able to adsorb at the electrode/solution interface at concentrations lower than the CMC. For ionic surfactants, close and above the CMC bilayers and surface micelles are formed, and well above that value multilayers are present (Figure 5.1) [197]. The surfactant films are usually prepared from solutions or dispersions (aqueous or organic solvent based) which are cast onto the electrode surfaces. After solvent evaporation, a water-insoluble multi-bilayered film structure is formed (self-assembled). These films resemble biomembranes stacked on solid electrodes and thus provide a biomembrane-like environment to the proteins [193,201]. Ionic surfactants such as didodecyldimethyl ammonium bromide (DDAB), dihexadecyl-phosphate (DHP), cetyltrimethylammonium bromide (CTAB) and dimyristoylphosphatidyl-choline (DMPC) are the most commonly used for electrode modification [201]. The structures of these and other surfactants used in the work described in this chapter are shown in Figure 5.2.

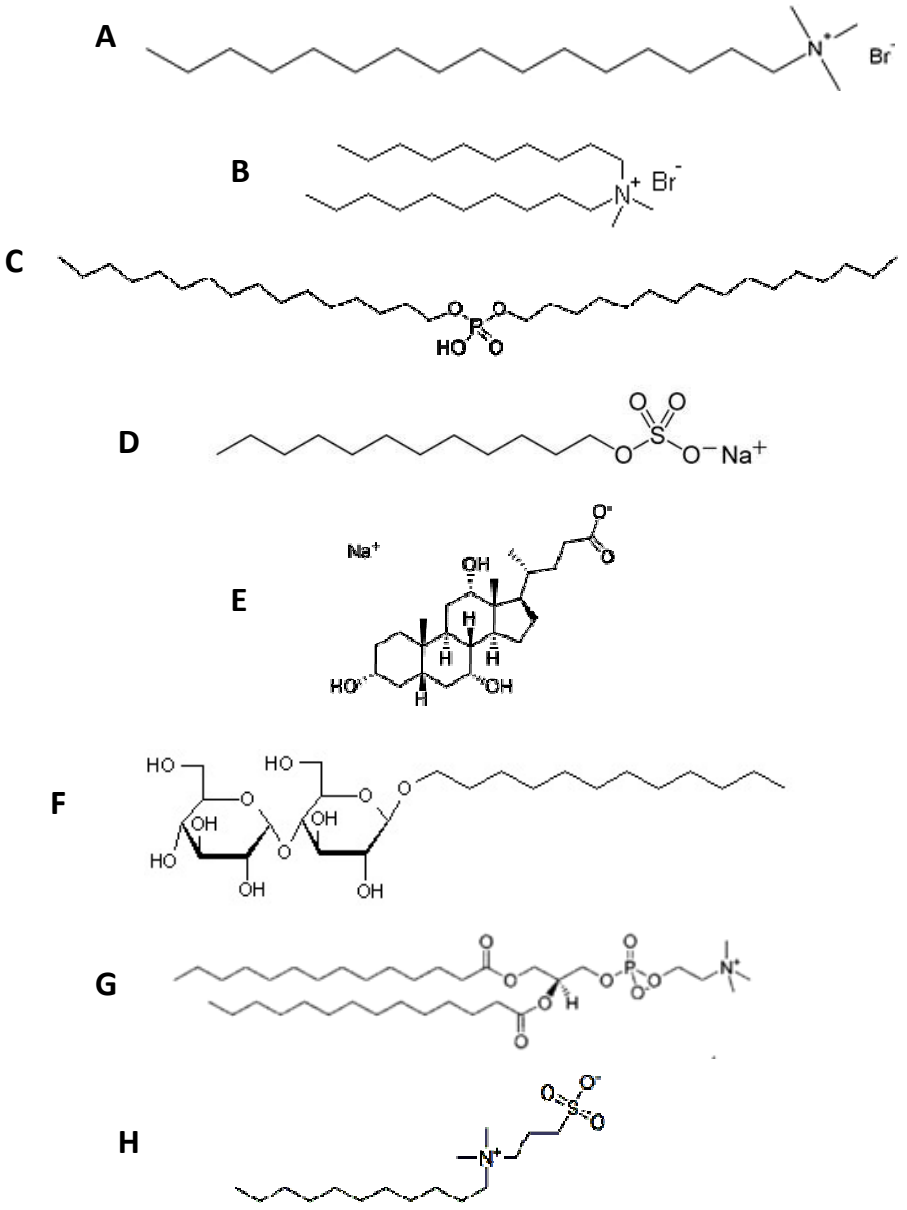


**Figure 5.2 -** Surfactant structures. Cationic head group: **A)** CTAB, **B)** DDAB; anionic: **C)** DHP, **D)** SDS, **E)** sodium choleate; non-ionic: **F)** DDM (n-dodecyl-β-D-maltoside); amphoteric: **G)** DMPC, **H)** Zwittergent 3-10.

Electrochemistry mainly takes advantage of two properties associated with these surface active agents: their ability to adsorb at interfaces and to generate membrane-like structures [197]. The proteins incorporated in surfactant films are expected to experience a more natural environment, closer to the physiological surroundings they are taken from.

Accordingly, surfactant films can help to promote and enhance protein electrochemistry and catalysis. Obvious cases are membrane-bound proteins [193], such as the enzyme employed in this thesis. Various soluble proteins have also shown enhanced electron transfer in surfactant films [192,194,197,202]. Myoglobin and cytochrome P450, for example, have showed good reversible electrochemistry in surfactant films of DDAB and DMPC at PG electrodes, as opposed to the bare ones, where no DET was observed. According to spectroscopic studies, both proteins were also able to keep their native conformations while embedded in the films [191,193,195-196].

The good performance of proteins in surfactant films has been associated to the strong adsorption of the surfactant at the electrode-film interface, therefore avoiding the denaturative adsorption of proteins or of other macromolecules that could block electron transfer [195]. Also, the well-defined microstructure and dynamics of the surfactant films, allows good diffusion within the layer. These films can also help to guide the orientation of immobilized proteins. This orientation may not be related with the surfactant headgroup charge but with the interaction between the protein and the hydrophobic bilayers [196,203]. Other advantages attributed to surfactant films are the increased degree of reversibility conferred to the electrochemical signals, the possibility to study the proteins both electrochemically and optically, the reduced amounts of sample required to prepare the films, their stability and the similarities with biomembranes [193,201].

The nature of the surfactant can have a strong impact on the redox properties of the protein. On one hand, electron transfer rates and catalysis are enhanced, on the other hand shifts in redox potentials can also be observed. These are probably associated with surfactant – protein interactions and with an electrical double-layer effect over the potential experienced by the proteins at the electrode-film interface [193].

This chapter reports the direct electrochemical response of *cc*NiR in surfactant cast films of DDM (n-dodecyl-β-D-maltoside), Zwittergent 3-10, SDS, sodium choleate, DDAB and CTAB. Owing to its location in the cell membrane, *cc*NiR is rather hydrophobic and is purified as high molecular weight aggregates [67]. Accordingly, the study of this enzyme is expected to benefit from mimicking its physiological hydrophobic environment. In addition, the use of surfactants is expected to disrupt the protein aggregates, thus allowing a different

interaction with the electrode, and possibly exposing different areas of the protein and specific heme groups. The enzyme was immobilized in surfactant films casted on pyrolytic graphite working electrodes. The redox activity of the enzyme in the absence and presence of substrate was characterized by electrochemical techniques. In addition to electrochemistry, UV-Vis spectroscopy was used to monitor the integrity of cc*NiR*.

## 5.2) Experimental

### 5.2.1) Reagents

cc*c*NiR was purified from *D. desulfuricans* ATCC 27774 cells as described in Annex 1. The specific activity was 300 U/mg and the protein content 1.0 mg/mL, in 0.1 M phosphate buffer pH 7.6. Sodium nitrite (Merck), tris(hydroxymethyl) aminomethane (Merck), potassium chloride (Merck), ethanol (Panreac), hydrochloric acid (Riedel-de-Haen), sodium hydroxide (Merck) sodium acetate (Merck), MES, HEPES, TAPS, CAPS (all from Sigma), Zwittergent 3-10 (Sigma), sodium dodecyl sulphate (Sigma), didecyldimethylammonium bromide (Aldrich), n-dodecyl-β-D-maltoside (Calbiochem), CTAB (Sigma), cholic acid (Sigma), sodium dithionite (Merck) were all analytical grade and used as received. Solutions were prepared with deionized water (resistivity 18 MΩcm) from a Millipore MilliQ water purification system.

### 5.2.2) Biolectrode preparation

The PG electrodes (self-made in glass tubes, with 4 mm diameter disks) were polished with alumina slurry (0.3 μm) from Buehler, thoroughly washed with water and ethanol and ultra-sonicated in deionized water for 5 min. Finally, the electrodes were washed with water and dried with compressed air.

cc*c*NiR–surfactant solutions were prepared by mixing 1.0 mg/mL of enzyme with 2 times the CMC of each surfactant (see Table 5.1). These mixtures were then incubated at room temperature (22 ± 2°C) for 30 minutes. Subsequently, 7.5 μL (6 μg of cc*c*NiR) of mixture were applied to the PGE and left to dry at room temperature for *ca.* 45 min. When not in use the electrodes were stored dry at 4°C.

**Table 5.1 -** Surfactant critical micellar concentrations.

| Surfactant | Type | CMC (mM) |
|---|---|---|
| **DDM** | Non-ionic | 0.18 |
| **Zwittergent 3-10** | Amphoteric | 32.5 |
| **SDS** | Anionic | 8.1 |
| **Cholic acid** | Anionic | 14 |
| **DDAB** | Cationic | 0.16 |
| **CTAB** | Cationic | 1.0 |

### 5.2.3) Electrochemical measurements

An Autolab PSTAT 12 potentiostat, monitored by the control and data acquisition software GPES 4.9, both from EcoChemie, was used for the electrochemical measurements. A Metrohm three electrode electrochemical cell consisting of a Radiometer Ag/AgCl reference electrode, a Pt counter electrode (also from Radiometer) and a self-made PGE was used. The supporting electrolyte (20 mL of 0.1 M KCl in 0.05 M tris-HCl buffer pH 7.6) was thoroughly purged with argon for 20 minutes. All experiments were performed at room temperature (22 ± 2°C).

The cyclic voltammetry experiments were performed with a 2.5 to 250 mV/s scan rate in a potential window of -0.1 to -0.8 V. To evaluate the response to nitrite, standard solutions of sodium nitrite (0.01, 0.1 and 1 M) were successively added to the cell. After each addition the cell was again purged with argon for *ca.* 30 s and the CV was recorded (20 mV/s). Nitrite catalytic currents were determined at the inversion potential -0.8 V.

The pH studies were performed in 0.1 M KCl in a universal buffer composition (sodium acetate, MES, HEPES, TAPS and CAPS) prepared at different pH values.

The values presented in the graphs and tables represent the average of three assays; error values and bars correspond to the standard deviation. All potentials are relative to the Ag/AgCl reference electrode (-197 mV *vs* NHE), unless stated otherwise.

### 5.2.4) UV-Vis spectroscopy

UV-vis spectroscopy was performed on a Shimadzu UV1800 spectrophotometer. The protein (*ca.* 0.1 mg/mL) was incubated for one hour with each detergent, at a final concentration of 2XCMC, in 0.1 M phosphate buffer pH 7.6. The UV-Vis spectra were then measured on a quartz cuvette (UV-Vis). Afterwards, sodium dithionite was added to the cuvette, to completely reduce the enzyme, and new spectra were taken.

## 5.3) Results and discussion

### 5.3.1) Non-catalytic direct electrochemistry of ccNiR in surfactant films

All the surfactants tested were used in a concentration corresponding to 2xCMC to ensure that biomembranes could be formed on the electrode from the micelles in solution and, in this way, equivalently compare the effects of the surfactants on the enzyme's electrochemical response. Cyclic voltammograms of ccNiR–surfactant films casted on PG electrodes are shown in Figure 5.3. While for SDS, DDM, cholic acid, Zwittergent 3-10 and ccNiR electrodes a single small and broad wave is observed in the cathodic scan at *ca.* -0.4 V, the cationic surfactants CTAB and DDAB CVs show well-defined peaks in both the reduction and oxidation scans at *ca.* -0.380 V and -0.250 V, respectively (scan rate 20 mV/s).

The enzyme's signal in the non-ionic, amphoteric and anionic detergents was identical to the control electrode (adsorbed ccNiR film only, Figure 5.3G) and also to the non-catalytic redox wave observed in both previously described immobilization systems: sol-gel (Chapter 3) and carbon nanotubes (Chapter 4). The peak potential was never shifted, no matter the surfactant type.

For the cationic surfactants, the signals were comparable with the previously reported non-catalytic peaks of ccNiR, obtained on edge orientated pyrolytic graphite with direct adsorption at the electrode surface (at pH 7 and 20°C the $E_{pc}$ and $E_{pa}$ peak potentials were -0.340 V and -0.280 V *vs* Ag/AgCl, respectively) [76].

The reported studies on heme proteins, like hemoglobin and myoglobin, considered that the DDAB surfactant films could favor a specific orientation of the proteins embedded in them, due to interaction with the cationic head group or the hydrocarbon chains of DDAB [195-196]. Since the cationic surfactants (DDAB and CTAB) produced CVs with peaks on both reduction and oxidation scans, this could indicate that the positively charged head groups of these compounds may influence the DET of ccNiR.

A pertinent factor for the enhanced electron transfer of the ccNiR–surfactant based bioelectrodes must be the hydrophobic environment provided by the films, certainly very suitable for the immobilization of this membrane associated protein. DDAB was the only insoluble surfactant used in this work and its cast films have proved to be highly stable [193] therefore they provided the most favorable microenvironment for the DET of ccNiR.

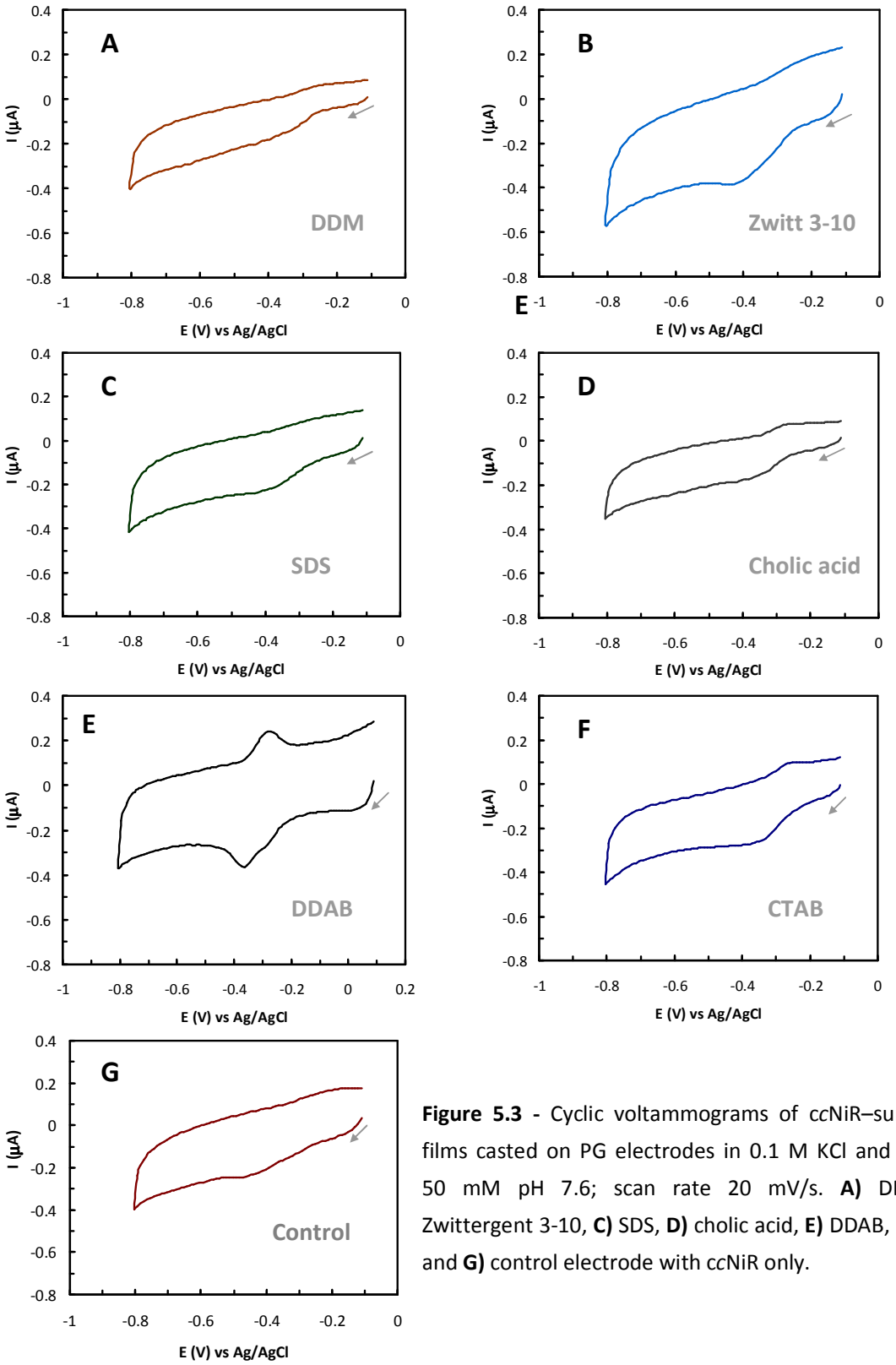


**Figure 5.3 -** Cyclic voltammograms of *cc*NiR–surfactant films casted on PG electrodes in 0.1 M KCl and tris-HCl 50 mM pH 7.6; scan rate 20 mV/s. **A)** DDM, **B)** Zwittergent 3-10, **C)** SDS, **D)** cholic acid, **E)** DDAB, **F)** CTAB and **G)** control electrode with *cc*NiR only.

Due to the novel features displayed by c*c*NiR in the DDAB films its electrochemical behavior was further investigated. Compared with other surfactants, DDAB greatly enhanced the DET of c*c*NiR with the PG electrode.

Figure 5.4A shows cyclic voltammograms of the c*c*NiR–DDAB films at different scan rates.

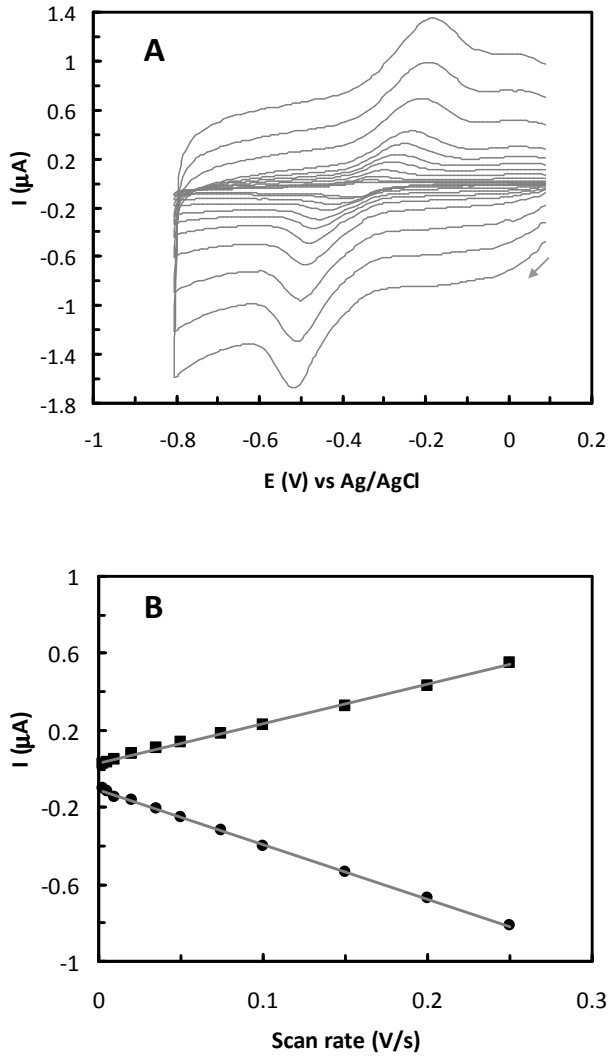


**Figure 5.4 - A)** Cyclic voltammograms of PG/c*c*NiR–DDAB electrode in 0.1 M KCl and 50 mM tris-HCl buffer pH 7.6 at different scan rates; from inside to outside: 0.0025, 0.005, 0.01, 0.02, 0.035, 0.05, 0.075, 0.1, 0.15, 0.2, 0.25 $V.s^{-1}$, respectively. **B)** Linear dependence of the cathodic (●) and anodic (■) peak currents on the potential scan rate. Linear regressions y = -2.85x - 0.11, $R^2$ = 0.999 and y = 2.05x + 0.03, $R^2$ = 0.998, respectively.

The cathodic and anodic peak currents increased linearly with scan rate which is consistent with a diffusionless electrochemistry (Figure 5.4B). The enzyme is thought to be adsorbed since no deviation from linearity is observed between peak current and scan rate up to 1 V/s (Figure 5.4B only shows up to 0.250 V/s). Nevertheless, even at slow scan rates the difference between cathodic and anodic peak potentials was quite high ($\Delta E_p$ = 141 mV at 20 mV/s) and increased with scan rate. This is the expected behavior for kinetically challenged electron transfer and shows that the electrode reaction is electrochemically non-reversible. In addition, there is a decrease in the area of the cathodic peaks with scan rate, which indicates that the protein is not adsorbed on the electrode [76] and that there could be in fact some diffusion within the DDAB film. This is consistent with the fluidity encountered in DDAB films in lamellar liquid crystal phase; this fluidity facilitates movement of proteins during voltammetry [204]. Diffusion-controlled electrochemistry has been observed for thick films (20 μm) of myoglobin in DDAB films; thin surfactant films, on the contrary, are characterized by thin-layer voltammetry [204]. No studies have been performed at this time to determine the cc*NiR–DDAB film thickness. Assuming that a cc*NiR monolayer contains 5 pmol.cm$^{-2}$, as predicted in reference [77] and the surface coverage was 73 pmol.cm$^{-2}$ (see below), it is expected that multiple layers of enzyme are formed.

Besides the increase of $\Delta E_p$ with scan rate, the ratio of cathodic peak current over the anodic one was *ca.* 1.5-2 and the widths at half height of the reduction signal were greater than that expected for an ideal one electron process ($\Delta E_{1/2}$=90 mV) varying between 120 and 170 mV, for the cathodic peaks and between 100 and 180 mV, for the anodic peaks. Based on this data the direct electrochemistry of cc*NiR in the DDAB surfactant films was considered to proceed by a quasi-reversible process.

The midpoint between the $E_{pc}$ and $E_{pa}$ values was practically constant over scan rates up to 250 mV/s. This average potential (-0.365 ± 8 mV *vs* Ag/AgCl), for the complex electrochemical signal, was quite similar to the reported non-catalytic signals of cc*NiR on edge pyrolytic graphite surfaces [76].

The surface concentration of cc*NiR in DDAB films was determined by integration of the cathodic non-catalytic peaks at low scan rates (<20 mV/s) using the method previously described in Chapter 2 (sections 2.2.2.3 and 2.3.2) [76]. This method considers that the

complete reduction of a $\alpha_2\beta$ complex of c*c*NiR involves 14 electrons (10 from the NrfA subunits and 4 from NrfH). The surface concentration of c*c*NiR in the DDAB films was determined to be 73 pmol.cm$^{-2}$. This accounts for 15% of the total amount of enzyme deposited on the electrode, suggesting that some protein may be lost or could remain not responding in the film. Similar electroactivity yields have been previously reported for heme proteins (*e.g.* hemoglobin) in DDAB surfactant films [194-195,202]. Taking into consideration that the only reversible non-catalytic signals reported for c*c*NiR were obtained with highly concentrated enzyme solutions (100 μM – 2 pmol applied) the DDAB surfactant film provides a suitable environment for the study of this protein using solutions of much lower concentration (*ca.* 6 μM – 0.3 pmol).

The pH of the buffer solution influences the electrochemistry of the c*c*NiR–DDAB films (Figure 5.5). An increase in pH has caused a negative shift in potentials for both the oxidation and reduction peaks. The potentials varied linearly with pH from 4 to 10.4 with a slope of -53.2 mV pH$^{-1}$ (Figure 5.5B), which is reasonably close to the theoretical value of -59 mV pH$^{-1}$ at 25°C indicating that a single proton transfer was coupled to the electron transfer. No obvious p$K_a$ was observed, as previously seen with the pH dependence of the broad non-resolved peaks of c*c*NiR in PG edge electrodes [76]. Such non-specific pH variation was assumed to be a result of the reduction of all of c*c*NiR's 14 heme groups, including the catalytic center, as probably is the case for the signals obtained herein.

Nonetheless, the possibility that the redox activity of one or more hemes is being favored in relation to the others should not be excluded. In fact, when low scan rates are used with the c*c*NiR–DDAB films, the cathodic wave reveals the presence of a second signal (a small shoulder can be observed in Figure 5.3E) at *ca.* -0.280 V, enforcing the idea that the electrochemical signals are a result of interaction and/or overlapping between multiple redox centers. This feature was not present in the anodic peak suggesting that the reaction being monitored is not completely reversible.

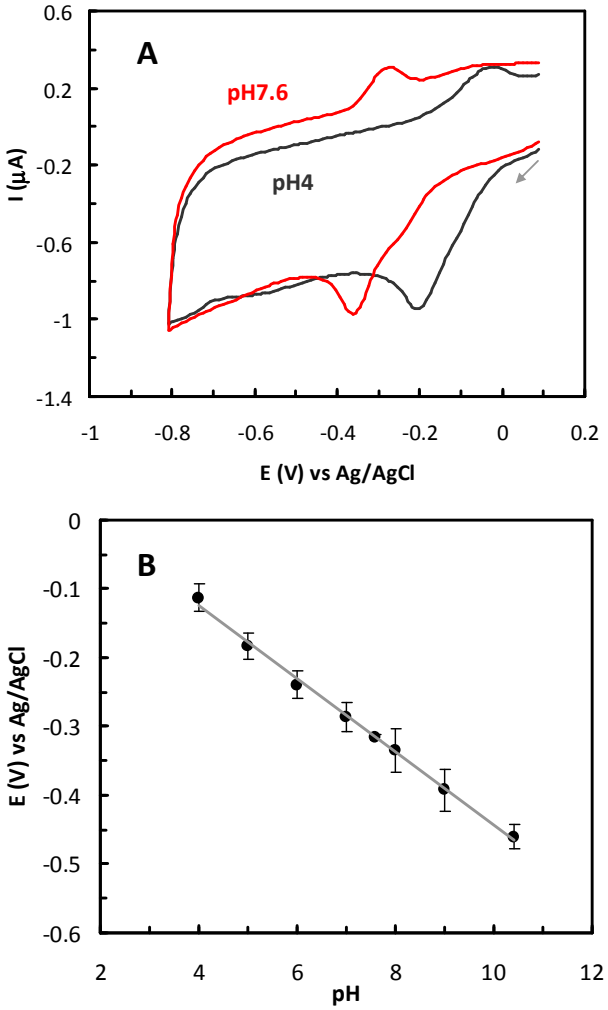


**Figure 5.5 -** Change in the potential of *cc*NiR's signal in DDAB films as a function of pH. **A)** Cyclic voltammograms of PG/*cc*NiR–DDAB electrode at pH 7.6 and pH 4; scan rate 20 mV/s. **B)** Linear dependence of the formal potential of the redox couple depicted in **A** on the pH. Linear regression $y = -0.0532x - 0.0885$, $R^2 = 0.997$.

### 5.3.2) UV-vis characterization of *cc*NiR in the presence of surfactants

A UV-vis characterization of the enzyme was performed in the presence of all tested compounds as a primary attempt to uncover any changes on the enzyme structure that may account for the unusual voltammetric responses (Figure 5.6).

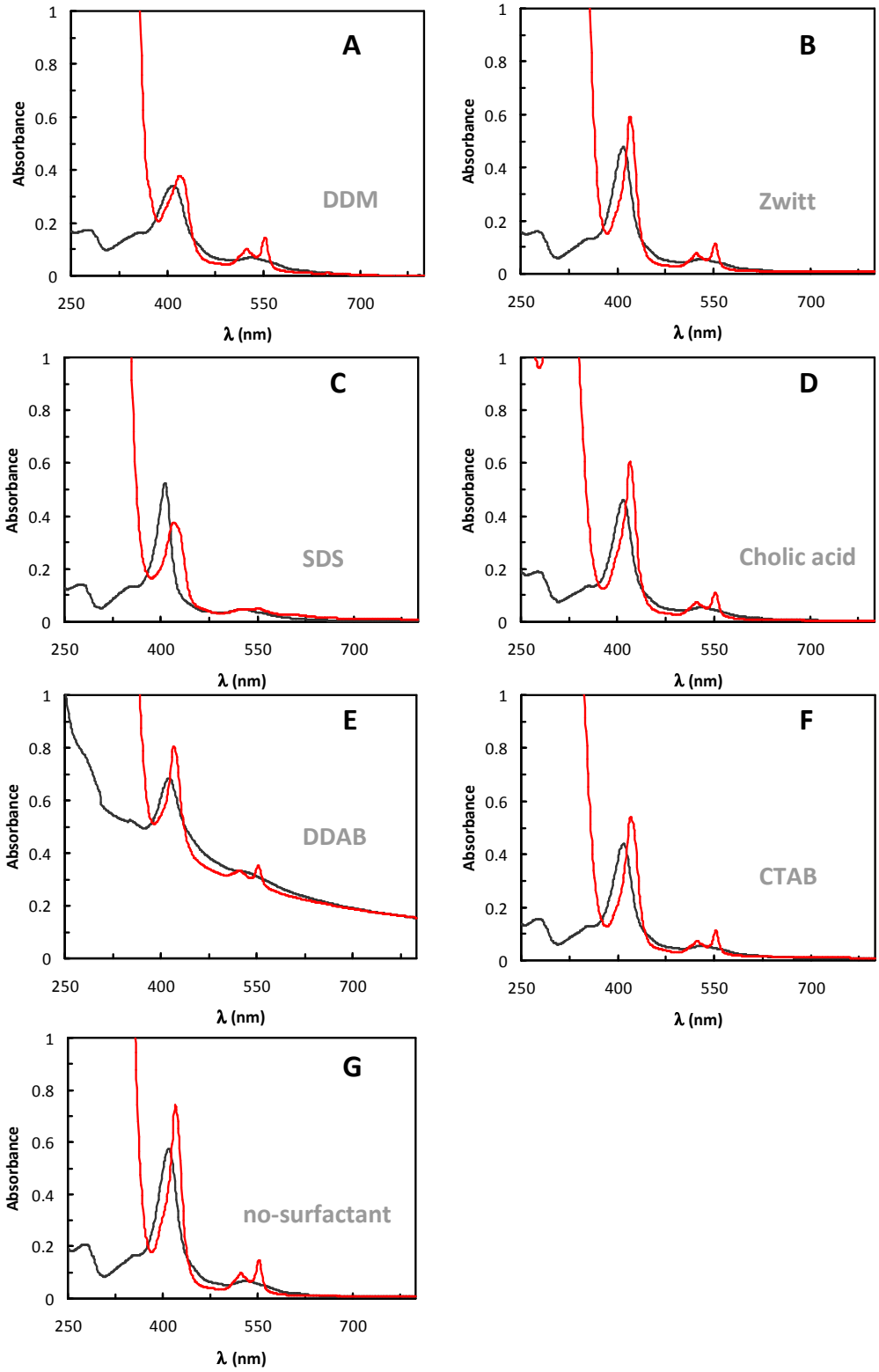


**Figure 5.6 -** UV-Vis spectra of **(gray line)** oxidized and **(red line)** dithionite reduced **A)** *cc*NiR–DDM, **B)** *cc*NiR–Zwittergent 3-10, **C)** *cc*NiR–SDS, **D)** *cc*NiR–cholic acid, **E)** *cc*NiR–DDAB, **F)** *cc*NiR–CTAB and **G)** *cc*NiR solutions after one hour incubation in 0.1 M phosphate buffer pH 7.6. Enzyme concentration was 0.1 mg/mL and surfactants were 2XCMC (*cf.* Table 5.1).

The position, intensity and width of the Soret absorption bands of heme proteins can be used as a measure of their possible denaturation [131,205]. The UV-Vis spectra in Figure 5.6 show that both oxidized and reduced spectra of cc*c*NiR are not affected by the majority of the surfactants, since there are no shifts in the absorption bands and their widths are also kept constant. Hence, no loss of enzyme integrity is expected. However, two surfactants do have particular spectra: SDS and DDAB.

The cc*c*NiR oxidized spectrum in SDS does not seem to be different but the reduced one is; although the absorption maxima are maintained, the Soret band is broadened and the overall absorption intensities diminish (Figure 5.6C). SDS is able to separate the subunits of cc*c*NiR and leads to partial denaturation of the enzyme but strikingly, it retains its nitrite activity [67]. SDS can possibly contribute to protein unfolding and consequently the heme spectroscopic signals are affected. Soret band broadening and decreased intensity was also observed for cytochrome P450 BM3 in SDS films. However, in that case, it was also accompanied by shifting to lower wavelengths as an indication of protein denaturation [206].

In the presence of DDAB the peaks corresponding to the Soret, $\alpha$ and $\beta$ bands of a typical cythochrome *c*-type protein, are neither shifted nor widened, in fact, the only change in the spectrum (Figure 5.6E) is a highly absorbing baseline. After several control experiments with all the components of the enzyme solution (ammonium sulfate and sodium choleate from the purification stages and the phosphate buffer) combined with the surfactant, no reasonable explanation was found.

In conclusion it seems that cc*c*NiR retains its native state in the presence of these surfactants and in the electroactive films. Most likely the surface active agents are disrupting the high molecular weight hydrophobic aggregates of the purified protein, but they are not affecting its structure. No further studies concerning the alterations induced by these compounds on the protein conformation were performed at this point. In fact, the main purpose of the work was to determine if the enzyme–surfactant films could in some way help improve the catalytic activity of cc*c*NiR. The electroactivity of the enzyme for nitrite was thus tested.

### 5.3.3) Nitrite reduction by *cc*NiR - surfactant films

The nitrite reducing activity of *cc*NiR–surfactant films on PG electrodes was evaluated by cyclic voltammetry in the presence of different concentrations of nitrite. This study was performed with only one of each type of surfactant: the non-ionic DDM, the amphoteric Zwittergent 3-10, the anionic SDS and the cationic DDAB. *cc*NiR was electroactive in all of the surfactant films. The voltammetric response had similar characteristics to the one obtained for sol-gel and CNT based bioelectrodes discussed in Chapters 3 and 4. The reduction peak current of *cc*NiR increased with the amount of nitrite in the cell as can be seen in Figure 5.7 CVs. The catalytic current increase was followed by a shifting peak potential to more negative values and eventually reached a limiting value, the typical behavior of enzyme saturation kinetics.

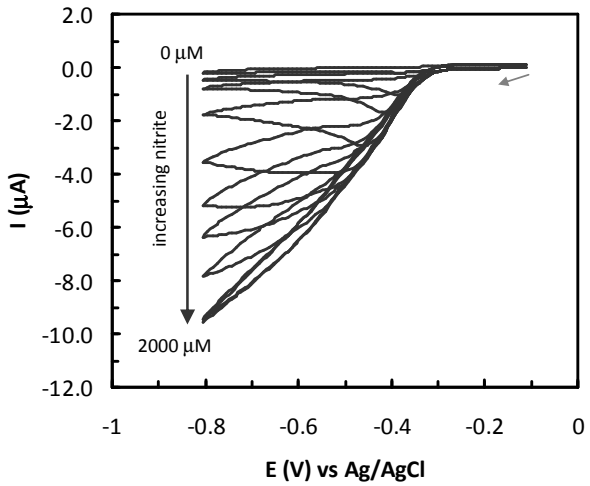


**Figure 5.7 -** Cyclic voltammograms of a PG/*cc*NiR–DDAB bioelectrode in the presence of varying nitrite concentrations.

The performance of the bioelectrodes was assessed and compared according to the sensitivity to nitrite, maximum current at saturating nitrite concentration (> 0.8 mM), lower limit of detection, amplitude of the linear range and catalytic efficiency (Table 5.2). The latter was expressed as the ratio of the reduction peak current in the presence and absence of nitrite ($J_{max}/J_0$).

**Table 5.2 -** Analytical characterization of PG/ccNiR–surfactant bioelectrodes.

| Surfactant | Linear range (μM) | Sensitivity ($mA.M^{-1}.cm^{-2}$) | Limit of detection (μM) | $J_{max}$ ($\mu A.cm^{-2}$) | $J_{max}/J_0$ |
|---|---|---|---|---|---|
| **No-surfactant** | 0.25 - 50 | 333 ± 30 | 0.113 | 27 ± 4 | 24 |
| **DDM** | 0.25 - 400 | 444 ± 30 | 0.184 | 267 ± 53 | 148 |
| **Zwittergent 3-10** | 0.25 - 400 | 394 ± 18 | 0.233 | 229 ± 34 | 140 |
| **SDS** | 0.25 - 150 | 346 ± 41 | 0.123 | 76 ± 14 | 47 |
| **DDAB** | 0.25 - 200/400 | 405 ± 66 | 0.229 | 75 ± 20 | 41 |

The ccNiR activity was improved with all the surfactants tested when compared to the control electrode with no surfactant. The sensitivity of the enzyme for nitrite increased only slightly with SDS, but for all other surfactants there were up to 20-30% increments (Figure 5.8). The improved performance of the ccNiR–surfactant films is clear when looking at the maximum current density values (Figure 5.9); these are far superior to the response of the control electrodes. With DDM and Zwittergent 3-10 almost ten times higher currents were observed, while for SDS and DDAB the response was more than a doubled.

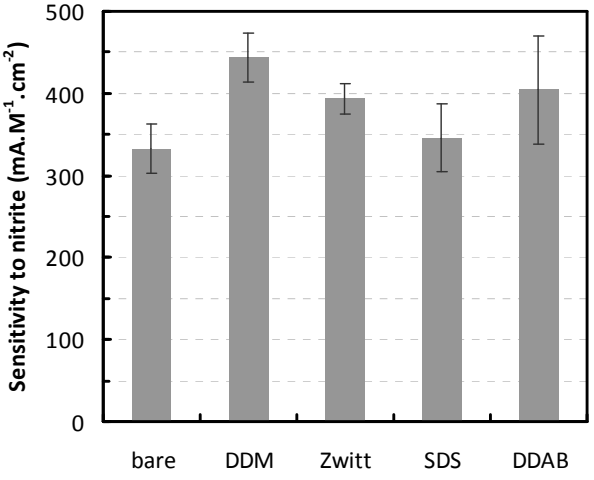


**Figure 5.8 -** Effect of surfactant type on the sensitivity of PG/ccNiR–surfactant bioelectrodes, as defined by the slope of the linear part of the calibration curve. Surfactant concentration was 2XCMC. Zwitt – Zwittergent 3-10.

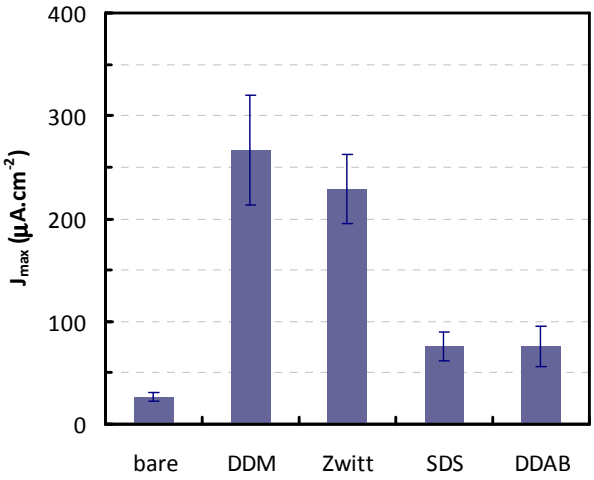


**Figure 5.9 -** Effect of surfactant type on the maximum current densities of PG/*cc*NiR–surfactant bioelectrodes at saturating nitrite concentrations (>0.8 mM). Surfactant concentration was 2XCMC. Zwitt – Zwittergent 3-10.

The catalytic currents had an extended linear correlation with the concentration of nitrite with all surfactants in comparison with the direct immobilization of *cc*NiR on the bare PGE (Table 5.2). This is due to the effect of the surfactant films on those bioelectrodes; they increased the diffusion barrier of nitrite to the immobilized enzyme. The linear range of the calibration curves was 0.25 – 400 µM with DDM and Zwittergent 3-10, and somewhat lower for the other two surfactants. The detection limits were similar on all bioelectrodes (*ca.* 0.1 - 0.2 µM). The catalytic efficiency followed the same trend of the other analytical parameters indicating DDM and Zwittergent 3-10 as the most appropriate surfactants to enhance *cc*NiR catalytic activity.

Overall, the nature of the surfactant affected nitrite catalysis. The specific interaction of *cc*NiR with each surfactant, governed by electrostatic effects like the local hydration, charge/nature of the head groups, electrolyte, etc., resulted in different response magnitudes. The ionic detergents were less suited than the non-ionic and zwiterionic for the enhancement of enzyme's activity. On the other hand, the biomembrane-like structures of the surfactant films provide more suitable surroundings for *cc*NiR. Apparently, this hydrophobic environment supplies a quite relevant contribution for the improvement of the activity.

In spite of providing good non-catalytic signals, DDAB did not confer a particularly high nitrite reducing activity. The response with both ionic surfactants, DDAB and SDS, was in fact lower than with the non-ionic and zwitterionic compounds. In the case of cc*c*NiR–SDS films it was expected that the enzyme would be active from previous activity tests performed in the presence of this compound [67]; nevertheless, it is interesting to notice that the nitrite catalysis was increased relatively to the control bioelectrode with no surfactant film, despite the partial denaturation. For sure, SDS disintegrates the large protein aggregates and therefore increases the exposure of the catalytic subunits contributing to the activity enhancement.

As mentioned before, the main interaction of proteins in surfactant films is expected to be related to the hydrophobic regions of the bilayers formed in this type of films, rather than the head groups [196,198]. Nevertheless, for cc*c*NiR, the cationic interaction with DDAB and CTAB was beneficial for the non-catalytic response but not for the catalysis.

DDM is the most attractive compound, providing the best analytical parameters (Table 5.2) including a wide linear range, the highest sensitivity, maximum current density and catalytic efficiency of all of the surfactant based bioelectrodes. Typically non-ionic surface active agents, like this alkylglucoside, are less denaturating than other reagents. They are also less prone to interfere in protein-protein interactions and therefore should not greatly affect important protein structural features [199-200].

The fact that all the surfactant modified electrodes provided a better electroactivity than bare PG surfaces suggests that the adsorption of these compounds on the electrodes is likely to play an important part in the enhancement of cc*c*NiR activity. The electrode surface becomes more enzyme “friendly”. Moreover, it is pertinent to assume that the surfactants worked as solubilizing agents to the high molecular weight aggregates this enzyme forms in solution, aiding in their dissociation. This is achieved by mimicking the natural bilayer environment of the protein, thus satisfying the hydrophobic nature of the membrane associated protein. The protein becomes enwrapped in the layer of protective surfactant, instead of forming aggregates. The dispersion of the cc*c*NiR complexes should increase the amount of functional enzyme available to exchange electrons with the electrode.

## 5.4) Conclusions

The direct electrochemistry of *cc*NiR was studied in films of surfactants casted on PG electrodes. Cationic compounds gave a pair of electrochemically non-reversible peaks not present either at bare electrode surfaces or with the other types of surfactants. Particularly, the electron transfer between *cc*NiR and PG electrodes was greatly promoted in the enzyme–DDAB films. The electrochemical process occurred at similar potentials to what has been formerly reported, so, despite the response enhancement, there was no decrease in the driving force for the reaction. The enzyme's non-catalytic response had much more defined peaks than previously reported; nevertheless, it was not possible, at this time, to conclude if the signals were from any particular heme. The peaks probably correspond to the interaction and/or overlapping of all the heme groups.

The electrochemical analysis of the pair of peaks in *cc*NiR–DDAB films showed a complex behavior with difusionless voltammetry characteristics, but the possibility for some diffusion within the surfactant film could not be ruled out. The reaction was non-reversible and more than one electron was being transferred. The formal potential was pH dependent suggesting that the redox reaction monitored was coupled to the transfer of one proton.

Visible spectra of *cc*NiR and surfactant mixtures indicated no major alterations of protein structure in the presence of these compounds, as shown by the Soret, $\alpha$ and $\beta$ absorption bands.

The activity of *cc*NiR for nitrite was compared in the different types of surfactant films by cyclic voltammetry. The enzyme–surfactant modified bioelectrodes showed improved activity, with increased sensitivity, maximum catalytic currents and wider linear ranges when compared to the DET of *cc*NiR in bare PG surfaces. This type of cast films shows great promise as the basis for fabricating nitrite biosensors. Particularly the non-ionic surfactant tested, DDM, which gave the best analytical performance with a 10 fold increase in maximum catalytic current and *ca.* 30% more sensitivity to nitrite.

The surfactant film modified electrodes provided a favorable environment for *cc*NiR to transfer electrons directly with PG electrodes. Most likely, the enzyme interaction with the partial hydrophobic environment contributed to its superior electrochemistry.

Future work should focus on how the cc*c*NiR complex is arranged in the presence of each of these surfactants. A gel filtration analysis of the protein–surfactant mixtures would allow determining the aggregation status of the protein. The film's thickness can be evaluated by ellipsometry and the stability of the protein films may be further tested using Raman spectroscopy and circular dichroism.

# Chapter 6

## *Desulfovibrio desulfuricans* ATCC 27774
## Respiratory Flexibility – a proteomic study

# Chapter 6 - *Desulfovibrio desulfuricans* ATCC 27774 Respiratory Flexibility – a proteomic study

## 6.1) Introduction

In order to develop a marketable enzyme based biosensor device the biocatalyst must be readily available and its production costs must be low. The mass production of enzymes is usually associated with overexpression strategies, which can be challenging and time consuming. cc*c*NiR overexpression is somewhat difficult since it is a complex protein with multiple redox centers. Expression and mutation studies have been reported for *E. coli* and *W. succinogenes* cc*c*NiR [69,207]. One issue is the need for encoding different systems involved in heme production, since the catalytic heme has a characteristic binding motif and therefore can not be produced by the regular *c*-type heme biosynthesis pathway available in bacteria. In particular, it requires the heme lyases encoded by the *nrf* operons [69]. *W. succinogenes* has been indicated as a valuable host for the production of multiheme cytochromes *c* allowing their expression in large scale, as well as the possibility to generate enzyme variants. It possesses the cytochrome *c* biogenesis machinery that allows the facile production of different types of hemes [207]. A simpler alternative strategy to produce higher amounts of the enzyme could reside on naturally overexpressing it by getting further knowledge over the regulation mechanisms of *D. desulfuricans* growth and how the production of that specific enzyme is controlled.

*Desulfovibrio desulfuricans* ATCC 27774 belongs to the sulfate reducing bacteria (SRB) group, which is constituted by a wide variety of microorganisms characterized by the ability to use sulfate as terminal electron acceptor, as a major component of their energy metabolism [208-209]. These bacteria can be found in anaerobic environments such as gastrointestinal tracts, marine sediments and soil sediments, where sulfate reduction is the dominant anaerobic biomineralization pathway [210]. These microorganisms can also be found close to oxic habitats, since they have proteins that allow them to sustain prolonged oxygen exposure [209,211]. In this way, they can grow in areas where nutrient availability is higher. The *D. desulfuricans* ATCC 27774 strain seems particularly adapted to grow in the presence of oxygen having a high tolerance for it [211].

SRB have a highly versatile metabolism as they can use a variety of electron donors (hydrogen, lactate, formate, pyruvate, alcohols) and acceptors (sulfate, sulfite, nitrate, nitrite) [210,212-213]. This enables them to easily adapt to changes in the environment and inhabit a multitude of locations. The molecular mechanisms beneath such versatility, which is related with the activation or repression of proteins under the different conditions, are still underexplored. The respiratory processes have important environmental consequences and attract scientific interest. The respiratory flexibility, for example, is frequently related with the modulation of the expression of different terminal oxido-reductases usually associated with membrane respiratory chains [214].

### 6.1.1) Final electron acceptors: nitrate *vs* sulfate

*D. desulfuricans* grows more rapidly and with higher yields with nitrate rather than with sulfate as electron acceptor. The changes in cellular metabolism that allow the switch in oxidizing substrates are not completely understood. Nitrate and nitrite reductases, for example, are overexpressed when these compounds are the only electron acceptors. In the presence of nitrate and sulfate, the thermodynamically less-favorable sulfate is preferred [215]. Nitrate reduction seems to occur only in the absence of sulfate and sulfide (the product from sulfate reduction), which strongly inhibits nitrate reduction by *D. desulfuricans* [215-217]. In a study by Marietou et al. it was shown that nitrate respiration is regulated at the transcriptional level with the nitrate reductase operon being induced by nitrate but repressed by sulfate [215]. Though, the nitrate reduction pathway is not completely expressed while sulfate is available; on the contrary, the sulfate reduction pathway is constitutively expressed when the cells grow with nitrate.

Cytochrome *c* nitrite reductase expression in *D. desulfuricans* is favored when the bacteria is grown in nitrate containing media [215]. Nevertheless, the *nrf* genes seem to be expressed constitutively in SRB and are present in sulfate grown bacteria [217-219]. *cc*NiR catalyzes the six-electron reduction of nitrite to ammonia in the final step of the dissimilatory pathway of nitrate ammonification [70]. Some nitrite reductases have also been shown to reduce sulfite to sulfide, thus forming the only known link between the nitrogen and sulfur biogeochemical cycles (Figure 6.1). The sulfite reductase activity in these enzymes is considerably lower than

their nitrite activity, still sometimes higher than the sulfite reductases enzymes themselves [64-65].

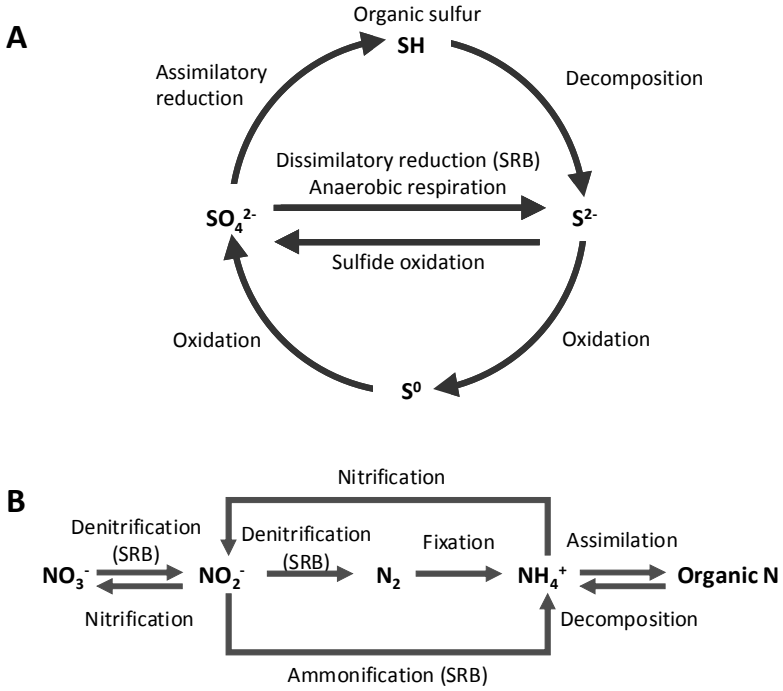


**Figure 6.1 -** Simplified **A)** Sulfur and **B)** Nitrogen cycles indicating steps were sulfate reducing bacteria are involved.

Besides the role in nitrate respiration, c*c*NiRs are thought to be involved in nitrite and NO detoxification processes. The latter has been reported in enteric bacteria that use NrfA to reduce NO [220-221]. Nitrite has been shown to inhibit SRB, and therefore the presence of c*c*NiR can sustain SRB in environments with millimolar concentrations of nitrite, *e.g.*, co-habitated by nitrate-reducing and sulfide-oxidizing bacteria [222-223]. This detoxification effect has been shown, for example, in *Desulfovibrio vulgaris* Hildenborough, which is unable to use nitrate as respiratory substrate, however it is able to cope with nitrite through the expression of *nrf* genes [74,218].

### 6.1.2) Economical impact

The interest on SRB extends over different areas. These microorganisms have been linked to health issues, since they can have a role in inflammatory bowel diseases [224]. They are involved in corrosion of metal equipment and souring of petroleum reservoirs, which can cause economical problems in the oil industry [225]. Furthermore, SRB ability to reduce toxic heavy metals is interesting for bioremediation [226-227]. The implications in these different areas are surely a consequence of the adaptability of the bacteria to different substrates and strongly compels studies regarding the understanding of its metabolism.

In this chapter a proteomic study was performed to evaluate the protein expression profiles of *D. desulfuricans* cells grown in nitrate or sulfate containing media. The changes at the protein level should indicate the molecular tools that confer the respiratory flexibility of this microorganism. This knowledge will help attain a better understanding over the modulation mechanisms that are activated by the cells to solve potential survival problems in adapting to different environments. The approach followed aimed to locate the proteins responsible for nitrate/sulfate respiratory flexibility in the proteomes of the differently grown cells and to identify these proteins by mass spectrometry (MS). The complete genome sequence of *Desulfovibrio desulfuricans* ATCC 27774 is available since 2009 (DOE Joint Genome Institute - www.jgi.doe.gov). This information will help in the future identification of proteins and in obtaining insights into the metabolic processes occurring in this microorganism.

### 6.1.3) Two-dimensional protein gel electrophoresis

The strategy followed herein made use of two-dimensional protein gel electrophoresis (2DE). With this technique complex protein mixtures can be separated according to their charge, during an isoelectric focusing (IEF), and size, in a sodium dodecyl sulfate polyacrylamide gel electrophoresis (SDS-PAGE) [228-230]. In this way the protein expression profiles of cells, tissues or organisms can be analyzed. In addition, the effects of specific conditions can be compared giving insights to the response mechanisms of a system to a

given perturbation. Moreover, 2DE can be performed in a micropreparative scale, allowing the purification of individual proteins for further analysis and identification [228,230-231].

Part of the work here described was done with differential in gel electrophoresis (DIGE) technique, which allows for simultaneous separation of up to three samples on a single gel [232-233]. The multiple samples are labeled with different fluorescent dyes which are co-migrated in the same gel. Figure 6.2 shows a basic scheme of the labeling chemistry.

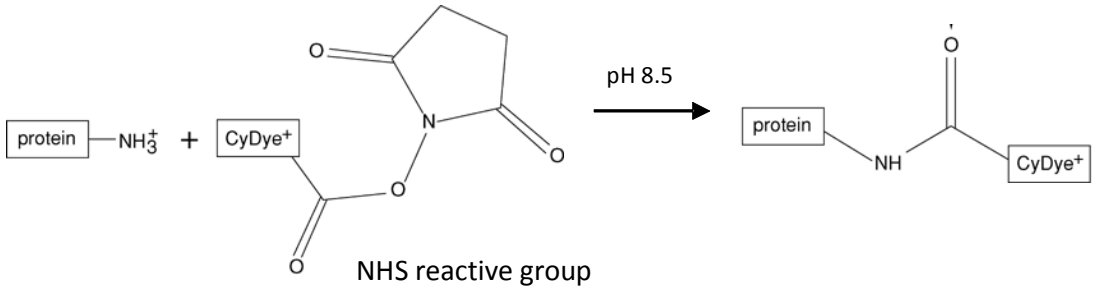


**Figure 6.2 -** Schematic presentation of the reaction of CyDye DIGE fluor minimal dyes with the amino group of a lysine residue of a protein [234].

The fluorescent dyes, such as the cyanine dyes (CyDyes) from GE used in this work, have an NHS-ester group which reacts with the amino group of a positively charged lysine residue on the protein. The dyes are also positively charged and so no net change in the protein isoelectric point is observed. In addition, they have very similar molecular masses, hence, both the charge and mass matching guarantees that a differently labeled protein will essentially co-migrate to the same point, during the electrophoresis. The procedure normally used is called "minimal labeling" since it was designed to ensure staining of one dye *per* protein molecule. Due to the different excitation wavelengths of each CyDye it is possible to acquire up to three images from one gel. The images resulting from consecutive excitation, with the appropriate wavelengths for each dye, are overlaid and normalized, whereby only the differences between the samples are visualized. Consequently, running discrepancies are eliminated. Additionally, the use of an internal standard (a mixture of all the samples under analysis) can compensate for experimental variation in spot quantities. DIGE experiments greatly facilitate image analysis and bring a new level of statistical confidence and reliability to 2D gel electrophoresis [232].

## 6.2) Experimental

### 6.2.1) Bacterial growth

The *Desulfovibrio desulfuricans* ATCC 27774 cells were grown under anaerobic conditions at 37°C in a semi-defined composition medium according to reference [235] which had either nitrate or sulfate (the electron acceptor substrates). The media composition is described in Tables 6.1, 6.2 and 6.3. The chemicals used in this work were analytical grade and were acquired from Sigma*, Merck**, Ridel-de-Haen†, Scharlau‡, Difco¤ Panreac¤¤, Roche•, Calbiochem••, GE Healthcare⌀ and Fluka⌀⌀.

**Table 6.1 -** Medium composition. The pH was adjusted to 7.45-7.55 with KOH. The solution was degassed by argon bubbling and sterilized by autoclaving (20 minutes at 120°C).

| Reagent | Concentration (g/L) |
|---|---|
| $KH_2PO_4$ ** | 0.5 |
| $NH_4Cl$ ** | 1.0 |
| $CaCl_2.2H_2O$ ** | 0.04 |
| Sodium lactate * | 6.0 |
| Sodium citrate † | 0.3 |
| Wolfes elixir | 1 mL (Table 6.2) |
| Casaminoacids ¤ | 2.0 |
| Tryptone ‡ | 2.0 |
| Vitamin solution | 2 mL (Table 6.3) |
| **For sulfate media** | |
| $Na_2SO_4$ ** | 4.5 |
| $MgSO_4.7H_2O$ ¤¤ | 0.060 |
| $FeSO_4.7H_2O$ ** | 0.004 |
| **For nitrate media** | |
| $NaNO_3$ ** | 2.4 |
| $MgCl_2.6H_2O$ ¤¤ | 0.050 |
| $FeCl_2.4H_2O$ ** | 0.003 |

**Table 6.2** - Composition of vitamin solution. The pH was adjusted to 7.4 with tris-HCl buffer 50 mM after dissolution of riboflavine with NaOH 1 M. The solution was sterilized with 0.2 µm filters.

| Reagent | Quantity for 200 mL |
|---|---|
| Vit. B2 – Riboflavine ** | 0.02 g |
| Vit. B3 – Nicotinic acid ** | 0.05 g |
| Vit. B1 – Tiamine ** | 0.06 g |
| Vit. B5 – Pentotenic acid ** | 0.06 g |
| Vit. B6 – Piridoxine ** | 0.06 g |
| Vit. B12 – Cianocobalamine • | 0.005 g |
| Vit. C – Ascorbic acid ** | 0.2 g |
| Vit. H – Biotine ØØ | 0.001 g |

**Table 6.3 -** Composition of Wolfes elixir. The pH was adjusted to 6.5 – 7.0 with KOH.

| Reagent | Concentration (g/L) |
|---|---|
| Nitriloacetic acid ØØ | 1.5 |
| $MgSO_4.7H_2O$ ¤¤ | 3.0 |
| $MnSO_4.H_2O$ ** | 0.5 |
| NaCl ǂ | 1.0 |
| $FeSO_4.7H_2O$ ** | 0.1 |
| $CoSO_4.7H_2O$ ** | 0.1 |
| $NiCl_2.6H_2O$ ** | 0.1 |
| $CuCl_2.2H_2O$ ** | 0.1 |
| $ZnSO_4.7H_2O$ ** | 0.1 |
| $CuSO_4.5H_2O$ ** | 0.01 |
| $AlK(SO_4)_2.12H_2O$ ** | 0.01 |
| $H_3BO_3$ ** | 0.01 |
| $Na_2MoO_4.2H_2O$ ** | 0.01 |
| $Na_2SeO_3.5H_2O$ ** | 0.001 |

Three pre-inoculums (100 mL) were prepared before the 1 or 2 L growths from which the bacterial cells were harvested. The inoculums were 10% of the total growth volume. Cells were harvested at 8, 16 and 24h. The growth rate was determined by measuring the optical density (OD) at 600 nm using a Shimadzu UV1800 spectrophotometer. Cell harvesting was done by centrifugation (Beckman Avanti J-25) of the culture media at 10000 g (10 or 15 min, 10°C). The pellet was then washed with a new centrifugation in phosphate buffer 10 mM, pH 7.6, suspended in a 1:3 proportion with the phosphate buffer and stored at -80°C.

### 6.2.2) Sample preparation

The *D. desulfuricans* cells were homogenized on a Potter-Elvejhem homogenizer (Multifix) in the presence of a protease inhibitor cocktail (Complete EDTA-free, Roche) and a mix of endonucleases (DNase I, Roche e RNase I, Sigma). The cells were lysed in a French-Press (Thermo-FA-080A) at *ca.* 16000 psi and centrifuged at 8000 g for 10 min at 4°C to eliminate cell debris in a Sigma 3K30 centrifuge. The supernatant constituted by the lysed cells was then ultracentrifuged (Beckman Optima L-70 centrifuge) to separate the soluble and membrane fractions (100000 g for 1h at 4°C).

### 6.2.3) Sample preparation for 2D and protein quantification

Both soluble and membrane protein extracts were solubilized in a 2D sample buffer composed of 7 M urea (Merck) , 2 M thiourea (Merck) and 2% (m/V) of CHAPS (Calbiochem). They were divided in small aliquots and stored at -80 °C.

Protein determination was performed with two different commercial protein quantification kits: the 2D Quant Kit (GE Healthcare) and the BioRad Protein Assay kit. The first method is based on the specific binding of copper ions to proteins. The proteins are first precipitated and then ressuspended in a copper-containing solution. The unbound copper is then measured with a colorimetric agent. The color density is inversely related to the protein concentration. The second protein quantification kit is based on the method of Bradford (a Coomassie® Brilliant Blue G-250 dye shifted from 465 nm to 595 nm maximum absorption when it binds to protein). Bovine serum albumin [Sigma] was used as protein standard solution in both methods. The results were comparable and the simpler BioRad Protein Assay method was therefore routinely used.

### 6.2.4) Two-Dimensional gel electrophoresis

Immobiline Dry strips (IPG) from GE Healthcare with a non-linear (NL) 3-10 pH gradient (18 cm long) were rehydrated over 12h in a 2D rehydration solution containing 7 M urea, 2 M thiourea, 2% (mV) of CHAPS, 0.5% (V/V) IPG buffer pH 3-10NL (GE), bromophenol blue (Merck) and 0.28% (m/V) DTT (GE). The sample (50 µg in DIGE and 60 µg in silver staining

experiments), diluted in a 1:9 proportion with the rehydration solution, was applied during the isoelectric focusing, with the use of sample cups (GE Healthcare).

In DIGE experiments, the soluble fractions of *D. desulfuricans* were added to the 2D sample buffer (CHAPS 2% (m/V), urea 7M, thiourea 2M) and labelled with Cy3 or Cy5 cyanine dyes (GE Healthcare). A pool consisting of equal amounts of every sample was prepared to be used as internal standard labeled with Cy2 dye. Nitrate and sulfate samples were combined and applied by sample-cup during isoelectric focusing to the same type of IPG strips.

The 1$^{st}$ dimension - the isoelectric focusing - was run in an Ettan IPGphor 3 unit (GE Healthcare) at 20°C with a 4 steps program (step 1 – 300 V fixed voltage for 3h, step 2 – voltage gradient up to 1000 V in 6h, step 3 – voltage gradient up to 10000 V in 3h and step 4 – 10000V fixed voltage for 3h) adding up to a total of 51.3 kV ran in 15h. After isoelectric focusing the strips were prepared for the second dimension by performing two equilibration steps in which the IPG strip was saturated with the buffer system required for the 2$^{nd}$ dimension separation. In the first step, the IPG strips were soaked and rocked for 15 minutes in 10 mg/mL of DTT in SDS equilibration buffer [6 M urea, 50 mM tris-HCl pH 8.8 (Merck and Riedel-de-Haen), 30% (V/V) glycerol (Panreac), 2% (m/V) SDS (Merck) and bromophenol blue], and in the second equilibration step the same procedure was repeated with 25 mg/mL of iodoacetamide (Merck).

For the 2$^{nd}$ dimension, SDS-PAGE was carried out with 12.5% acrilamide gels (21x27 cm) on a vertical unit (EttanDalt Six GE Healthcare) according to Laemmli [236]. The gel solution was prepared as described in Table 6.4. After casting the gel solution, 30% isopropanol (Riedel-de-Haen) was added to the top of the gels to allow an even polymerization line to be formed. The gels were polymerized overnight at room temperature. The IPG strips, equilibrated in the SDS equilibration buffer, were then applied on top of the gel and the glasses were sealed with 1% agarose solution in electrophoresis buffer [0.025 M tris, 0.192 M glycine (Panreac) and 0.2% SDS]. The SDS-PAGE was ran at 350 V constant voltage for *ca.* 3:30h after an initial 15 min step at 80 V to allow the sample to migrate from the IPG strip to the 2$^{nd}$ dimension gel.

**Table 6.4 -** SDS-PAGE gel preparation.

| Reagent | Concentration |
|---|---|
| Tris-HCl 1.5 M pH 8.8 | 0.375 M |
| Acrylamide:Bisacrylamide 40%:3% Ø | 12.5% |
| SDS 10% | 0.2% |
| TEMED Ø | 0.05% |
| PSA 10% Ø | 0.04% |

### 6.2.5) Gel staining

After electrophoresis, the gels were silver-stained following the protocol indicated in the PlusOne Silver Staining kit (GE Healthcare). A Coomassie Blue based method (PageBlue Protein Staining from Fermentas) was used for preparative gels, which is compatible with mass spectrometry analysis.

The gels were digitalized with GE Healthcare ImageScanner. Fluorescence images of the DIGE gels were acquired on a Typhoon 9400 scanner (GE Healthcare).

### 6.2.6) Gel analysis

Image analysis and statistical quantification of relative protein abundances was performed using ImageMaster 7.0 and DeCyder V5.0 software (GE Healthcare). The intensity level of the spots was determined by the relative spot volume of each protein compared to the normalized volume of proteins. The relative abundance of each protein spot was compared between the nitrate and sulfate conditions: the spots with an intensity ratio higher than 2 were considered significantly different.

### 6.2.6) Protein identification

The gel plugs containing the spots of interest were removed from Coomassie Blue stained preparative gels, where 300 µg of protein were applied. Protein identification was carried out using the peptide mass fingerprint (pmf) approach. After tryptic digestion, the samples were analyzed by matrix-assisted laser desorption ionization time-of-flight mass spectrometry (MALDI-TOF-TOF-MS) on a 4700 Proteomics analyzer (Applied Biosystems). The monoisotopic peptide masses were used to search for protein identification using Mascot software (http://www.matrixscience.com) against MSDB (http://csc-serve.hh.med.ic.ac.uk/msdb.html) and SwissProt databases.

## 6.3) Results and Discussion

### 6.3.1) Cell growth

The growth curves of *D. desulfuricans* cells in nitrate or sulfate based media are represented in Figure 6.3. They follow the expected trend with an initial lag phase of very slow growth (*ca.* 4h) after which the cells start growing at an exponential rate, up to 18h for nitrate cells and 19h for sulfate cells, when a stationary phase is reached.

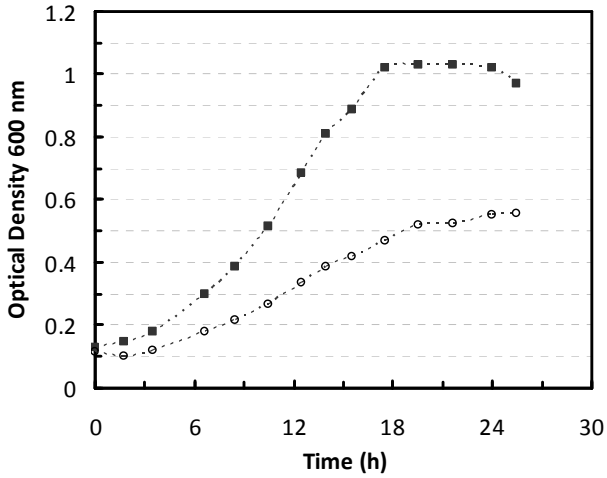


**Figure 6.3 -** Growth curves of *D. desulfuricans* cells in (■) nitrate and (○) sulfate based media.

As expected, the cells in nitrate media grow faster and give higher yields than the sulfate grown ones. Besides nitrate reduction being thermodynamically more favorable, this slower growth in sulfate containing media has been attributed to the fact that the final products of sulfate reduction (sulfide) might be toxic to the cells, therefore inhibiting their growth [215,219]. The maximum OD in the sulfate growths, determined in the stationary phase, was 54% of the one obtained in nitrate media. This value is similar to previously reported cell yields of sulfate *vs* nitrate grown *D. desulfuricans* cells (45% in Postgate medium at 30°C [215]).

The specific growth rate (μ) and the doubling time (Td) were determined by the semi-log plot of the exponential phase of the growth curves. The values are presented in Table 6.5 and confirm the favorable growth of the cells when nitrate is the terminal electron acceptor.

**Table 6.5 -** Specific growth rate (μ) and doubling time (Td) of *D. desulfuricans* cells grown in nitrate or sulfate media.

| Electron acceptor | μ ($h^{-1}$) | Td (h) |
|---|---|---|
| **Nitrate** | 0.1005 | 6.9 |
| **Sulfate** | 0.0848 | 8.2 |

### 6.3.2) *D. desulfuricans* soluble proteome

*D. desulfuricans* cells, from nitrate and sulfate media, were collected at three different times of the bacterial growth: at 8h, within the beginning of the exponential phase of growth; at 16h, the top of the exponential phase; and at 24h, the stationary phase. The proteins of the resulting six soluble fractions (nitrate 8h, nitrate 16h, nitrate 24h, sulfate 8h, sulfate 16h and sulfate 24h) were analyzed in a DIGE experiment to evaluate how the oxidizing substrate and the cell development phase influence protein expression in *D. desulfuricans*. The protein fractions from nitrate and sulfate growths were labeled with two different cyanine dyes (Cy3 and Cy5, respectively) and paired up according to the hours of growths. Additionally, an internal standard constituted by equal amounts of all six fractions was labeled with the third fluorescent dye (Cy2) and added to the sample applied in each gel. The proteomes are presented in Figures 6.4, 6.5 and 6.6.

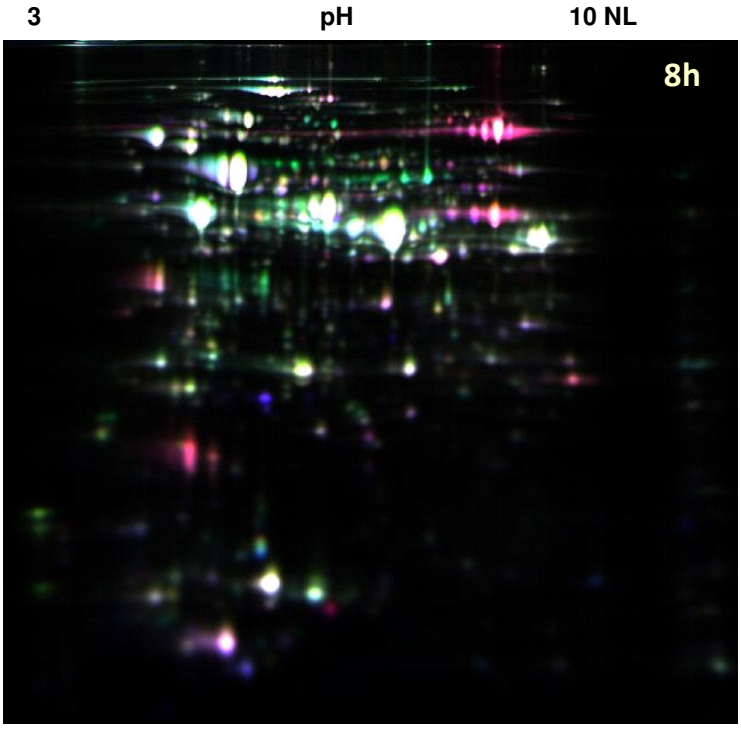


**Figure 6.4 -** Proteomic analysis of the soluble proteins fraction of *D. desulfuricans* grown for 8h with nitrate or sulfate media. Image overlay using DIGE technology resulting from one gel experiment containing three differentially labeled samples: nitrate Cy3 (green), sulfate Cy5 (red), and pooled-sample internal standard Cy2 (blue). Gel images are oriented with high molecular weight on top to low molecular weight towards the bottom of the gel. 50 µg of each labeled sample applied on an 18 cm IPG strip pH 3-10NL, 12.5% polyacrylamide gel.

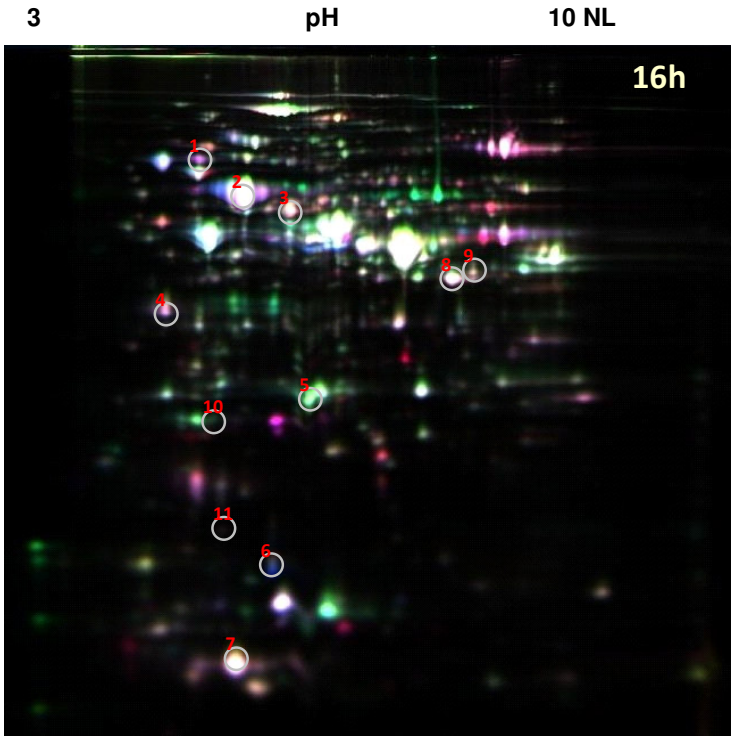


**Figure 6.5 -** Proteomic analysis of the soluble proteins fraction of *D. desulfuricans* grown for 16h with nitrate or sulfate media. Image overlay using DIGE technology resulting from one gel experiment containing three differentially labeled samples: nitrate Cy3 (green), sulfate Cy5 (red), and pooled-sample internal standard Cy2 (blue). Gel images are oriented with high molecular weight on top to low molecular weight towards the bottom of the gel. 50 µg of each labeled sample applied on an 18 cm IPG strip pH 3-10NL, 12.5% polyacrylamide gel. Circles indicate proteins identified by MS.

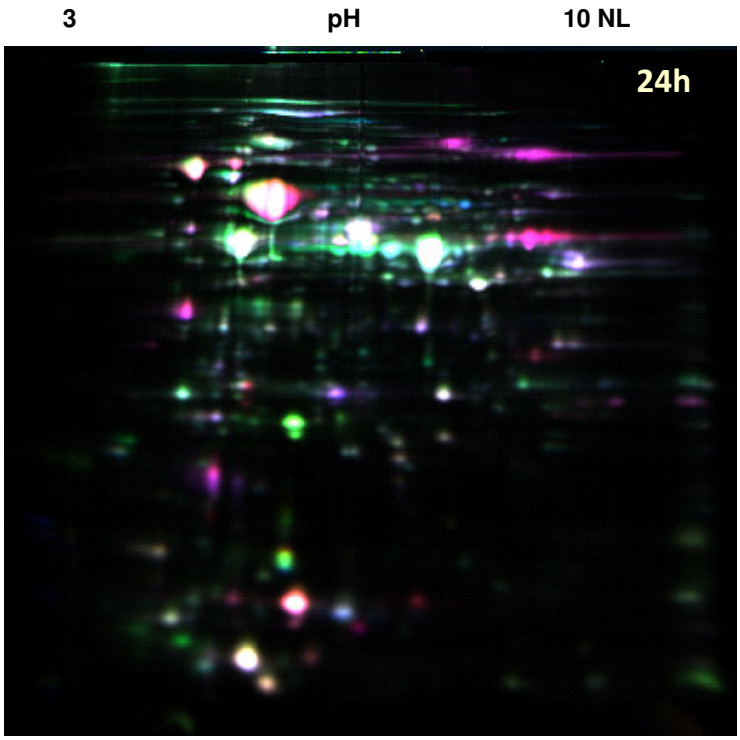


**Figure 6.6 -** Proteomic analysis of the soluble proteins fraction of *D. desulfuricans* grown for 24h with nitrate or sulfate media. Image overlay using DIGE technology resulting from one gel experiment containing three differentially labeled samples: nitrate Cy3 (green), sulfate Cy5 (red), and pooled-sample internal standard Cy2 (blue). Gel images are oriented with high molecular weight on top to low molecular weight towards the bottom of the gel. 50 µg of each labeled sample applied on an 18 cm IPG strip pH 3-10NL, 12.5% polyacrylamide gel.

Overall the soluble proteomes of the cells grown with nitrate or sulfate as electron acceptors had similar protein patterns no matter the growth stage. The electrophoretic maps showed a high abundance of protein spots with relative molecular weights between 65 and 35 kDa and with acidic character (in the 4-7 pH range). Using the DeCyder software for image analysis close to 1800 protein spots (matched) were detected in each of the six conditions representing the soluble proteomes.

Important differences could be clearly visualized in the form of green spots for nitrate up-regulated proteins and red spots for sulfate induced ones (Figures 6.4, 6.5 and 6.6). The protein spots showing a volume intensity ratio higher than two[1] were considered differentially expressed (Table 6.6).

**Table 6.6 -** Statistical analysis of the soluble fraction of *D. desulfuricans* proteome performed with DeCyder sotware. The up- and down-regulated spots represent two-fold variations in relative spot volume.

| Growth time | Number of spots/ matches | Down-regulated in nitrate | Up-regulated in nitrate |
|---|---|---|---|
| 8h | 1769 | 149 | 178 |
| 16h | 1800 | 144 | 161 |
| 24h | 1722 | 135 | 277 |

From the data analysis in Table 6.6 it is clear that the respiratory substrates have important consequences in the cellular composition, considerably affecting the protein expression levels in *D. desulfuricans*. In general, at least 15% of the protein spots had significant intensity variations between the nitrate *vs* sulfate medium, enabling the grouping of the 2D maps according to the oxidizing substrate.

Regarding the cell development no statistical evaluation was performed due to lack of biological replicates. From a general inspection of the gels, the major differences seem to be between the exponential and stationary phases (24h) of cell growth; the samples collected during the exponential phase (8 and 16h growths) exhibited more similar proteomic profiles.

In this study, the cells were grown in batch cultures, where important parameters for cell development, such as mixing, pH, nutrient availability and metabolite production, are difficult to control [237]. The bacteria harvested at different times of growth should reflect a heterogeneous population including cells in different stages of development, which can potentially be expressing a range of metabolic states at the same time. As a consequence,

[1] The significance of the two-fold variations must not be over estimated, seeing that no biological replicates were used. The DIGE experimental workflow reduces the need for technical replication for acquiring statistical significance to the variations observed between samples, but it does not exclude the need for biological replicates.

although the growth phase might have an impact on the biochemical reactions taking place in the cells, the abundance of proteins can also be related to the media composition at the stage of harvesting, which is changing over the time of growth [237]. It was decided to focus the attention on the cells grown up to the exponential phase (16h growths), since in this phase the nutrient availability should not be a limiting fact of cell development and the nature of the electron acceptor ought to have a more isolated effect over the protein expression.

In order to determine the influence of the respiratory substrate on the metabolism of *D. desulfuricans* its proteins must be identified and characterized. Coomassie blue stained preparative 2D gels from the 16h growth samples were used to remove protein spots to be analyzed by mass spectrometry. The spots identified so far were some of the most abundant in the gels; they are indicated by a red number in Figure 6.5 and are listed and characterized in Table 6.7.

From the 11 spots identified, some of the proteins are predicted to be located on the membrane. This indicates that the soluble fraction has some contaminations and the method for its separation from the membranes should be reviewed and improved.

For most of the proteins their estimated molecular weights and isoelectric point is in good agreement with their positioning in the gel maps; small variations are usually associated with post-transcription and post-translational modifications [228,238] (*e.g.* amino acid modification, cofactor integration, cleavage of signal sequences). Nevertheless, this was not true for proteins 2, 4 and 9. Furthermore, the pmf score for these proteins was quite low (see Table 6.7), so new identifications should be performed.

**Table 6.7 -** Proteins from the nitrate and sulfate soluble fractions of *D. desulfuricans* cells identified by MS-TOF-TOF analysis of protein spots from 2D gels. Mascot protein score thresholds were 54 and 78 for protein identifications indicated with * and $^{+}$, respectively. Biological processes, cell locations, MWs and pIs, are theoretical values predicted from sequence analysis according to databases and tools from the DOE Joint Genome Institute and ExPAsy Proteomics Server. Differential expression analysis was performed with ImageMaster 7.0 from GE Healthcare.

| Spot | Protein | MW | pI | Biological process | Cell location | Score | % coverage | Expression (Range ratio) |
|---|---|---|---|---|---|---|---|---|
| 1 | Heat shock protein Hsp90 | 74101 | 5.09 | Stress response | cytoplasm | 144* | 41 | 2.03 sulfate |
| 2 | Elongation factor G2 | 73162 | 5.86 | Protein biosynthesis | cytoplasm | $68^{+}$ | 30 | 1.18 |
| 3 | ATP synthase F1, α subunit | 54293 | 5.52 | ATP synthesis | membrane | 101* | 42 | 1.88 sulfate |
| 4 | Inorganic diphosphatase | 32741 | 4.91 | Phosphate metabolism | cytoplasm | 32* | 49 | 1.10 |
| 5 | Pyridoxine biosynthesis protein | 31489 | 5.45 | Pyridoxal metabolism | cytoplasm | 127* | 29 | 2.04 nitrate |
| 6 | UspA domain protein | 15655 | 5.36 | Stress response | cytoplasm | 85* | 47 | 2.20 nitrate |
| 7 | Sulfite reductase, γ subunit | 11873 | 5.14 | Redox processes | cytoplasm | $58^{+}$ | 25 | 1.76 sulfate |
| 8 | Extracellular ligand-binding receptor | 40760 | 6.86 | Type I periplasmic ligand-binding domain | membrane | 149* | 36 | 1.09 |
| 9 | Glyceraldehyde-3-phosphate dehydrogenase, type I | 37359 | 6.27 | Glucose metabolism | cytoplasm | 28* | 2 | 1.20 |
| 10 | Hydrogenase (NiFe) small subunit Hyd A | 33889 | 5.22 | Redox processes | membrane | 166* | 5 | 1.44 |
| 11 | Bacterioferritin | 19926 | 5.02 | Iron storage | cytoplasm | $80^{+}$ | 29 | 1.38 |

At this point of the work, only a few number of protein spots were analyzed and most of these did not present a differential relative abundance between nitrate and sulfate cells. Among these proteins, Hsp90 (spot 1), pyridoxine biosynthesis protein (spot 5) and UspA domain protein (spot 6) were the ones being differentially expressed (ratios > 2 in Table 6.7), the first in sulfate and the two latter in nitrate (*cf.* spots in Figure 6.5). Additionally, the $\alpha$ subunit of ATP synthase F1, and the $\gamma$ subunit of sulfite reductase (spots 3 and 7, respectively) were somewhat more abundant in sulfate growing conditions. Spot 3 will not be considered here, since it is a probable membrane contamination and therefore its up-regulation could derive from the poor extraction and separation processes, and might not have any biological significance.

As mentioned before, for the nitrate medium, a protein involved in pyridoxal metabolism was over-expressed. Interestingly, it has been annotated as being implicated in the production of pyridoxal phosphate, probably by incorporating ammonia into the pyridine ring. Seeing that ammonia is the final product of nitrate reduction, the up-regulation of this protein is consistent with the condition where this pathway is thought to be expressed.

The stress response proteins UspA domain and Hsp90 were up-regulated in nitrate and sulfate grown cells, respectively. While the first is usually expressed in the presence of stress agents inside cells, the second is involved in unfolded protein binding. Stress proteins are important for the protection and survival of cells, under different stress conditions (oxygen, salt, heat, osmotic, carbon starvation, stationary phase) [239]. Herein, they can probably be correlated with the end of the exponential phase of the growths and indicate the lowering of lactate concentration and the accumulation of potential stress products in the culture media.

Besides the proteins that are being affected by the growing media composition, the remaining identified ones are from diverse functional categories like protein biosynthesis, phosphate and glucose metabolism, detoxification and transport and oxidation-reduction processes.

### 6.3.3) *D. desulfuricans* membrane proteome

As mentioned in the experimental section 6.2.2 the membrane fraction was separated by ultracentrifugation of the disrupted bacterial cells. This fraction was solubilized and analyzed in the same way that the soluble one. Representative gels, stained with silver nitrate, are shown in Figures 6.7 and 6.8. Only the 16h growths membrane fractions were used in this part of the study.

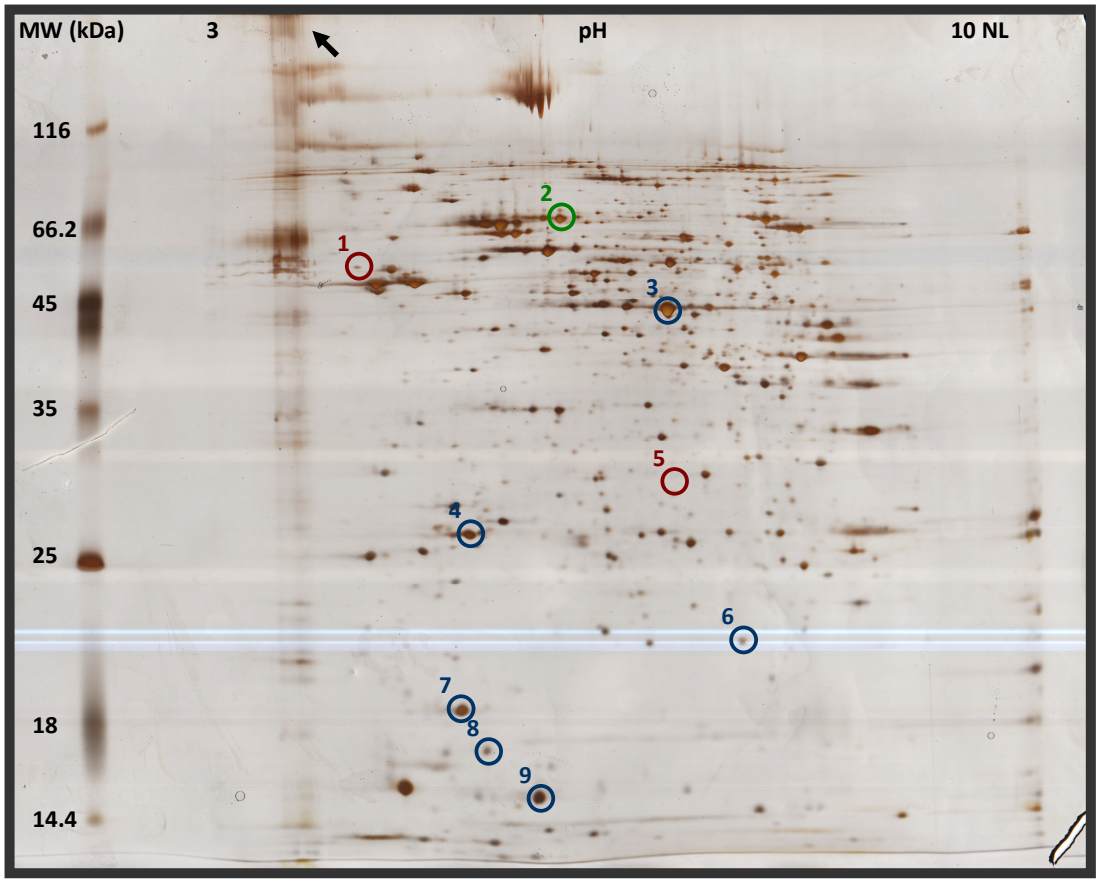


**Figure 6.7 -** Overview of the 2D gel profile of the membrane fraction of *D. desulfuricans* cells grown for 16h with nitrate media. Circles indicate proteins identified by MS: red ones refer to proteins up-regulated in sulfate growths, green to nitrate while blue circles indicate proteins without differential expression. The black arrow indicates the place of protein application in the 1$^{st}$ dimension gel strip by cup-loading. 60 µg of nitrate membrane sample were applied on an 18 cm IPG strip pH 3-10NL, 12.5% polyacrylamide gel stained with silver nitrate.

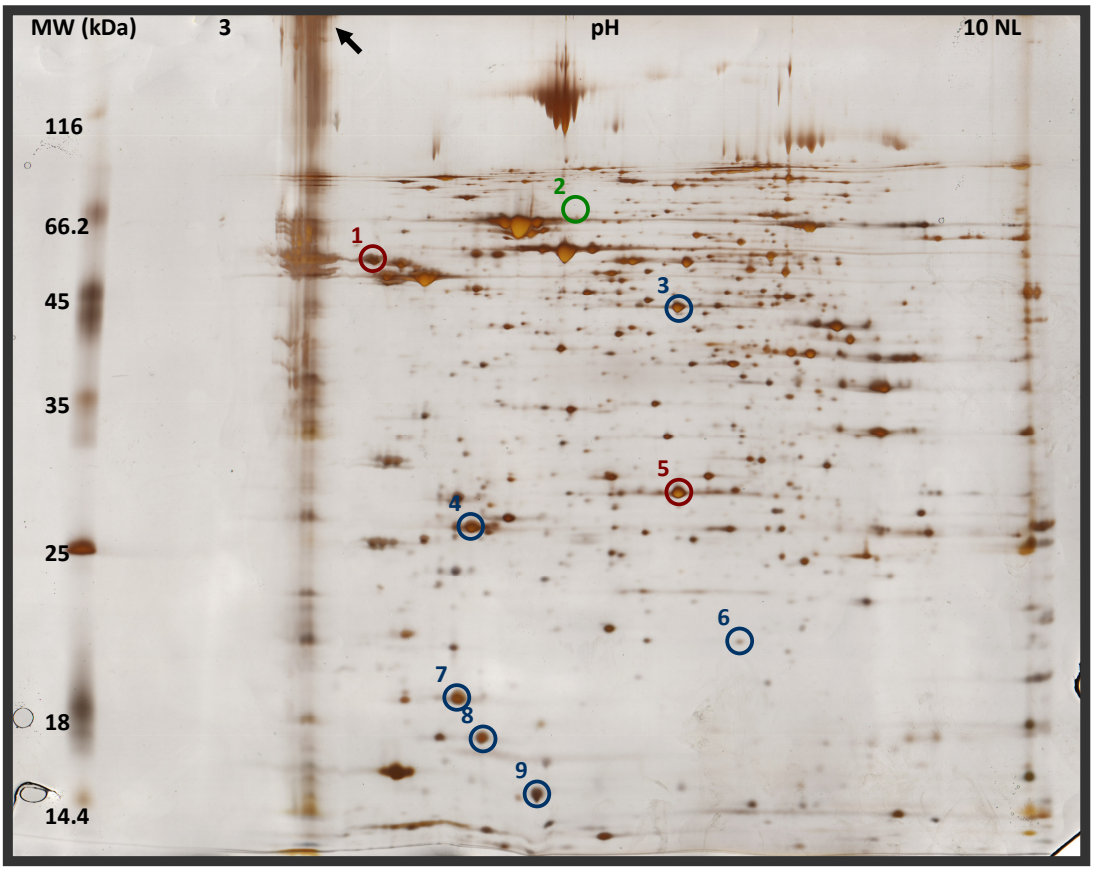


**Figure 6.8 -** Overview of the 2D gel profile of the membrane fraction of *D. desulfuricans* cells grown for 16h with sulfate media. Circles indicate proteins identified by MS: red ones refer to proteins up-regulated in sulfate growths, green to nitrate while blue circles indicate proteins without differential expression. The black arrow indicates the place of protein application in the 1st dimension gel strip by cup-loading. 60 µg of sulfate membrane sample were applied on an 18 cm IPG strip pH 3-10NL, 12.5% polyacrylamide gel stained with silver nitrate.

Although no specific protocol was used to solubilize the membrane fraction proteins, as frequently necessary [240], they are well represented in the proteome maps. Nevertheless, it appears that some proteins are not being separated due to some precipitation in the place were they were cup-loaded in the 1st dimension gel strip (*cf.* arrows in Figures 6.7 and 6.8).

The images of the 2D gels were processed with the Image Master software. A preliminary spot detection identified *ca.* 800 protein spots in the membrane proteomes of *D. desulfuricans*. These proteins were fairly distributed along the entire pH gradient; contrary

to what was observed in the soluble fraction, a sizeable amount of proteins was present in the alkaline portion of the gel (pH 6-9).

Although a similar protein pattern could be observed in the proteomes of the membrane fractions it was quite difficult to perform the matching of the gel maps. This was attributed to the technical difficulties (in the IEF and SDS-PAGE) of obtaining reproducible gels of membrane samples and to the low reproducibility of the silver staining. For these reasons, a detailed analysis of protein expression differences on the membrane proteome was not performed at this time. Nonetheless, variations between the nitrate and sulfate samples can be detected at the naked eye. In fact, when changing the electron acceptor substrate, the metabolic adjustments are in great part expected to be related with the respiratory chains associated to the cell membrane [214,226,241]. A preliminary assessment involving the analysis of a total of 8 gels with 70% of spots matched (4 for each condition representing two different biological replicate growths), indicates that the expression of approximately 100 proteins is altered between the nitrate/sulfate conditions.

Only 9 protein spots were collected from Coomassie blue stained preparative gels of the membrane fractions and analyzed by mass spectrometry. The results are listed in Table 6.8. From the 9 identified spots 4 are from putative cytoplasm proteins. This confirms the previously mentioned cross contamination of the membrane and soluble fractions.

The relative MW and isoelectric points of proteins 2, 4 and 8 (Table 6.8) were different from the predicted values – both the molecular weights and pIs were higher for all of them. Although their pmf score was good, new MS identification must be done to confirm these results. For the remaining proteins there was good agreement between the theoretical and experimental values.

**Table 6.8 -** Proteins from the nitrate and sulfate membrane fractions of *D. desulfuricans* cells identified by MS-TOF-TOF analysis of protein spots from 2D gels. Mascot protein score threshold was 54 for all identifications. Biological processes, cellular locations, MW, pI, are theoretical values predicted from sequence analysis according to databases and tools from the DOE Joint Genome Institute and ExPAsy Proteomics Server. Differential expression analysis was performed with ImageMaster 7.0 from GE Healthcare.

| Spot | Protein | MW | pI | Biological process | Cell location | Score | % coverage | Expression (Range ratio) |
|---|---|---|---|---|---|---|---|---|
| 1 | Hypothetical protein Ddes_1248 | 58886 | 4.73 | Undefined | undefined | 77 | 2 | 7.34 sulfate |
| 2 | Protein of unknown function (DUF224 cysteine-rich region domain protein) | 60621 | 5.5 | Putative redox processes | undefined | 109 | 19 | 12.05 nitrate |
| 3 | NAD(P)(+) transhydrogenase | 41332 | 5.95 | Redox processes | cytoplasm | 138 | 21 | 1.63 nitrate |
| 4 | ribosomal 5S rRNA E-loop binding protein Ctc/L25/TL5 | 22351 | 4.71 | Translation | cytoplasm | 163 | 76 | 1.08 |
| 5 | Hypothetical protein Ddes_0648 | 30449 | | Undefined | undefined | 166 | 50 | 46.14 sulfate |
| 6 | Hypothetical protein Ddes_0452 | 19915 | 6.22 | Undefined | undefined | 50 | 8 | 1.07 |
| 7 | Ribosomal protein L9 | 18311 | 5.03 | Translation | cytoplasm | 79 | 71 | 1.09 |
| 8 | ATP synthase F1, ε subunit | 14364 | 5.20 | ATP synthesis | membrane | 69 | 42 | 1.33 |
| 9 | UspA domain protein | 15655 | 5.36 | Stress response | cytoplasm | 66 | 52 | 1.55 nitrate |

Regarding the predicted cellular roles of the identified proteins, the cytoplasm contamination proteins 4, 7, 3 and 9 can be included in translation, energy metabolism and stress response processes. These proteins were not considered to be differentially expressed.

Like almost all proteins identified so far, proteins 4 and 7 have relatively intense gel spots. These are ribosomal proteins which were in fact predicted to be abundant in bacterial cells during the exponential phase [239].

Protein 9 – UspA domain protein – was also identified in the soluble proteome and was indicated to be up-regulated in nitrate grown cells; in the membrane proteome a relatively more intense spot was also quantified in the same oxidizing substrate medium.

The ε subunit of ATP synthase F1 is the only protein from the identified group that is annotated as membrane located. It is involved in energy production and conservation and it does not appear to be affected by changing nitrate to sulfate growing conditions.

Spots 1, 2, 5 and 6 were identified as hypothetical and unknown function proteins. Interestingly, with exception of the last one (Ddes_0452) the cell concentrations of these proteins are dependent on the electron acceptor substrate. Accordingly, these up- and down-regulated proteins could be key effectors in the adaptation of *D. desulfuricans* to different substrate availability indicating that there may be unknown mechanisms involved in respiratory flexibility and in SRB adaptation to changing conditions [242]. This is consistent with the importance of hypothetical proteins (no similar protein has yet been identified in other organisms) in cell function [243]. In the future these proteins should be studied to understand their structure/function and roles in *D. desulfuricans* ATCC 27774 metabolism.

### 6.3.4) Soluble and membrane proteomes - considerations

There are 2382 protein coding genes on the complete genome sequence of *Desulfovibrio desulfuricans* ATCC 27774 strain (DOE Joint Genome Institute - www.jgi.doe.gov). The pH gradient used in the 2D experiments was quite broad and therefore allowed a widened view of the proteome. About 1800 protein spots were identified in the soluble fraction and 800 more in the membrane fraction, accounting for a total of 2600 proteins. The elevated number of spots can be a result of the samples cross contamination (some proteins are simultaneously present in both soluble and membrane fractions).

On the other hand, such an extensive representation of the proteome confirms the suitability of the 2D technique, and in particular of the methodology here used, for the comprehensive study of this bacterium. The proteome maps represent not only the expression part of the genome, but also the variation of several active forms and post-translational modifications of proteins from a single gene. The observation of multiple spots for some proteins reflects, for example, different timings of expression, post-transcriptional control, isoforms, cleavage of signal peptides, etc. [228,238]. In this way, this proteomic approach provided an active view of the organism, reflecting the constant changes and responses to different situations.

### 6.3.5) cc*NiR in the proteome of *D. desulfuricans*

cc*NiR is expected to be overexpressed when *D. desulfuricans* cells are grown with nitrate [215]. In an attempt to identify this enzyme in the proteome maps by protein co-migration, the membrane fraction was mixed with cc*NiR and this mixture was analyzed in a 2DE experiment.

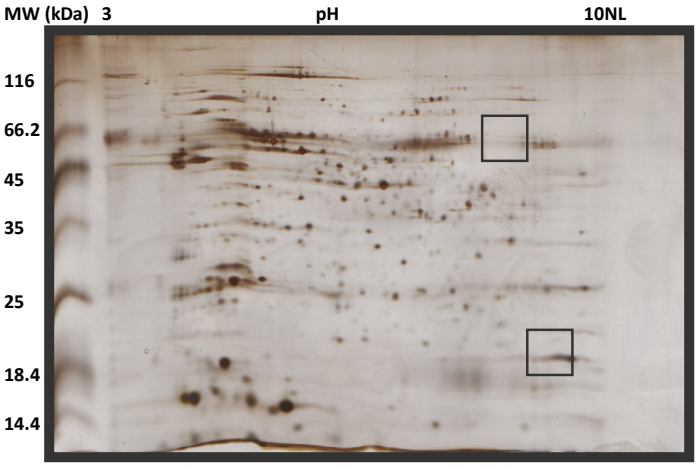


**Figure 6.9 -** Co-migration gel of membrane fraction of *D. desulfuricans* cells grown in nitrate media and cc*NiR. Gray squares indicate the expected coordinates of NrfA and NrfH subunits. 5 µg of nitrate membrane sample and 5 µg of purified cc*NiR were applied on an 7 cm IPG strip pH 3-10NL, 12.5% polyacrylamide gel stained with silver nitrate.

Since the same amount of pure protein and membrane sample was applied (5 µg each), very intense protein spots corresponding to the NrfA (61 kDa, pI 8.1) and NrfH (19 kDa, pI 9) subunits of c*c*NiR were expected. However, the co-migrated gel (Figure 6.9) has no increased protein spots, which suggested that the protein did not migrate at least in the second dimension gel.

In order to verify this hypothesis the pure enzyme was ran in a set of tests in native polyacrilamide gels, where different sample buffers were tested in order to solubilize the protein. Besides the regular rehydration solution used in the 2D experiments, and described in section 6.2.4, the protein was incubated for 1 h at 30°C with identical solutions but with increased detergent concentration and with two different detergents: ABS-14 (a sulfobetaine frequently used for the solubilization of complex samples for 2DE) and Zwitergent 3-10 (a zwiterionic compound which is used to obtain crystals of this enzyme). In this way, the final composition of the solubilization solutions was 7 M Urea, 2 M thiourea, 0.5% IPG, 0.28% DTT and a) 2% CHAPS, b) 4% CHAPS c) 2% CHAPS & 2% ASB-14 and d) 2% CHAPS & 2% Zwittergent 3-10.


**Figure 6.10 -** PAGE analysis of c*c*NiR samples (10 µg) incubated with 2D solubilization solutions: 7 M Urea, 2 M thiourea, 0.5% IPG, 0.28% DTT and **a)** 2% CHAPS, **b)** 4% CHAPS **c)** 2% CHAPS & 2% ASB-14 and **d)** 2% CHAPS & 2% Zwittergent 3-10. 10 % Polyacrylamide native gel, stained with Coomassie blue.

As observed in Figure 6.10, none of the treated samples allowed *cc*NiR to completely enter the gel and effectively be separated. Hence, the procedure used to solubilize the proteins was not effective for *cc*NiR. A different protocol must be used in the future, probably with detergents or extraction kits specific for membrane proteins.

## 6.4) Conclusions

The study presented in this chapter provided a proteomic overview of the soluble and membrane protein content of *Desulfovibrio desulfuricans* ATCC 27774. The proteomes of cells grown in nitrate and sulfate containing media were obtained. The study should be taken as a preliminary assessment, since no sufficient biological and technical reproduction of proteomes was performed yet. For these reasons the statistical analysis of the results should be interpreted with some care.

The study was based on 2D electrophoresis and mass spectrometry. Using image analysis software it was possible to identify *ca.* 1800 and 800 protein spots in the soluble and membrane fractions, respectively, of the *D. desulfuricans* cells grown either with nitrate or sulfate as oxidizing substrates. According to the genome sequence, this represented an excessive number of proteins. This could mean that the samples are cross contaminated and quite a lot of proteins are present in both the soluble and membrane fractions. But more importantly, it shows that the methodology followed herein allows a very wide overview of the dynamic and changing nature of the proteome. As a result, more information than the one provided by the static genomic data can be gathered, namely, indications over the functional state of the bacteria.

For the soluble proteome a DIGE experiment was performed, which included an internal standard to normalize protein spot intensity in the samples. This facilitated the proteomic analysis and allowed a higher degree of confidence in the results. In the 16h growths, corresponding to the top of the exponential phase of bacterial development, *ca.* 15% of proteins had expression differences above a two fold threshold and, thus, these were considered significantly changing as a result of *D. desulfuricans* using nitrate or sulfate as electron acceptor substrate.

Regarding the membrane fraction 12% of proteins were preliminary evaluated as having important variation when changing from a nitrate to a sulfate medium.

The changes at the protein level indicate that this SRB possesses differentiated sets of metabolic pathways to adapt to different conditions. The results demonstrate that varying from a sulfate to a nitrate containing medium impacts the cell metabolism and, as a result, differential protein expression is observed.

The identification of 20 proteins from both the soluble and membrane fractions was achieved by peptide mass fingerprinting. Proteins from several functional categories have been recognized, namely protein biosynthesis, glucose, pyridoxal and phosphate metabolism, detoxification and transport, redox processes, translation, energy metabolism, stress response as well as putative proteins of unknown function. Most of the identifications correspond to abundant proteins in the gels that have no significant concentration variation between nitrate and sulfate grown cells. Nevertheless, it was found that stress response proteins were overexpressed in both nitrate and sulfate soluble proteomes. This was attributed to the approach of the end of the exponential phase and a possibly low nutrient availability and accumulation of cell metabolism by-products in the growth media. The up-regulated proteins in the membrane fraction were hypothetical or proteins of unknown function. This suggested that yet to be studied mechanisms are involved in the respiratory adaptability of this bacterium.

Important differences in protein content were found in the samples coming from the nitrate or sulfate containing media, indicative of different respiratory mechanisms being activated in the presence of each of the final electron acceptors. The future identification of these proteins by peptide mass fingerprinting will allow an overview over the pathways which may be affected by the changing electron acceptors.

*cc*NiR, the protein central to this thesis, was not identified in the proteome maps, and therefore no conclusions over its expression conditions could be assessed. It was not possible to solubilize it in any of the conditions tested so far. Its membrane/hydrophobic character and size were the most probable impediments.

# Chapter 7

# Conclusions and Future Perspectives

# Chapter 7 - Conclusions and Future Perspectives

## 7.1) Remarks on *cc*NiR DET based biosensors

This thesis describes the construction of third generation electrochemical biosensors for nitrite determination using the cytochrome *c* nitrite reductase isolated from *Desulfovibrio desulfuricans* ATCC 27774.

The study of the homogeneous kinetics of the enzyme made it clear that the common spectrophotometric methods and redox mediator compounds, used to estimate kinetic parameters, influence the obtained values. The redox mediators, for example, may dock differently with the enzyme molecules. As a result, care must be taken when comparing different sets of parameters. Globally it was confirmed that below -250 mV *vs* NHE, nitrite is fully converted to ammonia and that the enzyme activity is favored by quite negative reducing power (*e.g.* conferred by methyl viologen). This study has also established that c*c*NiR films immobilized in pyrolytic graphite electrodes, and tested by protein film voltammetry, have a catalytic activity comparable to the enzyme in solution ($k_{cat}$ was 738 $s^{-1}$ in solution and 762 $s^{-1}$ on PG). The fact that the kinetic constant of the free and immobilized enzyme were similar gave good perspectives for the use of c*c*NiR in direct electron transfer based biosensors, without important losses of nitrite reducing activity.

Several immobilizing strategies where used to construct the c*c*NiR biosensors. Yet, for transduction a common platform was utilized - pyrolytic graphite electrodes. Table 7.1 lists the parameters that characterize the analytical and kinetic behavior of c*c*NiR in all the biosensor constructs, as well as some additional information regarding the preparation and analysis of the bioelectrodes, namely, the potential at which the catalytic currents were determined and the amount of enzyme used.

The two bare electrode configurations had different kinetic and analytical behavior as expected due to the different enzyme quantity used. So, the analysis of the results should be focused on the general trends and main characteristics of the responses and not on the absolute values, which can not be directly compared.

**Table 7.1 -** Analytic and kinetic parameters of *cc*NiR biosensors. All configurations were based on pyrolytic graphite electrodes. Analysis was performed by cyclic voltammetry except for the sol-gel configuration in which amperometry was also used. The stability was determined as the electrode being able to maintain at least 90% of its initial response to nitrite and up to no more catalytic current being observed (values in parenthesis). ND – not determined. *– Value determined with rotating disk electrode.

| | **Bioelectrode configuration** | | | | | | |
|---|---|---|---|---|---|---|---|
| **Parameter** | **Sol-gel** | **SWCNT** | **SWCNT/ laponite** | **MWCNT_$O_2$** | **Bare** | | **DDM** |
| **ccNiR (pmol)** | 74 | 50 | 50 | 50 | 50 | 42 | 42 |
| **Sensitivity ($mA.M^{-1}.cm^{-2}$)** | 430 | 2400 | 580 | 951 | 520 | 333 | 444 |
| **Linear range (µM)** | 0.25 - 50 | 2.1 - 150 | 1.3 - 400 | 1 - 400 | 0.6 - 150 | 0.25 - 50 | 0.25 - 400 |
| **LOD (µM)** | 0.12 | 2.1 | 1.3 | 1.4 | 0.6 | 0.11 | 0.18 |
| **Stability (days)** | 15 (>180) | 1 (>240) | 90 (>240) | ND | 1 (ND) | 1 (ND) | ND |
| **$J_{max}$ ($\mu A.cm^{-2}$)** | 69 | 1500 | 513 | 796 | 216 | 27 | 267 |
| **$K_M$ (µM)** | (27*) 44 | 715 | 918 | 1227 | 43 | 49 | 469 |
| **$E_{measurement}$ (V) *vs* NHE** | -0.703 | -0.558 | -0.558 | -0.558 | -0.558 | -0.603 | -0.603 |

Regarding the analytical performance of the nitrite biosensors, generally a good sensitivity was attained with all configurations. The values are in the same order of magnitude than the ones obtained with other biosensing devices described in the literature (Table 1.1 in Chapter 1).

With the exception of the SWCNT based bioelectrode, the lower limits of quantification are well suited for nitrite detection in real samples, specifically for drinking waters, in agreement with EU regulations (0.1 ppm, *i.e.*, 2.2 µM).

The linear ranges varied according to the electrode modification; the SWCNT/laponite, MWCNT_$O_2$ and surfactant modified electrodes presenting the most extended ones. Despite this, the values are still bellow the nitrite dynamic ranges observed with configurations based on the combination of MET (mediated electron transfer) and polymeric immobilization systems presented in Table 1.1 (Chapter 1).

The sol-gel based sensor permitted the incorporation of c*c*NiR in a porous membrane where it retained electronic contact with the electrode surface and its catalytic activity for a long time (although it did decrease significantly after the first two weeks of sensor preparation). The sol-gel proved to be a very versatile material; the matrix was optimized based on a quite hydrophobic precursor, which was compatible with the protein, while at the same time allowed the easy diffusion of the small substrate molecules. Nevertheless, the response to nitrite was limited, as low $J_{max}$, sensitivity and linear range were observed. As an encapsulating matrix, sol-gel played its role of guarantying the extension of the lifetime of the enzyme, as compared to bare pyrolytic graphite surfaces (that have immediate response decreases after the 1$^{st}$ day of use).

The strategy presented in Chapter 4 was based on the increase of the electrode surface areas by depositing multiple layers of carbon nanotubes. These nanostructured bio-electrodes greatly enhanced the electrocatalytic activity of c*c*NiR in different types of carbon electrodes (GC and PG), but it was the pyrolytic graphite ones that gave the best results, highlighting the role of graphene based platforms for the enhancement of c*c*NiR's activity. The currents observed in these biosensors far surpassed the normal immobilization of c*c*NiR directly on electrodes or with other materials (sol-gel and surfactants) as can be judged by the elevated $J_{max}$ and sensitivity values in Table 7.1. This was most likely a consequence of a higher amount of electroactive enzyme (and not total quantity initially deposited on the electrode) contacting the transducing surfaces. The use of chemically modified MWCNTs constituted a promising approach since these could be dispersed in water. In the future such materials should be used to better preserve the catalytic activities of the enzyme and to facilitate electrode preparation. Besides the high currents and sensitivity obtained with these treated nanomaterials, a widened range of linear response to nitrite was also provided. This could be related with the highly conducting modification of the electrode, also functioning as a diffusion barrier to the analyte, just as additional polymeric layers would.

As a probable result of the biocompatibility of the modification and of the greater amount of c*c*NiR being electroactive on the SWCNT bioelectrodes, their response was kept for a very long time. Moreover, the addition of protective polymeric layers, *e.g.* laponite, supported the maintenance of the nitrite activity without significant sensitivity variations (during *ca.* 90

days no lower than 90% response was observed as compared to the 1st use of the biosensor). As in the case of the sol-gel biosensor, the enzyme remained residually active for an extended period of time (over 180 days). This trend indicates c*c*NiR as a suitable bioreceptor for the development of robust nitrite sensing devices and confirms the usefulness of those protective immobilizing layers in prolonging the lifetime of the biodevices. Furthermore, these configurations provided a better performance when compared to previously described second generation biosensors based on nitrite reductases and redox mediators [42-45].

The use of surfactant molecules to immobilize c*c*NiR on PG electrodes was another good improvement towards the enhancement of the enzyme's catalytic activity. These compounds were thought to be disrupting the hydrophobic complexes of this enzyme, exposing the catalytic subunits and thus allowing a more efficient DET with the electrode. They also provided a biomembrane like friendly environment for the encapsulation of this membrane associated protein. In the future, this type of compounds and specifically less denaturating non-ionic ones, like DDM, are to be considered to help increase the activity of the c*c*NiR in any system it might be applied in.

The kinetic parameters of c*c*NiR were different in all of the biosensor configurations as they were affected by the immobilization materials. No turnover numbers were calculated due to the difficulties in determining the electrode coverage. The $K_M$s were identical for the sol-gel and the bare electrode configurations; however, both the CNT and surfactant based bioelectrodes had increased affinity constants due to the diffusion constrains those materials generate on the enzyme's interaction with nitrite.

Another interesting biosensor characteristic that could be modulated by the type of electrode modification was the response to interfering species. From the compounds studied - nitrate, sulfite, sulfate, ammonium and hydroxylamine - the last was the most problematic, since it is an intermediate of c*c*NiR reduction reaction of nitrite to ammonium. The sol-gel matrix used in the biosensor described in Chapter 3 was able to greatly reduce the response to that compound (2.2% of the response to an equal amount of nitrite) relatively to the SWCNT sensor (20%) and others described in the literature [43], therefore being the most selective biosensor.

A good indication to the use of these devices as nitrite quantification methods in real sample analysis was given by the sol-gel based sensor. An accurate quantification of nitrite in river water samples was achieved.

Some of the issues regarding the implementation of nitrite biosensors were addressed in this work. The potentiality for use in real sample analysis, the enhancement of the c*c*NiR activity with CNTs and surfactants, the ability to protect the enzyme with polymer layers, assuring the biosensor's long term stability, and the possibility to modulate the selectivity with specific matrices, constitute important advances for nitrite biosensing with nitrite reductases.

## 7.2) Remarks on the proteomic study of *D. desulfuricans* cells

It was not possible to identify c*c*NiR in the proteomics analysis performed on the *D. desulfuricans* cells, because the protein does not enter the gels due to its hydrophobic/membrane character. The study did however allow getting a general overview on the proteins that are induced by different respiratory substrates.

As expected, the proteomes showed indications of the flexibility of *D. desulfuricans* to the use of nitrate or sulfate as terminal electron acceptors. A future identification of the proteins being differentially expressed will provide the opportunity to look at the global regulation involved in biological processes that allow this adjustment. No key conclusions could be attained because the up- and down-regulated proteins identified so far are related with stress response processes and are of hypothetical proteins of unknown functions. Nevertheless, this 2DE – MS based proteomic approach was rather promising for the understanding and identification of the regulatory networks in *D. desulfuricans*.

## 7.3) Future work

Regarding the biochemical characterization of c*c*NiR, future endeavors should cover the study of the enzyme's interaction with substrates other than nitrite and hydroxylamine. A systematic study of enzyme inhibition, the influence of pH, ionic strength, and temperature should be very useful to understand the kinetic mechanism of c*c*NiR and for developing a

robust electrochemical biosensor. Additionally, the study of the reaction by differential electrochemical mass spectrometry may allow determining the identities of the intermediates and products formed during the catalytic reaction.

In the future, it will be essential to create sensor platforms where the orientation of the enzyme molecules is possible. This will guarantee a greater reproducibility of the responses obtained (in this work a 10% or less general variation in the response, from one preparation to another, was observed). This could be achieved by the use of functionalized materials.

Another important issue to be addressed in the future is the problem of oxygen removal from the samples to be analyzed. Important advances were made with the CNT configurations which, due to the great enhancement in currents, should at least allow the detection of nitrite reducing activity at higher potentials, less prone to direct interference of oxygen.

The implementation of these or other improved systems in disposable configurations based on screen-printed electrodes is also a step envisioned for the future.

The production of sizeable amounts of proteins is also a pending issue; this could be achieved through the heterologous overexpression of this enzyme or by the understanding of the mechanisms that regulate its production in bacteria.

The creation of mutant variants with some type of modification that allow a greater activity or a way to bind or orientate it on an electrode surface, modified or not, is also to take into account in the next developments.

Finally, regarding the proteome of *D. desulfuricans* a more comprehensive study with an increased number of replicate growths and gels should raise the level of statistical confidence over the results. Also the cell cultivation methods must be reassessed due to the difficulties in controlling the growth of the bacteria in shake flasks. More controllable environments such as bioreactors, where several parameters, that influence cell growth, can be regulated (*e.g.* pH, mixing and nutrient availability) should be used for the growth of cells.

# References

## References


1. Clark, L.C., Jr.; Lyons, C. Electrode systems for continuous monitoring in cardiovascular surgery. *Ann N Y Acad Sci* **1962**, *102*, 29-45.
2. Thévenot, D.R.; Toth, K.; Durst, R.A., et al. Electrochemical biosensors: recommended definitions and classification *Pure Appl Chem* **1999**, *71*, 2333-2348.
3. Almeida, M.G. Biossensores: Modernas Ferramentas para Monitorização e Controlo Analítico. *Boletim de Biotecnologia* **2005**, *79*, 12-23.
4. Xu, Z.; Chen, X.; Dong, S. Electrochemical biosensors based on advanced bioimmobilization matrices. *TrAC, Trends Anal Chem* **2006**, *25*, 899-908.
5. Rodriguez-Mozaz, S.; Alda, M.J.L.d.; Marco, M.-P., et al. Biosensors for environmental monitoring: A global perspective. *Talanta* **2005**, *65*, 291-297.
6. Kissinger, P.T. Biosensors - A perspective. *Biosens Bioelectron* **2005**, *20*, 2512-2516.
7. Rogers, K.R.; Williams, L.R. Biosensors for environmental monitoring: a regulatory perspective. *TrAC, Trends Anal Chem* **1995**, *14*, 289-294
8. Sharma, S.K. Biomolecules for development of biosensors and their aplications. *Curr Appl Phys* **2003**, *3*, 307-316.
9. Dutt, J.; Davis, J. Current strategies in nitrite detection and their application to field analysis. *J Environ Monit* **2002**, *4*, 465-471.
10. Moorcroft, M.J.; Davis, J.; Compton, R.G. Detection and determination of nitrate and nitrite: a review. *Talanta* **2001**, *54*, 785-803.
11. Ellis, G.; Adatia, I.; Yazdanpanah, M., et al. Nitrite and nitrate analyses: a clinical biochemistry perspective. *Clin Biochem* **1998**, *31*, 195-220.
12. Hord, N.G.; Tang, Y.; Bryan, N.S. Food sources of nitrates and nitrites: the physiologic context for potential health benefits. *Am J Clin Nutr* **2009**, *90*, 1-10.
13. Correia, M.; Barroso, Â.; Barroso, M.F., et al. Contribution of different vegetable types to exogenous nitrate and nitrite exposure. *Food Chem* **2010**, *120*, 960-966.
14. Siu, D.C.; Henshall, A. Ion chromatographic determination of nitrate and nitrite in meat products. *J Chromatogr A* **1998**, *804*, 157-160.
15. Skovgaard, N. Microbiological aspects and technological need: Technological needs for nitrates and nitrites. *Food Addit Contam* **1992**, *9*, 391-397.
16. Larsson, S.C.; Orsini, N.; Wolk, A. Processed Meat Consumption and Stomach Cancer Risk: A Meta-Analysis. *J Natl Cancer Inst* **2006**, *98*, 1078-1087.
17. Lijinsky, W. N-Nitroso compounds in the diet. *Mutation Research/Genetic Toxicology and Environmental Mutagenesis* **1999**, *443*, 129-138.
18. http://www.inorganics.basf.com/p02/CAPortal/en_GB/portal/Stickoxide/content/Produktgruppen/Stickoxide/Stickoxide
19. Dutton, R. Problems with volatine corrosion inhibitorsin the metal finishing industry. *Met Finish* **2004**, *102*, 12-15.
20. Galloway, J.N.The Global Nitrogen Cycle of the chapter. In *Treatise on Geochemistry*, Heinrich, D.H., Karl, K.T., Eds.; Pergamon: Oxford, Country, 2003; pp. 557-583.
21. Victorin, K. Review of the genotoxicity of nitrogen oxides. *Mutat Res* **1994**, *317*, 43-55.

22. Smolders, A.; Lucassen, E.; Bobbink, R., et al. How nitrate leaching from agricultural lands provokes phosphate eutrophication in groundwater fed wetlands: the sulphur bridge. *Biogeochemistry* **2010**, *98*, 1-7.
23. Camargo, J.A.; Alonso, Á. Ecological and toxicological effects of inorganic nitrogen pollution in aquatic ecosystems: A global assessment. *Environ Int* **2006**, *32*, 831-849.
24. Lundberg, J.O.; Gladwin, M.T.; Ahluwalia, A., et al. Nitrate and nitrite in biology, nutrition and therapeutics. *Nat Chem Biol* **2009**, *5*, 865-869.
25. Dejam, A.; Hunter, C.J.; Schechter, A.N., et al. Emerging role of nitrite in human biology. *Blood Cells Mol Dis* **2004**, *32*, 423-429.
26. Eiserich, J.P.; Patel, R.P.; O'Donnell, V.B. Pathophysiology of nitric oxide and related species: free radical reactions and modification of biomolecules. *Molecular Aspects of Medicine* **1998**, *19*, 221-357.
27. Sun, J.; Zhang, X.; Broderick, M., et al. Measurement of Nitric Oxide Production in Biological Systems by Using Griess Reaction Assay. *Sensors* **2003**, *3*, 276-284.
28. Bryan, N.S.; Fernandez, B.O.; Bauer, S.M., et al. Nitrite is a signaling molecule and regulator of gene expression in mammalian tissues. *Nat Chem Biol* **2005**, *1*, 290-297.
29. Bryan, N.S.; Grisham, M.B. Methods to detect nitric oxide and its metabolites in biological samples. *Free Radic Biol Med* **2007**, *43*, 645-657.
30. Helmke, S.M.; Duncan, M.W. Measurement of the NO metabolites, nitrite and nitrate, in human biological fluids by GC-MS. *J Chromatogr B Analyt Technol Biomed Life Sci* **2007**, *851*, 83-92.
31. Pelletier, M.M.; Kleinbongard, P.; Ringwood, L., et al. The measurement of blood and plasma nitrite by chemiluminescence: pitfalls and solutions. *Free Radic Biol Med* **2006**, *41*, 541-548.
32. Guevara, I.; Iwanejko, J.; Dembinska-Kiec, A., et al. Determination of nitrite/nitrate in human biological material by the simple Griess reaction. *Clin Chim Acta* **1998**, *274*, 177-188.
33. Dai, Z.; Liu, S.; Ju, H., et al. Direct electron transfer and enzymatic activity of hemoglobin in a hexagonal mesoporous silica matrix. *Biosens Bioelectron* **2004**, *19*, 861-867.
34. Zhao, G.; Xu, J.-J.; Chen, H.-Y. Interfacing myoglobin to graphite electrode with an electrodeposited nanoporous ZnO film. *Anal Biochem* **2006**, *350*, 145-150.
35. Larsen, L.H.; Damgaard, L.R.; Kjær, T., et al. Fast responding biosensor for on-line determination of nitrate/nitrite in activated sludge *Wat Res* **2000**, *34*, 2463-2468
36. Reshetilov, A.N.; Iliasov, P.V.; Knackmuss, H.J., et al. The Nitrite Oxidizing Activity of *Nitrobacter* Strains as a Base of Microbial Biosensor for Nitrite Detection. *Anal Lett* **2000**, *33*, 29 - 41.
37. Einsle, O.; Kroneck, P.M. Structural basis of denitrification. *Biol Chem* **2004**, *385*, 875-883.
38. Moura, I.; Moura, J.J. Structural aspects of denitrifying enzymes. *Curr Opin Chem Biol* **2001**, *5*, 168-175.
39. Richardson, D.J.; Watmough, N.J. Inorganic nitrogen metabolism in bacteria. *Curr Opin Chem Biol* **1999**, *3*, 207-219.

40. Kiang, C.H.; Kuan, S.S.; Guilbault, G.G. A novel enzyme electrode method for the determination of nitrite based on nitrite reductase. *Anal Chim Acta* **1975**, *80*, 209-214.
41. Scharf, M.; Moreno, C.; Costa, C., et al. Electrochemical studies on nitrite reductase towards a biosensor. *Biochem Biophys Res Commun* **1995**, *209*, 1018-1025.
42. Silva, S.D.; Cosnier, S.; Almeida, M.G., et al. An efficient poly(pyrrole–viologen)-nitrite reductase biosensor for the mediated detection of nitrite. *Electrochem Comm* **2004**, *6*, 404-408.
43. Almeida, M.G.; Silveira, C.M.; Moura, J.J. Biosensing nitrite using the system nitrite redutase/Nafion/methyl viologen - a voltammetric study. *Biosens Bioelectron* **2007**, *22*, 2485-2492.
44. Chen, H.; Mousty, C.; Cosnier, S., et al. Highly sensitive nitrite biosensor based on the electrical wiring of nitrite reductase by [ZnCr-AQS] LDH. *Electrochem Comm* **2007**, *9*, 2241-2246.
45. Zhang, Z.; Xia, S.; Leonard, D., et al. A novel nitrite biosensor based on conductometric electrode modified with cytochrome c nitrite reductase composite membrane. *Biosens Bioelectron* **2009**, *24*, 1574-1579.
46. Strehlitz, B.; Grundig, B.; Schumacher, W., et al. A Nitrite Sensor Based on a Highly Sensitive Nitrite Reductase Mediator-Coupled Amperometric Detection. *Anal Chem* **1996**, *68*, 807-816.
47. Strehlitz, B.; Grundig, B.; Vorlop, K., et al. Artificial electron donors for nitrate and nitrite reductases usable as mediators in amperometric biosensors. *Journal of Anal Chem* **1994**, *349*, 676-678.
48. Ferretti, S.; Lee, S.-K.; MacCraith, B.D., et al. Optical biosensing of nitrite ions using cytochrome cd1 nitrite reductase encapsulated in a sol–gel matrix. *Analyst* **2000**, *125*, 1993-1999.
49. Rosa, C.C.; Cruz, H.J.; Vidal, M., et al. Optical biosensor based on nitrite reductase immobilised in controlled pore glass *Biosens Bioelectron* **2002**, *17*, 45-52
50. Serra, A.S.; Jorge, S.R.; Silveira, C.M., et al. Cooperative use of cytochrome cd1 nitrite reductase and its redox partner cytochrome c552 to improve the selectivity of nitrite biosensing. *Anal Chim Acta* **2011**, *693*, 41-46.
51. Wu, Q.; Storrier, G.D.; Pariente, F., et al. A Nitrite Biosensor Based on a Maltose Binding Protein Nitrite Reductase Fusion Immobilized on an Electropolymerized Film of a Pyrrole-Derived Bipyridinium. *Anal Chem* **1997**, *69*, 4856-4863.
52. Quan, D.; Min, D.G.; Cha, G.S., et al. Electrochemical characterization of biosensor based on nitrite reductase and methyl viologen co-immobilized glassy carbon electrode. *Bioelectrochemistry* **2006**, *69*, 267-275.
53. Quan, D.; Nagarale, R.K.; Shin, W. A Nitrite Biosensor Based on Coimmobilization of Nitrite Reductase and Viologen-Modified Polysiloxane on Glassy Carbon Electrode. *Electroanalysis* **2010**, *22*, 2389-2398.
54. Sasaki, S.; Karube, I.; Hirota, N., et al. Application of nitrite reductase from Alcaligenes faecalis S-6 for nitrite measurement. *Biosens Bioelectron* **1998**, *13*, 1-5.
55. Astier, Y.; Canters, G.W.; Davis, J.J., et al. Sensing nitrite through a pseudoazurin-nitrite reductase electron transfer relay. *ChemPhysChem* **2005**, *6*, 1114-1120.

56. Tepper, A.W. Electrical contacting of an assembly of pseudoazurin and nitrite reductase using DNA-directed immobilization. *J Am Chem Soc* **2010**, *132*, 6550-6557.
57. Bamford, V.A.; Angove, H.C.; Seward, H.E., et al. Structure and spectroscopy of the periplasmic cytochrome c nitrite reductase from Escherichia coli. *Biochemistry* **2002**, *41*, 2921-2931.
58. Liu, M.C.; Peck, H.D., Jr. The isolation of a hexaheme cytochrome from Desulfovibrio desulfuricans and its identification as a new type of nitrite reductase. *J Biol Chem* **1981**, *256*, 13159-13164.
59. Simon, J.; Gross, R.; Einsle, O., et al. A NapC/NirT-type cytochrome c (NrfH) is the mediator between the quinone pool and the cytochrome c nitrite reductase of Wolinella succinogenes. *Mol Microbiol* **2000**, *35*, 686-696.
60. Einsle, O.; Messerschmidt, A.; Stach, P., et al. Structure of cytochrome c nitrite reductase. *Nature* **1999**, *400*, 476-480.
61. Costa, C.; Moura, J.J.; Moura, I., et al. Hexaheme nitrite reductase from Desulfovibrio desulfuricans. Mossbauer and EPR characterization of the heme groups. *J Biol Chem* **1990**, *265*, 14382-14388.
62. Einsle, O.; Messerschmidt, A.; Huber, R., et al. Mechanism of the six-electron reduction of nitrite to ammonia by cytochrome c nitrite reductase. *J Am Chem Soc* **2002**, *124*, 11737-11745.
63. Stach, P.; Einsle, O.; Schumacher, W., et al. Bacterial cytochrome c nitrite reductase: new structural and functional aspects. *J Inorg Biochem* **2000**, *79*, 381-385.
64. Lukat, P.; Rudolf, M.; Stach, P., et al. Binding and reduction of sulfite by cytochrome c nitrite reductase. *Biochemistry* **2008**, *47*, 2080-2086.
65. Pereira, I.C.; Abreu, I.A.; Xavier, A.V., et al. Nitrite reductase from Desulfovibrio desulfuricans (ATCC 27774)--a heterooligomer heme protein with sulfite reductase activity. *Biochem Biophys Res Commun* **1996**, *224*, 611-618.
66. Rodrigues, M.L.; Oliveira, T.F.; Pereira, I.A., et al. X-ray structure of the membrane-bound cytochrome c quinol dehydrogenase NrfH reveals novel haem coordination. *Embo J* **2006**, *25*, 5951-5960.
67. Almeida, M.G.; Macieira, S.; Goncalves, L.L., et al. The isolation and characterization of cytochrome c nitrite reductase subunits (NrfA and NrfH) from Desulfovibrio desulfuricans ATCC 27774. Re-evaluation of the spectroscopic data and redox properties. *Eur J Biochem* **2003**, *270*, 3904-3915.
68. Rodrigues, M.L.; Oliveira, T.; Matias, P.M., et al. Crystallization and preliminary structure determination of the membrane-bound complex cytochrome c nitrite reductase from Desulfovibrio vulgaris Hildenborough. *Acta Crystallogr Sect F Struct Biol Cryst Commun* **2006**, *62*, 565-568.
69. Clarke, T.A.; Mills, P.C.; Poock, S.R., et al. Escherichia coli cytochrome c nitrite reductase NrfA. *Methods Enzymol* **2008**, *437*, 63-77.
70. Simon, J. Enzymology and bioenergetics of respiratory nitrite ammonification. *FEMS Microbiol Rev* **2002**, *26*, 285-309.
71. Cunha, C.A.; Macieira, S.; Dias, J.M., et al. Cytochrome c nitrite reductase from Desulfovibrio desulfuricans ATCC 27774. The relevance of the two calcium sites in the structure of the catalytic subunit (NrfA). *J Biol Chem* **2003**, *278*, 17455-17465.

72. Einsle, O.; Stach, P.; Messerschmidt, A., et al. Cytochrome c Nitrite Reductase from Wolinella succinogenes. *J Biol Chem* **2000**, *275*, 39608-39616.
73. Clarke, T.A.; Hemmings, A.M.; Burlat, B., et al. Comparison of the structural and kinetic properties of the cytochrome c nitrite reductases from Escherichia coli, Wolinella succinogenes, Sulfurospirillum deleyianum and Desulfovibrio desulfuricans. *Biochem Soc Trans* **2006**, *34*, 143–145.
74. Pereira, I.A.; LeGall, J.; Xavier, A.V., et al. Characterization of a heme c nitrite reductase from a non-ammonifying microorganism, Desulfovibrio vulgaris Hildenborough. *Biochim Biophys Acta* **2000**, *1481*, 119-130.
75. Liu, M.-C.; Costa, C.; Moura, I.[21] Hexaheme nitrite reductase from Desulfovibrio desulfuricans (ATCC 27774) of the chapter. In *Methods in Enzymology*, Harry D. Peck, J.J.L., Eds.; Academic Press: Country, 1994; Volume 243 Volume 243, pp. 303-319.
76. Almeida, M.G.; Silveira, C.M.; Guigliarelli, B., et al. A needle in a haystack: the active site of the membrane-bound complex cytochrome c nitrite reductase. *FEBS Lett* **2007**, *581*, 284-288.
77. Angove, H.C.; Cole, J.A.; Richardson, D.J., et al. Protein film voltammetry reveals distinctive fingerprints of nitrite and hydroxylamine reduction by a cytochrome c nitrite reductase. *J Biol Chem* **2002**, *277*, 23374-23381.
78. Gwyer, J.D.; Richardson, D.J.; Butt, J.N. Diode or tunnel-diode characteristics? Resolving the catalytic consequences of proton coupled electron transfer in a multi-centered oxidoreductase. *J Am Chem Soc* **2005**, *127*, 14964-14965.
79. Gwyer, J.D.; Richardson, D.J.; Butt, J.N. Inhibiting Escherichia coli cytochrome c nitrite reductase: voltammetry reveals an enzyme equipped for action despite the chemical challenges it may face in vivo. *Biochem Soc Trans* **2006**, *34*, 133-135.
80. Gwyer, J.D.; Angove, H.C.; Richardson, D.J., et al. Redox-triggered events in cytochrome c nitrite reductase. *Bioelectrochemistry* **2004**, *63*, 43-47.
81. Gwyer, J.D.; Richardson, D.J.; Butt, J.N. Resolving complexity in the interactions of redox enzymes and their inhibitors: contrasting mechanisms for the inhibition of a cytochrome c nitrite reductase revealed by protein film voltammetry. *Biochemistry* **2004**, *43*, 15086-15094.
82. Gwyer, J.D.; Zhang, J.; Butt, J.N., et al. Voltammetry and in situ scanning tunneling microscopy of cytochrome C nitrite reductase on Au(111) electrodes. *Biophys J* **2006**, *91*, 3897-3906.
83. Wonderen, J.H.v.; Burlat, B.; Richardson, D.J., et al. The Nitric Oxide Reductase Activity of Cytochrome c Nitrite Reductase from Escherichia coli. *J Biol Chem* **2008**, *283*, 9587-9594.
84. Schröder, I.; Roberton, A.M.; Bokranz, M., et al. The membraneous nitrite reductase involved in the electron transport of Wolinella succinogenes. *Arch Microbiol* **1985**, *140*, 380-386.
85. Clarke, T.A.; Kemp, G.L.; Van Wonderen, J.H., et al. Role of a conserved glutamine residue in tuning the catalytic activity of Escherichia coli cytochrome c nitrite reductase. *Biochemistry* **2008**, *47*, 3789-3799.
86. Armstrong, F.A.; Heering, H.A.; Hirst, J. Reactions of Complex Metalloproteins Studied by Protein-Film Voltammetry. *Chem Soc Rev* **1997**, *26*, 169-179.

87. Leger, C.; Bertrand, P. Direct electrochemistry of redox enzymes as a tool for mechanistic studies. *Chem Rev* **2008**, *108*, 2379-2438.

88. Nicholas, J.D.; Nason, A. Determination of nitrate and nitrite *Methods Enzymol* **1957**, *3*, 981-984.

89. Searcy, R.L.; Simms, N.M.; Foreman, J.A., et al. A study of the specificity of the Berthelot colour reaction. *Clin Chim Acta* **1965**, *12*, 170-175.

90. Duhovny, D.; Nussinov, R.; Wolfson, H. Efficient Unbound Docking of Rigid Molecules In Gusfield et al., Ed. Proceedings of the 2'nd Workshop on Algorithms in Bioinformatics(WABI) Rome, Italy, Lecture Notes in Computer Science 2452. In Springer Verlag, 2002.

91. Schneidman-Duhovny, D.; Inbar, Y.; Nussinov, R., et al. PatchDock and SymmDock: servers for rigid and symmetric docking. *Nucleic Acids Res* **2005**, *33*, W363-367.

92. Pettersen, E.F.; Goddard, T.D.; Huang, C.C., et al. UCSF Chimera--a visualization system for exploratory research and analysis. *J Comput Chem* **2004**, *25*, 1605-1612.

93. Pisa, R.; Stein, T.; Eichler, R., et al. The nrfI gene is essential for the attachment of the active site haem group of Wolinella succinogenes cytochrome c nitrite reductase. *Mol Microbiol* **2002**, *43*, 763-770.

94. Tipton, K.F. Principles of enzyme assay and kinetic studies, in Enzyme Assays A Practical Approach (Eisenthal, R and Danson, M J, eds ) In Oxford University Press, 1993.

95. Monk, P.M.S. Fundamentals of Electroanalytical Chemistry. In John Wiley & Sons, 2002.

96. Wang, J. Amperometric biosensors for clinical and therapeutic drug monitoring: a review. *J Pharm Biomed Anal* **1999**, *19*, 47-53.

97. Willner, B.; Katz, E.; Willner, I. Electrical contacting of redox proteins by nanotechnological means. *Curr Opin Biotechnol* **2006**, *17*, 589-596.

98. Gorton, L.; Lindgren, A.; Larsson, T., et al. Direct electron transfer between heme-containing enzymes and electrodes as basis for third generation biosensors. *Anal Chim Acta* **1999**, *400*, 91-108.

99. Wu, Y.; Hu, S. Biosensors based on direct electron transfer in redox proteins. *Microchim Acta* **2007**, *159*, 1-17.

100. Barreau, S.; Miller, J.N. Highlight. Sol-gel systems for biosensors. *Anal Commun* **1996**, *33*, 5H-6H.

101. Avnir, D.; Braun, S.; Lev, O., et al. Enzymes and Other Proteins Entrapped in Sol-Gel Materials. *Chem Mater* **1994**, *6*, 1605-1614.

102. Wang, J. Sol-gel materials for electrochemical biosensors. *Anal Chim Acta* **1999**, *399*, 21-27.

103. Gupta, R.; Chaudhury, N.K. Entrapment of biomolecules in sol-gel matrix for applications in biosensors: problems and future prospects. *Biosens Bioelectron* **2007**, *22*, 2387-2399.

104. Livage, J.; Coradin, T.; Roux, C. Encapsulation of biomolecules in silica gels. *J Phys Condens Matter* **2001**, *13*, R673-R691.

105. Lin, J.; Brown, C.W. Sol-gel glass as a matrix for chemical and biochemical sensing. *TrAC, Trends Anal Chem* **1997**, *16*, 200-211.

106. Airoldi, C.; Farias, R.F. Alcóxidos como precursores na síntese de novos materiais através do processo sol-gel. *Química Nova* **2004**, *27*, 84-88.
107. Avnir, D. Organic Chemistry within Ceramic Matrixes: Doped Sol-Gel Materials. *Acc Chem Res* **1995**, *28*, 328-334.
108. Lev, O.; Tsionsky, M.; Rabinovich, L., et al. Organically Modified Sol-gel Sensors. *Anal Chem* **1995**, *67*, 22A - 30A.
109. Dave, B.C.; Dunn, B.; Valentine, J.S., et al. Sol-gel encapsulation methods for biosensors. *Anal Chem* **1994**, *66*, 1120A-1127A.
110. Walcarius, A. Electroanalysis with Pure, Chemically Modified and Sol-Gel-Derived Silica-Based Materials. *Electroanalysis* **2001**, *13*, 701-718.
111. Hench, L.L.; West, J.K. The sol-gel process. *Chem Rev* **1990**, *90*, 33-72.
112. Pandey, P.C.; Upadhyay, S.; Pathak, H.C. A New Glucose Biosensor Based on Sandwich Configuration of Organically Modified Sol-Gel Glass. *Electroanalysis* **1999**, *11*, 59-64.
113. Pandey, P.C.; Upadhyay, S.; Pathak, H.C. A new glucose sensor based on encapsulated glucose oxidase within organically modified sol–gel glass. *Sens Actuators, B* **1999**, *60*, 83-89.
114. Couto, C.M.C.M.; Araújo, A.N.; Montenegro, M.C.B.S.M., et al. Application of amperometric sol-gel biosensor to flow injection determination of glucose. *Talanta* **2002**, *56*, 997-1003.
115. Narang, U.; Prasad, P.N.; Bright, F.V., et al. A Novel Protocol to Entrap Active Urease in a Tetraethoxysilane-Derived Sol-Gel Thin-Film Architecture. *Chem Mater* **1994**, *6*, 1596-1598.
116. Di, J.; Shen, C.; Peng, S., et al. A one-step method to construct a third-generation biosensor based on horseradish peroxidase and gold nanoparticles embedded in silica sol-gel network on gold modified electrode. *Anal Chim Acta* **2005**, *553*, 196-200.
117. Gomes, S.P.; Odlozilikova, M.; Almeida, M.G., et al. Application of lactate amperometric sol-gel biosensor to sequential injection determination of L-lactate. *J Pharm Biomed Anal* **2007**, *43*, 1376-1381.
118. Ramanathan, K.; Kamalasanan, M.N.; Malhotra, B.D., et al. Immobilization and Characterization of Lactate Dehydrogenase on TEOS Derived Sol-Gel Films. *J Sol-Gel Sci Technol* **1997**, *10*, 309-316.
119. Aylott, J.W.; Richardson, D.J.; Russell, D.A. Optical Biosensing of Nitrate Ions Using a Sol-Gel Immobilized Nitrate Reductase. *Analyst* **1997**, *122*, 77-80.
120. Sun, Y.X.; Wang, S.F. Direct electrochemistry and electrocatalytic characteristic of heme proteins immobilized in a new sol-gel polymer film. *Bioelectrochemistry* **2007**, *71*, 172-179.
121. McDonagh, C.; Sheridan, F.; Butler, T., et al. Characterisation of sol-gel-derived silica films. *J. Non-Cryst Solids* **1996**, *194*, 72-77.
122. Collinson, M.M.; Howells, A.R. Sol-gels and electrochemistry: research at the intersection. *Anal Chem* **2000**, *72*, 702A-709A.
123. Bharathi, S. Sol-gel-derived nanocrystalline gold-silicate composite biosensor. *Anal Commun* **1998**, *35*, 29-31.
124. Wang, J.; Pamidi, P.V.A. Sol−Gel-Derived Gold Composite Electrodes. *Anal Chem* **1997**, *69*, 4490-4494.

125. Rabinovich, L.; Lev, O. Sol-Gel Derived Composite Ceramic Carbon Electrodes. *Electroanalysis* **2001**, *13*, 265-275.
126. Tsionsky, M.; Gun, G.; Glezer, V., et al. Sol-Gel-Derived Ceramic-Carbon Composite Electrodes: Introduction and Scope of Applications. *Anal Chem* **1994**, *66*, 1747-1753.
127. Gun, J.; Lev, O. Sol-gel derived, ferrocenyl-modified silicate-graphite composite electrode: Wiring of glucose oxidase. *Anal Chim Acta* **1996**, *336*, 95-106.
128. Jena, B.K.; Raj, C.R. Electrochemical Biosensor Based on Integrated Assembly of Dehydrogenase Enzymes and Gold Nanoparticles. *Anal Chem* **2006**, *78*, 6332-6339.
129. Wang, J.; Pamidi, P.V.A.; Zanette, D.R. Self-Assembled Silica Gel Networks. *J Am Chem Soc* **1998**, *120*, 5852-5853.
130. Pandey, P.C.; Upadhyay, S.; Pathak, H.C., et al. Studies on Ferrocene Immobilized Sol-Gel Glasses and Its Application in the Construction of a Novel Solid-State Ion Sensor. *Electroanalysis* **1999**, *11*, 950-956.
131. Dave, B.C.; Miller, J.M.; Dunn, B., et al. Encapsulation of Proteins in Bulk and Thin Film Sol-Gel Matrices. *J Sol-Gel Sci Technol* **1997**, *8*, 629-634.
132. Siebert, F.; Hildebrandt, P. Heme Proteins. In *Vibrational Spectroscopy in Life Science*, Wiley-VCH Verlag GmbH & Co. Weinheim, 2008.
133. Cai, C.; Chen, J. Direct electron transfer and bioelectrocatalysis of hemoglobin at a carbon nanotube electrode. *Anal Biochem* **2004**, *325*, 285-292.
134. Wang, S.; Xie, F.; Liu, G. Direct electrochemistry and electrocatalysis of heme proteins on SWCNTs-CTAB modified electrodes. *Talanta* **2009**, *77*, 1343-1350.
135. McCreery, R.L. Advanced carbon electrode materials for molecular electrochemistry. *Chem Rev* **2008**, *108*, 2646-2687.
136. Wang, J. Nanomaterial-based electrochemical biosensors. *Analyst* **2005**, *130*, 421-426.
137. Balasubramanian, K.; Burghard, M. Biosensors based on carbon nanotubes. *Anal Bioanal Chem* **2006**, *385*, 452-468.
138. Davis, J.J.; Coleman, K.S.; Azamian, B.R., et al. Chemical and biochemical sensing with modified single walled carbon nanotubes. *Chemistry* **2003**, *9*, 3732-3739.
139. Gong, K.; Yan, Y.; Zhang, M., et al. Electrochemistry and electroanalytical applications of carbon nanotubes: a review. *Anal Sci* **2005**, *21*, 1383-1393.
140. Gooding, J.J. Nanostructuring electrodes with carbon nanotubes: A review on electrochemistry and applications for sensing. *Electrochim Acta* **2005**, *50*, 3049-3060.
141. Jacobs, C.B.; Peairs, M.J.; Venton, B.J. Review: Carbon nanotube based electrochemical sensors for biomolecules. *Anal Chim Acta* **2010**, *662*, 105-127.
142. Rivas, G.A.; Rubianes, M.D.; Rodriguez, M.C., et al. Carbon nanotubes for electrochemical biosensing. *Talanta* **2007**, *74*, 291-307.
143. Trojanowicz, M. Analytical applications of carbon nanotubes: a review. *TrAC, Trends Anal Chem* **2006**, *25*, 480-489.
144. Wang, J. Carbon-Nanotube Based Electrochemical Biosensors: A Review. *Electroanalysis* **2005**, *17*, 7-14.
145. Banks, C.E.; Compton, R.G. Exploring the electrocatalytic sites of carbon nanotubes for NADH detection: an edge plane pyrolytic graphite electrode study. *Analyst* **2005**, *130*, 1232-1239.

146. Banks, C.E.; Moore, R.R.; Davies, T.J., et al. Investigation of modified basal plane pyrolytic graphite electrodes: definitive evidence for the electrocatalytic properties of the ends of carbon nanotubes. *Chem Commun* **2004**, 1804-1805.
147. Ji, X.; Kadara, R.O.; Krussma, J., et al. Understanding the Physicoelectrochemical Properties of Carbon Nanotubes: Current State of the Art. *Electroanalysis* **2010**, *22*, 7-19.
148. Rao, C.N.R.; Satishkumar, B.C.; Govindaraj, A., et al. Nanotubes. *Chem Phys Chem* **2001**, *2*, 78-105.
149. Hamada, N.; Sawada, S.-i.; Oshiyama, A. New one-dimensional conductors: Graphitic microtubules. *Phys Rev Lett* **1992**, *68*, 1579.
150. Saito, R.; Fujita, M.; Dresselhaus, G., et al. Electronic structure of chiral graphene tubules. *Appl Phys Lett* **1992**, *60*, 2204-2206.
151. Dresselhaus, M.S.; Lin, Y.M.; Rabin, O., et al. Nanowires and nanotubes. *Mater Sci Eng, C* **2003**, *23*, 129-140.
152. Peigney, A.; Laurent, C.; Flahaut, E., et al. Specific surface area of carbon nanotubes and bundles of carbon nanotubes. *Carbon* **2001**, *39*, 507-514.
153. Journet, C.; Maser, W.K.; Bernier, P., et al. Large-scale production of single-walled carbon nanotubes by the electric-arc technique. *Nature* **1997**, *388*, 756-758.
154. Kingston, C.T.; Simard, B. Fabrication of Carbon Nanotubes. *Anal Lett* **2003**, *36*, 3119 - 3145.
155. Thess, A.; Lee, R.; Nikolaev, P., et al. Crystalline Ropes of Metallic Carbon Nanotubes. *Science* **1996**, *273*, 483-487.
156. Balasubramanian, K.; Burghard, M. Chemically Functionalized Carbon Nanotubes. *Small* **2005**, *1*, 180-192.
157. Furtado, C.A.; Kim, U.J.; Gutierrez, H.R., et al. Debundling and Dissolution of Single-Walled Carbon Nanotubes in Amide Solvents. *J Am Chem Soc* **2004**, *126*, 6095-6105.
158. Valcárcel, M.; Cárdenas, S.; Simonet, B.M. Role of Carbon Nanotubes in Analytical Science. *Anal Chem* **2007**, *79*, 4788-4797.
159. Britto, P.J.; Santhanam, K.S.V.; Rubio, A., et al. Improved Charge Transfer at Carbon Nanotube Electrodes. *Adv Mater* **1999**, *11*, 154-157.
160. Hiura, H.; Ebbesen, T.W.; Tanigaki, K. Opening and purification of carbon nanotubes in high yields. *Adv Mater* **1995**, *7*, 275-276.
161. Liu, J.; Rinzler, A.G.; Dai, H., et al. Fullerene Pipes. *Science* **1998**, *280*, 1253-1256.
162. Moore, R.R.; Banks, C.E.; Compton, R.G. Basal Plane Pyrolytic Graphite Modified Electrodes: Comparison of Carbon Nanotubes and Graphite Powder as Electrocatalysts. *Anal Chem* **2004**, *76*, 2677-2682.
163. Vairavapandian, D.; Vichchulada, P.; Lay, M.D. Preparation and modification of carbon nanotubes: Review of recent advances and applications in catalysis and sensing. *Anal Chim Acta* **2008**, *626*, 119-129.
164. Chen, J.; Hamon, M.A.; Hu, H., et al. Solution Properties of Single-Walled Carbon Nanotubes. *Science* **1998**, *282*, 95-98.

165. Cosnier, S.; Holzinger, M. Design of carbon nanotube-polymer frameworks by electropolymerization of SWCNT-pyrrole derivatives. *Electrochim Acta* **2008**, *53*, 3948-3954
166. Katz, E.; Willner, I. Biomolecule-Functionalized Carbon Nanotubes: Applications in Nanobioelectronics. *Chem Phys Chem* **2004**, *5*, 1084-1104.
167. Davis, J.J.; Coles, R.J.; Allen, H., et al. Protein electrochemistry at carbon nanotube electrodes. *Journal of Anal Chem* **1997**, *440*, 279-282.
168. Valentini, F.; Amine, A.; Orlanducci, S., et al. Carbon Nanotube Purification: Preparation and Characterization of Carbon Nanotube Paste Electrodes. *Anal Chem* **2003**, *75*, 5413-5421.
169. Rubianes, M.D.; Rivas, G.A. Carbon nanotubes paste electrode. *Electrochem Commun* **2003**, *5*, 689-694.
170. Britto, P.J.; Santhanam, K.S.V.; Ajayan, P.M. Carbon nanotube electrode for oxidation of dopamine. *Bioelectrochem Bioenerg* **1996**, *41*, 121-125.
171. Wang, J.; Musameh, M. Carbon nanotube screen-printed electrochemical sensors. *Analyst* **2004**, *129*, 1-2.
172. Gooding, J.J.; Wibowo, R.; Liu, J., et al. Protein electrochemistry using aligned carbon nanotube arrays. *J Am Chem Soc* **2003**, *125*, 9006-9007.
173. Yu, X.; Chattopadhyay, D.; Galeska, I., et al. Peroxidase activity of enzymes bound to the ends of single-wall carbon nanotube forest electrodes. *Electrochem Commun* **2003**, *5*, 408-411.
174. Fei, S.; Chen, J.; Yao, S., et al. Electrochemical behavior of l-cysteine and its detection at carbon nanotube electrode modified with platinum. *Anal Biochem* **2005**, *339*, 29-35.
175. Zhao, L.; Liu, H.; Hu, N. Assembly of layer-by-layer films of heme proteins and single-walled carbon nanotubes: electrochemistry and electrocatalysis. *Anal Bioanal Chem* **2006**, *384*, 414-422.
176. Musameh, M.; Wang, J.; Merkoci, A., et al. Low-potential stable NADH detection at carbon-nanotube-modified glassy carbon electrodes. *Electrochem Commun* **2002**, *4*, 743-746.
177. Salimi, A.; Banks, C.E.; Compton, R.G. Abrasive immobilization of carbon nanotubes on a basal plane pyrolytic graphite electrode: application to the detection of epinephrine. *Analyst* **2004**, *129*, 225-228.
178. Deng, S.; Jian, G.; Lei, J., et al. A glucose biosensor based on direct electrochemistry of glucose oxidase immobilized on nitrogen-doped carbon nanotubes. *Biosens Bioelectron* **2009**, *25*, 373-377.
179. Guiseppi-Elie, A. Direct electron transfer of glucose oxidase on carbon nanotubes. *Nanotechnology* **2002**, *13*, 559.
180. Wang, M.; Shen, Y.; Liu, Y., et al. Direct electrochemistry of microperoxidase 11 using carbon nanotube modified electrodes. *Journal of Anal Chem* **2005**, *578*, 121-127.
181. Prakash, P.A.; Yogeswaran, U.; Chen, S.-M. Direct electrochemistry of catalase at multiwalled carbon nanotubes-nafion in presence of needle shaped DDAB for H2O2 sensor. *Talanta* **2009**, *78*, 1414-1421.

182. Salimi, A.; Noorbakhsh, A.; Ghadermarz, M. Direct electrochemistry and electrocatalytic activity of catalase incorporated onto multiwall carbon nanotubes-modified glassy carbon electrode. *Anal Biochem* **2005**, *344*, 16-24.
183. Wang, J.; Li, M.; Shi, Z., et al. Direct Electrochemistry of Cytochrome c at a Glassy Carbon Electrode Modified with Single-Wall Carbon Nanotubes. *Anal Chem* **2002**, *74*, 1993-1997.
184. Zhao, G.-C.; Zhang, L.; Wei, X.-W., et al. Myoglobin on multi-walled carbon nanotubes modified electrode: direct electrochemistry and electrocatalysis. *Electrochem Commun* **2003**, *5*, 825-829.
185. Ionescu, R.E.; Cosnier, S.; Marks, R.S. Protease amperometric sensor. *Anal Chem* **2006**, *78*, 6327-6331.
186. Haddad, R.; Cosnier, S.; Maaref, A., et al. Non-covalent biofunctionalization of single-walled carbon nanotubes via biotin attachment by pi-stacking interactions and pyrrole polymerization. *Analyst* **2009**, *134*, 2412-2418.
187. Gonçalves, A.G.; Figueiredo, J.L.; Órfão, J.J.M., et al. Influence of the surface chemistry of multi-walled carbon nanotubes on their activity as ozonation catalysts. *Carbon* **2010**, *48*, 4369-4381.
188. Holzinger, M.; Bouffier, L.; Villalonga, R., et al. Adamantane/beta-cyclodextrin affinity biosensors based on single-walled carbon nanotubes. *Biosens Bioelectron* **2009**, *24*, 1128-1134.
189. Haddad, R.; Cosnier, S.; Maaref, A., et al. Electrochemical Characterization of Biotin Functionalized and Regular Single-Walled Carbon Nanotube Coatings. Application to Amperometric Glucose Biosensors. *Sens Lett* **2009**, *7*, 801-805.
190. Shao, Y.; Wang, J.; Wu, H., et al. Graphene Based Electrochemical Sensors and Biosensors: A Review. *Electroanalysis* **2010**, *22*, 1027-1036.
191. Guto, P.M.; Rusling, J.F. Myoglobin retains iron heme and near-native conformation in DDAB films prepared from pH 5 to 7 dispersions. *Electrochem Commun* **2006**, *8*, 455-459.
192. Nassar, A.-E.F.; Rusling, J.F.; Kumosinski, T.F. Salt and pH effects on electrochemistry of myoglobin in thick films of a bilayer-forming surfactant. *Biophys Chem* **1997**, *67*, 107-116.
193. Rusling, J.F. Enzyme Bioelectrochemistry in Cast Biomembrane-Like Films. *Acc Chem Res* **1998**, *31*, 363-369.
194. Lu, Z.; Huang, Q.; Rusling, J.F. Films of hemoglobin and didodecyldimethylammonium bromide with enhanced electron transfer rates. *Journal of Anal Chem* **1997**, *423*, 59-66.
195. Nassar, A.-E.F.; Willis, W.S.; Rusling, J.F. Electron Transfer from Electrodes to Myoglobin: Facilitated in Surfactant Films and Blocked by Adsorbed Biomacromolecules. *Anal Chem* **1995**, *67*, 2386-2392.
196. Rusling, J.F.; Nassar, A.E.F. Enhanced electron transfer for myoglobin in surfactant films on electrodes. *J Am Chem Soc* **1993**, *115*, 11891-11897.
197. Vittal, R.; Gomathi, H.; Kim, K.-J. Beneficial role of surfactants in electrochemistry and in the modification of electrodes. *Adv Colloid Interface Sci* **2006**, *119*, 55-68.

198. Wang, F.; Chen, X.; Xu, Y., et al. Enhanced electron transfer for hemoglobin entrapped in a cationic gemini surfactant films on electrode and the fabrication of nitric oxide biosensor. *Biosens Bioelectron* **2007**, *23*, 176-182.
199. le Maire, M.; Champeil, P.; Moller, J.V. Interaction of membrane proteins and lipids with solubilizing detergents. *Biochim Biophys Acta* **2000**, *1508*, 86-111.
200. Seddon, A.M.; Curnow, P.; Booth, P.J. Membrane proteins, lipids and detergents: not just a soap opera. *Biochimica et Biophysica Acta (BBA) - Biomembranes* **2004**, *1666*, 105-117.
201. Hu, N. Direct electrochemistry of redox proteins or enzymes at various film electrodes and their possible applications in monitoring some pollutants. *Pure Appl Chem* **2001**, *73*, 1979-1991.
202. Mimica, D.; Zagal, J.H.; Bedioui, F. Electroreduction of nitrite by hemin, myoglobin and hemoglobin in surfactant films. *J Electroanal Chem* **2001**, *497*, 106-113.
203. Zhang, Z.; Rusling, J.F. Electron transfer between myoglobin and electrodes in thin films of phosphatidylcholines and dihexadecylphosphate. *Biophys Chem* **1997**, *63*, 133-146.
204. Brajter-Toth, A.; Chambers, J.Q. Electroanalytical methods for biological materials. In Marcel Dekker, 2002.
205. George, P.; Hanania, G. A spectrophotometric study of ionizations in methaemoglobin. *Biochem J* **1953**, *55*, 236-243.
206. Udit, A.K.; Hill, M.G.; Gray, H.B. Electrochemistry of Cytochrome P450 BM3 in Sodium Dodecyl Sulfate Films. *Langmuir* **2006**, *22*, 10854-10857.
207. Kern, M.; Simon, J. Production of recombinant multiheme cytochromes c in Wolinella succinogenes. *Methods Enzymol* **2011**, *486*, 429-446.
208. Steger, J.L.; Vincent, C.; Ballard, J.D., et al. Desulfovibrio sp. genes involved in the respiration of sulfate during metabolism of hydrogen and lactate. *Appl Environ Microbiol* **2002**, *68*, 1932-1937.
209. Fournier, M.; Aubert, C.; Dermoun, Z., et al. Response of the anaerobe Desulfovibrio vulgaris Hildenborough to oxidative conditions: proteome and transcript analysis. *Biochimie* **2006**, *88*, 85-94.
210. Cypionka, H. Oxygen respiration by desulfovibrio species. *Annu Rev Microbiol* **2000**, *54*, 827-848.
211. Lobo, S.A.L.; Melo, A.M.P.; Carita, J.N., et al. The anaerobe Desulfovibrio desulfuricans ATCC 27774 grows at nearly atmospheric oxygen levels. *FEBS Lett* **2007**, *581*, 433-436.
212. Moura, I.; Bursakov, S.; Costa, C., et al. Nitrate and nitrite utilization in sulfate-reducing bacteria. *Anaerobe* **1997**, *3*, 279-290.
213. Postgate, J.R.; Campbell, L.L. Classification of Desulfovibrio species, the nonsporulating sulfate-reducing bacteria. *Bacteriol Rev* **1966**, *30*, 732-738.
214. Richardson, D.J. Bacterial respiration: a flexible process for a changing environment. *Microbiology* **2000**, *146 ( Pt 3)*, 551-571.
215. Marietou, A.; Griffiths, L.; Cole, J. Preferential Reduction of the Thermodynamically Less Favorable Electron Acceptor, Sulfate, by a Nitrate-Reducing Strain of the Sulfate-Reducing Bacterium Desulfovibrio desulfuricans 27774. *J Bacteriol* **2009**, *191*, 882-889.

216. Dalsgaard, T.; Bak, F. Nitrate Reduction in a Sulfate-Reducing Bacterium, Desulfovibrio desulfuricans, Isolated from Rice Paddy Soil: Sulfide Inhibition, Kinetics, and Regulation. *Appl Environ Microbiol* **1994**, *60*, 291-297.
217. Mitchell, G.J.; Jones, J.G.; Cole, J.A. Distribution and regulation of nitrate and nitrite reduction by Desulfovibrio and Desulfotomaculum species. *Arch Microbiol* **1986**, *144*, 35-40.
218. Haveman, S.A.; Greene, E.A.; Stilwell, C.P., et al. Physiological and gene expression analysis of inhibition of Desulfovibrio vulgaris hildenborough by nitrite. *J Bacteriol* **2004**, *186*, 7944-7950.
219. Seitz, H.-J.; Cypionka, H. Chemolithotrophic growth of Desulfovibrio desulfuricans with hydrogen coupled to ammonification of nitrate or nitrite. *Arch Microbiol* **1986**, *146*, 63-67.
220. Mills, P.C.; Rowley, G.; Spiro, S., et al. A combination of cytochrome c nitrite reductase (NrfA) and flavorubredoxin (NorV) protects Salmonella enterica serovar Typhimurium against killing by NO in anoxic environments. *Microbiology* **2008**, *154*, 1218-1228.
221. Poock, S.R.; Leach, E.R.; Moir, J.W., et al. Respiratory detoxification of nitric oxide by the cytochrome c nitrite reductase of Escherichia coli. *J Biol Chem* **2002**, *277*, 23664-23669.
222. Haveman, S.A.; Greene, E.A.; Voordouw, G. Gene expression analysis of the mechanism of inhibition of Desulfovibrio vulgaris Hildenborough by nitrate-reducing, sulfide-oxidizing bacteria. *Environ Microbiol* **2005**, *7*, 1461-1465.
223. Greene, E.A.; Hubert, C.; Nemati, M., et al. Nitrite reductase activity of sulphate-reducing bacteria prevents their inhibition by nitrate-reducing, sulphide-oxidizing bacteria. *Environ Microbiol* **2003**, *5*, 607-617.
224. Roediger, W.E.; Moore, J.; Babidge, W. Colonic sulfide in pathogenesis and treatment of ulcerative colitis. *Dig Dis Sci* **1997**, *42*, 1571-1579.
225. Hamilton, W.A. Bioenergetics of sulphate-reducing bacteria in relation to their environmental impact. *Biodegradation* **1998**, *9*, 201-212.
226. Rodionov, D.A.; Dubchak, I.; Arkin, A., et al. Reconstruction of regulatory and metabolic pathways in metal-reducing delta-proteobacteria. *Genome Biol* **2004**, *5*, R90.
227. Lloyd, J.R. Microbial reduction of metals and radionuclides. *FEMS Microbiol Rev* **2003**, *27*, 411-425.
228. Dutt, M.J.; Lee, K.H. Proteomic analysis. *Curr Opin Biotechnol* **2000**, *11*, 176-179.
229. Görg, A.; Drews, O.; Lück, C., et al. 2-DE with IPGs. *Electrophoresis* **2009**, *30*, S122-S132.
230. Görg, A.; Weiss, W.; Dunn, M.J. Current two-dimensional electrophoresis technology for proteomics. *Proteomics* **2004**, *4*, 3665-3685.
231. Wittmann-Liebold, B.; Graack, H.R.; Pohl, T. Two-dimensional gel electrophoresis as tool for proteomics studies in combination with protein identification by mass spectrometry. *Proteomics* **2006**, *6*, 4688-4703.
232. Alban, A.; David, S.O.; Bjorkesten, L., et al. A novel experimental design for comparative two-dimensional gel analysis: two-dimensional difference gel electrophoresis incorporating a pooled internal standard. *Proteomics* **2003**, *3*, 36-44.
233. Lilley, K.S.; Friedman, D.B. Difference gel electrophoresis DIGE. *Drug Discovery Today: Technologies* **2006**, *3*, 347-353.

234. Chakravarti, B.; Gallagher, S.R.; Chakravarti, D.N.Difference Gel Electrophoresis (DIGE) Using CyDye DIGE Fluor Minimal Dyes of the chapter. In *Current Protocols in Molecular Biology*, Eds.; John Wiley & Sons, Inc.: Country, 2001; pp.

235. Zinkevich, V.; Beech, I.B. Screening of sulfate-reducing bacteria in colonoscopy samples from healthy and colitic human gut mucosa. *FEMS Microbiol Ecol* **2000**, *34*, 147-155.

236. Laemmli, U.K. Cleavage of structural proteins during the assembly of the head of bacteriophage T4. *Nature* **1970**, *227*, 680-685.

237. Elias, D.A.; Tollaksen, S.L.; Kennedy, D.W., et al. The influence of cultivation methods on Shewanella oneidensis physiology and proteome expression. *Arch Microbiol* **2008**, *189*, 313-324.

238. Blackstock, W.P.; Weir, M.P. Proteomics: quantitative and physical mapping of cellular proteins. *Trends in Biotechnol* **1999**, *17*, 121-127.

239. Luo, Q.; Hixson, K.K.; Callister, S.J., et al. Proteome Analysis of Desulfovibrio desulfuricans G20 Mutants Using the Accurate Mass and Time (AMT) Tag Approach. *Journal of Proteome Research* **2007**, *6*, 3042-3053.

240. Rabilloud, T. Membrane proteins and proteomics: love is possible, but so difficult. *Electrophoresis* **2009**, *30 Suppl 1*, S174-180.

241. Matias, P.M.; Pereira, I.A.C.; Soares, C.M., et al. Sulphate respiration from hydrogen in Desulfovibrio bacteria: a structural biology overview. *Prog Biophys Mol Biol* **2005**, *89*, 292-329.

242. Redding, A.M.; Mukhopadhyay, A.; Joyner, D.C., et al. Study of nitrate stress in Desulfovibrio vulgaris Hildenborough using iTRAQ proteomics. *Briefings in Functional Genomics & Proteomics* **2006**, *5*, 133-143.

243. Elias, D.A.; Monroe, M.E.; Marshall, M.J., et al. Global detection and characterization of hypothetical proteins in Shewanella oneidensis MR-1 using LC-MS based proteomics. *Proteomics* **2005**, *5*, 3120-3130.

244. Dias, J.M.; Cunha, C.A.; Teixeira, S., et al. Crystallization and preliminary X-ray analysis of a membrane-bound nitrite reductase from *Desulfovibrio desulfuricans* ATCC 27774. *Acta Crystallogr D Biol Crystallogr* **2000**, *56*, 215-217.

## Annex 1 - Protein purification

c*c*NiR was obtained from *Desulfovibrio desulfuricans* ATCC 27774 membranes as described in [58,75,244]. The process was performed at 4°C with phosphate buffer 0.1 M pH 7.6.

### *ccNiR extraction from membranes*

The membranes were washed with phosphate buffer and centrifuged in a Beckman ultracentrifuge at 100.000 *g* for 2 hours. The supernatant was discarded and the membranes were again suspended in buffer. Sodium choleate was added (3 mg/mL) and the suspension was left to incubate for 24 h under slow magnetic stirring. The membrane suspension was centrifuged again, in the same conditions. The supernatant was stored and the membranes were ressuspended in buffer and the washing procedure was repeated, after which sodium choleate was added to the suspension. The procedures were repeated with sodium choleate concentrations of 4, 4.5, 5, 6 and 6.5 mg/mL; washing procedures were executed in between. The red fractions rich in nitrite reductase were obtained between 4-6 mg/mL of detergent.

### *Salting in/ salting out fractioning*

The c*c*NiR containing supernatants were fractioned with ammonium sulfate at 35, 40, 45, 48 and 52% saturation. After incubation for 1 hour the red precipitates were recovered by centrifugation at 13200 *g* for 30 minutes and dissolved in a minimum volume of phosphate buffer.

### *Gel filtration*

The fractions were applied on a gel filtration column Superdex 200 (Amersham) equilibrated with phosphate buffer 100 mM pH7.6. The enzyme was then eluted with the same buffer; the nitrite reductase containing fractions were pooled, concentrated and stored at -20°C.

The c*c*NiR purity was checked by denaturant polyacrylamide electrophoresis and by UV-vis spectroscopy. Pure protein fractions in a 12.5% SDS-PAGE gel presented an intense 61 kDa band of the NrfA subunit and a band of weak intensity of 19 kDa (NrfH subunit). c*c*NiR

displayed a typical cytochrome c-type UV-vis spectra, with peaks at 280, 409 e 534 nm in the oxidized form and at 420.5, 523.5 e 553.5 nm when dithionite reduced. The purity index of cc*NiR* ($Abs_{409nm}/Abs_{280nm}$) was *ca.* 3.4.

## Annex 2 - Determination of the initial rates of enzyme reaction

For the continuous enzymatic assay described in section 2.2.2.2 only three mediators were used: methyl viologen ($\varepsilon_{604nm}$=13.6 $mM.cm^{-1}$), diquat ($\varepsilon_{460nm}$=2.7 $mM.cm^{-1}$) and phenosafranine ($\varepsilon_{540nm}$=18.4 $mM.cm^{-1}$); the respective reactions are:

$$NO_2^- + 6MV^{+\cdot} + 8H^+ \rightarrow NH_4^+ + 6MV^{2+} + 2H_2O \quad \text{(A2.1)}$$

$$NO_2^- + 6DQ^{+\cdot} + 8H^+ \rightarrow NH_4^+ + 6DQ^{2+} + 2H_2O \quad \text{(A2.2)}$$

$$NO_2^- + 3PSH_2^+ + 8H^+ \rightarrow NH_4^+ + 3PS^{2+} + 2H_2O + 6H^+ \quad \text{(A2.3)}$$

From the assay data collected (mediator absorbance variation with time), the initial rates of reaction were determined by two methods: assuming a zero-order reaction or a pseudo-1$^{st}$ order reaction.

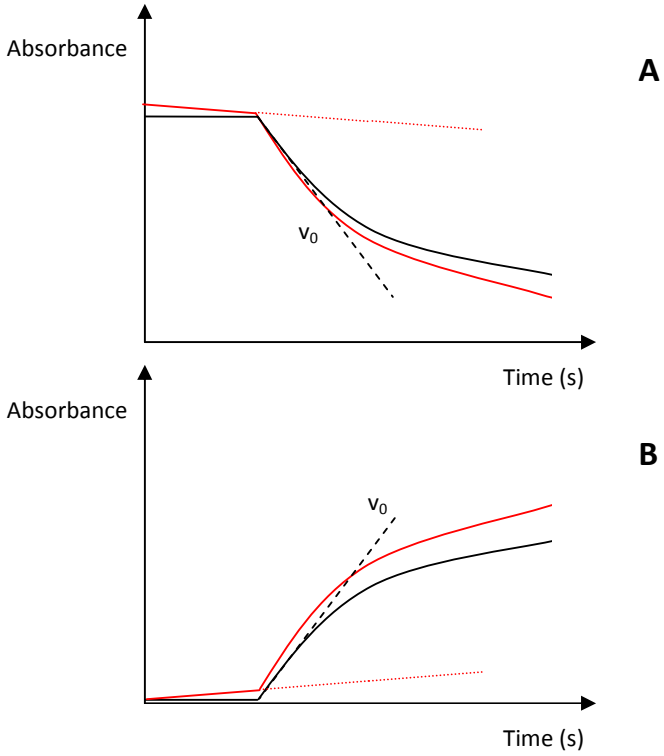


**Figure A2.1 -** Typical absorbance *vs* time plots for **A)** MV and DQ assays, **B)** PS assays. The red lines are the assays and the black lines correspond to the baseline subtraction. $v_0$ is the initial rate of reaction.

***Pseudo 1st order reaction:***

The equation for the rate of reaction is:

$$v_0 = \frac{d[NO_2^-]}{dt} = k[NO_2^-]_0 \qquad \text{(A2.4)}$$

where $v_0$ is the initial rate of reaction, k is the rate constant and $[NO_2^-]_0$ is the initial nitrite concentration. The previous equation is integrated:

$$\int_{[NO_2^-]_0}^{[NO_2^-]} \frac{d[NO_2^-]}{[NO_2^-]} = -k\int_0^t dt \Leftrightarrow \ln[NO_2^-] - \ln[NO_2^-]_0 = kt \Leftrightarrow [NO_2^-] = [NO_2^-]_0 e^{-kt} \qquad \text{(A2.5)}$$

Linearizing the previous equation:

$$\ln\left(\frac{[NO_2^-]}{[NO_2^-]_0}\right) = -kt \qquad \text{(A1.4)} \qquad \text{(A2.6)}$$

The nitrite concentration during the assay is $[NO_2^-]_0 + \Delta[NO_2^-]$ (the initial concentration plus the variation during the assay). The previous equation can thus be represented by:

$$\ln\left(\frac{1}{[NO_2^-]_0} \times [NO_2^-]_0 + \Delta[NO_2^-]\right) = -kt \qquad \text{(A2.7)}$$

According to the reaction stoichiometry for each nitrite molecule that is consumed 6 MV/DQ and 3 PS molecules are used. Accordingly, the equation for MV, DQ and PS are respectively:

$$\Delta[NO_2^-] = \frac{\Delta[MV^{+\cdot}]}{6} = \frac{\Delta Abs_{604nm}}{13.6 \times 6} \qquad \text{(A2.8)}$$

$$\Delta[NO_2^-] = \frac{\Delta[DQ^{+}]}{6} = \frac{\Delta Abs_{460nm}}{2.7 \times 6} \qquad \text{(A2.9)}$$

$$\Delta[NO_2^-] = \frac{\Delta[PSH_2^{+}]}{3} = \frac{\Delta Abs_{540nm}}{18.4 \times 3} \qquad \text{(A2.10)}$$

These equations can be introduced in equation A1.6. For MV:

$$\ln\left(\frac{1}{[NO_2^-]_0} \times [NO_2^-]_0 + \frac{\Delta Abs_{604nm}}{13.6 \times 6}\right) = -kt \Leftrightarrow \qquad \text{(A2.11)}$$

$$\Leftrightarrow \ln\left(\frac{\Delta Abs_{604nm} + [NO_2^-]_0 \times 13.6 \times 6}{[NO_2^-]_0 \times 13.6 \times 6}\right) = -kt \Leftrightarrow \qquad \text{(A2.12)}$$

$$\Leftrightarrow \ln\left(\Delta Abs_{604nm} + [NO_2^-]_0 \times 13.6 \times 6\right) - \underbrace{\ln\left([NO_2^-]_0 \times 13.6 \times 6\right)}_{\text{Constant value for each assay}} = -kt \qquad \text{(A2.13)}$$

In this way the slope of the graphic plot of $\ln(\Delta Abs_{604nm}+13,6x6x[NO_2^-]_0)$ versus the assay time (t) is –k. Identical expressions were used for the other mediators. The k values are used in the equation for the rate of reaction to obtain the initial reaction rates $v_0$:

$$v_0 = k[NO_2^-]_0 \qquad \text{(A2.14)}$$

***Zero order reaction:***

This method was employed when the initial linear part of the assay was long enough to allow the direct calculation of the initial rate reaction by plotting a tangent to the assay curve. In this case, the rate equation is independent of the concentration of the substrates, because they are saturating:

$$v_0 = k \qquad \text{(A2.15)}$$

So, the initial rate can be determined, for MV, by:

$$v_0 = \frac{\Delta Abs_{604nm}}{\Delta t \times 13.6 \times 6} \qquad \text{(A2.16)}$$